FAULT-CONTROLLED HYDROTHERMAL ALTERATION OF PALAEOPROTEROZOIC MANGANESE ORE IN WESSELS MINE, KALAHARI MANGANESE FIELD

by

ALBERT MEIRING BURGER

dissertation
submitted in fulfillment
for the degree of

MASTER OF SCIENCE

in

GEOLOGY

in the

FACULTY OF SCIENCE

at the

RAND AFRIKAANS UNIVERSITY

SUPERVISOR: PROF. N. J. BEUKES
CO-SUPERVISOR: DR. A.S.E. KLEYENSTüBER

DECEMBER 1994

ACKNOWLEDGMENTS

I would like to thank the following:

MINTEK for their financial support.

Samancor for their logistical support.

Mr. E. Karberg of the analytical chemistry department of Samancor at Hotazel for chemical analyses.

The analytical chemistry department at MINTEK for chemical analyses and the use of instrumentation at MINTEK.

The geological and administrative personnel of Samancor at Hotazel, especially Mr. R. Arnot, Miss C. Lathy and Mr. D. McIver for their help and assistance during field and follow-up work. Also the administrative personnel of Samancor at Hotazel and Wessels Mine for making my stay comfortable and smooth running.

Patrick and his underground sampling team at Wessels Mine, for assistance during field work as well as advice and guidance during the project.

Dr. Hsue-Wen Yeh of the Hawaii Institute of Geophysics in Honolulu, USA for stable isotope analyses.

My co-supervisor at MINTEK, Dr. A.S.E. Kleyenstüber for his guidance, help and advice, XRD and SEM analyses.

The personnel and post graduate students at the Geological department of the Rand Afrikaans University, especially Dr. M. Buxton, Mrs. N. Day, Mr. H. Dirr, Mr. H. Jonker, Mrs. E. Maritz, Mr. V. Morel, Mr. K. Mokgatla (for answering the phone) Prof. C. Roering and Mr. J. Gutzmer for sharing his "manganese knowledge". Mr. D. Selepe and Mr. M. Baloy for cutting and polishing thin sections and Mr. H. Leteane for tea.

My parents and brothers for their love, encouragement and financial support.

My fiancé Ilané for her love, encouragement and understanding.

My supervisor Prof. N.J. Beukes for his guidance, help and advice which made it possible.

All thanks to God who made it possible for everyone of us, through his everlasting love.

Hieride tesis is opgedra aan my broer Francois.

25/11/1970 - 10/07/1994

Opsomming

Die Kalaharimangaanveld, ongeveer 60km noordwes van Kuruman in die Noord-Kaapprovinsie geleë, bevat die grootste landelike mangaanafsettings ter wêreld. Dit bestaan grootliks uit laegraadse sedimentêre Mamatwantipe erts (met tot 38 gewigspersent Mn) wat ongeveer 97 persent van die ertsreserwes uitmaak. Ongeveer 3 persent van die bekende reserwes bestaan uit hoëgraadse Wesselstipe erts (met 'n gemiddeld van tussen 42 en 48 gewigspersent Mn) wat voorkom in die noordwestelike deel van die afsetting. In hierdie gedeelte van die afsetting word die opeenvolging verplaas deur 'n stelsel van noord-suidstrekkende normale verskuiwings. Verskuiwingsones is veryster en die oorspronklike sedimentêre Mamatwantipe erts is hidrotermaal opgegradeer langs verskuiwings tot hoëgraadse Wesselstipe erts. Relikte van Mamatwantipe erts is bewaar in the sentrale gedeeltes van verskuiwingsblokke. Mamatwantipe erts bestaan hoofsaaklik uit braunietlutiet en die mangaankarbonaat kutnahoriet met ondergeskikte kalsiet. In kontras bestaan Wesselstipe erts uit hausmanniet, bixbyiet, brauniet II en manganiet en ondergeskikte sekondêre minerale soos kalsiet, chlinochloor, gaudefroyiet en andradiet.

Hidrotermale verandering van Mamatwantipe erts na Wesselstipe erts behels hoofsaaklik loging van SiO_2 uit die sisteem en 'n oksidering van mangaankarbonate na mangaanoksiedes. In effens veranderde Mamatwantipe erts is sferiese klein kutnahoritiese konkresies vervang deur hausmanniet en kalsiet. Brauniet is verander na brauniet II deur 'n loging van SiO_2. Die volgende stadium van verandering behels 'n transformasie van brauniet II na bixbyiet en oksidering van al die mangaankarbonaat na hausmanniet en vorming van kalsiet en andradiet as aarsteenminerale. Die hoogste graad Wesselstipe erts bestaan hoofsaaklik uit hausmanniet. Dit is langs verskuiwingssones gekonsentreer. In die onmiddelike omgewing van verskuiwingsones is die mangaanerts gehematitiseer en van die hausmanniet is ysterryk. Die ysterryke hausmanniet (met tot 15 gewigspersent Fe) is hoogs magneties. In die oorgangsone tussen hoëgraadse hausmannietryke Wesselstipe erts en die verysterde sone is 'n sekondêre fase van massiewe braunietryke erts ontwikkel. Dit is moontlik veroorsaak deur die herpresipitasie van silika, geloog uit Mamatwantipe erts deur die hidrotermale vloeistowwe. Die hematietryke verskuiwingsones bevat heelwat kalsiet en tot 'n mindere mate ook kwarts.

Normale verskuiwings het blykbaar as kanale vir hidrotermale vloeistowwe gedien. Hidrotermale oplossings, wat verantwoordelik was vir die opgradering van die erts,

was blykbaar ryk in tweevalente yster en alkalies om silika te kan loog uit primêre Mamatwantipe erts. Fe_2O_3 is in verskuiwingssones gepresipiteer, terwyl mangaan gemobiliseer is as Mn^{2+} om as hausmanniet te presipiteer meer distaal tot die verskuiwingsone. Silikaloging deur die hidrotermale oplossings het veroorsaak dat brauniet verander is na brauniet II wat op sy beurt weer verander is na bixbyiet. Langs die veranderingsfront, tussen Mamatwantipe- en Wesselstipe erts, was die oplossings oksiderend soos aangedui word deur die verandering van mangaan karbonate na hausmanniet en die vorming van kalsiet. Hidrotermale verandering het blykbaar plaasgevind in 'n tipe van konveksiesel met SiO_2 en Ca wat geloog is vanuit Mamatwan-tipe erts en geherpresipiteer is in die nabyheid van die normale verskuiwings in die vorm van sekondêre brauniet en kalsiet.

Die laterale mineralogiese sonering in die ertse mag moontlikhede inhou vir selektiewe mynbou van verskillende tipes ertse. Die ontdekking van magnetiese hausmanniet in die ertse mag moontlik toepassing vind in geofisiese eksplorasie na hoëgraadse Wesselstipe erts, sowel as in die skeiding van verskillende erts grade.

Abstract

The Kalahari manganese field, situated some 60km northwest of Kuruman in the Northern Cape Province, contains the world's largest known land-based manganese deposits. Low-grade sedimentary Mamatwan-type ore (containing up to 38 weight percent Mn) dominates and constitutes about 97 percent of the ore reserves. It is composed of finely intergrown braunite and Mn-carbonate. High-grade Wessels-type ore (containing on average between 42 and 48 weight percent Mn) constitutes about 3 percent of the known reserves and occurs in the northwestern part of the deposit. Here the sequence is displaced by a system of north-south striking normal faults. Fault zones are ferruginized and alongside faults sedimentary Mamatwan-type ore has been upgraded by hydrothermal alteration to Wessels-type ore. Pockets of Mamatwan-type ore are present in cores of fault blocks. Wessels-type ore consists mainly of hausmannite, bixbyite, braunite II and manganite, and subordinate secondary minerals such as calcite, clinochlore, gaudefroyite and andradite.

Hydrothermal alteration of Mamatwan-type ore to Wessels-type ore involved essentially leaching of SiO_2 from the system and oxidation of manganese-carbonates to manganese oxides. In slightly altered Mamatwan-type ore kutnahoritic ovoids are replaced by hausmannite and residual calcite remaining and braunite altered to braunite II through leaching of SiO_2. The next stage of alteration involves transformation of braunite II into bixbyite and oxidation of all manganese carbonate into hausmannite and formation of calcite or andradite as gangue minerals. Highest grade Wessels-type ore is essentially composed of hausmannite. In proximity to fault zones hematitization of manganese ore took place and hausmannite is iron-rich. This iron-rich hausmannite (containing up to 15 weight percent Fe) is highly magnetic, as indicated by magnetic susceptibility and other paleomagnetic studies. In the transition zone between hematite-rich fault zones and high-grade hausmannite-rich Wessels-type ore, a secondary phase of massive braunite is developed, as a result of reprecipitation of earlier leached silica. The hematite-rich fault zones may contain abundant calcite and some quartz.

Normal faults apparently acted as conduits for hydrothermal fluids. Hydrothermal solutions, responsible for the upgrading of the ore, were presumably rich in ferrous iron and alkaline in order to mobilize Mn^{2+} and turned less alkaline to neutral with relative high temperature (± 300°C), to leach silica from primary Mamatwan-type ores. The solution precipitated ferric iron as Fe_2O_3 adjacent to normal faults, while mobilizing manganese as Mn^{2+} to precipitate it more distal to the fault zone as

hausmannite. Leaching of SiO_2 by the hydrothermal solution caused transformations from braunite into braunite II and bixbyite. Along the alteration front, between Mamatwan- and Wessels-type ore, solutions were oxidizing as indicated by the transformation of Mn-carbonates into hausmannite and calcite. Hydrothermal alteration apparently took place in a type of convection cell with SiO_2 and Ca leached from Mamatwan-type ore and re-precipitated in proximity to the normal faults in the form of a secondary braunite and calcite.

Identification of systematic lateral mineralogical variations in Wessels-type ore, relative to ferruginized normal fault zones holds potential for selective mining of different ore types. Similarly the presence of magnetic hausmannite may find future application in geophysical exploration for high-grade Wessels-type ore, as well as in the separation of different grades of ore.

CONTENTS

CHAPTER I INTRODUCTION

1.1 STATEMENT OF PROBLEM

The Kalahari Manganese Field is the biggest land-based manganese deposit in the world. It is situated about 60km northwest of Kuruman in the Northern Cape Province, South Africa. It is the main producer of manganese ore in South-Africa, with estimated reserves of about 13 billion metric tons at Mn content of 20-48 weight percent (Taljaardt, 1982). The primary ores are of sedimentary origin, interbedded with iron-formation of the Hotazel Formation, of the Transvaal Supergroup. Three ore beds are present, preserved within five structural controlled basins comprising from North to South the Leinster, Avontuur, Hotazel, Langdon Annex and Kalahari deposits (Fig. 1.1). The Kalahari deposit is by far the largest and economically the only one being exploited.

The Wessels mine is situated in the northern part of the Kalahari deposit. In this area Hotazel strata is displaced by normal and thrust faults (Beukes and Smit, 1987; Grobbelaar, 1988). In the vicinity of normal faults, primary low grade sedimentary manganese ores (Mamatwan-type ore) have been altered to high grade Wessels-type manganese ore. Definition of ore types is after Kleyenstüber (1984). Mamatwan-type ore has an average manganese content of 37,5 weight percent and Wessels-type ore an average manganese content of 48 weight percent. In addition, zones of ferruginization occur within the latter ore beds, making part of this high-grade ore unmineable.

The process of upgrading of low-grade ore to high-grade ore and controls on the distribution of high-grade ores and zones of ferruginization are poorly understood. The aim of this study is to provide geological explanations for controls on, and processes responsible for enrichment of the low grade Mamatwan-type ore to the higher grade Wessels-type ore. Solution of the question may have wide-ranged economic applications, especially in light of the fact that only 3 percent of the known reserves in the Kalahari manganese field are represented by high-grade Wessels-type ore. Knowledge about the origin of Wessels-type ore may be applied to locate (both on a regional and a mine exploration scale) new high-grade ore reserves and also possibly lhelp in planning selective mining of different high-grade ore types.

1.2 LOCALITY

The study was undertaken at the Wessels mine, owned by the Samancor-group, situated in the northern part of the Kalahari deposit (Fig. 1.2). The mine, which is an underground operation, is ideally suited for such a study, because it is the type locality for Wessels-type ore. However, within the mine, parts of the manganese ore beds cannot be mined because of ferruginization and because high-grade Wessels-type ore grades laterally into low-grade Mamatwan-type ore. Underground ore grade maps of the mine indicate significant lateral variation in grade and chemical composition of ore beds apparently related to certain structures in the Mine. Structures which have most significant influence on the composition of ore beds are represented by north-south trending normal faults that displace the manganese beds resulting in a system of horst and graben structures. High-grade ore development and ferruginization appear to be directly related to the system of normal faults. Underground operations opened up many of these features, making it possible to study and sample lateral transitions from Mamatwan-type ore into Wessels-type ore and from the latter into zones of ferruginization. Detailed petrographic and geochemical analyses of lateral transition zones between different ore types can thus be undertaken.

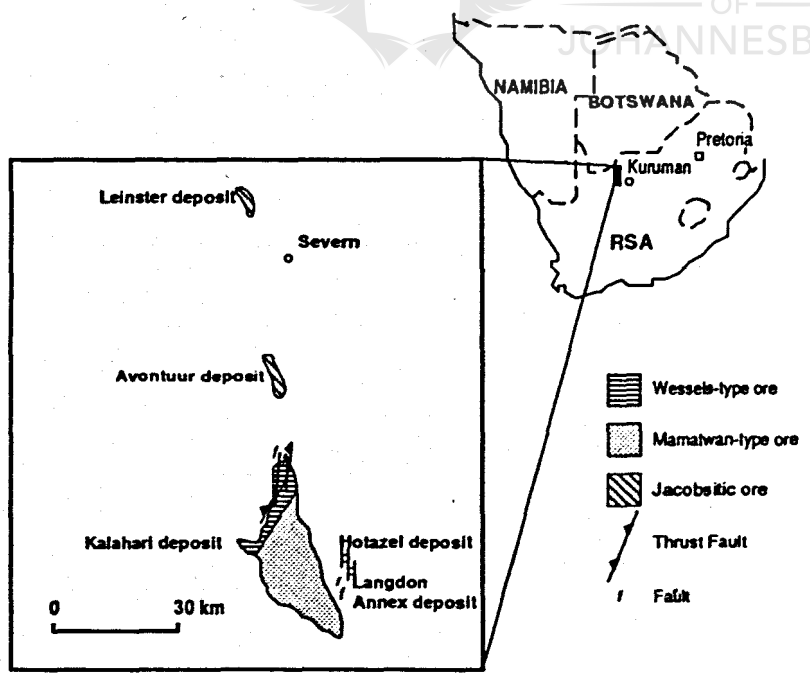

Figure 1.1 Locality of the Kalahari manganese deposit in South Africa and distribution of five known deposits representing structurally preserved erosional relicts of original much more extensive occurrences of manganese (after Miyano and Beukes, 1987).

1.3 MINING ACTIVITIES

Mining in the Kalahari area of the Northern Cape Province include production of diamonds, blue asbestos, limestone, iron and manganese. A summary of the history of mining of the area comes from a book, Kaias and cocopans (Hocking, 1983), published by Hollards in South Africa. Mining has been taking place since the stone age, with the production of primitive tools, from banded iron-formation. Prehistoric man also mined hematite, limonite and specularite for use as body paint (Hocking, 1983). Later on, in the 19th century, alluvial diamond digging started along the Vaal and Orange Rivers, with kimberlite pipes exploited near Kimberley.

In 1884 crocidolite was discovered near Kuruman in the Asbestos Hills. In time, especially before the first world war, crocidolite was one of the main minerals produced from the Kuruman area, for insulation material in boilers on warships.

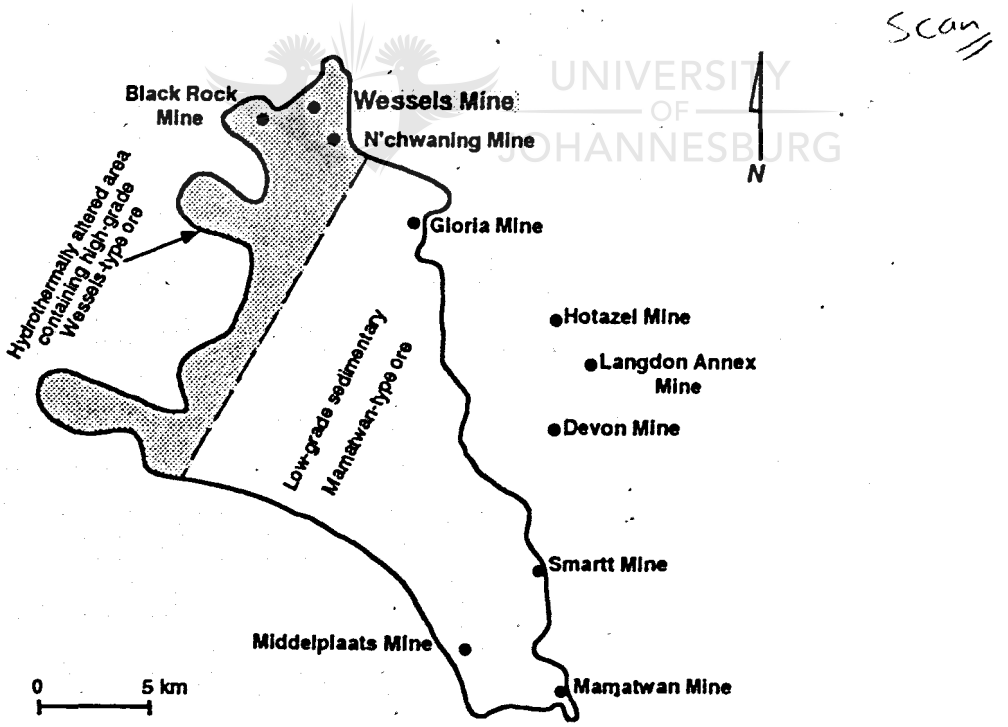

Figure 1.2 Outline of the Kalahari deposit showing the distribution of areas in which low-grade Mamatwan-type ores dominate and areas in which high-grade Wessels-type ores are present (redrawn after Kleyenstüber, 1985).

In 1907 a government geologist, A.W. Rogers, noted manganese at Black Rock (Fig. 1.2) in the Kalahari manganese deposit. However, the deposit received no further attention for a very long time, because all activities were directed at the manganese deposit associated with the Cambellrand carbonates in the Postmasburg manganese field. In 1926 Union Manganese was launched and investigated several farms containing manganese in the Postmasburg area and took out options. In the same year another company, South African Manganese Ltd., was registered and bought options on farms close to those of Union Manganese. In November 1930 the railway reached Postmasburg for transport of ore from the Beeshoek manganese mine, which mined very low-grade ore. A few other deposits were also mined, such as Kapstewel and Lohatla. In 1936 Anglovaal entered the manganese market and launched a new company named Associated Manganese Mines of South Africa Ltd., today known as Ammosal or Assmang. They opened a new mine on the farm Gloucester. By now (1936) the railroad reached the Lohatlha manganese mine.

The first manganese mine to open in the Kalahari manganese deposit was Black Rock (Fig. 1.2), opened in 1940 by Ammosal. It was also one of the first underground manganese mines in the world. In 1953 South African Manganese opened the Smartt mine (Fig. 1.2), which is a low-grade open pit mine in the eastern part of the Kalahari deposit. During this time Associated Manganese developed a new open pit mine north of the Smartt mine, called Devon. It has since been worked out. Devon lies approximately 4km south of Hotazel and is situated in a graben structure.

In the mid 1950s manganese was discovered on the farm Langdon (Fig. 1.2), north of Devon by a "diviner", looking for water on the property, who was reported to have seen "masses of black rock". This open pit mine was worked by the company National Manganese. The ore pillar left between Langdon and Devon mines were later mined as the Langdon Annex operation. Most of these mines stopped operation in the late 1970's to early 1980's

Shortly after Langdon was discovered, high-grade ore was reported by Dr. L.G. Boardman from a graben structure on the farm Hotazel (Fig. 1.2). An open pit mine, named Hotazel Mine, was opened during November 1959 and with it the village Hotazel developed. A high-grade ore, named Hotazel super grade, was mined here until well into the 1980's, first in open pit operations and later as an underground operation. Zones of ferruginization occurred in the Hotazel deposit

and South African Manganese was forced to look for another source of manganese ore with low iron content. Thus exploration started at Mamatwan (Fig. 1.2), with a drilling program, while Ammosal opened a mine on Adams, a farm immediately adjacent. Shortly afterwards Mamatwan mine was opened with only a pillar separating the two open pits. Mamatwan mine is still in operation, with vast ore reserves left, while Adams is mined out.

During 1976 Anglo American Corporation of South Africa decided to develop an underground manganese mine for low-grade ore on Middelplaats (Fig. 1.2), neighbouring Mamatwan. Work on the shaft was finished in 1979. The mine extends to a depth of 489 metres. In 1982 the mine was sold to South African Manganese, now known as Samancor (since its merger with Amcor i.e. African Metals Corporation). Samancor closed down the mine, because enough low-grade ore is produced by the Mamatwan mine to satisfy the market. The first totally mechanized underground mine in the Kalahari manganese field was Gloria mine (Fig. 1.2) which opened in 1977.

Hotazel Mine closed down temporarily in 1978 because of difficult mining conditions and fluctuating market prices. It opened again in 1981 and was mined sporadically until the late 1980's. However, with ore reserves at Hotazel starting to become depleted in the 1970's, South African Manganese started exploration on the Wessels deposit (Fig. 1.2). Wessels Mine began production in 1978 and before long it was the largest underground manganese mine in the world. At approximately the same time Associated Manganese opened the N'Chwaning I underground mine, situated to the south of the Wessels mine (Fig. 1.2). N'Chwaning I later closed down, because of a 60 meter down displacement of the ore beds to the west by a normal fault, and N'Chwaning II mine was opened (Fig. 1.2). Similar high-grade manganese ores are mined at Wessels and N'Chwaning. These two mines are at present the main producers of manganese ores from the Kalahari manganese field, supplemented by low-grade ore from the Mamatwan Mine. Mamatwan ore is at present upgraded by roasting, whereby the CO_2 is removed from the carbonates in the ore, to produce a Mn-ore sinter suitable for use in a submerged arc furnace.

1.4 PREVIOUS WORK

A.W. Rogers (1908) indicated the location of the Black Rock manganese deposit on a small-scale map of the Kuruman area. This was the only outcrop of manganese that eventually led to the discovery of the giant Kalahari manganese field (Boardman, 1941).

J. de Villiers (1956) and Kupferburger et al. (1965) discussed the geological setting of the Kalahari manganese field. However, in these early years after the discovery, the mineralogical composition and genesis of the ore received little attention.

J. de Villiers (1960) compiled a comprehensive review on the manganese deposits of the Union of South Africa. In it information on all aspects of the manganese producers of South Africa are given; concentrating on geology, mineralogy, origin of the ores, mining and history of production. The Kalahari and Postmasburg deposits are described and an evaluation of ore reserves given.

Boardman (1961) gives a broad account of the occurrence of manganese in South Africa, indicating the location and distribution of the geological formations in which deposits are situated.

The first detailed mineralogical studies were by P.R. De Villiers and Herbstein (1967). They determined the mineral properties of ferrian braunite. The crystal structure of this braunite was determined much later by J.P.R de Villiers (1980). It contains less SiO_2 than normal braunite, and is referred to as braunite II.

P.R. de Villiers (1970) undertook the first comprehensive study on the geology and mineralogy of the Kalahari manganese field. He concentrated mainly on samples from Adams, Black Rock, Devon, Hotazel, Langdon, Mamatwan and Smartt mines, and a few diamond drill cores that were available at that time. Thirty minerals from the deposits are described by him.

Geological maps of the Postmasburg (Moen, 1977) and Kuruman (Moen, 1979) areas, with explanatory notes, have been published by the South African Geological Survey.

Kleyenstüber (1979) investigated the products formed during the reduction of Mamatwan-type manganese ore in furnaces. He concentrated on mineralogical changes and presented a possible reduction mechanism for Mamatwan-type ore .

Mineralogic aspects of manganese deposits of Griqualand West were investigated by J.E. de Villiers (1983) to determine if the iron-content of manganese sesquioxides may be utilized to determine the temperature of formation of ores at various localities. He states that judging by mineralogical and textural features of the sesquioxides, the Postmasburg and the Kalahari deposits are genetically related and formed due to hydrothermal processes. De Villiers (1992) later reiterated this statement, but Beukes (1992) pointed out that abundant sedimentary features are present in the Kalahari deposits and that later hydrothermal activity only led to upgrading in the sedimentary ores in specific areas. Beukes (1992) also indicates that the Kalahari- and Postmasburg deposits are not genetically related.

A mineralogical study of the mineralogy of the Mamatwan ore body was done by Nel (1984). He characterized the ore of the Mamatwan mine geochemically, as well as mineralogically. This work enabled the mine to deliver ore for specific applications according to mineralogy and not only on chemical grade as was done previously. His findings were later published by Nel et al. (1986). At the same time Jennings (1986) discusses the geology of the neighbouring Middelplaats Mine, an underground operation.

The mineralogy of the Hotazel Formation and associated manganese deposits are described by Kleyenstüber (1984). The emphasis is on the composition of the various manganese minerals. He established the terms Mamatwan-type ore and Wessels-type ore and states that the latter is related to hydrothermal alteration.

A basin analysis of the Voëlwater Subgroup was undertaken by Beukes (1985). He describes the relationship between the Gamagara- and Mapedi Formations, as well as thrust fault deformation in the area.

Kleyenstüber (1985) did an intensive mineralogical study on the whole of the Kalahari manganese field. This work gave an overview of the different minerals and their parageneses encountered in the Voëlwater Subgroup. He discusses 55 different minerals, with an explanation of their origin. He also suggests that

hydrothermal alteration of Mamatwan-type ore to high-grade Wessels-type ore is related to the period of thrust deformation in the basin. He also describes the mineralogy of the Hotazel Formation (Kleyenstüber, 1986), and gives attention to the fine grained gangue minerals.

Beukes and Smit (1987) present stratigraphic and structural evidence that major thrust faults displace early Palaeoproterozoic Transvaal and Olifantshoek strata near the western margin of the Kaapvaal craton in Griqualand West. These thrust faults also duplicate manganese beds in the Kalahari deposit.

Miyano and Beukes (1987) discuss the physiochemical environments for the formation of quartz-free manganese oxide ores from the Hotazel Formation of the Kalahari Manganese Field. They do it on the basis of phase relations in the system Mn-Fe-Si-O, and qualitatively in the system Ca-Mn-Fe-Si-O. These phase relations are also applicable to the estimation of physiochemical environments of other manganese deposits with a deficiency in SiO_2. Miyano and Beukes (1988) also used carbon dioxide fugacity to determine stability fields for quartz-free manganese oxide ores from the Kalahari manganese field in the presence of $CaCO_3$.

Metamorphic silicate minerals, sugillite in particular, and their relation to hydrothermal activity in the lower manganese ore body at the Wessels mine, are discussed by Dixon (1988). He also presents radiometric age dating results suggesting that some of the hydrothermal alteration took place some 1250 m.y. ago.

The N'Chwaning mine, mining the same orebody as the Wessels mine, was described briefly in terms of its location, geology and history by Grobbelaar (1988).

Von Bezing et al. (1991) gives an update of minerals found in the Kalahari manganese field. It is an update of the list given by Wilson and Dunn (1978). The new list contains 120 minerals. He also presents some excellent photographs of the spectacular specimens of some secondary minerals occurring in the Kalahari deposit (especially in the N'Chwaning and Wessels mine). The Kalahari manganese field is world renown for these mineral specimens.

Kleyenstüber (1993) discusses characteristics of the different main ore types present in the Kalahari manganese field. The three unconformities (of different age) that intersect the ore beds, are mentioned, as well as the overprint left by them on the mineralogical composition of ore beds.

Gutzmer and Cairncross (1993) reports on recent mineral discoveries in the Wessels Mine, made in 1992. The article also presents excellent photographs of the minerals described.

Tsikos (1994) gives an overview of the possible source and conditions of deposition and diagenesis of the manganese and especially the banded iron-formations of the Voëlwater Subgroup. Similarities between the Voëlwater iron-formation and other major Superior-type iron-formations are discussed.

Numerous abstracts on the Kalahari manganese field have been submitted to geological congresses all over the world, through the years. Not all will be quoted, but a list as comprehensive as possible is given.

Abstracts on manganese deposits associated with the Transvaal Supergroup in the Northern Cape Province of South Africa were submitted by Beukes (1984), Beukes (1988), Kleyenstüber (1988), Beukes (1989), Beukes (1993), Beukes and Gutzmer (1994), Beukes (1994). Hydrothermal alteration, diagenesis and sedimentation of manganese ores in the Kalahari manganese field are discussed by Beukes et al. (1982), Beukes (1984), Beukes (1986), Beukes and Kleyenstüber (1986), Beukes (1989), Gutzmer (1993). Description of individual mineral phases and their chemical composition are given by Burger et al. (1994) and Beukes et al. (1994).

Gutzmer (1993) and Gutzmer and Beukes (in press) discuss the systematics of mineralogical variations in transition zones from low-grade Mamatwan-type ore to high-grade Wessels-type ore in the N'Chwaning mine. They suggest that it is related to a system of normal faults and ferruginization. The present thesis was in actual fact devised to test these theories in the neighbouring Wessels Mine.

1.5 AIM OF STUDY AND METHODS APPLIED

This present study is aimed at describing the lateral transition from low-grade Mamatwan-type ore, through high-grade Wessels-type ore, into zones of ferruginization associated with large-scale north-south trending normal faults in Wessels Mine. It is intended to test the model for hydrothermal alteration given by Gutzmer and Beukes (in press). It is also intended at establishing geological parameters responsible for hydrothermal upgrading of Mamatwan-type ore to Wessels-type ore and to determine factors that control the distribution of the high-grade ore.

The following analytical techniques were applied to reach this goal: underground mapping and sampling of sections from zones of ferruginization, through high-grade Wessels-type ore, into low-grade Mamatwan-type ore, XRD-analysis, petrographic descriptions, microprobe analysis, whole rock XRF chemical analysis, stable isotope analysis of carbonate minerals and magnetic susceptibility measurements.

CHAPTER II GEOLOGICAL SETTING

2.1 REGIONAL GEOLOGICAL SETTING

Of the five known manganese deposits in the Kalahari manganese field, the Kalahari deposit is the largest, covering an area of 35 km x 15 km. Manganese beds are confined to the Hotazel Formation of the Postmasburg Group of the Transvaal Supergroup (Söhnge, 1977; Beukes, 1980). The manganese beds occur interbedded in host rock iron-formation (Fig. 2.1).

The Hotazel Formation is conformably overlies pillow lava and jaspilites of the Ongeluk Formation (Fig. 2.1). In the central part of the Kalahari deposit the Mooidraai Formation, composed of dolomite and limestone, overlies the Hotazel Formation with a conformable contact (Fig. 2.2A). The Transvaal Supergroup is overlain with marked angular unconformity by late Palaeoproterozoic red beds of the Mapedi and Lucknow Formations of the Olifantshoek Group (Fig. 2.3). Prior to the deposition of the red beds, the Transvaal Supergroup was folded and peneplained by erosion. The Kalahari deposit is preserved in an old synclinal structure (Fig. 2.2C) below the unconformity at the base of the Mapedi shale of the Olifantshoek Group. Manganese is preserved in this structure below the red beds. Later the red beds tilted to the west so that the manganese deposits are preserved in the ancient syncline below the red beds, with the axis of the syncline tilted to the northwest (Fig. 2.2A and 2.2B).

The Transvaal Supergroup and Olifantshoek Group are unconformably overlain by late Carboniferous-, early Permian diamictite of the Dwyka Formation of the Karoo Supergroup (with a thickness of up to 130 metres in glacial paleovalleys) (Fig. 2.1). The Dwyka Formation is in turn unconformably overlain by unconsolidated sediments of the Kalahari Formation composed of calcrete, gravels, clay and aeolian sand up to 125 metres thick.

The topography is absolutely flat with the only noticeable topographic landmark in the area represented by Black Rock, a small hill composed of Hotazel iron-formation and manganese ore beds. It represents the only natural outcrop of the manganese deposits in the entire Kalahari manganese field.

The Hotazel Formation contains three manganese beds, each forming the centre of three symmetrical cycles of sedimentation (Fig. 2.3). The cycles are

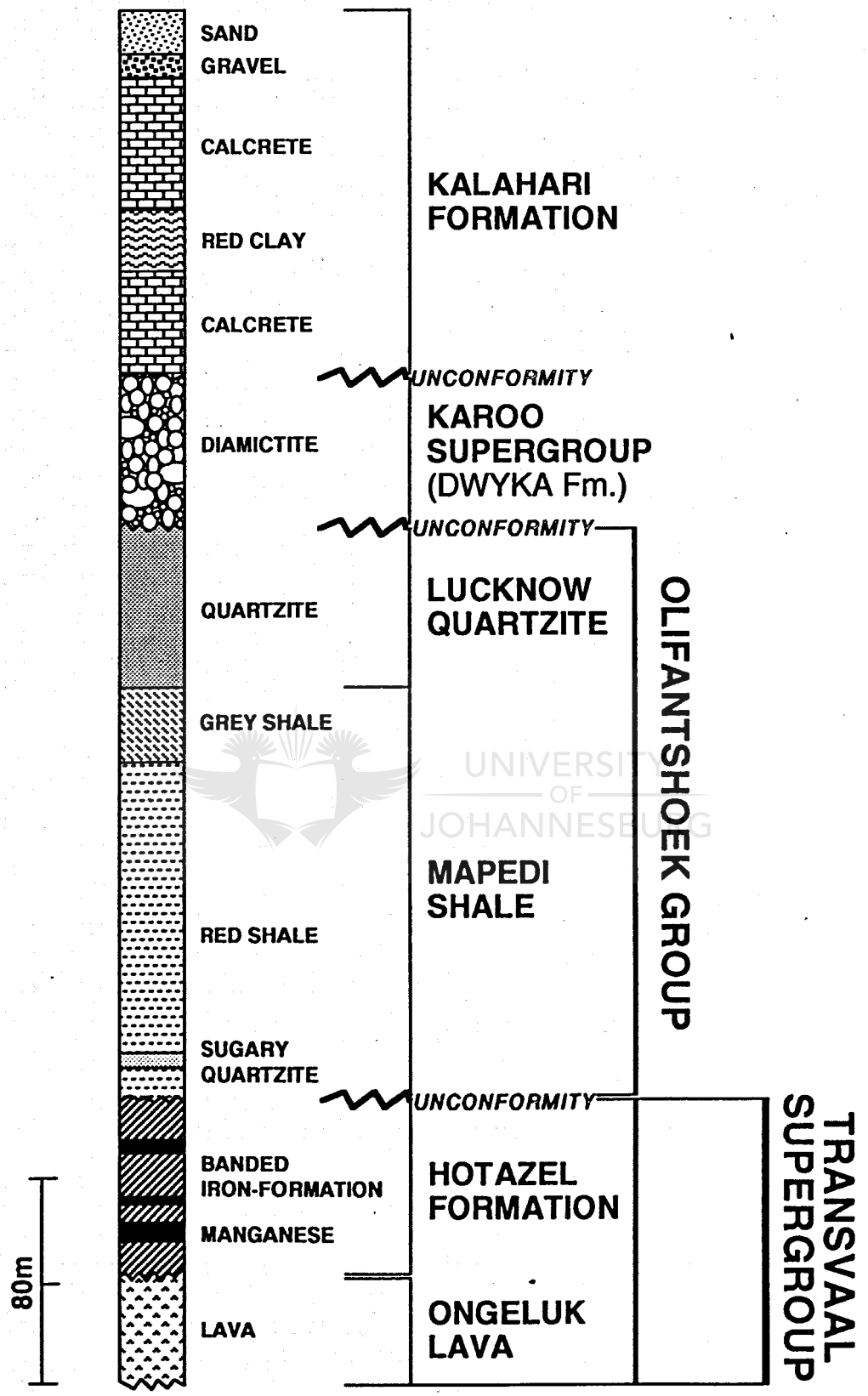

Figure 2.1 Stratigraphical column at Wessels Mine.

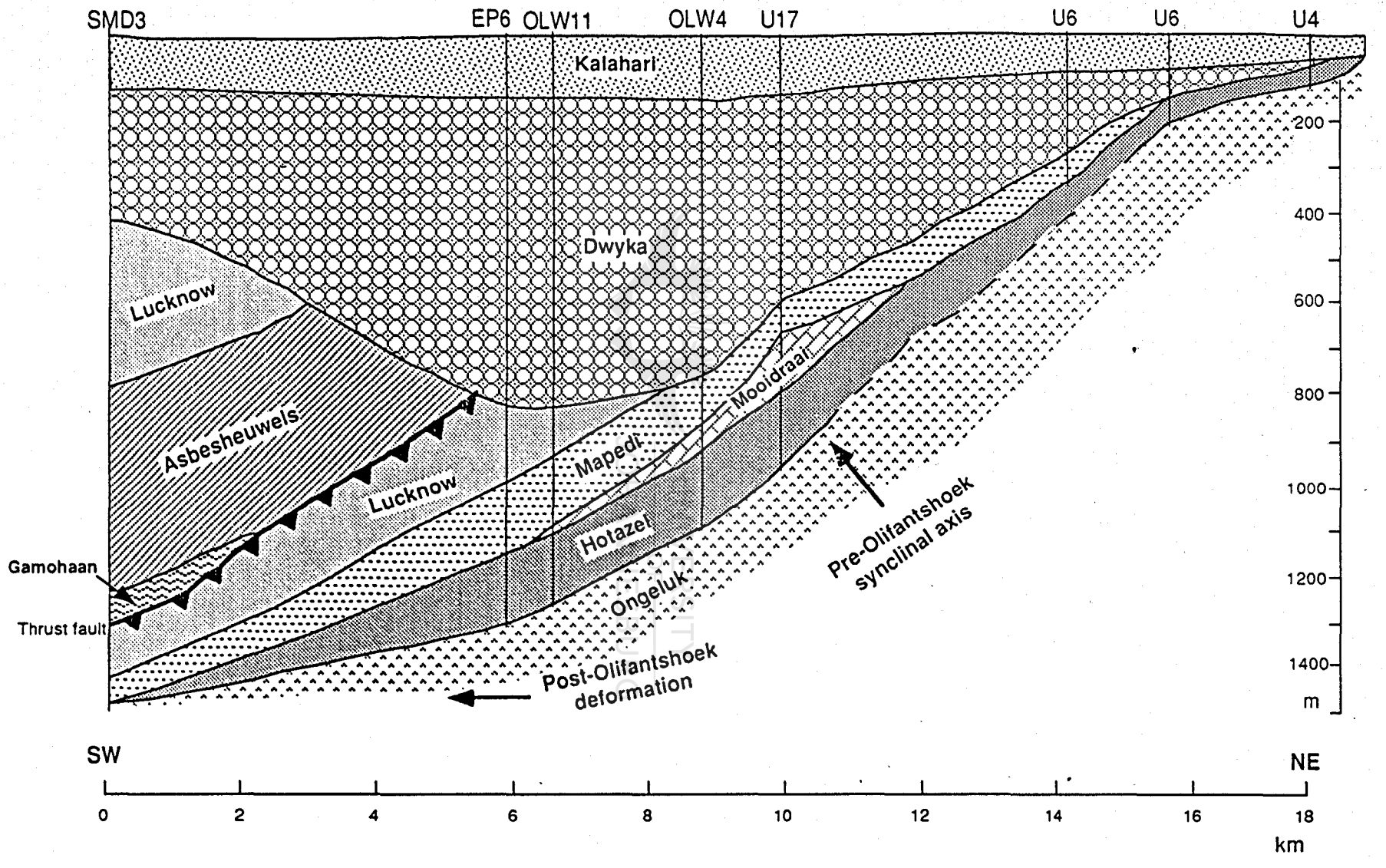

Figure 2.2A. Northeast-southwest stratigraphical section through the Kalahari basin, showing the relationship of the major formations. Redrawn after Beukes, 1985.

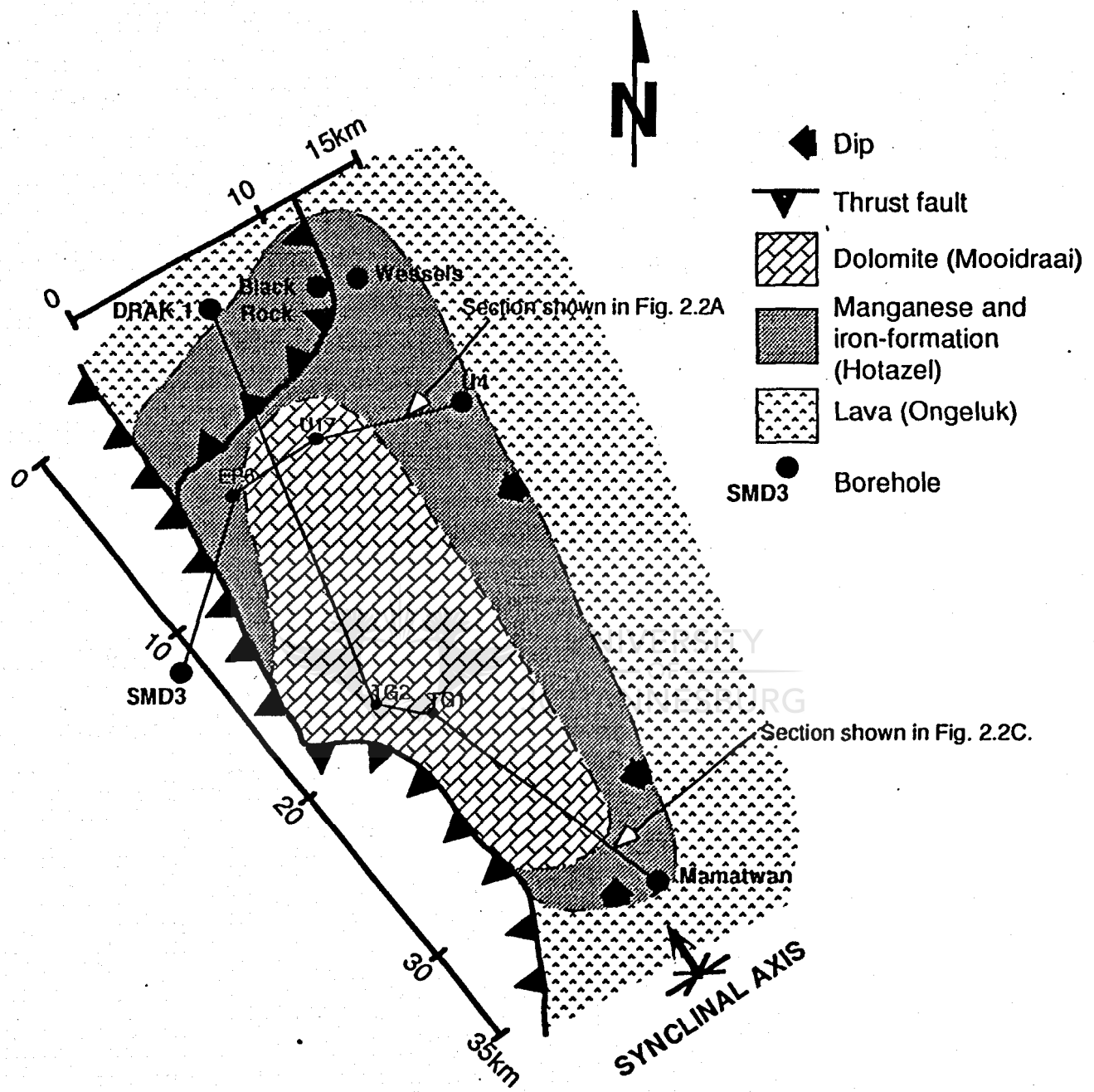

Figure 2.2B. Paleosyncline of the Kalahari deposit, below the Dwyka and Kalahari Formations. Redrawn after Beukes, 1985.

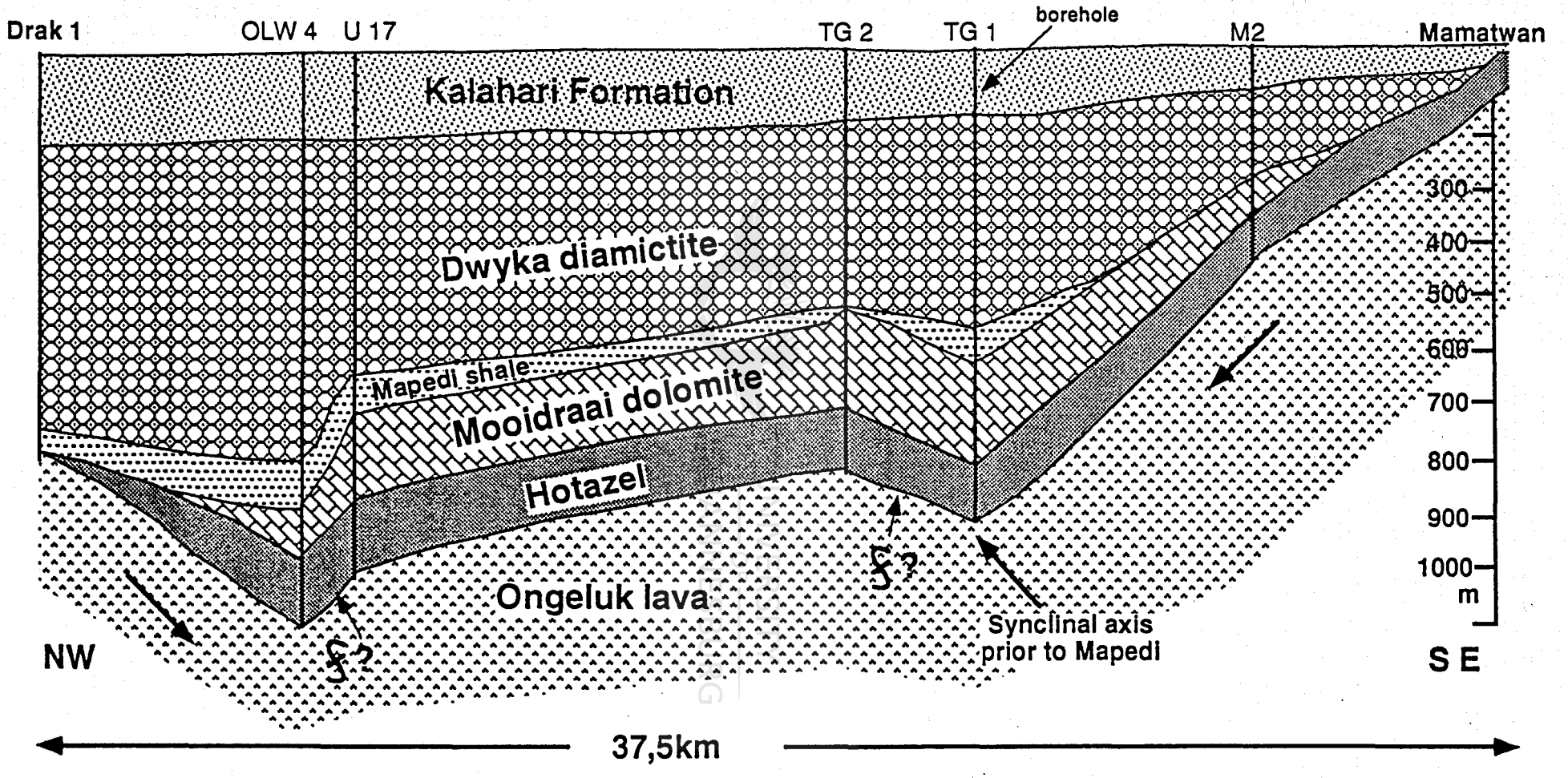

Figure 2.2C. Northwest-southeast stratigraphic section through the Kalahari syncline. See Fig. 2.2B for borehole positions (redrawn after Beukes, 1985).

composed of iron-formation <-> hematite lutite <-> manganese lutite (in the centre of the cycle) (Beukes et al., 1982) (Fig. 2.3). Of the three manganese ore beds, the lowermost one is the thickest, varying between 4 and 40m in thickness (De Villiers, 1970). It is also economically the most important. The middle bed is poorly developed and maybe absent in some areas. It is on average about one meter thick (De Villiers, 1970). The upper bed rarely exceeds five metres in thickness and consists mostly of low-grade manganese ore. Virtually all the manganese ore is mined from the lower ore bed, which at the Wessels mine is between 4 and 8 metres thick.

North-south striking normal faults displace the manganese ore beds in the Wessels- N'Chwaning area with a mean throw of between 5 and 10 meters. Some faults display almost no displacement and then there are others, reported in the N'Chwaning area, with a displacement of almost 60 meters. Downthrows are almost invariably to the west (Fig. 2.4). Minor east-west striking faults are also present. Normal faults of this system are also responsible for preservation of the Hotazel and Langdon deposits, in old grabens below the Kalahari Formation.

Towards the west of the Wessels mine there is evidence of large scale overthrusting (Fig. 2.2A). The thrusts duplicated the sequence and is also responsible for the Black Rock outcrop. The normal faults apparently post-date the red beds of the overlying Olifantshoek Group, but pre-dates the thrust event. Thrusting is related to the formation of the Kheiss orogen 1700 - 1800 m.y. ago (Stowe, 1986; Beukes and Smit, 1987). Development of high-grade Wessels-type ore is apparently related to this area of normal and thrust fault deformation (Kleyenstüber, 1985).

The age of the Hotazel Formation is not very well constrained. The Ongeluk lava conformably underlying the Hotazel Formation, define a Pb-Pb isochron that indicates an apparent age of 2239 ± 90 m.y. (Armstrong, 1987). In contrast the Hartley lava of the overlying Olifantshoek Group, above the Lucknow quartzites, define a Rb-Sr isochron that indicates an age of 2026 ± 180 m.y. with a Pb-Pb determined age of 1830 ± 400 m.y. (Armstrong, 1987) (Fig. 2.5). Söhnge (1977) estimates the age of sedimentation of the Hotazel Formation at about 2100 m.y.. Bostonite dykes encountered in the Wessels Mine were dated through Rb-Sr isotopes by Dixon (1988) at about 1350 m.y. old. The age of the dykes pre-dates the age of sugillite, a hydrothermal mineral occurring in the manganese beds, which is associated with the later stages of the hydrothermal

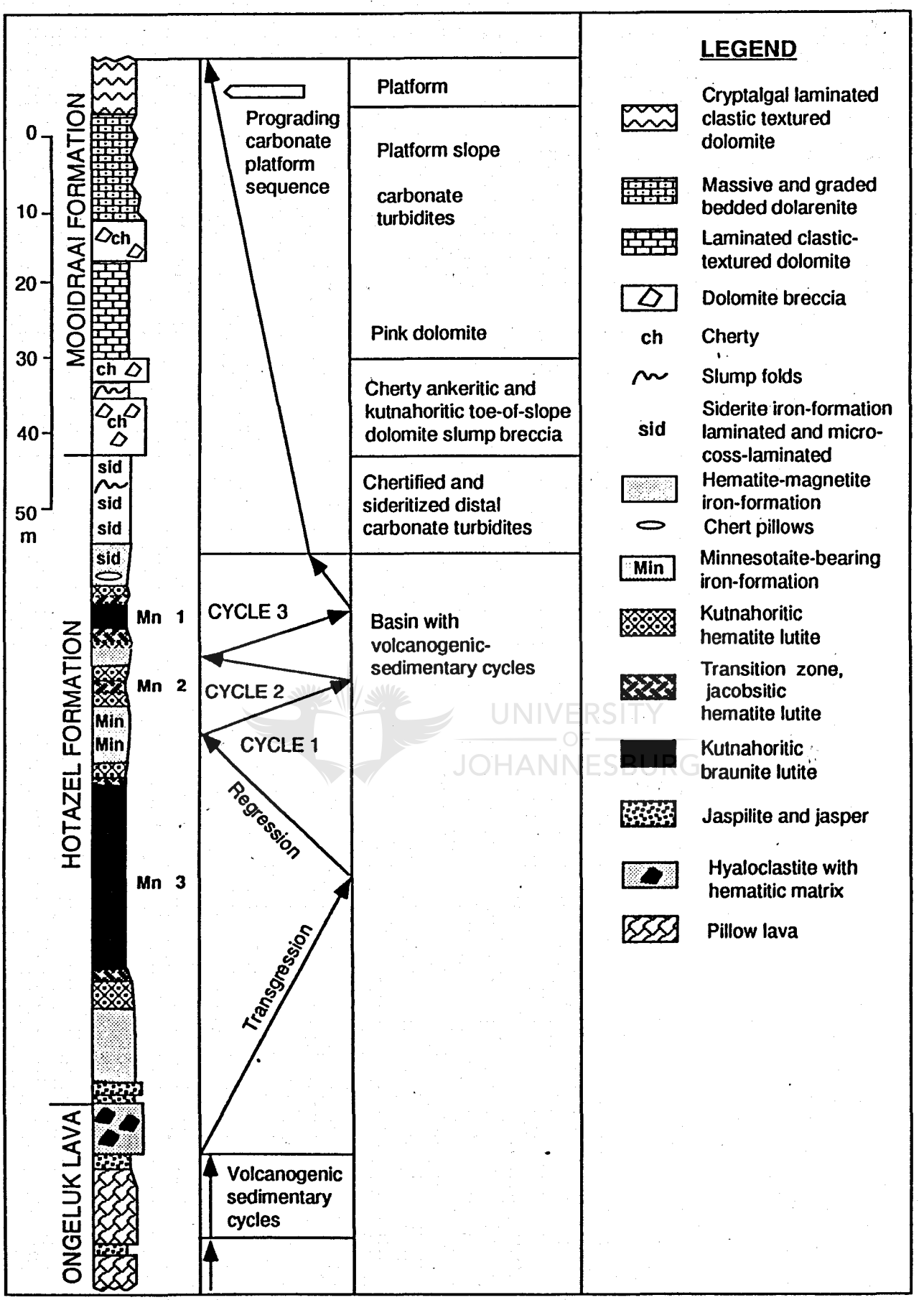

Figure 2.3. Stratigraphical profile of the Voëlwater Subgroup, indicating the three symmetrical cycles of sedimentation containing the sedimentary manganese ore beds in the Hotazel Formation (After Beukes et al., 1982).

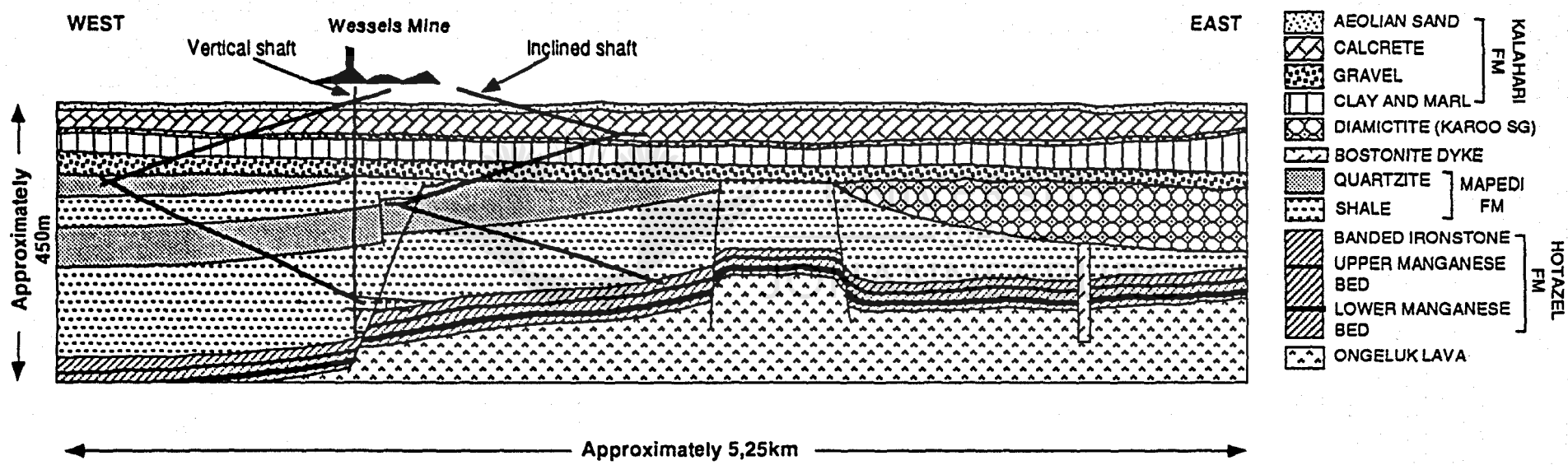

Figure 2.4. East-west section through Wessels Mine indicating major faults and dykes, the Dwyka glacial valley and stratigraphy of the mine. Redrawn after Samancor information brochure (Manganese ore, undated).

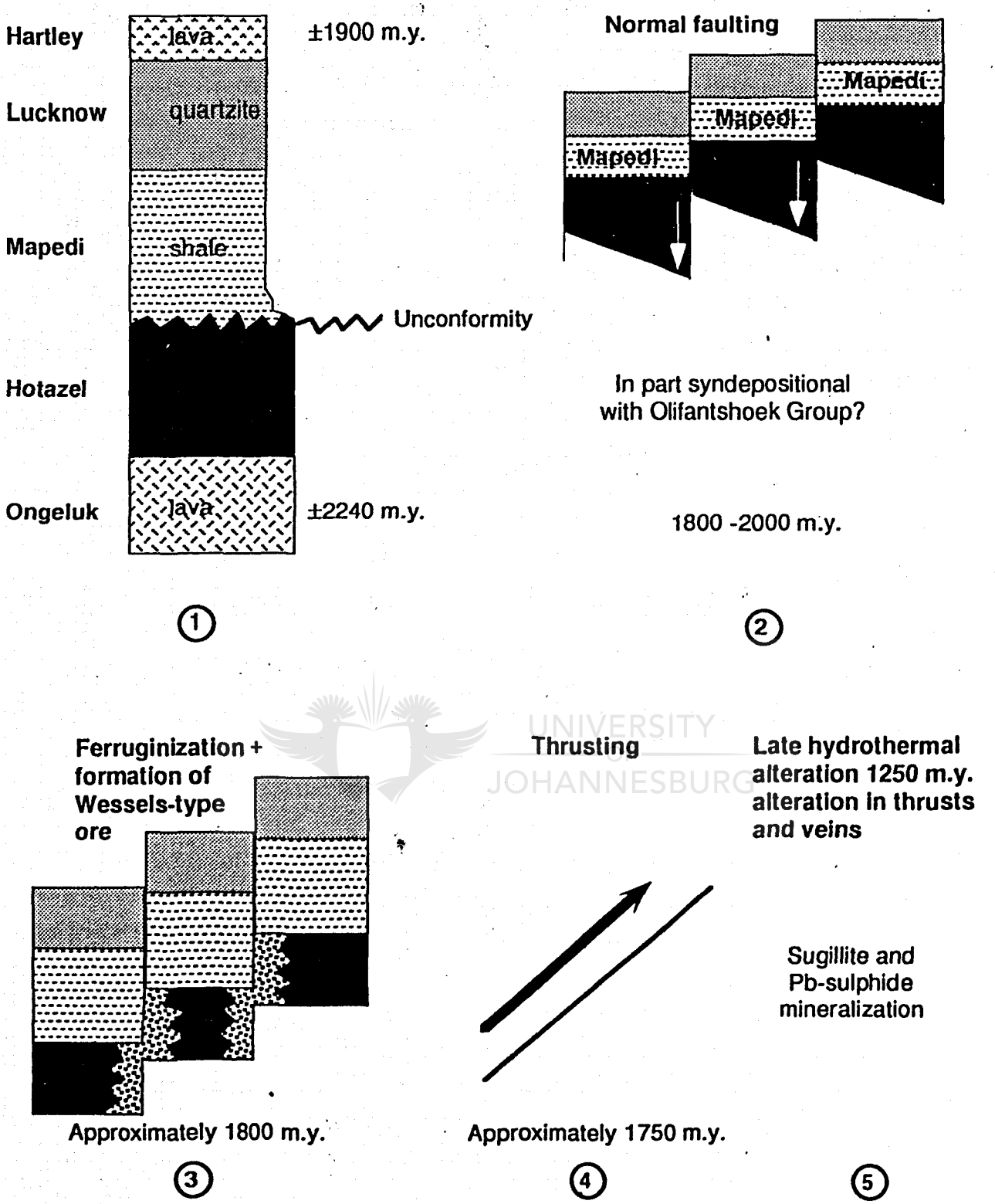

Figure 2.5. A summary of the timing of depositional, deformational and hydrothermal alteration events in the Kalahari manganese field.

event responsible for upgrading the ore. The formation of the sugillite-forming hydrothermal event was dated by Pb-Pb isotopes at 1270 ± 30 m.y. (Dixon, 1988). The bostonite dykes also display hydrothermal alteration, so this age seems to be correct relative to the age of bostonite dykes. As mentioned earlier, thrusting related to the Kheiss orogeny, took place some 1700 - 1800 m.y. ago. Normal faults in the Wessels mine area post-date the deposition of the Mapedi shale and pre-date thrusting, so that faulting must have taken place some 1800 - 2000 m.y. ago (Fig. 2.4). The age of the main phase of hydrothermal alteration is unknown. Dixon (1988) gives it an age of 1250 m.y. as the latest phase of alteration and Kleyenstüber (1985) recognizes hydrothermal mineral assemblages in thrust planes, also suggesting a younger age. However ferruginization and the main phase of hydrothermal alteration appear to be restricted to normal faults, which would suggest that it took place before thrusting some 1800 - 2000 m.y. ago; perhaps during, or shortly after formation of the normal faults (Fig. 2.5).

2.2 DETAILED GEOLOGICAL SETTING AND SAMPLING OF ORE

A map of Wessels mine on which normal faults, ferruginized zones and bostonite dykes are shown relative to mined out areas indicate that manganese ore is not mined adjacent to major normal faults (Fig. 2.6). The main reason for this is that the manganese ore beds are ferruginized along the faults and secondly that some loss of ground due to normal faulting is present (Fig. 2.7). Unmined areas of low-grade Mamatwan-type ore occur in the centre of fault blocks (Fig. 2.6). High-grade Wessels-type ore is developed inbetween the areas of unmined Mamatwan-type ore and the ferruginized zones along faults.

The Wessels-type manganese ore is coarse-grained, rather massive, black in colour and vuggy, often with a metallic lustre in high-grade areas close to the ferruginized zones. This contrasts with the dull very fine-grained and laminated nature of the primary sedimentary Mamatwan-type ore, preserved in the central part of fault blocks. Mamatwan-type ore has a spotted appearance due to the presence of tiny ovoidal carbonate concretions. Ferruginized zones along fault planes are also very fine grained with a bluish metallic lustre and irregular subhorizontal to vertical banding. Only the lowermost manganese ore bed of the Hotazel Formation is mined in the Wessels mine. The ore beds are slightly undulating to very gently folded. Dips range between 2 and 15 degrees in a westerly direction.

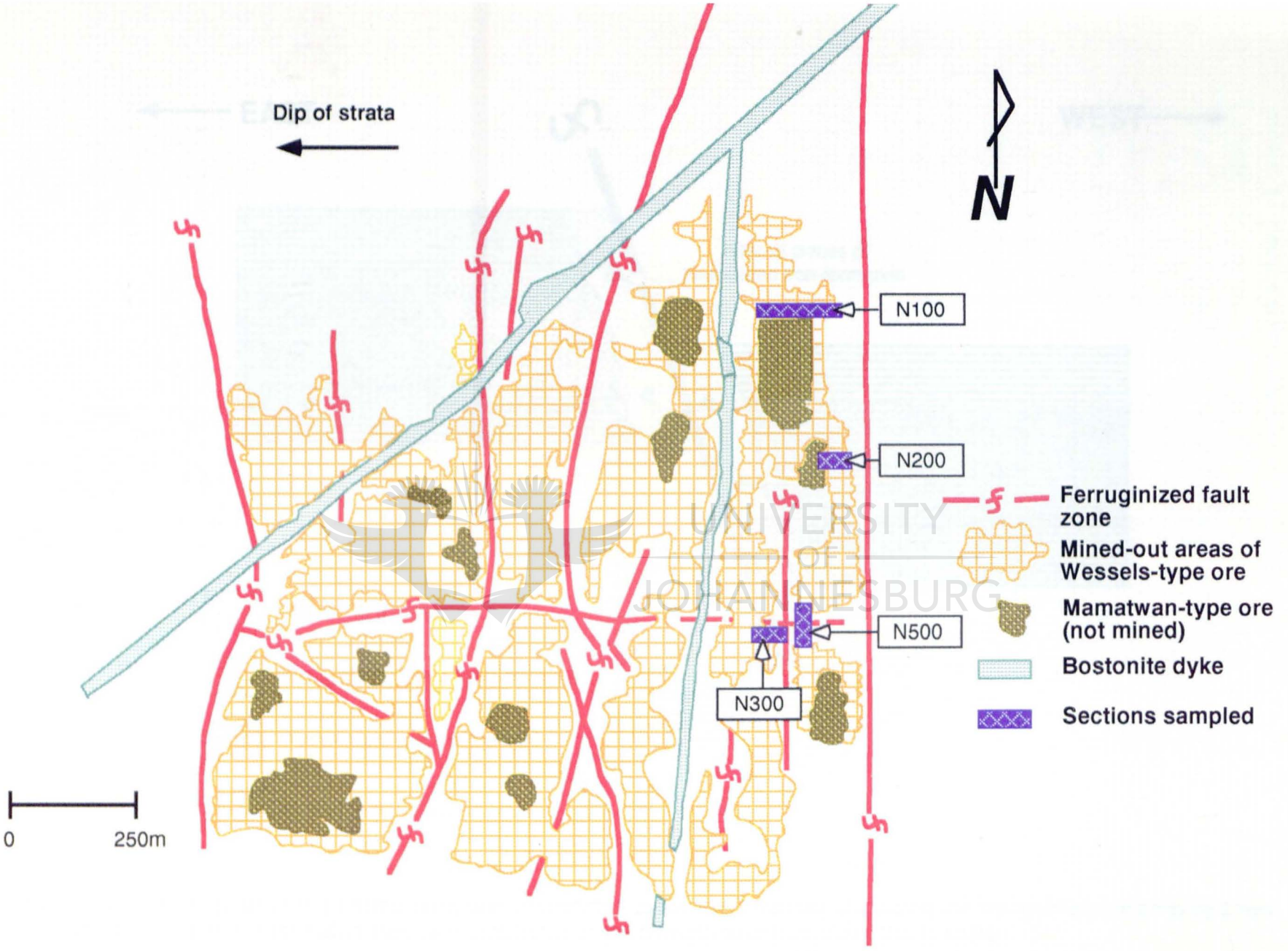

Figure 2.6. Simplified map of the Wessels Mine showing the normal fault pattern, areas of mined out high-grade Wessels-type ore and unmined areas composed of Mamatwan-type ore in the centre of fault blocks. Note unmined ferruginized zones along normal faults. Bostonite dykes intruded along normal faults and also crosscut some of the faults.

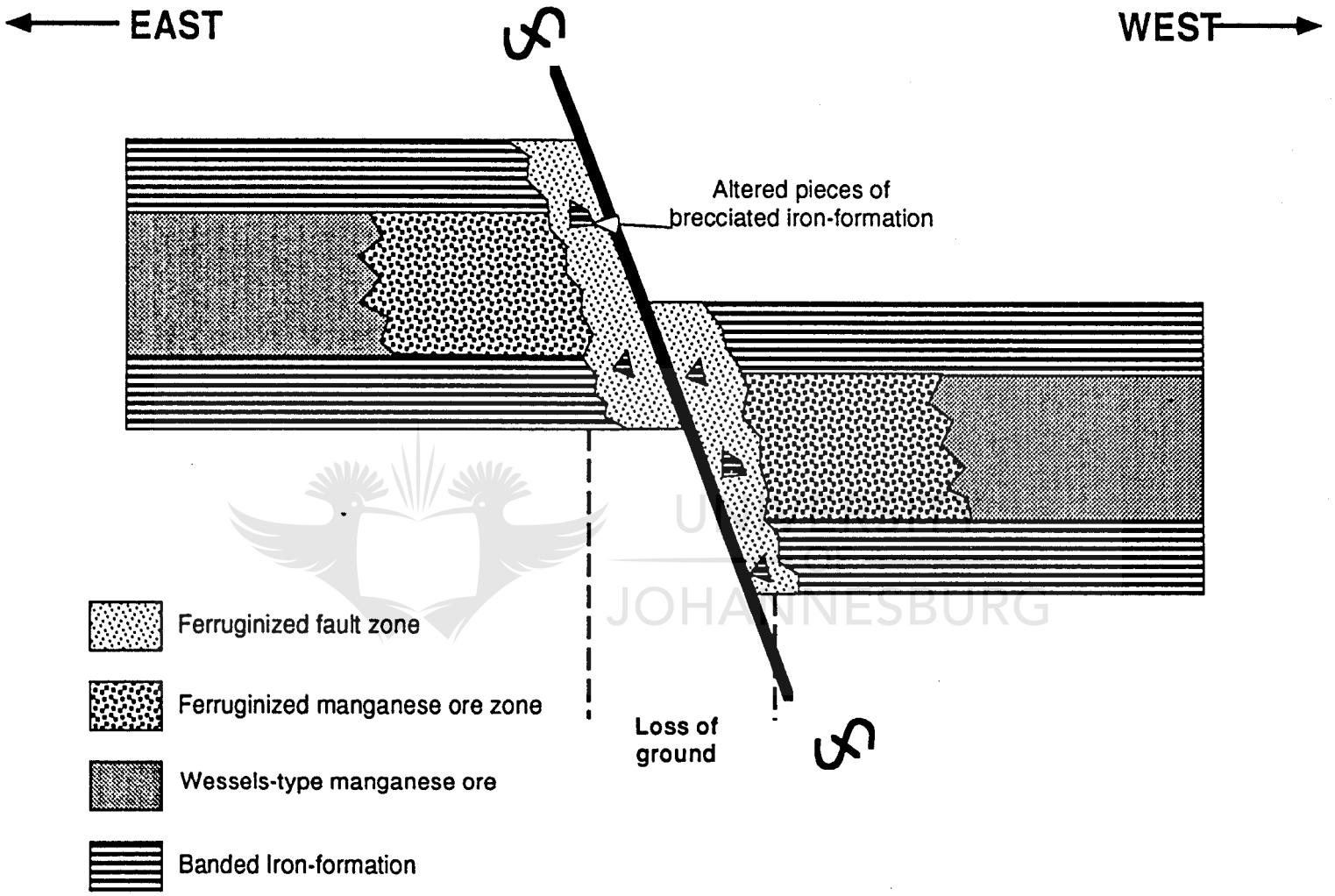

Figure 2.7. Schematic diagram of a normal fault, with downthrow to the west, typically displacing the manganese ore beds by a few metres. Altered clasts of iron-formation may be incorporated in the ferruginizsed fault zone. Not to scale.

Three grades of ore are mined at the Wessels Mine namely, Wessels high-grade (WH), Wessels low-grade (WL) and W4 ore. WH has a manganese-content of more than 50 weight percent and an iron-content of 8 - 10 weight percent. WL has a manganese-content of between 48 and 50 weight percent and an iron-content of 9 - 11 weight percent. It is the main ore product. W4 has a manganese-content of 40 - 48 weight percent and contains 12 - 18 weight percent iron. The ore is mined by the room and pillar technique down to a depth of about 450m below surface. The pillars have the advantage that they can be used for sampling in mined out areas; as was the case in the present study.

Only the lower manganese bed at Wessels Mine was sampled. Samples were taken along sections displaying lateral transitions from low grade Mamatwan-type ore into areas of high-grade Wessels-type ore, and whenever possible, into zones of ferruginization along faults. Three traverses were identified as suitable for sampling (Fig. 2.6) after studying grade maps of ore and after reconnaissance inspection. These traverses are illustrated in figures 2.8 to 2.14. In addition a traverse was sampled, for comparative purposes, through a ferruginized zone not connected with a north-south trending normal fault, but related to an east-west trending normal fault (Fig. 2.12).

Selected hand samples of sufficient size to enable petrographic and geochemical analysis, were taken. In order to eliminate possible effects of vertical zonation in ore beds, samples were taken at specific distance below the "grade line" in the ore beds. The "grade line" is a thin, red hematite lamina approximately 4mm thick, that occurs consistently in the middle of the lower manganese ore bed at Wessels Mine. Samples were taken about 1,1m below the grade line where possible. However, this distance varied between 1m and 1,2m because of the hardness of the ores and difficulty to get samples out from pillar faces. Along section N300, difficulties were experienced in finding the grade line because of the proximity to the fault and its ferruginized zone. In this specific area the lower banded iron-formation unit was used as a reference line during the sampling process.

2.3 DESCRIPTION OF TRAVERSES SAMPLED

2.3.1 SECTION N100

Section N100 is some 200m long and extends from low grade Mamatwan-type ore in the west, through high grade Wessels-type ore, into a ferruginized zone

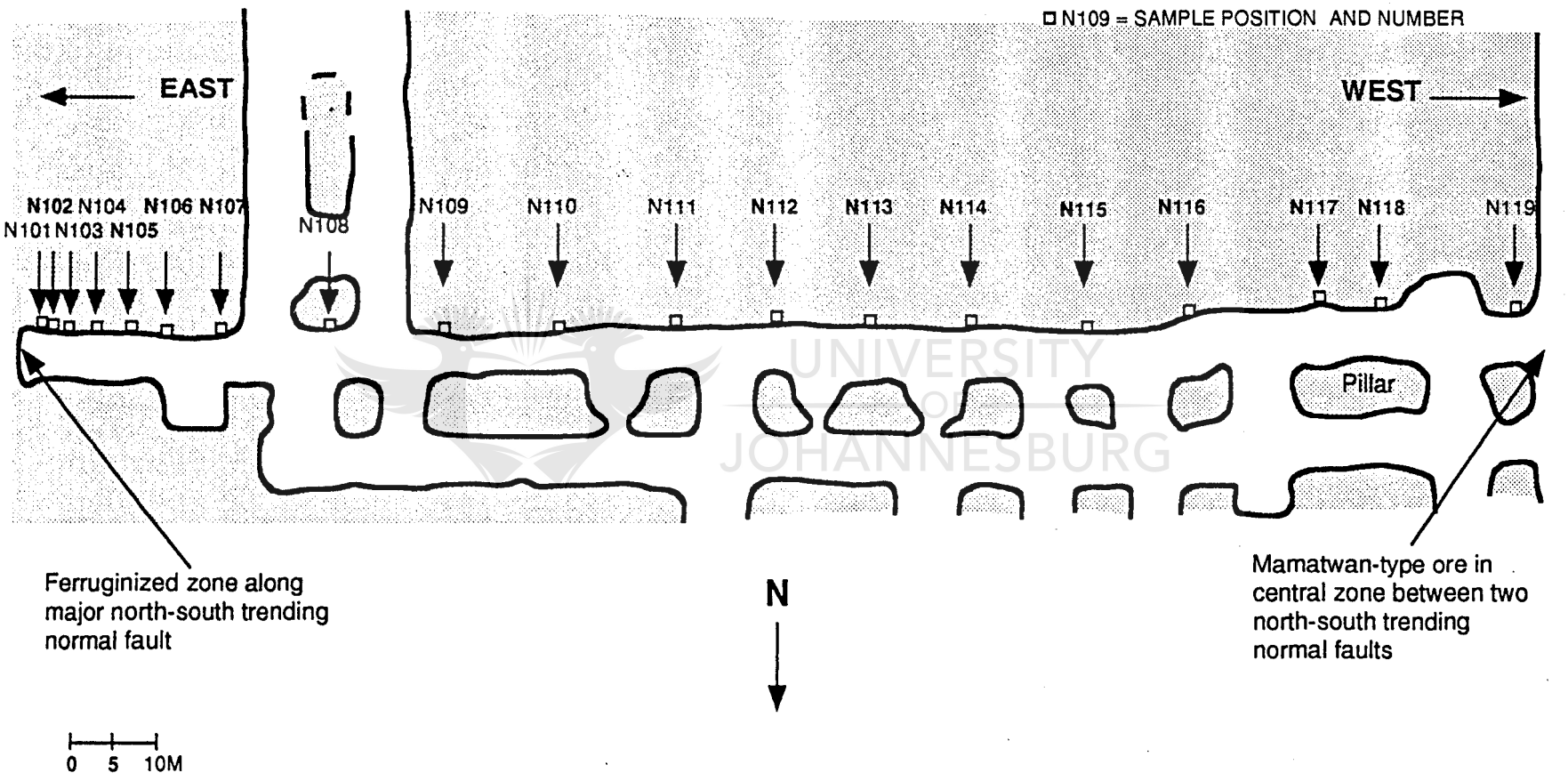

Figure 2.8. Plan view of section N100.

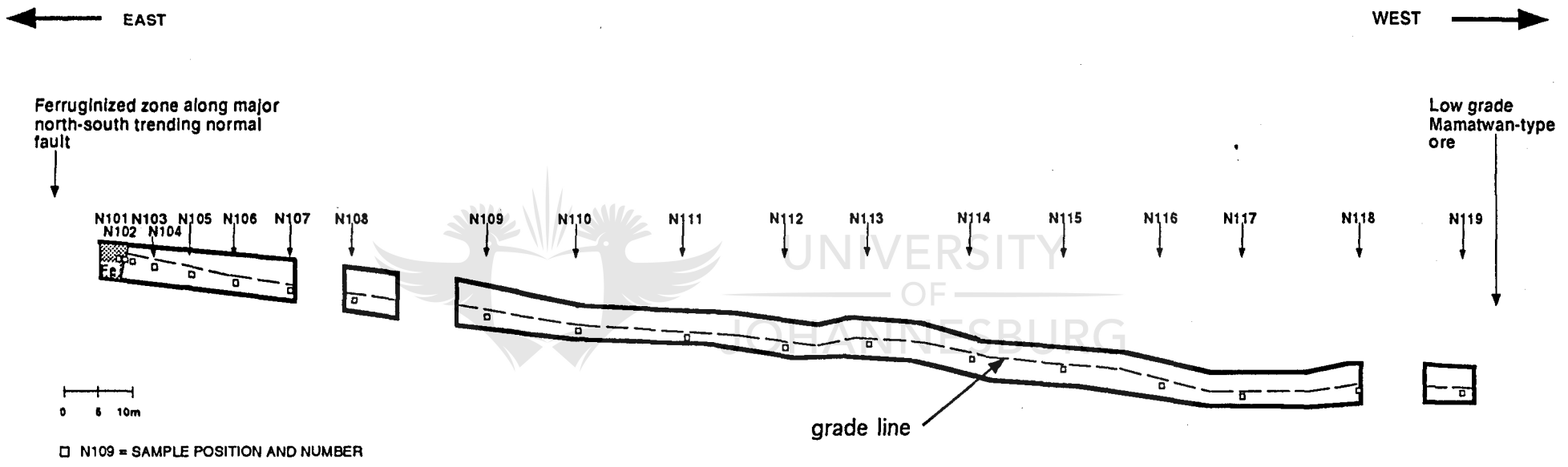

Figure 2.9. Section N100 with sample positions indicated by small rectangles relative to the grade line.

along a major north-south trending normal fault in the east (Fig. 2.8). Samples were taken along a south facing stope wall. Along the section slight undulations, with a wavelength of about 35m, are visible in the ore bed (Fig. 2.9). The regional dip is about 10° to the west. Samples N101 and N102, on the eastern end of the section, were taken in close proximity to each other, with sample N101 in the ferruginized ore and sample N102 on the border between ferruginized ore and high-grade ore. The other samples were evenly spaced, about 10 metres apart. Sample N119 was sampled in the Mamatwan-type ore, and the rest, samples N102 - N118, in the Wessels-type ore.

2.3.2 SECTION N200

Section N200 is a short section of some 40m long (Fig. 2.10). It represents a transition from a low-grade Mamatwan-type ore pocket, in the central part of a fault block in the west, through high-grade Wessels-type ore into a ferruginized zone along a major north-south trending normal fault in the east. Sample N201 comes from the border with the ferruginized ore, in close proximity to sample N202, which is situated in the high-grade Wessels-type ore bordering the ferruginized zone. Bedding, still visible in the samples, is distorted and folded in the ferruginized ore. The grade line is gently undulating with regional dip in the order of 10° to the west (Fig. 2.11).

2.3.3 SECTION N300

Section N300 (Fig. 2.12) is a section that extends from high-grade Wessels-type ore into a north-south trending normal fault. Downthrow of the fault is one of few cases where it occurs to the east. Regional dip is to the west at about 10°, but next to the fault the beds are dragged down to the east, towards sample N228, which was taken in a large vug in the fault plane itself. As mentioned earlier, it was difficult to find the grade line and not all the samples were taken relative to it (Fig. 2.13). Where the grade line became distorted, samples were taken about 2m above the banded iron-formation in the footwall of the manganese ore bed, and may have been sampled in places into the basal lutite zone.

2.3.4 SECTION N500

Section N500 (Fig. 2.12) extends from a zone of high grade ore, through a zone of ferruginization (indicated on mine maps). No displacement of the grade-line

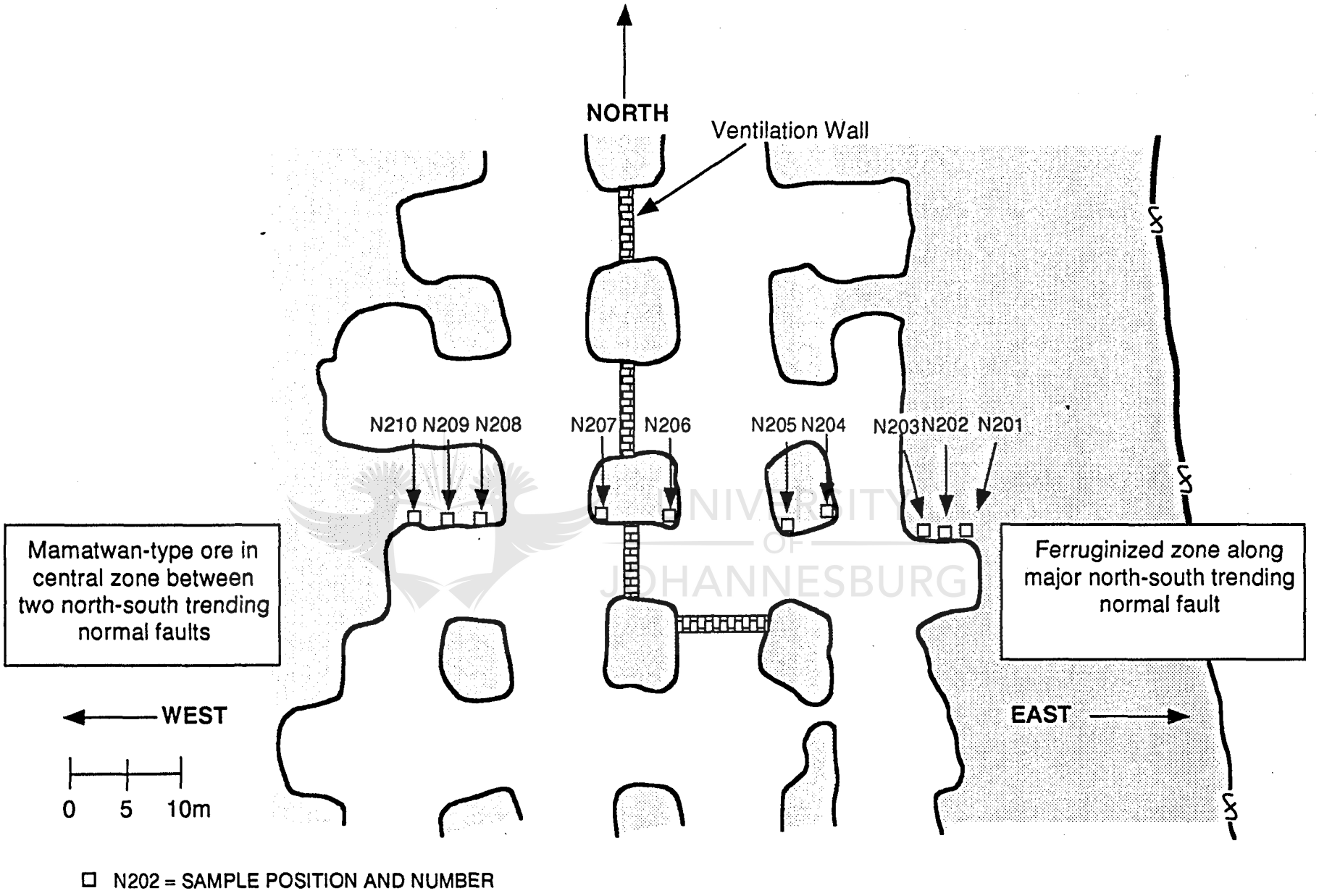

Figure 2.10. Plan view of section N200

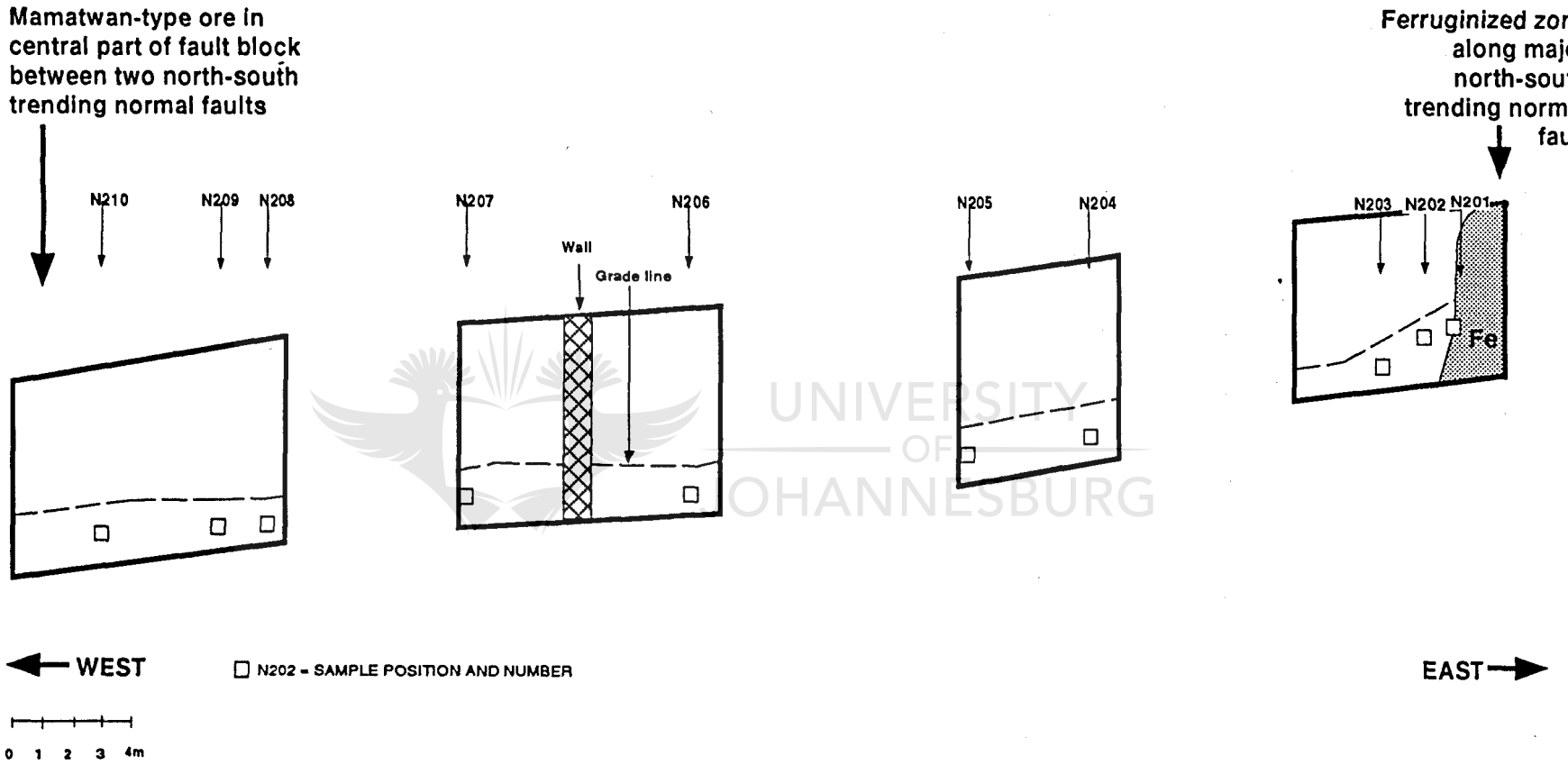

Figure 2.11. Section N200 with sample positions indicated by small rectangles relative to the grade line.

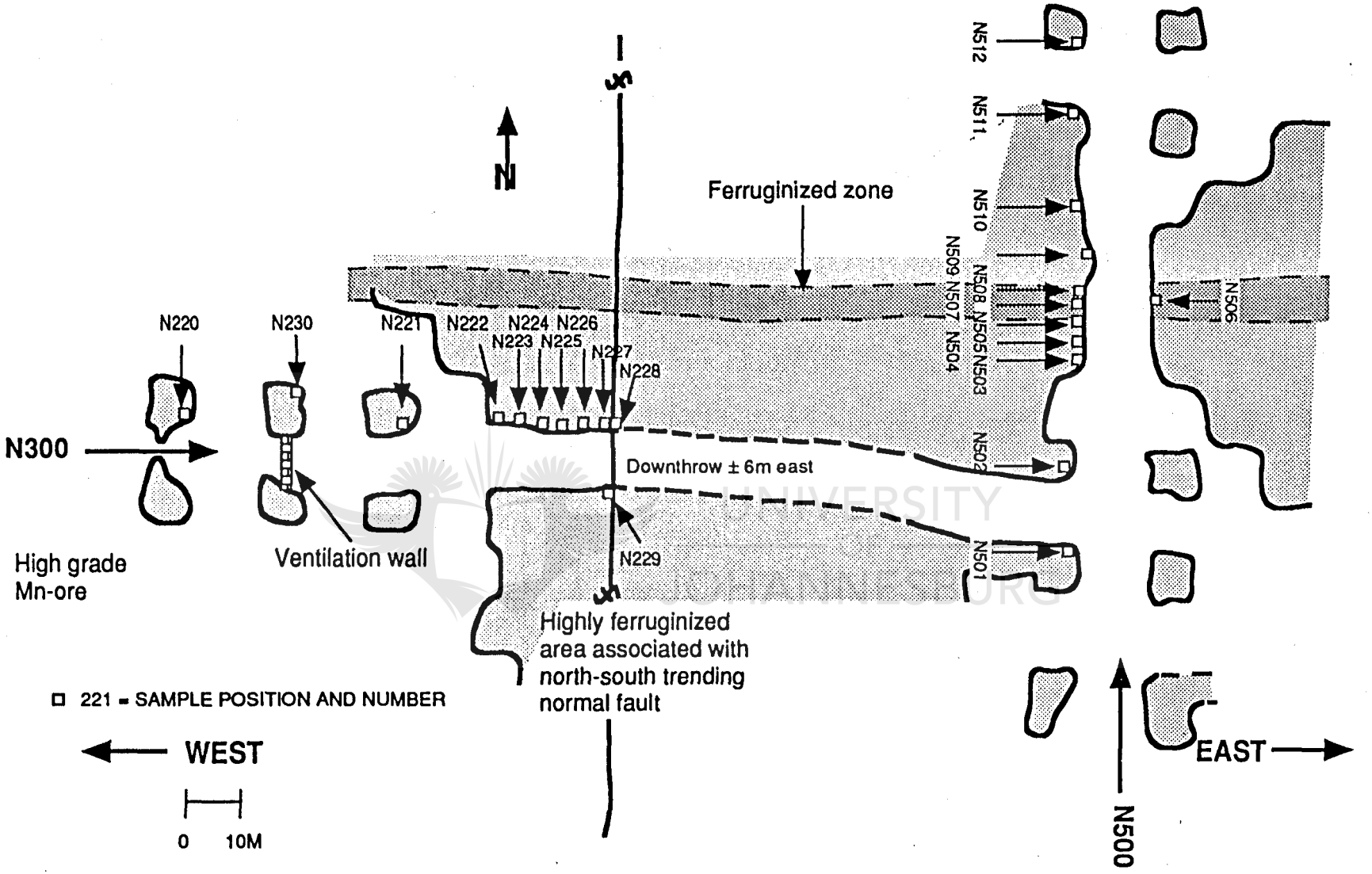

Figure 2.12. Plan view of sections N300 and N500. The "ferruginized" zone is also indicated.

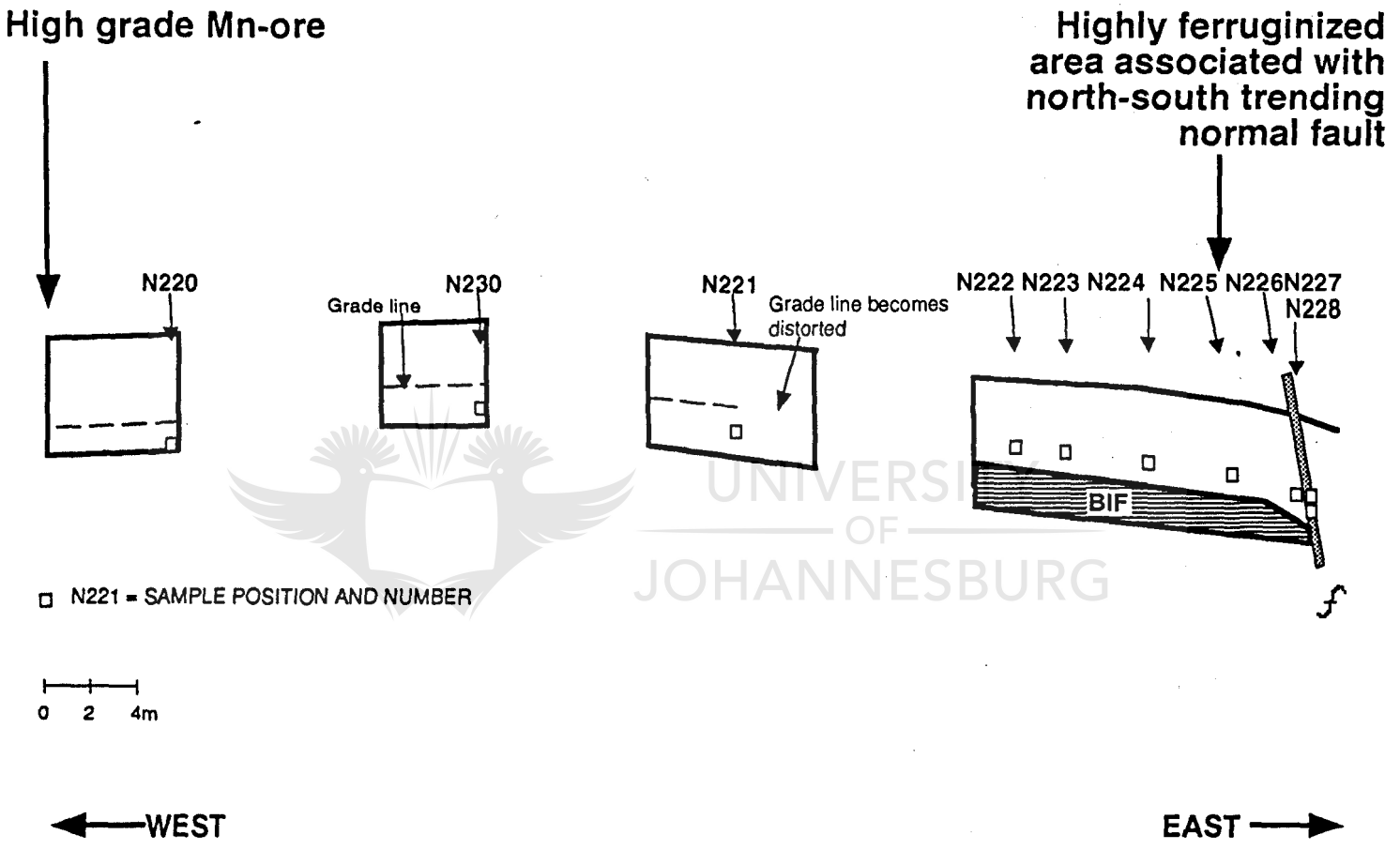

Figure 2.13. Section N300 with sample positions indicated by small rectangles relative to the grade line.

is shown on both sides of the zone of ferruginization (Fig. 2.14). The ferruginized zone in the middle of the section proved to be composed of mainly quartz and Mn-diopside. In hand sample, clasts of banded rock surrounded by metasomatized silica are visible, together with clasts of altered banded iron-formation. It is therefore speculated that this "ferruginized" zone is merely a small graben structure or zone of weakness caused by the influence of a nearby east-west trending normal fault and filled by breccia of overlying strata. Brecciation of roof rock may also have been caused by circulating hydrothermal fluids. Ferruginization is evident along the borders of the "ferruginized" zone and in the immediately adjacent high-grade Wessels-type ore. Sugilite is present in the ferruginized zone and was sampled along the eastern wall of the adit (sample N206, Fig. 2.12).

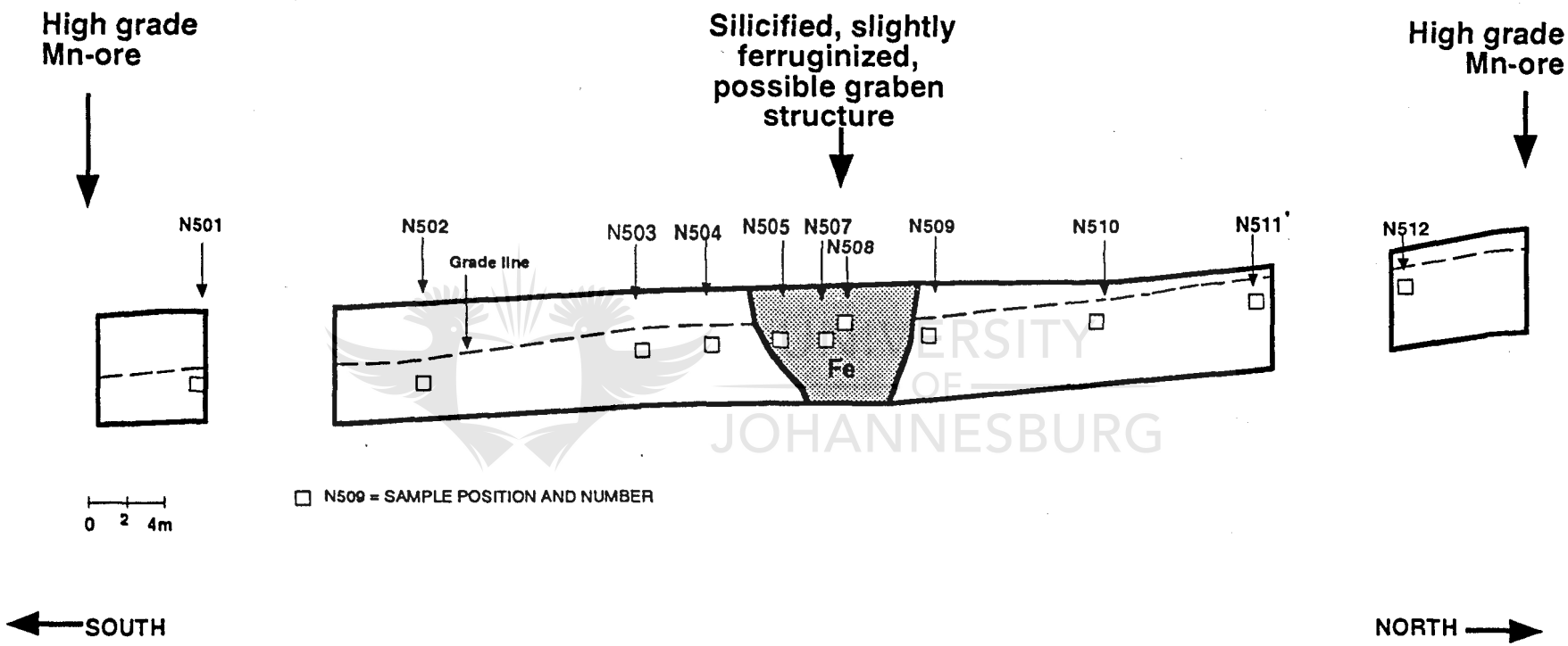

Figure 2.14 Section N500 with sample positions indicated by small rectangles relative to the grade line.

CHAPTER III MACROSCOPIC DESCRIPTION OF ORES

3.1 DEFINITION OF ORE TYPES

Hand specimens are described in terms of texture, because the ores are black in colour and it is difficult, almost impossible, to distinguish between the different ore minerals in hand specimen. In order to make the initial descriptions, use was made of some petrography and XRD analyses.

A study of the various sections indicated a rather simple grouping of ore types (Fig. 3.1 to 3.4). Zones of ferruginization are characterized by very fine grained, massive to irregularly banded hematite ore. A massive fine grained braunitic ore is also present, typically immediately adjacent to the ferruginized ore, which will be referred to as secondary braunite ore. Highest-grade ore, referred to as massive hausmannite-rich ore, is coarse grained and rather massive in texture Cleavage planes of minerals display a metallic lustre. Very little light-coloured inclusions of gangue minerals are present. This is in contrast to another high-grade type of ore, referred to as vuggy hausmannite-rich ore, which is coarse-grained and very porous, with abundant light-grey gangue minerals infilling vugs or pores. A fourth common type of ore is composed of medium- to fine grained ore minerals, with remnant sedimentary lamination and quite abundant calcite filled vugs. One of the main minerals is braunite II and the ore is referred to as braunite II-rich ore. It is typically developed in the transition zone between vuggy hausmannite-rich ore and residual low-grade Mamatwan-type ore. Mamatwan-type ore is laminated ore, fine-grained with abundant small carbonate ovoids. In summary it can thus be stated that there are basically six types of ore, namely hematite ore, secondary braunite-rich ore, massive hausmannite-rich ore, vuggy hausmannite-rich ore, braunite II-rich ore and Mamatwan-type ore.

3.2 LATERAL VARIATIONS ALONG SECTIONS

3.2.1 SECTION N100

Sampling was conducted from Mamatwan-type ore (Pl 3.1), composed of carbonate ovoids set in a finely laminated, very fine grained matrix of black braunite-rich sedimentary ore. In the direction of the ferruginized zone, medium grained braunite II-rich ore with residual lamina are present (Pl. 3.2). Obliteration of some lamina took place and small secondary vugs or pores are

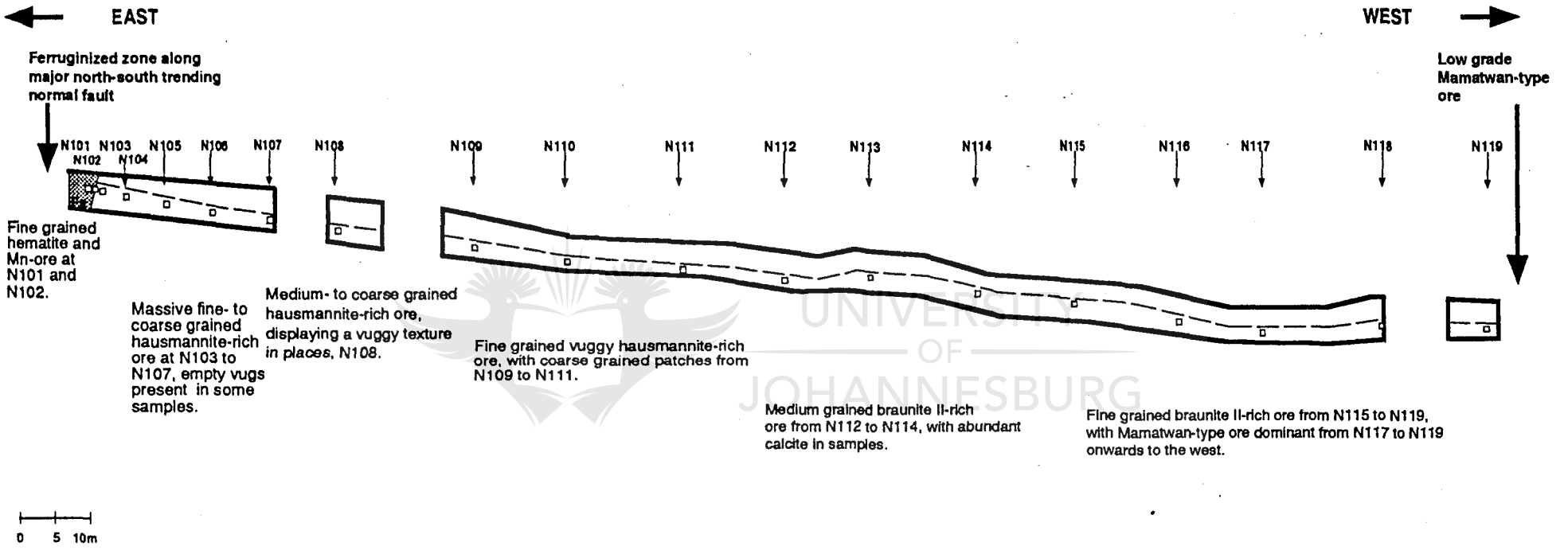

Figure 3.1. Section N100 with a macroscopic description of the textures found in the different ore types.

appearing in the ore. More proximal to the ferruginized zone even higher-grade ore is encountered, with almost no lamination preserved (Pl. 3.3) and with abundant white calcite filling small vugs. In some samples the calcite is absent (Pl. 3.4).

Closer to the ferruginized zone, coarse grained vuggy, hausmannite-rich ore is present with abundant gangue minerals like calcite in vugs (Pl. 3.5). Lamination is totally absent. This coarse grained ore grades over into massive coarse-grained, hausmannite-rich ore, with virtually no vugs, proximal to the ferruginized zone (Pl. 3.5). Cleavage planes in this high-grade hausmannite-rich ore display a metallic lustre. In a narrow zone between the ferruginized ore and the hausmannitic ore, a fine-grained massive, secondary braunite-rich ore is present. It replaces coarse grained hausmannite-rich ore (Pl. 3.7). No sedimentary structures are preserved. In the ferruginized fault zone hematite ore with a bluish-grey metallic colour is developed.

3.2.2 SECTION N200

The sampled section started in the transition zone between Wessels- and Mamatwan-type ores. In this transition zone, Mamatwan-type ore is present in which original kutnahorite ovoids have been replaced by hausmannite. In direction of the fault zone, ovoids quickly disappear and lamination is partly destroyed to form thicker lamination. This ore grades over into medium- to coarse grained, calcitic vuggy hausmannite-rich ore (Pl. 3.5), with no layering preserved. More proximal to the ferruginized zone high-grade massive coarse grained, hausmannitic ore with little secondary pores or visible gangue minerals, are present (Pl. 3.6). Metallic lustre is visible on the cleavage planes of rough samples. Secondary ore is developed immediately adjacent to the ferruginized zone. This ore is very fine-grained and display undulating banding. Undulating, metallic grey coloured residual bedding alternate with more bluish-grey hematite bands.

3.2.3 SECTION N300

Samples of section N300 taken in the west, furthest away from the ferruginized fault zone, are composed of medium- to coarse grained, massive hausmannite-rich ore. This ore grades, in direction of the fault zone, over into medium- to fine grained, massive secondary braunite-rich ore. In the ferruginized zone itself, the ore is bluish-red in colour with abundant crosscutting white calcite-filled

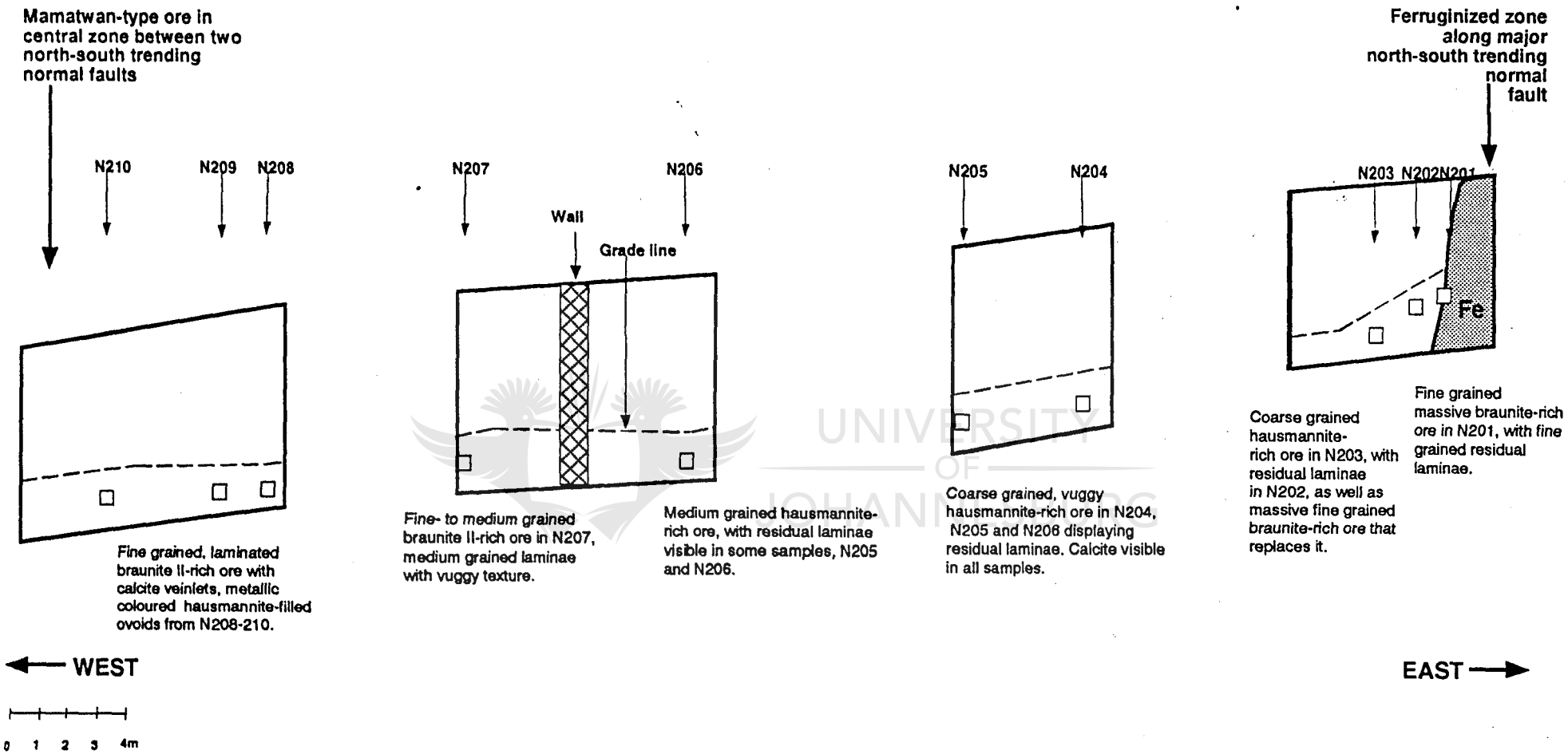

Figure 3.2. Section N200 with a macroscopic description of the textures encountered in the different ore types.

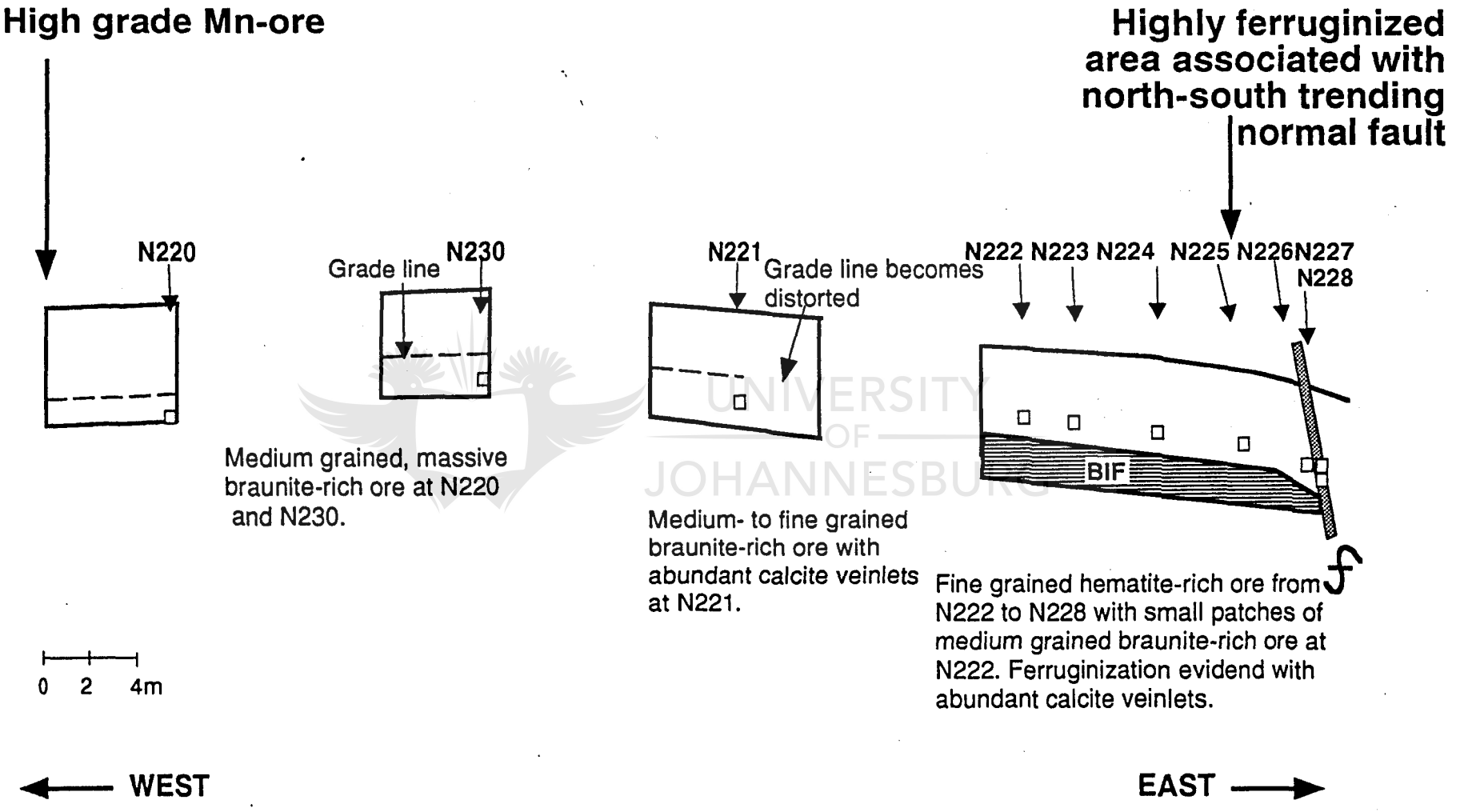

Figure 3.3. Section N300, with a macroscopic description of textures encountered in the different ore types.

Plate 3.1. Mamatwan-type ore, with white, calcite ovoids in some laminae and brownish kutnahoritic ovoids in others, set in a very fine-grained braunite matrix. Sample N119.

Plate 3.2. White calcitic ovoids visible along laminae which are obliterated by alteration in higher-grade vuggy braunite II-type ore at the bottom of the sample. Sample N116.

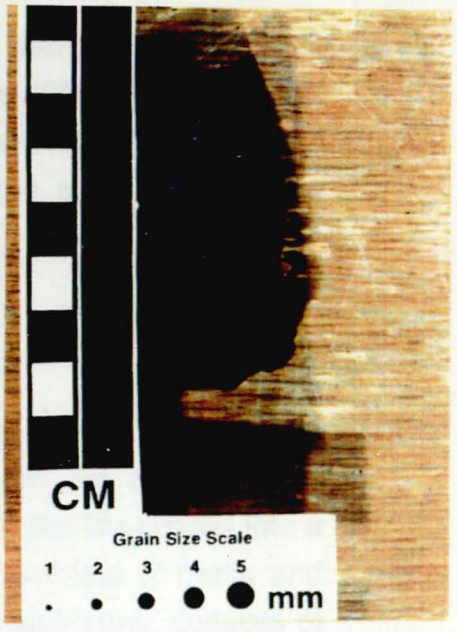

Plate 3.3. Fine grained braunite II-type ore with faintly preserved sedimentary lamination. Sample N115.

Plate 3.4. Fine grained hausmannite-rich ore with only a few small vugs. Dark finer grained phases are present in the ore, together with more medium-grained patches, giving it a replacement texture. Sample N107.

Plate 3.5. Coarse grained, vuggy hausmannite-rich ore with abundant, white calcite filling vugs in the ore. Sedimentary laminations are absent (blade marks may be mistaken for laminations). Note veinlet of calcite at top of sample. Sample N204.

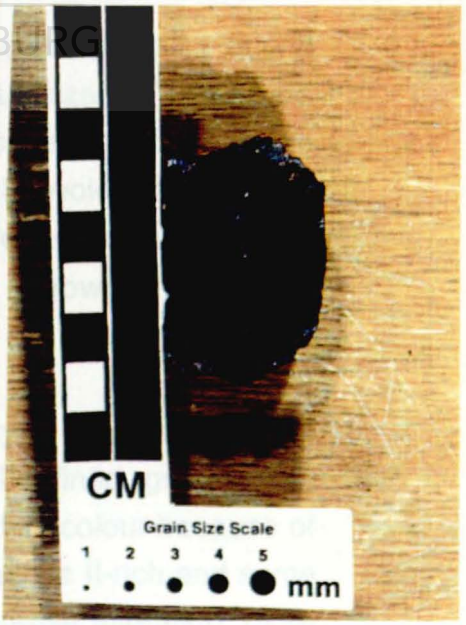

Plate 3.6. Coarse-grained, massive hausmannite-rich ore with virtually no gangue minerals present. Sample N204.

veinlets. Thick undulating banding is present in some samples. In the fault plane itself, banded hematite ore with botryoidal texture (Pl. 3.8), is present. Botryoidal hematite line large vugs in the ore. Gangue minerals such as calcite and barite and in some cases pyrite, are also present in some of the large secondary vugs.

3.2.4 SECTION N500

Ore types in section N500 are symmetrically distributed on both sides of the ferruginized fault zone. Coarse-grained hausmannite-rich ore is developed distal from the fault zone. In the direction of the fault zone, the ore grades into a medium-grained massive black manganite-rich ore with veinlets of barite and calcite in sample N503. Ore immediately adjacent to the fault zone, consists of fine-grained, massive, secondary braunite-rich ore. In the fault zone fine-grained yellow-brown banded silicified rocks are present (Pl. 3.9). Fragments of altered banded iron-formation are present surrounded by quartz. On the eastern side of the adit, in sample N506, a pocket of sugilite is developed surrounded by quartz.

3.3 INTEGRATED MODEL OF LATERAL VARIATIONS IN ORE TYPES

From the above observations a general model could be constructed for lateral zonation in manganese ores relative to zones of ferruginization (Fig. 3.5). Primary Mamatwan-type ore, preserved in the centre of fault blocks, is fine crystalline and laminated with abundant small brownish ovoidal kutnahorite concretions. Thin calcite-filled veinlets may crosscut the ore. The veinlets may also be filled with hausmannite (Pl. 3.1). The ore display a brown to lightbrown streak.

In the transition zone between Wessels and Mamatwan-type ores, ore become medium-grained and sedimentary lamination is less well defined, grading into thicker residual layering (Pl. 3.2). Ovoids change into a white colour because of transition to calcite. The ore changes from braunite to braunite II-rich and some of the ovoids are replaced by hausmannite. With more intense alteration, more proximal to the ferruginized zone, the calcite ovoids start disappearing (Pl. 3.3) and they are replaced by Mn-oxide minerals. Residual layering also disappear (Pl. 3.4) and ores tend to become massive. Ores also are more black in colour in this typical braunite II-rich ore type.

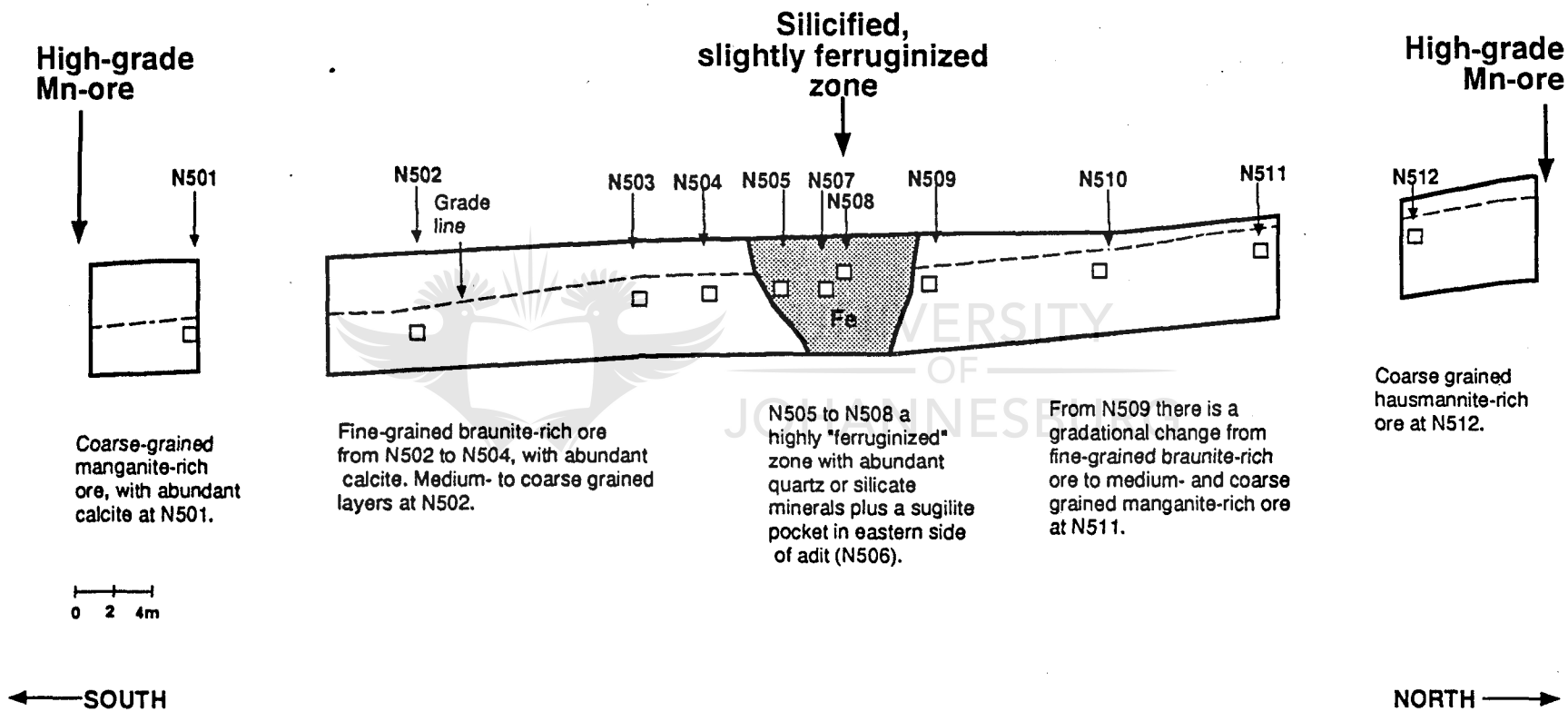

Figure 3.4. Section N500 with a macroscopic description of textures encountered in the different ore types.

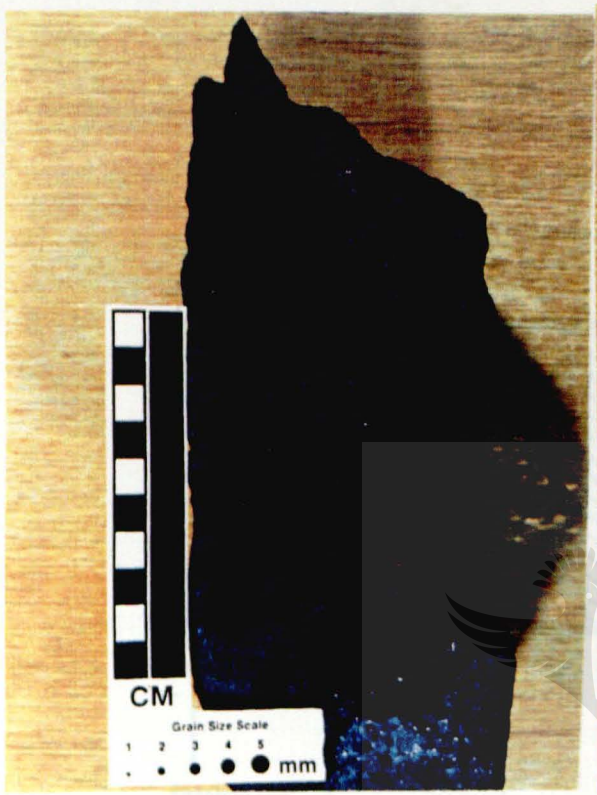

Plate 3.7. Coarse grained hausmannite-rich ore with metallic luster on cleavage planes of hausmannite. Massive fine-grained braunite-rich ore replacing hausmannite-rich ore is present in the top part of the sample. No lamination is preserved. Sample N102.

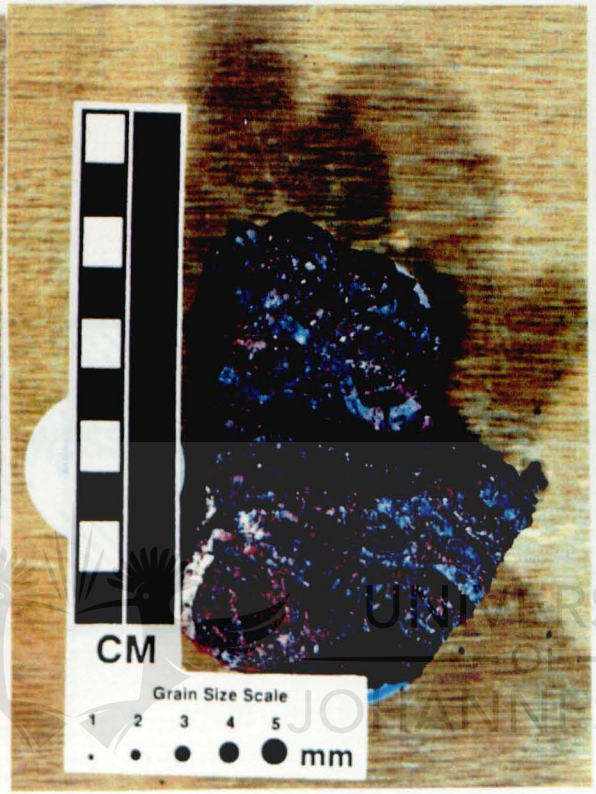

Plate 3.8. Banded hematite-rich ore with botryoidal texture from fault plane. Sample N229.

Plate 3.9. Altered iron-formation clast in fault zone (top), together with a block of silicified ore (bottom). Sample N505.

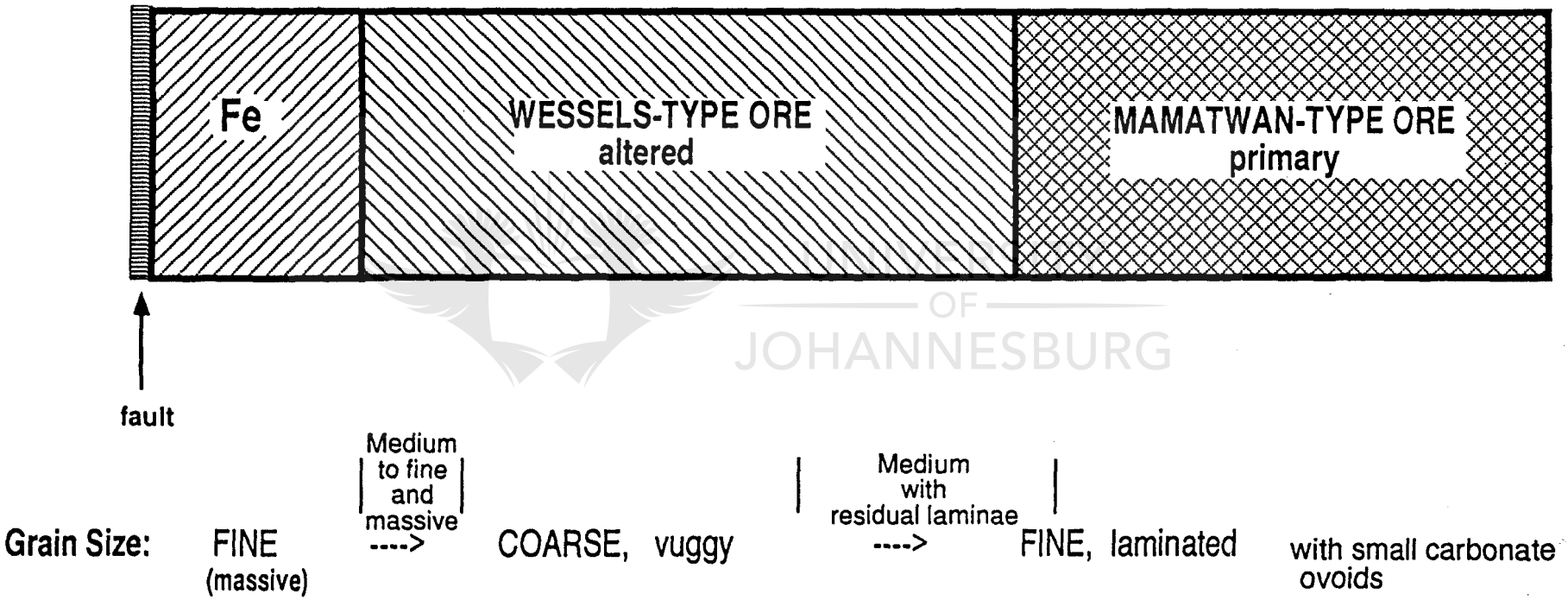

Figure 3.5. Model illustrating the general character of Wessels-type ore, relative to primary Mamatwan-type ore on one side, in central areas of fault blocks and ferruginized fault zones on the other.

Closer to the zone of ferruginization, vuggy coarse-grained rather massive hausmannite-rich ores predominate. The vugs probably represent signs of leaching of certain components of the ore during alteration (Pl. 3.5). In some cases the vugs are filled with light-coloured secondary minerals such as clinochlore, calcite and gaudefroyite. In direction of the fault zone this ore is dense, massive hausmannite-rich with metallic lustre and very little gangue minerals present. This represents the highest grade Wessels-type manganese ore. This ore then becomes replaced by fine grained massive braunite-rich ore.

Ferruginized zones are composed of dense banded metallic hematite-rich ores or by silicified ores with clasts of iron-formation cemented by quartz and/or calcite. Abundant calcite-filled veinlets are present (Fig. 3.5).

It must be noted however, that although the alteration in texture and ore types is described as gradual, it is only used to describe the main trend present, when moving from one ore type into another. Sudden transitions from one ore type to another may occur locally, with sharp contacts between different ore types in places, even crosscutting of different ore types over bedding. The overall pattern of upgrading and downgrading of Mn-ores are however gradational in its overall mineralogical extent.

CHAPTER IV LATERAL MINERALOGICAL VARIATIONS

4.1 QUALITATIVE X-RAY DIFFRACTION ANALYSES

All samples taken in the four sections were analyzed by X-ray diffraction (XRD), to identify the main minerals. This information defined mineral zonation patterns along the various sections. It also was of great help for identification of minerals during follow-up petrographic studies. Analyses were undertaken with a Siemens D-500 diffractometer, using Cu K-α radiation, a step size of 0,4° 2θ and counting time of 0,5 seconds/step. Samples were scanned from 4° to 80° 2θ. Due to overlap of reflection peaks, some minor minerals present could not be recognized with the XRD analyses. Minerals encountered are summarized in Table 4.1.

Table 4.1 Minerals encountered in manganese ores during XRD analyses. Also given are the ideal chemical formulae of the various minerals.

HAUSMANNITE	Mn_3O_4	**Mn-OXIDES**
BIXBYITE	$(Mn,Fe)_2O_3$	
MAROKITE	$CaMn_2O_4$	
BRAUNITE II	$Ca_{0,5}(Mn,Fe)_7Si_{0,5}O_{12}$	
BRAUNITE	Mn_7SiO_{12}	
MANGANITE	$MnO(OH)$	
FEITKNECHTITE	ß-$MnO(OH)$	
HEMATITE	Fe_2O_3	
JACOBSITE	$MnFe_2O_4$	
CRYPTOMELANE	KMn_8O_{16}	
CALCITE	$CaCO_3$	**CARBONATE**
GAUDEFROYITE	$Ca_4Mn_3(BO_3)_3(CO_3)(O,OH)_3$	**Boron containing carbonate**
BARITE	$BaSO_4$	**SULPHATE**
AEGERINE	$Na(Fe,Mn)Si_2O_6$	**SILICATES**
ANDRADITE	$Ca_3Fe_2(SiO_4)_3$	
CLINOCHLORE	$(Mg,Fe)_5AlSi_3O_{10}(OH)_8$	
QUARTZ	SiO_2	
DIOPSIDE (Mn)	$(Ca,Mn)(Mg,Fe,Mn)Si_2O_6$	
INESITE	$Ca_2Mn_7Si_{10}O_{28}(OH)_2.5H_2O$	
SUGILITE	$(K,Na)(Na,Fe^{3+})_2(Li_2Fe^{3+})Si_{12}O_{30}$	
BRUCITE	$Mg(OH)_2$	**HYDROXIDES**

4.2 MINERALOGICAL VARIATION ALONG SECTION N100

XRD results on samples from section N100 indicate that Mamatwan-type ore on the western side of the section (sample N119) is composed of braunite with minor braunite II and trace amounts of hausmannite and calcite (Fig. 4.1). The trace amount of hausmannite and calcite present most probably come from the carbonate ovoids. It is known that kutnahorite transforms to hausmannite and calcite during alteration (Kleyenstüber, 1985). Sample N118 and N117 are similar in composition to sample N119, i.e. Mamatwan-type ore, but lack calcite. Trace amounts of gangue minerals, such as barite, andradite and clinochlore start appearing in sample N118 and N117. In the transition zone to Wessels-type ore braunite disappears (sample N116) and abundant braunite II and hausmannite are present.

High-grade ore, with hausmannite as the major phase and minor braunite II, occurs from sample N115 through to sample N112. More proximal to the fault zone, bixbyite appears in sample N111 and becomes a main mineral phase in proximity to the fault zone in samples N106 - N107. Immediately adjacent to the ferruginized fault zone braunite again predominates and is especially abundant in sample N102. Hausmannite is now only present in trace amounts. Hematite is the dominant mineral in the ferruginized fault zone. Calcite is also conspicuous in the fault zone and immediately next to it. Gangue minerals such as barite, brucite, andradite, clinochlore and gaudefroyite occur sporadically as trace amounts in the Wessels-type ore. However, gaudefroyite appears more persistently close to the ferruginized fault zone. These gangue minerals are absent in the fault zone itself. Cryptomelane occurs in trace amounts in samples N110 and N111.

4.3 MINERALOGICAL VARIATION ALONG SECTION N200

In the western part of the section, on the border with Mamatwan-type ore (sample N210), braunite is the major phase, with minor hausmannite and trace amounts of calcite and clinochlore (Fig. 4.2). Moving away from the Mamatwan-type ore, in the transition zone to Wessels-type ore (samples N209 and N208), braunite II starts to appear as main phase, with minor hausmannite and braunite and trace amounts of clinochlore and barite (Fig. 4.2).

Braunite disappears in Wessels-type ore proper (samples N207 - N203), leaving hausmannite as major phase (samples N207 to N203) and braunite II

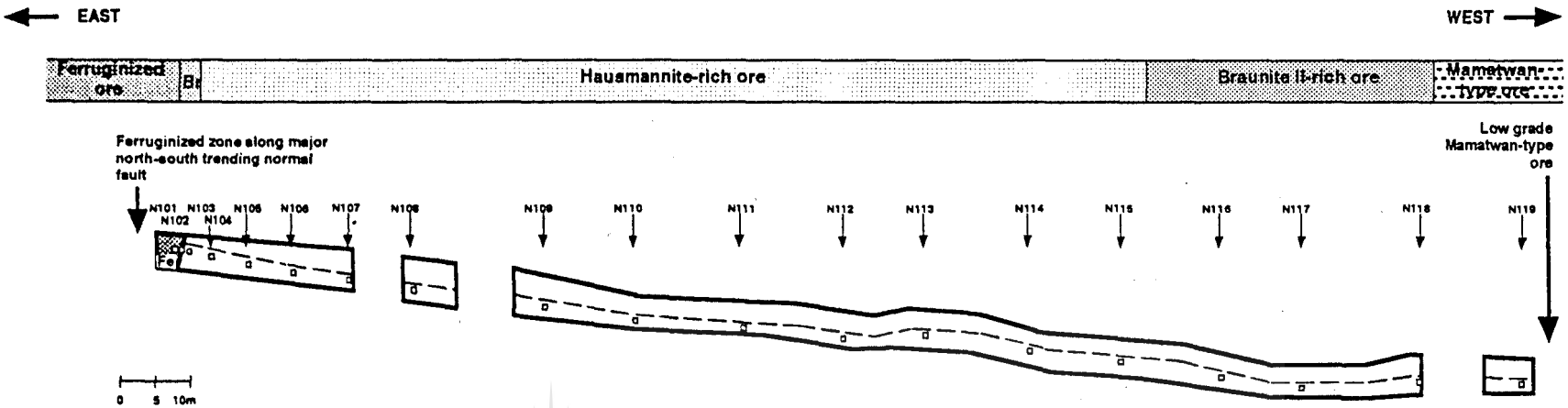

	N101	N102	N103	N104	N105	N106	N107	N108	N109	N110	N111	N112	N113	N114	N115	N116	N117	N118	N119
HAUSMANNITE		x	xxx	xxx	xxx	xxx	xxx	xx	xxx	xxx	xxx	xxx	xxx	xxx	xxx	xx	x	x	x
BIXBYITE			x			xxx	xxx	xx	x		x								
BRAUNITE II	x	xxx	x	x	x	xx	xx	x	xx		x	xx	xxx	xx	xx	xxx	xx	x	xx
BRAUNITE	x	xx	x							x							xxx	xxx	xxx
MANGANITE								xxx	x	x									
HEMATITE	xxx	x	x	x				x	x					x		x			
CALCITE	xx	xxx				xx		x	x	x					x	x			x
BARITE					x	x		x		x			x		x	x		x	
BRUCITE					x							x	x						
ANDRADITE								x					x				x		
CLINOCHLORE			x	x				x	x	x	x	x	x	x	x	x	x		
NATROLITE														x	x				
CRYPTOMELANE										x	x								
GAUDEFROYITE			x		x	x	x		x		x				x				

Figure 4.1. XRD results on samples from section N100. Main mineral phases are indicated by three x's, minor phases by two x's and trace amounts by one x.

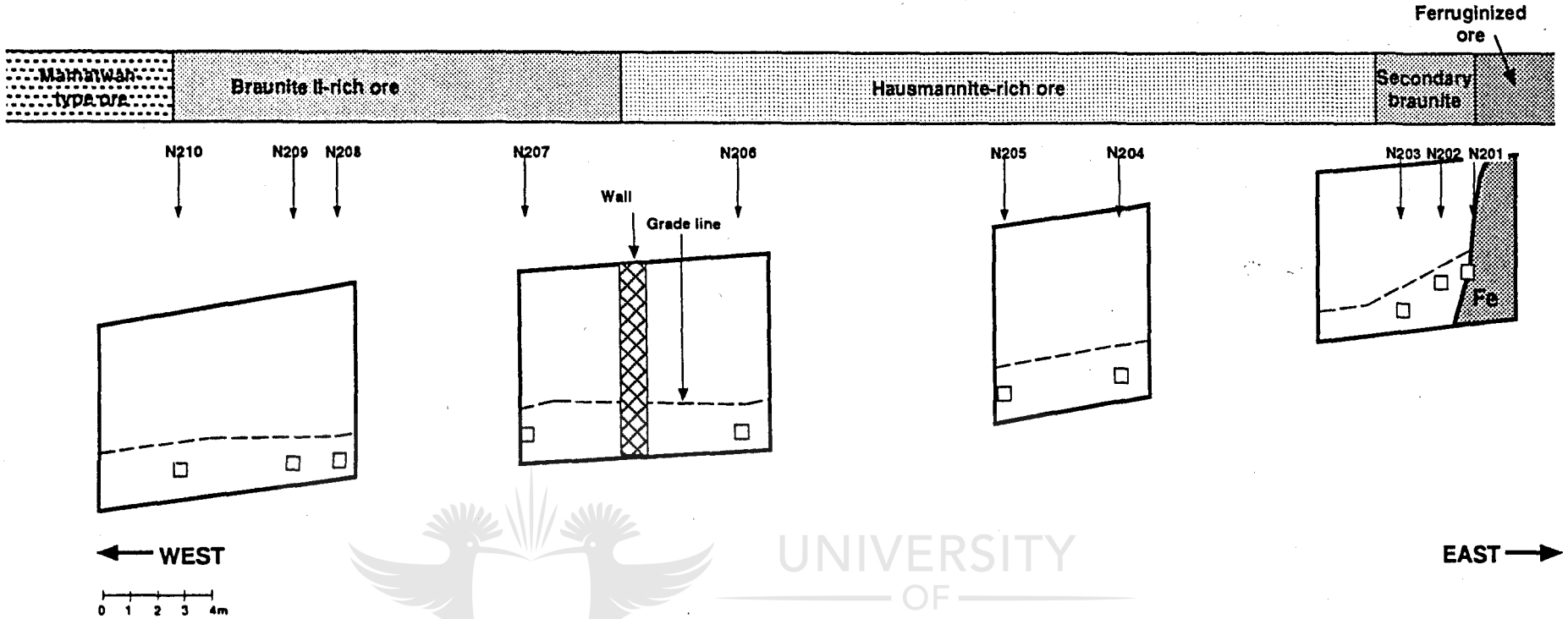

	N210	N209	N208	N207	N206	N205	N204	N203	N202	N201
HAUSMANNITE	xx	xx	xx	xxx	xxx	xxx	xxx	xxx	xx	
JACOBSITE									x	
BRAUNITE II		xxx	xxx	xx	xx	x		x	xxx	
BRAUNITE	xxx	xx	xx						xx	xxx
BIXBYITE			x		x	xx	x	x	x	x
MANGANITE										
HEMATITE			x	x	x	x	x		xx	xx
CALCITE	x	x				x	x	x	xx	xxx
BARITE	x		x				x	x	x	
BRUCITE				x	x		x			
ANDRADITE								x		xx
CLINOCHLORE	x	x	x		x	x	x	x	x	
NATROLITE			x							
CRYPTOMELANE	x									
FEITKNECHTITE			x		x					

Figure 4.2 XRD results of mineral abundances in samples along section N200. Main mineral phases are indicated by three x's, minor phases by two x's and trace mineral phases by one x.

as minor phase (samples N207 and N206). Trace amounts of calcite, clinochlore, brucite, barite, natrolite and andradite are present.

Very close to the ferruginized fault zone (sample N202) braunite II is the main phase with minor hausmannite, braunite, hematite, jacobsite and calcite (Fig. 4.2). Immediately adjacent to the ferruginized fault zone (sample N201), hausmannite and braunite II are absent, and braunite and calcite are major phases with hematite and andradite as minor phases (Fig. 4.2).

4.4 MINERALOGICAL VARIATION ALONG SECTION N300

Along the western side of section N300 (samples N220 and N230) braunite II is the major phase with trace amounts of hausmannite, manganite and calcite. In direction of the fault zone, the next sample (N221) contains braunite as major phase with braunite II as minor phase and hausmannite in trace amounts. In samples N222 - N228, in the direction of the fault, hematite is the major phase with no manganese ore minerals present, except in sample N223 which contains minor to trace amounts of hausmannite, braunite II and braunite. However, it is in the area of these samples that the grade line in the ore bed could not be recognized and it is quite possible that some samples were taken close to the bottom hematite lutite zone of the manganese ore bed (refer to Fig. 2.3 for position of hematite lutite). Trace amounts of calcite and sometimes clinochlore, are present in the hematite-rich ore.

4.5 MINERALOGICAL VARIATION ALONG SECTION N500

Section N500 displays symmetrical variation of manganese mineral assemblages on both sides of the ferruginized fault zone (Fig. 4.4). Most distal to the fault zone, manganite is the major mineral in high-grade ore with subordinate hausmannite and braunite II. On the south side of the fault zone bixbyite is associated with the manganite.

In the direction of the ferruginized zone, braunite II becomes the major manganese mineral with minor manganite. Trace amounts of brucite and calcite represent the gangue minerals. In the fault zone itself only minor braunite is present with Mn-diopside the major mineral in association with aegerine, hematite and calcite. Quartz is also a major constituent of the mineral assemblage in the centre of the fault zone. Cryptomelane is developed immediately adjacent to the fault zone, in the ore rich in braunite II.

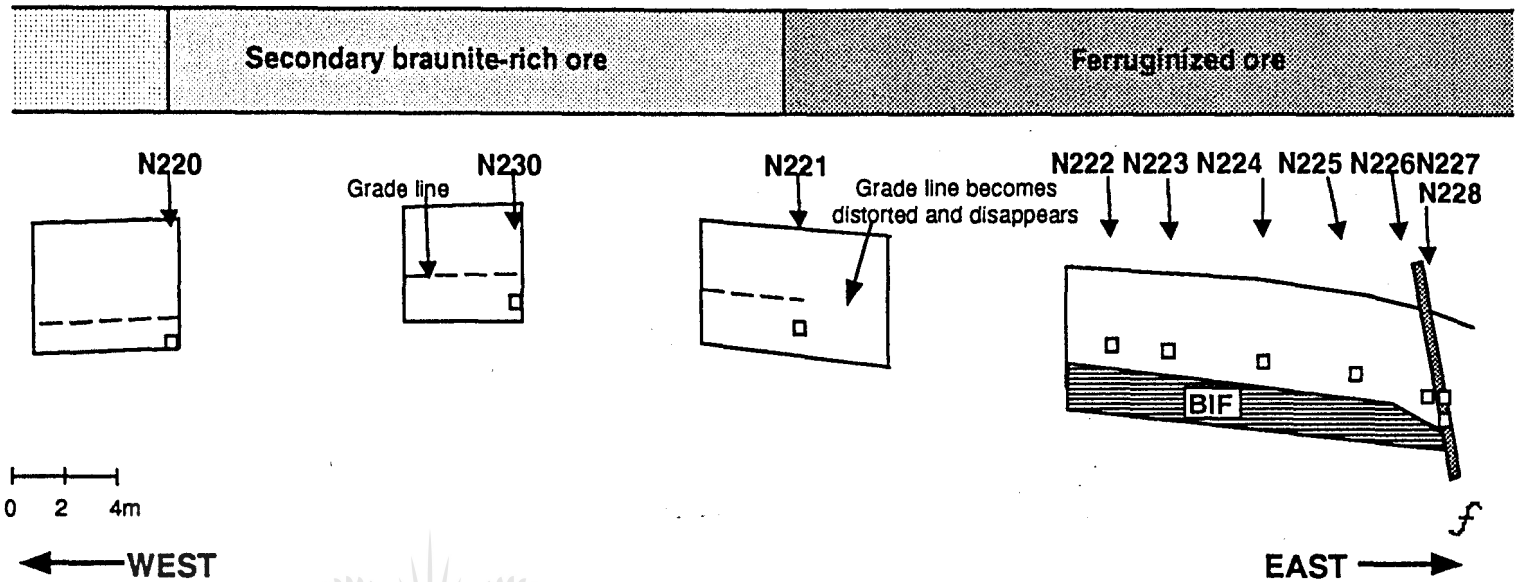

	N220	N230	N221	N222	N223	N224	N225	N226	N227	N228
HAUSMANNITE	x	x	x		x					
BRAUNITE II	xxx	xxx	xx		x					
BRAUNITE			xxx		xx					
BIXBYITE										
MANGANITE	x								x	
HEMATITE				xxx	xxx	xxx	xxx	xxx	xxx	xxx
CALCITE	x	xx	x	x	x	x	x	x	x	x
BARITE								x		
BRUCITE										
ANDRADITE										
CLINOCHLORE					x			x	x	

Figure 4.3. Mineralogical variations along section N300 as determined by XRD analyses. Main mineral phases indicated by three x's, minor mineral phases by two x's and trace amounts by one x.

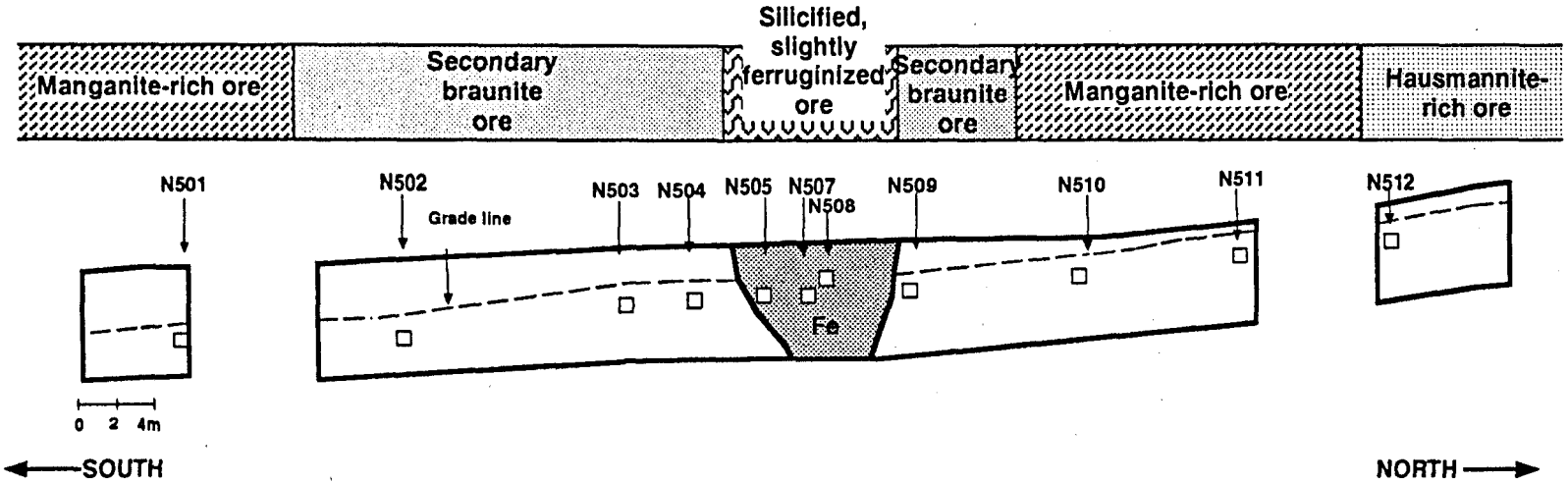

	N501	N502	N503	N504	N505	N507	N508	N509	N510	N511	N512
HAUSMANNITE				x					X	XX	XX
BRAUNITE II	X	XXX	XXX	XXX	XX			XXX	x	X	X
BIXBYITE	XXX							XXX			
MANGANITE	XXX	XX	XX	X				X	XXX	XXX	XXX
HEMATITE					XX	X	XXX				
CALCITE		X	X	X		X		X	XX	X	X
BARITE											
BRUCITE	X	X	X	X				X			
ANDRADITE											
CLINOCHLORE			X				X				
CRYPTOMELANE			X	X				X			
FEITKNECHTITE			X					X			
DIOPSIDE (Mn)					XXX	XXX	XX				
AEGIRINE					XX						
GAUDEFROYITE		X									
INESITE			X								
QUARTZ						XXX	XX				

Figure 4.4. Mineralogical variations along section N500 as determined by XRD analyses. Main mineral phases indicated by three x's, minor phases by two x's and trace amounts by one x.

Feitknechtite appears to be associated with the cryptomelane. Trace amounts of gaudefroyite and inesite are present (Fig. 4.4).

4.6 INTEGRATED MODEL OF LATERAL MINERALOGICAL VARIATION

The XRD analyses of the various sections sampled indicate a definite zonation in mineral assemblages relative to ferruginized fault zones on one side and unaltered sedimentary Mamatwan-type ore on the other (Fig. 4.5). In the ferruginized zone hematite is associated with minor calcite. The hematite-rich ore grades sharply into a relatively thin zone of massive braunite-rich ore (seldom more than a few metres in width) in turn grading into ore containing abundant braunite II. These two ore types replace earlier formed, very high-grade hausmannite-rich ore (Pl. 3.7). The secondary braunite-rich ore grades laterally into typical Wessels-type ore, composed essentially of hausmannite and some bixbyite. More distal to the zone of ferruginization the hausmannite-rich ore grades over into braunite II-rich ore in turn grading into Mamatwan-type ore containing braunite and kutnahorite. The major carbonate phase in Wessels-type ore is calcite with gangue minerals such as clinochlore, gaudefroyite, barite and andradite. There is no definite trend visible in the occurrence of these gangue minerals.

This zonation implies that, in moving from low-grade primary sedimentary Mamatwan-type ore into the high-grade Wessels-type ore, a gradual loss of silica takes place. This is indicated by the fact that in primary Mamatwan-type ore braunite is present, containing a theoretical silica content of 10 weight percent. It is replaced by braunite II containing only about 5 weight percent SiO_2 in its crystal structure. In turn this ore grades into hausmannite and bixbyite ore containing no SiO_2 in their crystal structures. The only silica left in the samples is that which is present in trace amounts of the andradite garnet sometimes developed in the ore (Fig. 4.5).

In proximity to the ferruginized fault zones silica is again introduced into the system with the formation of secondary phases of braunite II and braunite, replacing hausmannite-rich Wessels-type ore.

There are variations in mineral zonation present in certain areas, for instance section N500, where slightly different structures occur. Here mostly Mn-oxides containing Mn^{3+} (manganite) occur, together with feitknechtite, which forms on the Mn-ore - meteoric water interface according to Kleyenstüber (1985). The

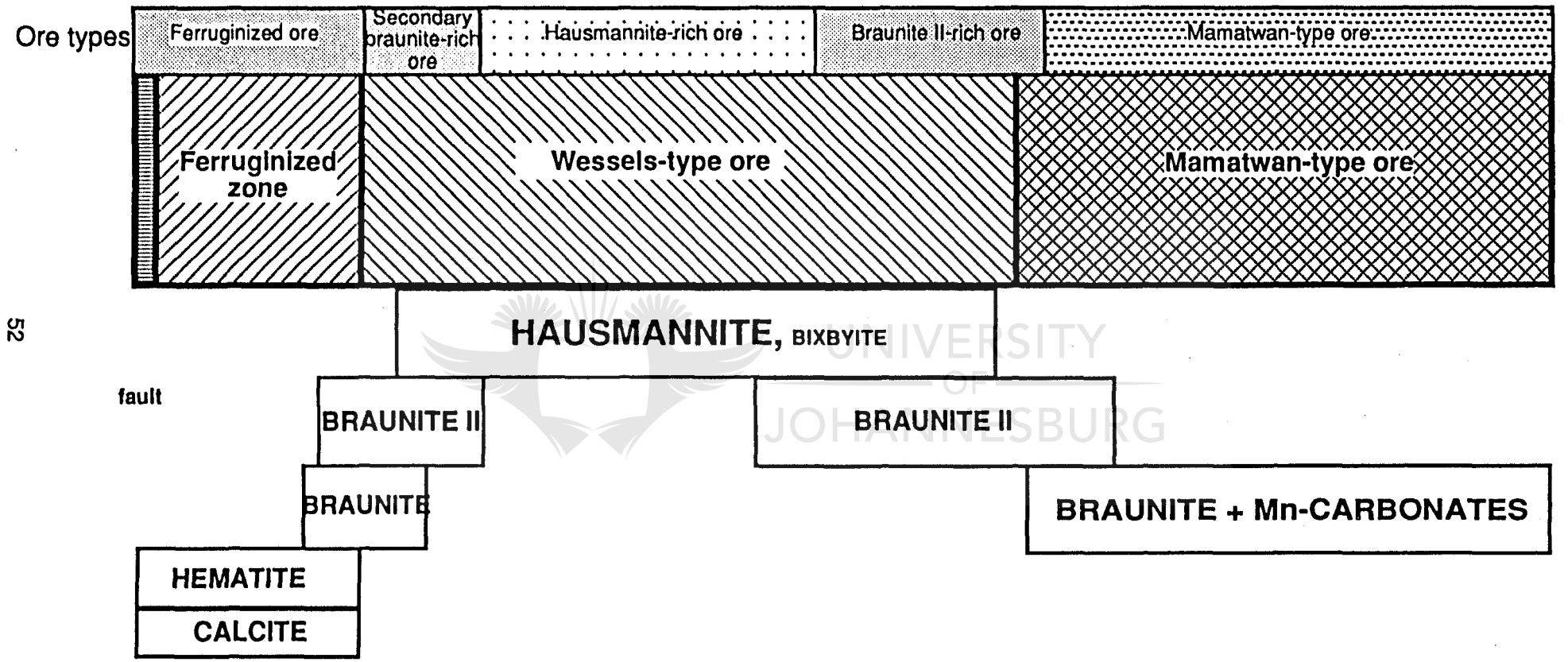

Figure 4.5. Model of distribution (zonation) of major mineral assemblages in Wessels-type ore relative to ferruginized fault zones on one side and unaltered primary Mamatwan-type ore on the other.

general pattern however, display a similarity to that encountered in the other sections, with only the major, high-grade Mn-minerals that differ.

Some variations from the ideal model of lateral mineralogical zonation are present. For example in section N500 manganite is developed in association with feitknechtite in the high-grade ore. According to Murray et al. (1985) feitknechtite forms experimentally at low temperature (0 °C) when Mn^{2+} is oxidized in a bicarbonate solution, it is metastable and goes over into manganite with time. At higher temperature (25 °C) hausmannite and some feitknechtite forms, with hausmannite changing into feitknechtite, which change into manganite with time (Murray et al., 1985). A later stage of formation, not connected with the main alteration event is suggested for this mineral pair (feitknechtite and manganite) that possibly formed due to meteoric water percolating through weak zones, with an alkaline oxidizing signature.

CHAPTER V LATERAL PETROGRAPHIC VARIATIONS AND MINERAL PARAGENESIS

Petrographic studies were undertaken using a Nikon OPTIPHOT-POL microscope mounted with a Nikon FX-35WA camera. Polished thin sections were used to facilitate reflected and transmitted light work. The XRD study was of great help in identifying minerals. Some mineral phases were identified by means of X-ray Debye-Scherrer camera work. The different ore types are described petrographically as it varies from Mamatwan-type ore, through the various high-grade ores up to the ferruginized zone (Fig. 5.1).

Sedimentary Mamatwan-type ore consists of primary braunite in a kutnahoritic matrix, with hematite specks as inclusions in the braunite. Carbonate ovoids, consisting of kutnahorite and manganoan calcite occur in the finely intergrown braunite-kutnahorite matrix. The ovoids are replaced by hausmannite and calcite (Pl. 5.1 and 5.2), as first indication of alteration.

Braunite II-rich ore, occuring between the Mamatwan-type ore and the high-grade hausmannite-rich ore, consists mainly of braunite II. It is found that the primary, fine grained braunite, as well as carbonate ovoids of Mamatwan-type ore, are replaced by braunite II with a yellow-grey colour (Pl. 5.3). The braunite II crystals are much larger in size (0,025mm) than the primary matrix braunite (0,01mm), indicating that recrystallization took place during formation of the braunite II. The fine primary laminations are disturbed and seems "thicker", due to replacement of fine grained braunite crystals by more medium- to coarse grained braunite II crystals. Small light grey metallic hematite specks occur as inclusions in the braunite II. The braunite II seems to be replacing the braunite ore by first replacing the kutnahorite matrix, containing the primary braunite. No kutnahorite is left in this ore. Gaudefroyite is encountered as a secondary ore mineral associated with braunite II . Andradite also occur in this ore type as gangue mineral. It is characterized by euhedral crystals with reddish internal reflection under uncrossed Nicols. Andradite is also found in rare cases, as rounded crystal masses in a braunitic matrix. In this case it apparently replaced the carbonate ovoids of the primary ore (Pl. 5.4). This ore type, encountered in the braunite II-rich ores, has a mottled appearance (Pl. 5.5). All the carbonate ovoids in this ore type, except for the rarely encountered andradite-bearing mottled ore type, are infilled by calcite with euhedral hausmannite crystals concentrated in the core of ovoids (Pl. 5.1 and 5.2). Veinlets filled with gaudefroyite and hausmannite may crosscut braunite II-rich ore (Pl. 5.6).

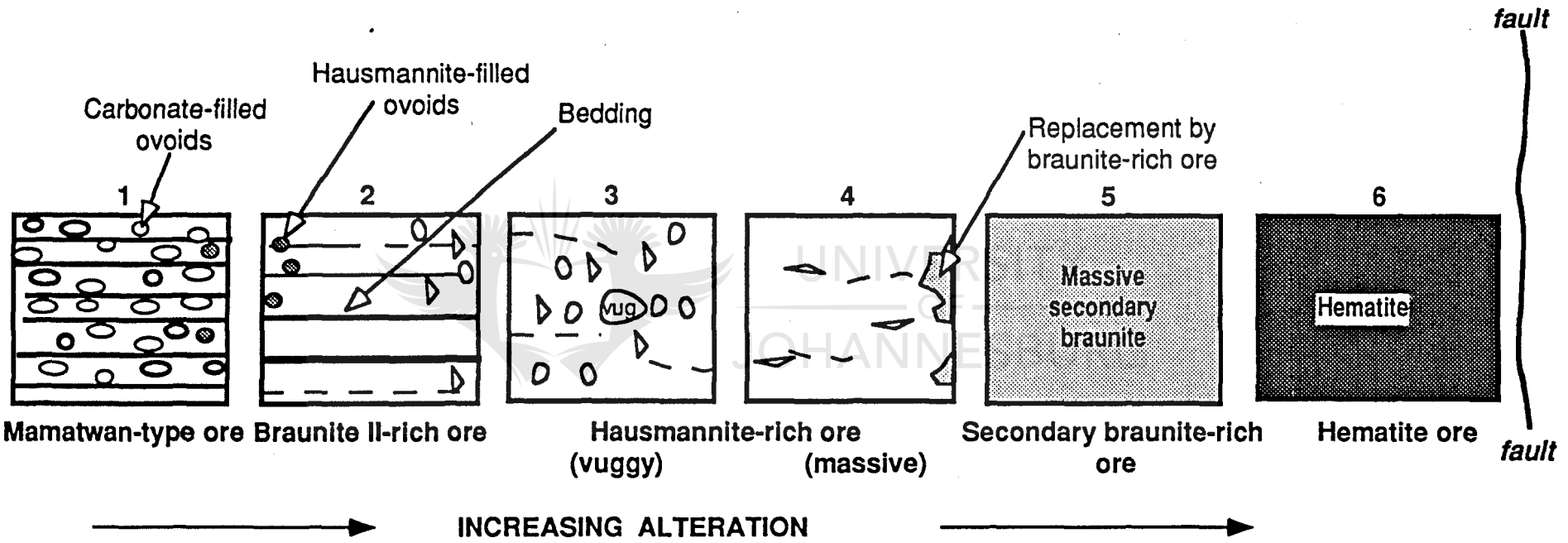

Figure 5.1. Schematic illustration of the six main ore types present in lateral gradations from Mamatwan-type ore through Wessels-type ore into hematite-rich ore along fault zones.

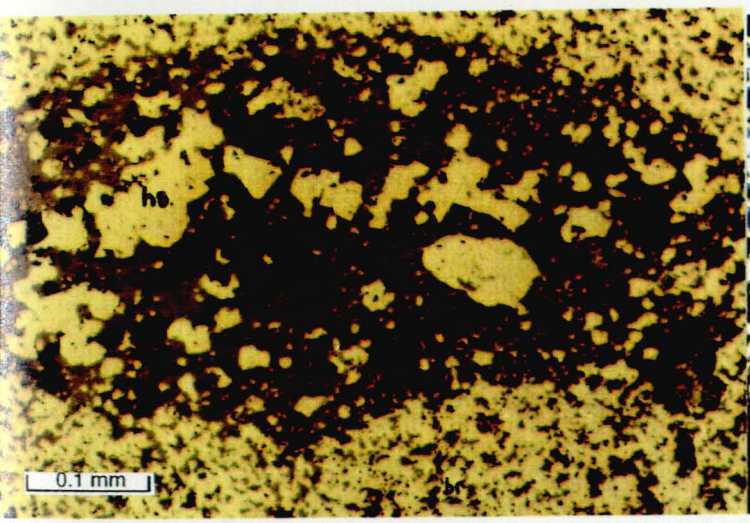

Plate 5.1. Calcite-filled ovoid surrounded by a matrix of finely intergrown braunite (br) and kutnahorite. Euhedral hausmannite (hs) developed in the core of the ovoid. Sample N119, Mamatwan-type ore (reflected light).

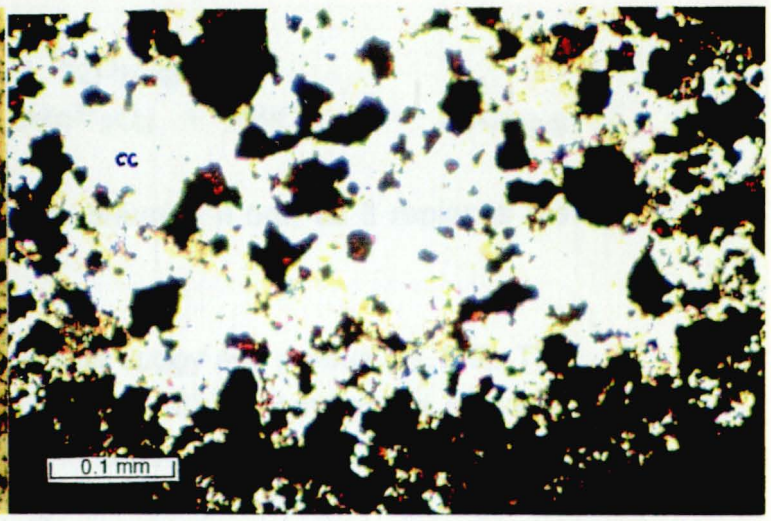

Plate 5.2. Calcite (cc) ovoid surrounded by a braunite-kutnahorite matrix. Euhedral hausmannite displaying red internal reflections, present in center of the ovoid where calcite has replaced the original Mn-carbonates. Sample N118, Mamatwan-type ore (transmitted light).

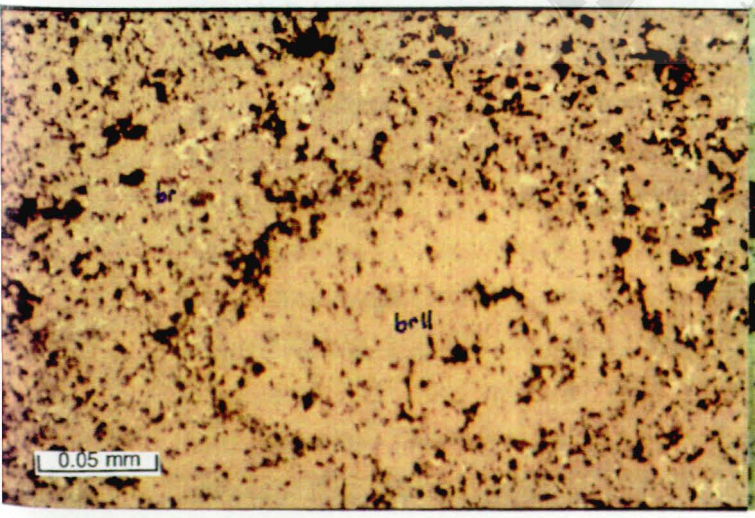

Plate 5.3. Yellow-brown braunite II (br II) which replaced an original carbonate ovoid. Braunite II is also replacing the matrix braunite. Small hematite specks are present in the sample. Sample N208, braunite II-rich ore (reflected light).

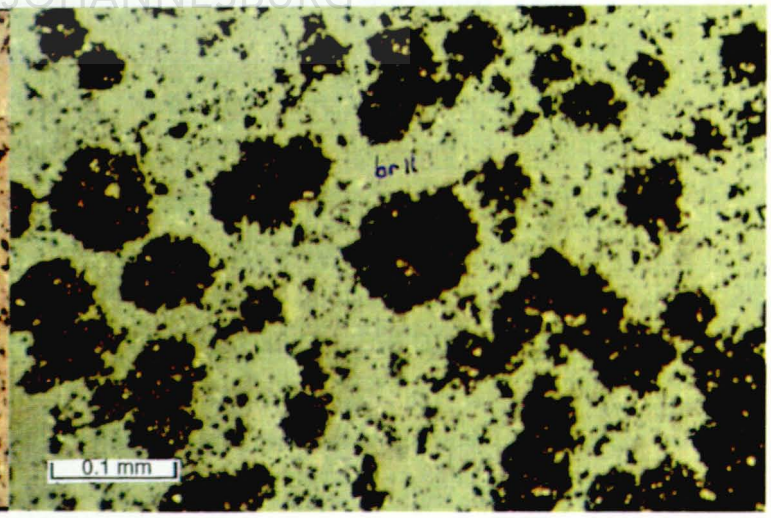

Plate 5.4. Mottled texture in braunite caused by spherical andradite (and) which replaced the primary carbonate ovoids. Braunite II is replacing the andradite and surrounding braunite-rich matrix. Small hematite inclusions are visible in the matrix. Sample N113, braunite II-rich ore (reflected light).

Low Si braunite with a skeletal texture, referred to as braunite (new) by Kleyenstüber (1985), replaces braunite II (Pl. 5.7), as well as hematite by the reaction

$6Mn^{2+}Mn^{3+}{}_6SiO_{12} + 3Fe_2O_3 + 2CaCO_3 + {}^3/_2O_{2(aq)}$ ---->

$6Ca_{0,34}(Mn,Fe)^{3+}{}_6Si_{0,34}O_{10} + 3Mn^{3+}{}_2O_3 + 4SiO_{2(aq)} + 2CO_{2(aq)}$

(Gutzmer, 1993).

Euhedral hausmannite inclusions appear in braunite II ore, as it replaces the braunite II mineral(Pl. 5.8).

The hausmannite-rich Wessels-type ore is very vuggy and porous (Pl. 5.9). The vugs may be filled or partly filled by calcite (Pl. 5.10); in some cases also with barite and clinochlore (Pl. 5.11), especially in larger vugs. A fibrous later phase of gaudefroyite is encountered in large vugs (Pl. 5.12). In hausmannite-rich ore braunite II is subordinate to absent, because it is replaced by hausmannite. The hausmannite is fine grained with patches of medium- to coarse grained crystals, displaying light yellow and blue birefringence under slightly crossed polars, and polysynthetic twinning (Pl. 5.13). Small anhedral inclusions of mostly braunite II, are present in the hausmannite (Pl. 5.14, 5.15 and 5.16), especially in proximity to the secondary braunite-rich ore near fault zones. Hematite specks are often included in the different manganese ore minerals. Braunite II is also replaced by low Si braunite (Pl. 5.7), in the hausmannite-rich ore. The low Si braunite displays a porous skeletal texture with gaudefroyite often infilling the pores. This skeletal low Si braunite replaces braunite II and in turn is being replaced by euhedral bixbyite and hausmannite that occur as euhedral inclusions in bixbyite. Thus it would appear that hausmannite replaces bixbyite. Patches in this hausmannite-rich ore type are composed of very medium- to coarse-grained hausmannite (Pl. 5.17) with larger vugs. Massive, very coarse-grained patches of hausmannite (±1mm), containing no vugs, are also present. This very coarse hausmannite may be replacing the finer grained hausmannite (±0,01mm) (Pl. 5.18 and 5.9) and, contain less hematite inclusions than the finer-grained hausmannite. The finer grained hausmannite may have been formed due to the reaction sequence:

braunite --> braunite II --> low Si braunite --> bixbyite,

where hausmannite replaces bixbyite (thus obtaining the high Fe-content observed in chapter 6). The fine grained hausmannite is of an older generation and is in places overprinted by a younger generation of the coarser grained hausmannite, an observation also made by Kleyenstüber (1985). Andradite with subhedral crystal edges, occurs in large vugs as gangue mineral (Pl. 5.17) and probably formed when silica, liberated from the braunites by the reaction:

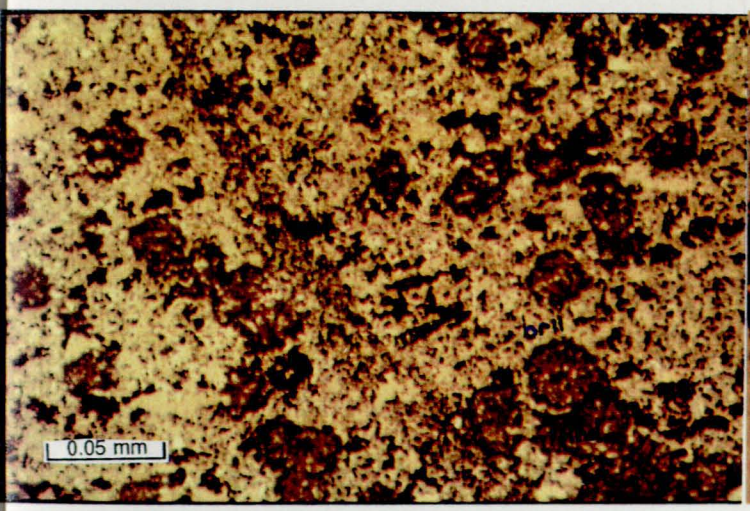

Plate 5.5. Mottled textured braunite II-rich ore. Andradite apparently replacing earlier Mn-carbonate ovoids. Braunite is replaced by braunite II and hausmannite. Numerous hematite specks are visible, especially in the andradite ovoids. Sample N208 (reflected light).

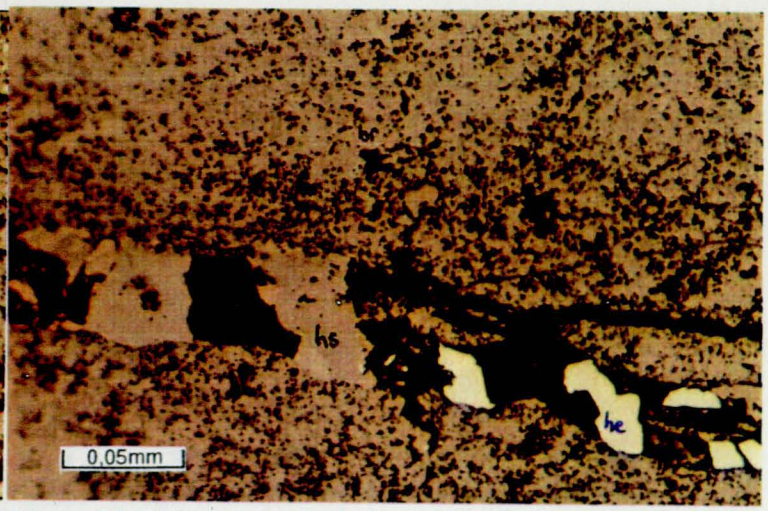

Plate 5.6. Veinlet composed of gaudefroyite, hausmannite and specularite (he) in braunite II-rich ore. Sample N118 (reflected light).

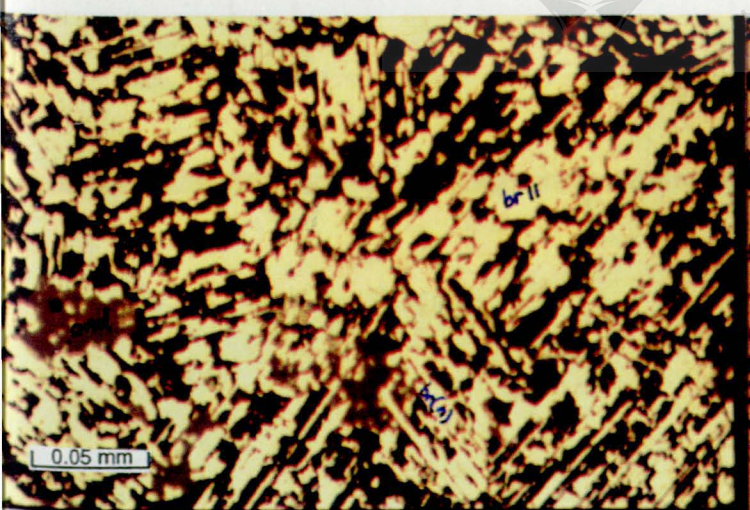

Plate 5.7. Example of skeletal texture in low Si braunite ("braunite new") -bearing ore. Only the very thin bladelike crystals have the composition of 'braunite (new)'. The blocky crystals and 'thicker'blades are composed of braunite II. Andradite fills some of the pores. Sample N209, braunite II-rich ore (reflected light).

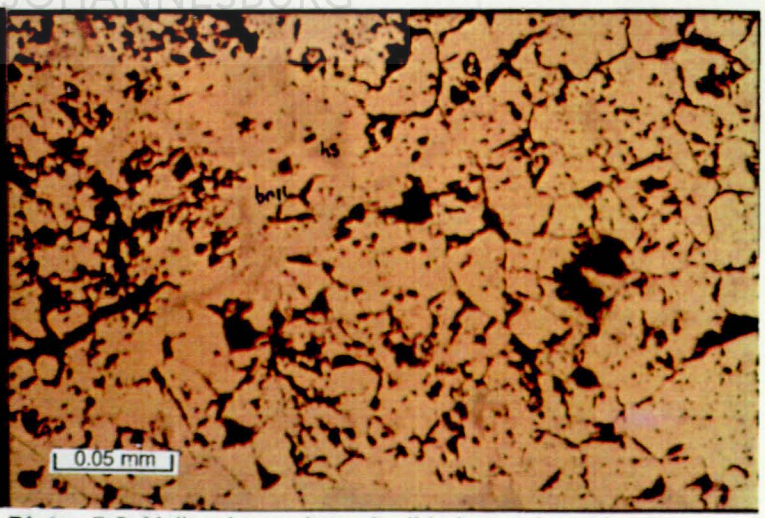

Plate 5.8. Yellow-brown braunite II being replaced by hausmannite. Sample N208, braunite II-rich ore (reflected light).

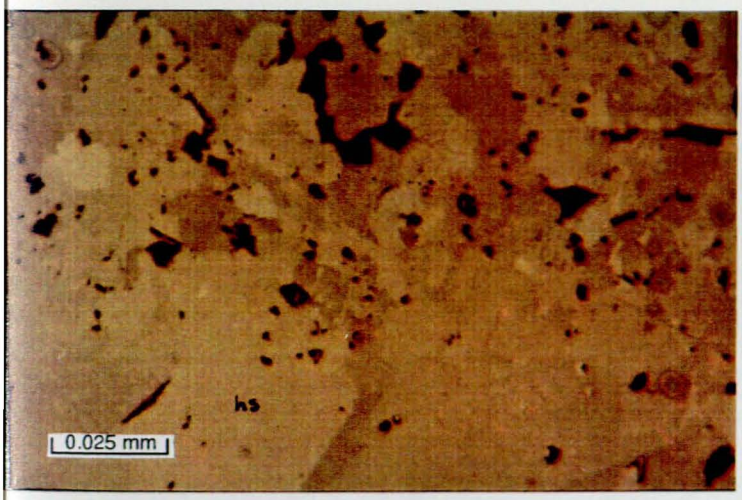

Plate 5.9. Small vugs developed in medium- to coarse grained hausmannite-rich ore. Sample N208 (reflected light).

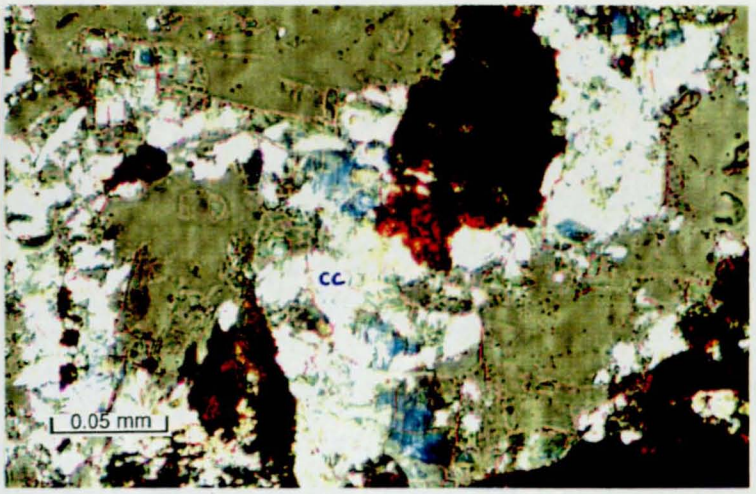

Plate 10. Large vugs, filled with calcite (white) in hausmannite-rich ore. Dark areas with red internal reflections are composed of hausmannite. Sample N108 (transmitted light).

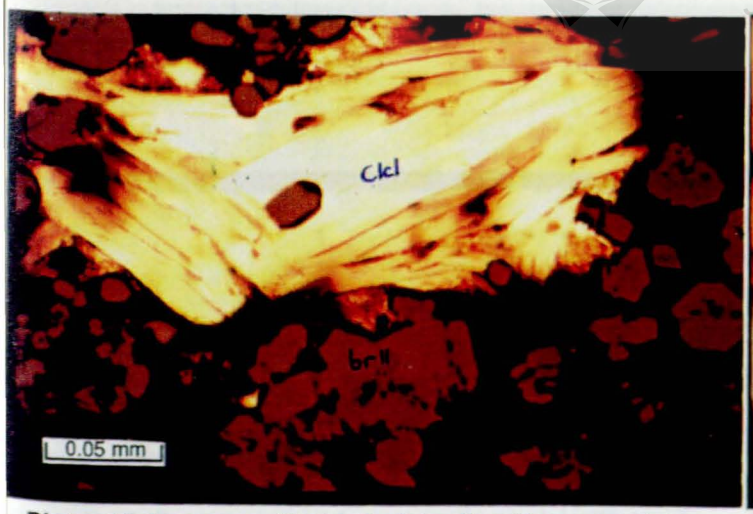

Plate 11. Large vug, filled with platy clinochlore, containing small inclusions of braunite II, in medium grained braunite II-rich ore. Sample N509 (transmitted light).

Plate 5.12. Fibrous gaudefroyite developed in large vugs in hausmannite-rich ore. Sample N204 (transmitted light).

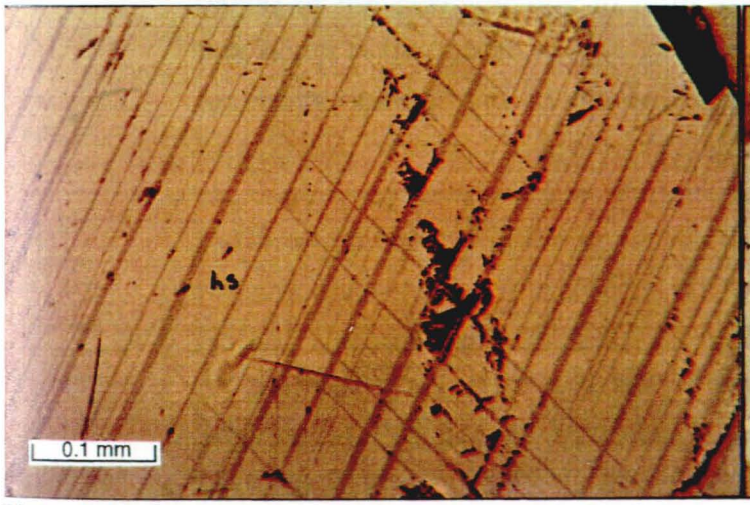

Plate 5.13. Coarse grained hausmannite crystal with distinct polysynthetic twinning. Wall of a vug visible in the upper right hand corner. Sample N204, hausmannite-rich ore (reflected light).

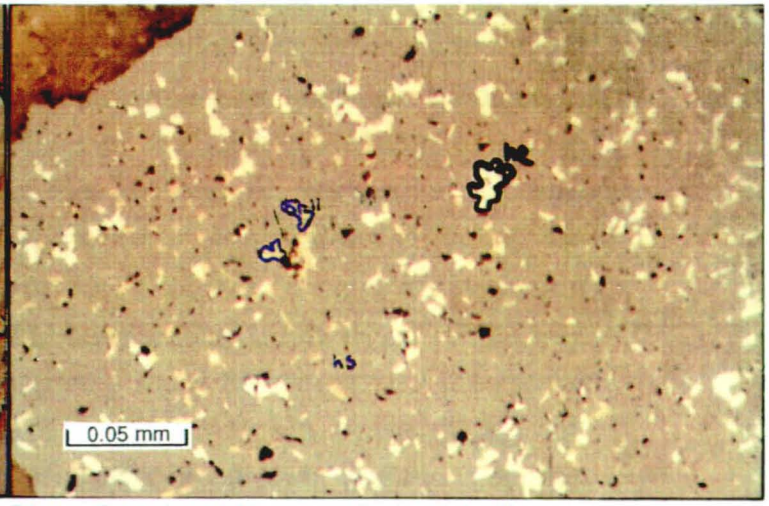

Plate 5.14. Large hausmannite crystal with numerous inclusions of hematite (white) and braunite II (yellow). Sample N203, hausmannite-rich ore (reflected light).

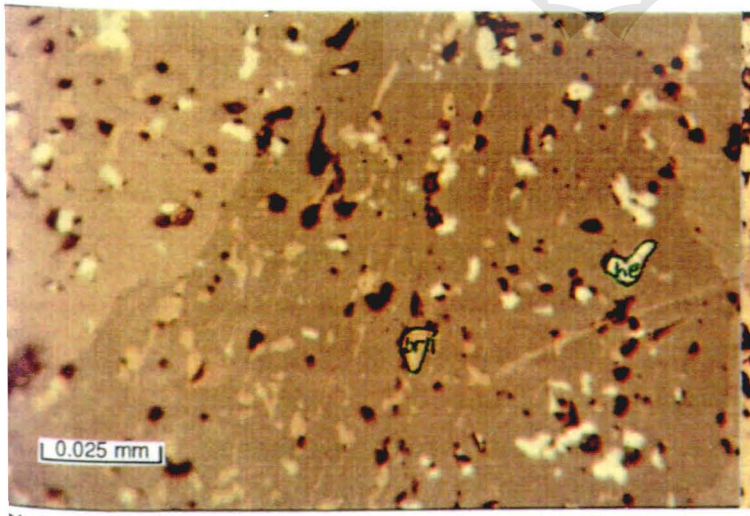

Plate 5.15. Coarse grained hausmannite crystal with small yellow inclusions of braunite II, aligned along cleavage planes of hausmannite and irregularly distributed white hematite inclusions. Braunite II is apparently replacing the hausmannite. Sample N203 (reflected light).

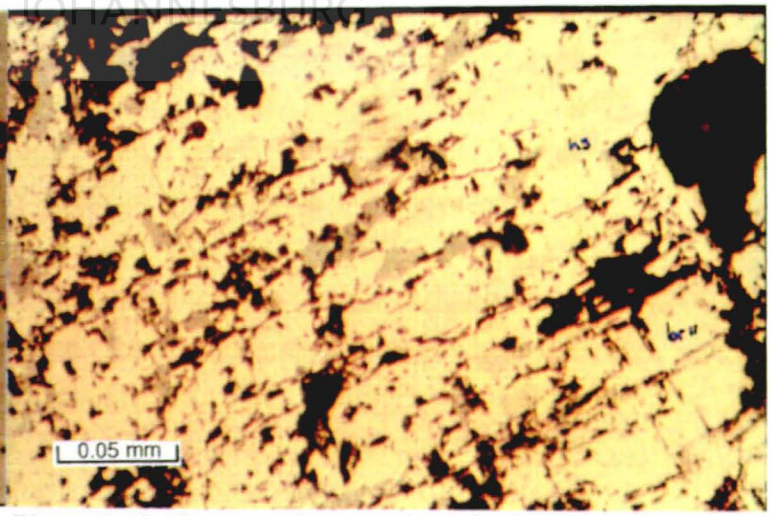

Plate 5.16. Massive yellow-grey braunite II, with greyish anhedral inclusions of hausmannite. Sample N220, secondary braunite-rich ore (reflected light).

braunite -> braunite II -> bixbyite,
reacts with Fe from hematite (in specks) and secondary calcite (in vugs and veins) of the surroundings to form andradite (Kleyenstüber, 1985). The vugs that occur in the hausmannite-rich ore are mostly filled by calcite, gaudefroyite, andradite, barite and in cases hydrothermal minerals such as clinochlore, brucite and natrolite. These minerals show that the fluids that caused alteration must have contained trace amounts of Na, Mg and Al. Manganite, an olive coloured pleochroic, anisotropic mineral, occurs in some areas in high-grade hausmannite-rich ores (samples N108-N110, N220 and in samples in section N500). The manganite is replaced by euhedral hausmannite (Pl. 5.19) as well as braunite II (Pl. 5.20 and 5.21). Manganite must have replaced the earlier sedimentary Mamatwan-type ore. In section N500 marokite is associated with braunite II, bixbyite and hausmannite. It consist of purplish, stubby, prismatic crystals (Pl. 5.22), which are replaced by braunite II. Marokite must have formed during oxidation of carbonates when large amounts of Ca was present in the hydrothermal fluids. The bixbyite associated with this ore also display no hematite inclusions, indicating that it replaces hematite specks present in the phases (braunite II, manganite and hausmannite) that it replaces.

In the transition zone between hausmannite-rich ore and massive secondary braunite-rich ore, immediately adjacent to the ferruginized fault zones, hausmannite is being replaced by braunite II along twin lamellae (Pl. 5.23). Hausmannite is still the main phase, but skeletal low Si braunite and euhedral braunite II starts forming as inclusions in the hausmannite as they replace the hausmannite, probably due to a secondary influx of silica into the ore. Large, cubic, yellow-grey, slightly anisotropic bixbyite crystals are also present in hausmannite, although rarely. It is found here that low Si braunite with the skeletal texture starts forming in hausmannite and is then in turn replaced by a more massive braunite II. This may develop into an ore where massive braunite II almost totally replaces the hausmannite-rich ore. This braunite II contains anhedral inclusions of hausmannite (Pl. 5.16). It also contains relicts of skeletal low Si braunite that is now being replaced and overgrown by braunite II (Pl. 5.24 and 5.25). Gaudefroyite occurs in vugs in the ore (Pl. 5.26). It is associated with braunite II. Veinlets filled with specularite and/or calcite are also present (Pl. 5.27). The massive secondary braunite-rich ore next to hematite ore is composed of densely intergrown braunite crystals, often partly replaced by specularite (Pl. 5.28). In rare instances primary ovoids, now totally replaced by calcite, may be present in the massive secondary braunite (Pl. 5.29).

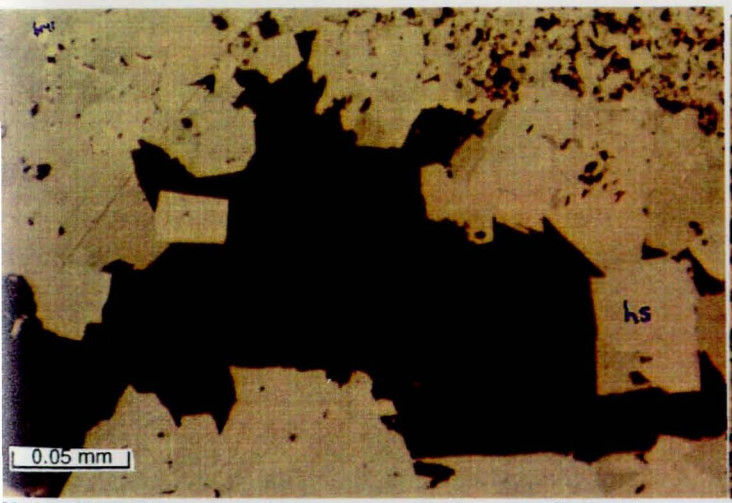

Plate 5.17. Large vug in hausmannite-rich ore filled with euhedral hausmannite crystals along walls and andradite in centre. Grey-yellow inclusions of braunite II are visible in the euhedral hausmannite crystals. Sample N103 (reflected light).

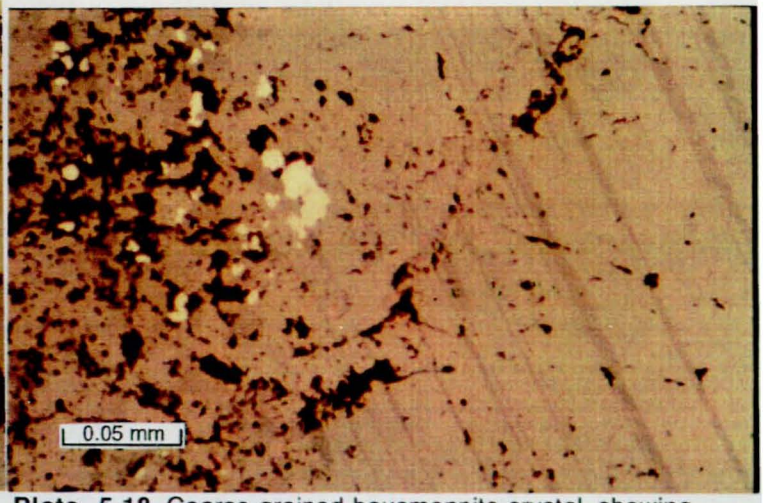

Plate 5.18. Coarse-grained hausmannite crystal, showing polysynthetic twinning. Large hematite specks are visible (white) together with dark brown gaudefroyite as secondary mineral. Finer-grained hausmannite on left side of photo appears to be replaced by coarse-grained twinned hausmannite. Sample N204, hausmannite-rich ore (reflected light).

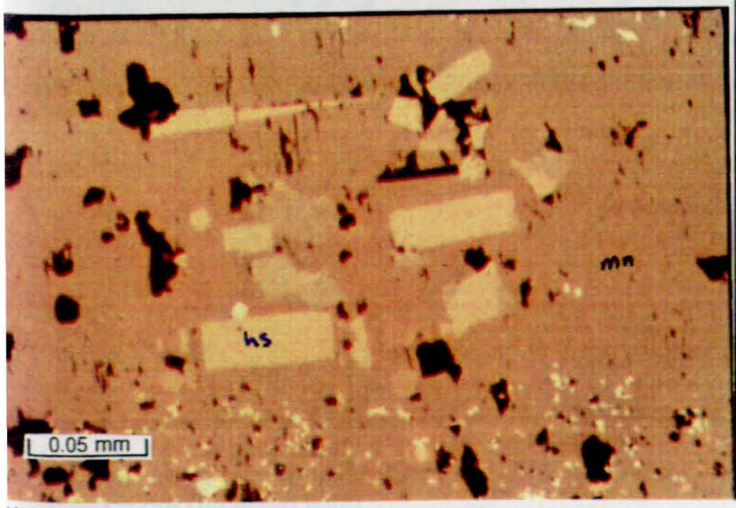

Plate 5.19. Euhedral hausmannite crystals, replacing manganite. Hematite inclusions (white) are present in some of the manganite. Sample N510, manganite-rich ore (reflected light).

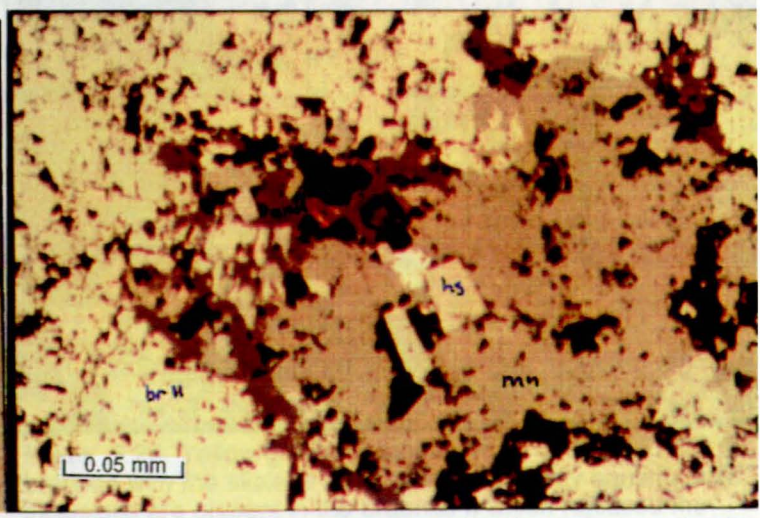

Plate 5.20. Euhedral hausmannite and yellow-grey braunite II replacing olive coloured manganite, with andradite as gangue mineral. Sample N220, secondary braunite-rich ore. (reflected light).

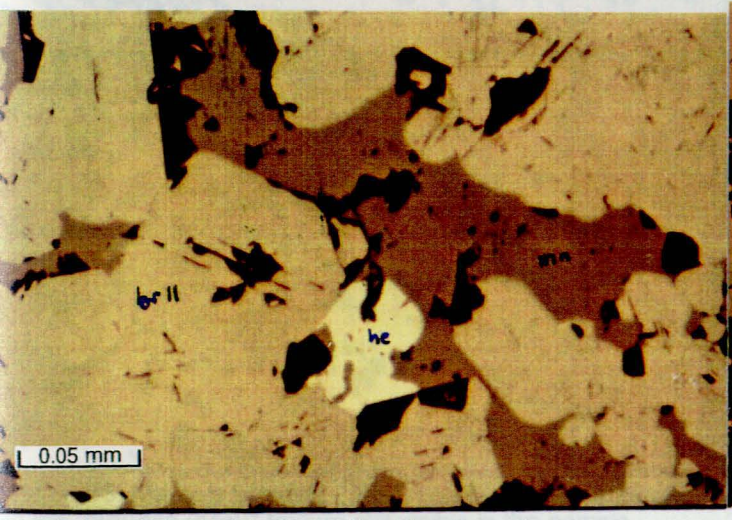

late 5.21. Euhedral braunite II with olive-coloured anganite and associated specularite (he), interstitially and in ugs. Sample N509, secondary braunite-rich ore (reflected ght).

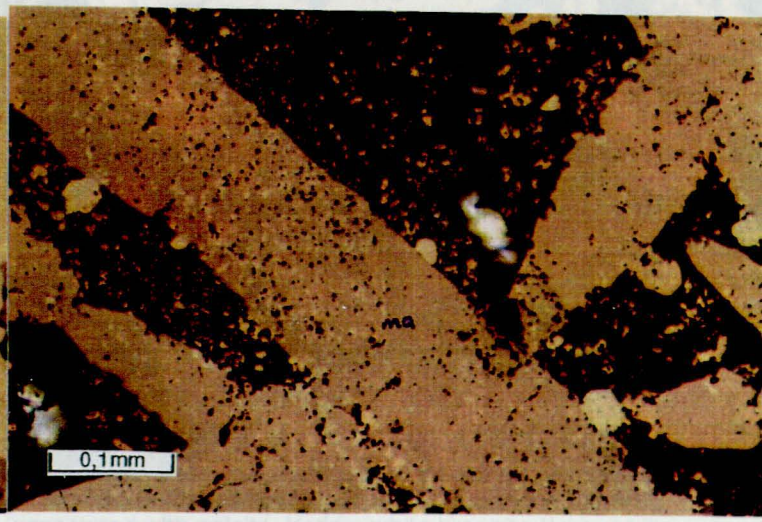

Plate 5.22. Brown stubby prismatic marokite crystals occuring in calcite which contains small inclusions of braunite II. White hematite specks are present in the marokite. Sample N510, manganite-rich ore (reflected light).

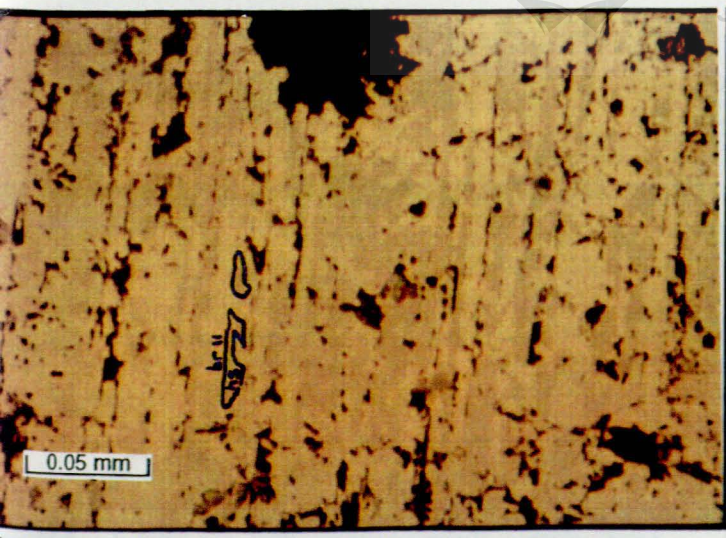

late 5.23. Yellow-grey braunite II replacing blue-grey ausmannite along twin lamellae. Sample N220, secondary raunite-rich ore (reflected light).

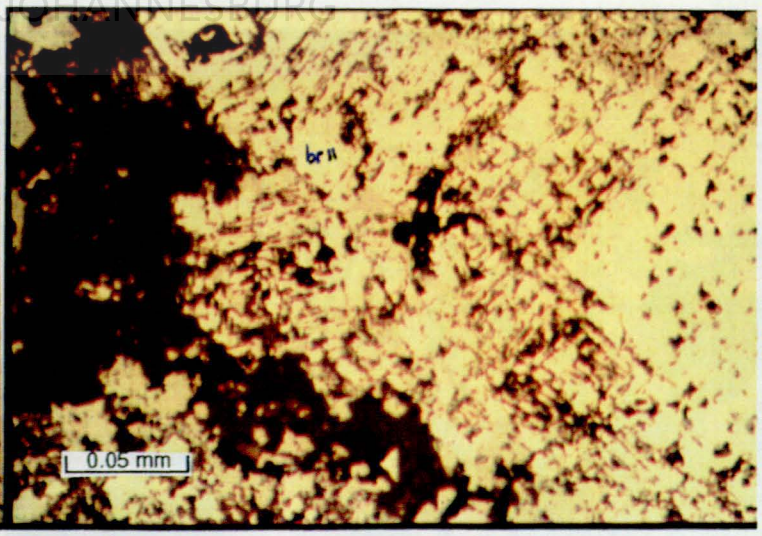

Plate 5.24. Yellow-grey massive braunite II replacing low Si braunite with the skeletal texture. Anhedral grey hausmannite inclusions are present in the braunite II which replaced the hausmannite. Brown gaudefroyite is filling vugs. Sample N220, secondary braunite-rich ore (reflected light).

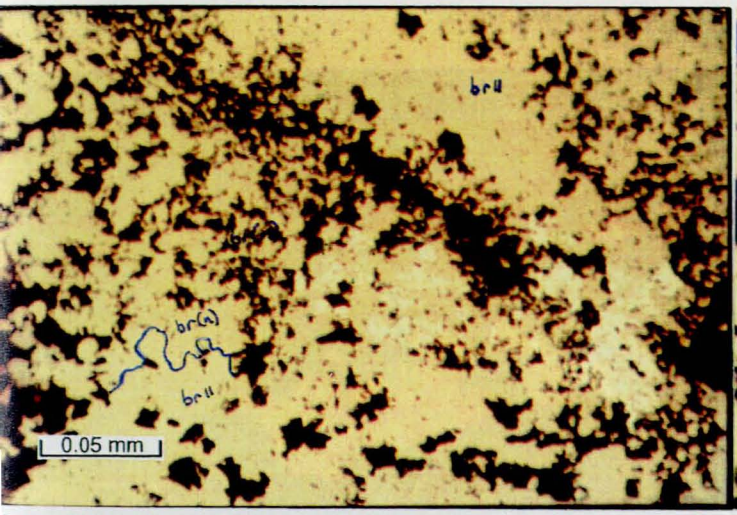

late 5.25. Massive braunite II that replaced earlier braunite II ith the "braunite (new)" texture still visible in the sample. umerous hematite specks (white) are visible in the sample. ample N230, secondary braunite ore (reflected light).

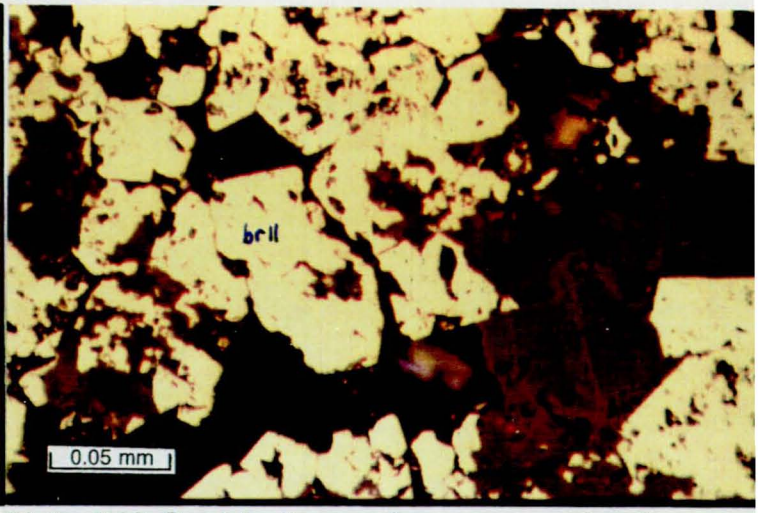

Plate 5.26. Gaudefroyite occurring as gangue mineral, associated with calcite. Yellow-white braunite II occurs as euhedral crystals and seems to be replaced by gaudefroyite in places. Sample N221, secondary braunite-rich ore (reflected light).

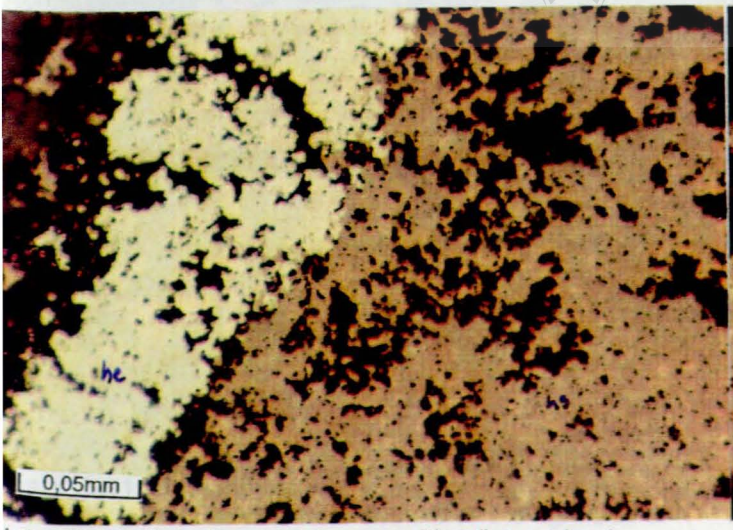

late 5.27. Hematite veinlet crosscutting fine-grained ausmannite-rich ore. Sample N202, from transition zone etween hausmannite-rich ore and secondary braunite-rich ore eflected light).

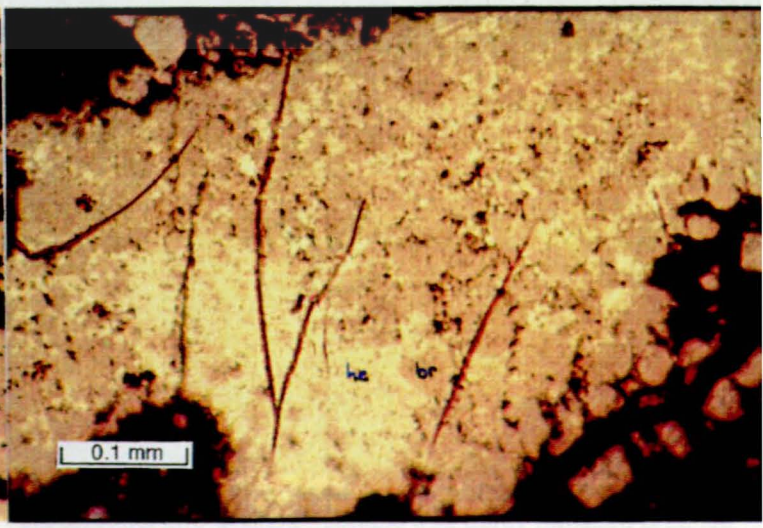

Plate 5.28. Massive braunite being replaced by hematite (white). Sample N201M, from transition zone between secondary braunite-rich ore and hematite ore along fault zone (reflected light).

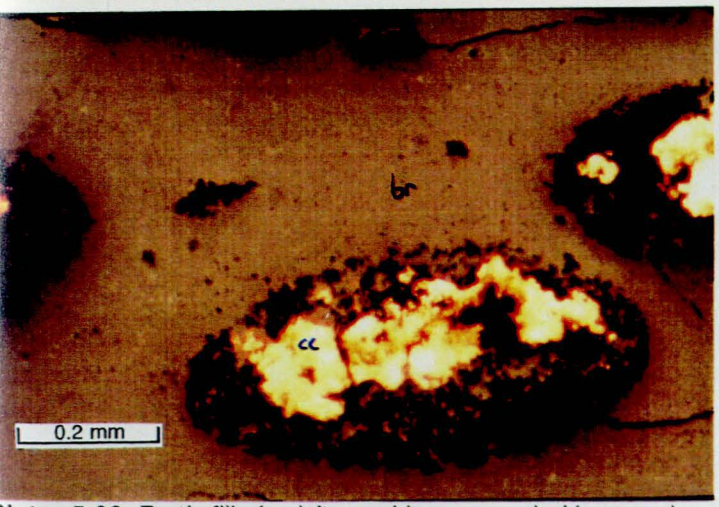

Plate 5.29. Partly filled calcite ovoids, surrounded by massive, secondary braunite with hematite specks (white). Sample N201, secondary braunite-rich ore (reflected light).

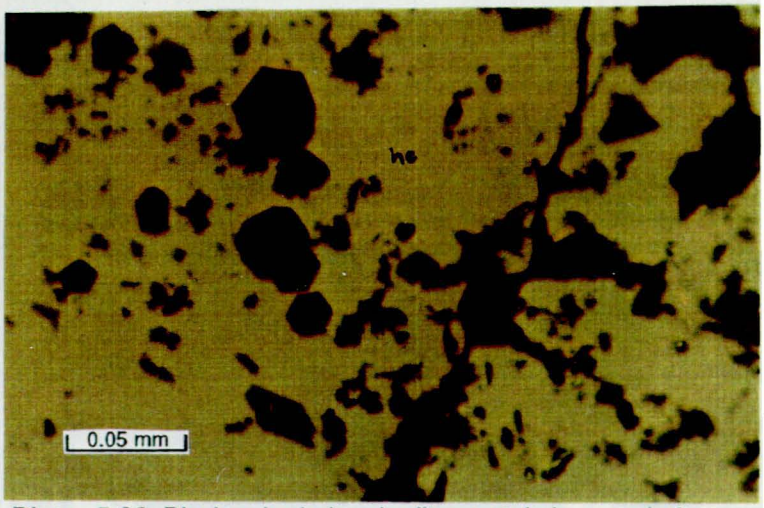

Plate 5.30. Black euhedral andradite crystals in specularite (he), together with grey euhedral hausmannite. Sample N103, hausmannite-rich ore (reflected light).

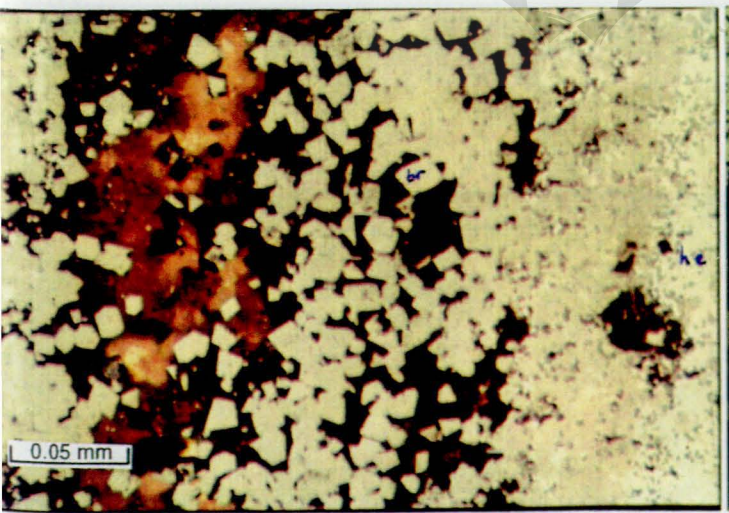

Plate 5.31. Euhedral braunite in a calcite filled veinlet crosscutting braunite-, hematite-rich ore on the right side of photograph. Sample N201, border between secondary braunite-rich ore and hematite ore (reflected light).

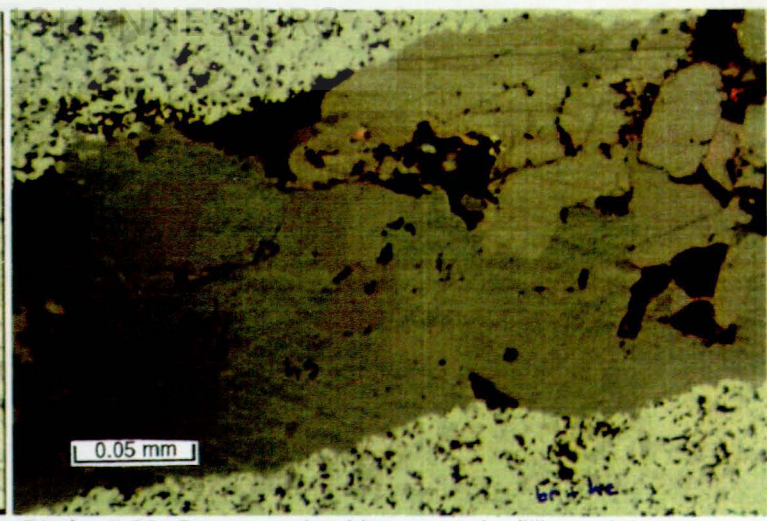

Plate 5.32. Coarse grained hausmannite filling veinlet crosscutting fine-grained hematite that partly replaced braunite. Sample N101, ferruginized ore on border with secondary braunite-rich ore (reflected light).

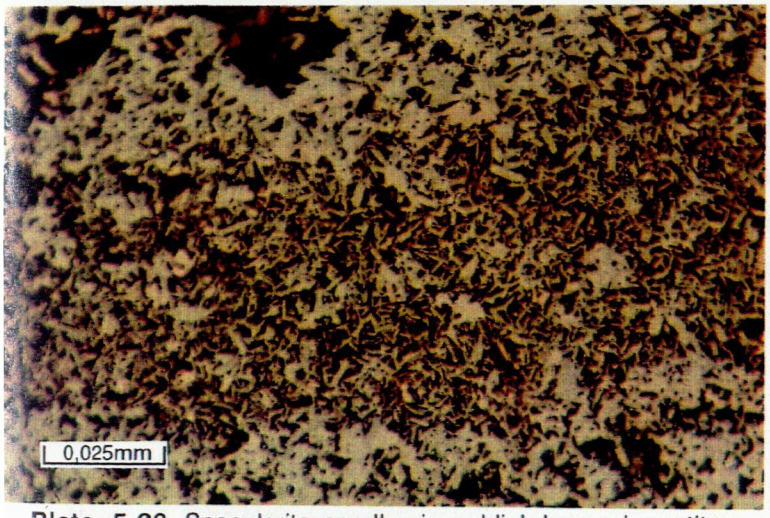

Plate 5.33. Specularite needles in reddish-brown hematite lutite. Sample N223, hematite-rich ore (reflected light).

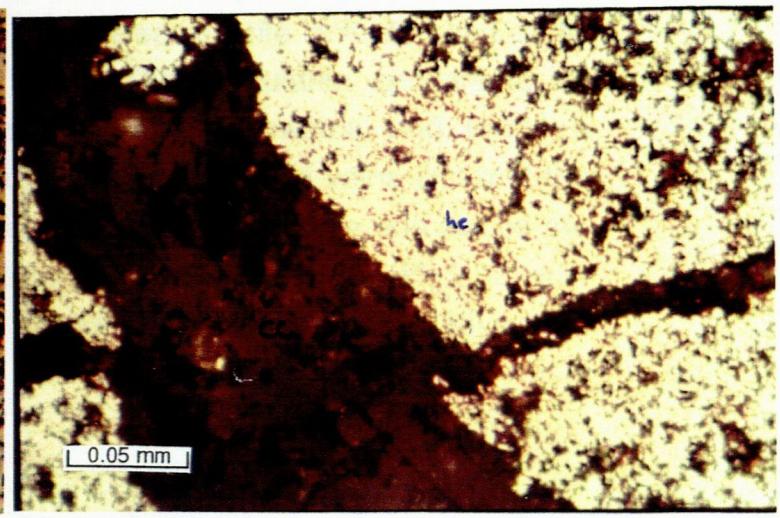

Plate 5.34. Sample consisting of secondary hematite (white) that totally replaced all primary ore minerals. Two generations of calcite veinlets crosscut the sample. Sample N223, hematite ore (reflected light).

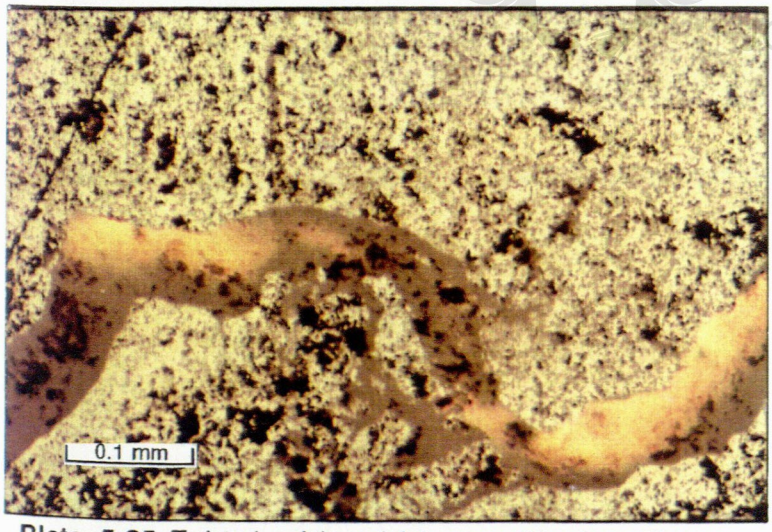

Plate 5.35. Twisted, calcite veinlet crosscutting hematite ore. Sample N223 (reflected light).

Hematite-rich ore, in ferruginized zones, is composed of dusty hematite, needlelike specularite and calcite. Specularite occurs associated with euhedral andradite crystals (Pl. 5.30) and is derived from recrystallization of hematite. Along the border with the braunite-rich ore the specularite infiltrated and partly replaced the braunite (Pl. 5.27 and 5.30). The specularite appears to be replacing the braunite crystals from the outsides inwards and forms a honeycomb texture (Pl. 5.27). In some places hausmannite veins crosscut the braunite and hematite (Pl. 5.31). Veinlets filled with specularite and calcite are common. Secondary euhedral braunite occurs in sparitic calcite (Pl. 5.32) with inclusions of specularite. Recrystalized lath-shaped specularite (Pl. 5.33) occurs in a matrix of fine crystalline hematite and sparitic calcite in veinlets (Pl. 5.34 and 5.35).

CHAPTER VI MINERAL CHEMISTRY

6.1 INTRODUCTION

A CAMECA CAMEBAX microprobe coupled to a Link eXL II EDS was used to obtain data on the composition of different minerals. An adsorption current of $3{,}48 \times 10^{-8}$ Amp for a cobalt tube and an acceleration voltage of 15 kV were used for analyses.

6.2. HAUSMANNITE

During this study it was found that some of the hausmannite in Wessels-type ore was magnetic. Crushed hausmannite-rich samples were separated by a common hand magnet into magnetic and "non magnetic" fractions of hausmannite. The particles were mounted in Perspex and polished for Energy dispersive spectometry (EDS) analyses. Manganese values were calculated to Mn^{3+} and Mn^{2+} values according to the method described by Kleyenstüber (1985) (samples with an M at the end of the number indicates a magnetic sample; the same sample numbers without the M at the end is not necessarily non magnetic, but less magnetic (N205ML is magnetic hausmannite, of the same hand specimen, analyzed at a later stage)). The analyses of samples from traverse N200 are given in Table 6.1. These are average values of which the statistical data are given in Appendix I.

Table 6.1. Mean values of EDS analyses of hausmannite from section N200. Magnetic samples indicated with an M at the end of sample number.

Element	N202M	N203	N203M	N204	N204M	N205	N205M	N205ML	N207	N207M	N209	N210	N119
SiO_2	0.23	*	*	*	*	*	*	0.20	*	0.21	*	*	0.67
Al_2O_3	*	*	*	*	*	*	*	*	*	*	*	*	*
MnO	32.45	32.57	33.09	32.47	32.45	32.62	31.79	32.87	31.09	32.30	31.11	32.13	31.68
Fe_2O_3	5.27	1.95	3.77	2.76	4.81	1.12	11.32	5.93	2.47	6.24	4.93	2.97	1.82
Mn_2O_3	61.71	64.98	62.93	64.38	62.64	65.78	57.14	61.14	65.79	61.20	63.06	64.68	63.98
MgO	0.54	*	*	*	*	*	*	*	0.23	0.29	0.92	*	0.43
CaO	*	*	*	*	*	*	*	*	*	*	*	*	0.40
Na_2O	*	*	*	*	*	*	*	*	*	*	*	*	*
Total	100.35	100.14	100.23	100.19	100.33	100.08	100.73	100.39	100.16	100.36	100.29	100.17	100.20

* Values < 0,20 wt%

Magnetic hausmannite shows consistently a higher iron-content than the non magnetic hausmannites (Fig. 6.1). Fe^{3+} apparently replaces Mn^{3+} in the structure of the magnetic hausmannite (Fig. 6.1). The Fe^{3+}/Mn^{3+} ratios of the hausmannites, plotted against their position relative to the ferruginized fault zone in the traverse N200, indicate a general increase in the iron-content of the hausmannite as the ferruginized fault zone is approached (Fig. 6.2). Hausmannite in Mamatwan-type ore, i.e. euhedral hausmannite developed in carbonate ovoids (sample N119), contains the lowest concentration of iron (Fig. 6.2).

As mentioned in the previous chapter, two generations of hausmannite are present in hausmannite-rich ore namely, fine- and coarse-grained hausmannite. The coarser-grained hausmannite, which replaces the fine-grained hausmannite, typically represent the non-magnetic hausmannite with relatively low iron contents. The fine-grained hausmannite contains relatively more iron and is magnetic. Some of the magnetic hausmannite contains up to 11,32 wt percent Fe_2O_3. The average Fe_2O_3 contents is between about 4 and 6 wt percent in magnetic samples and 1,1 - 4 wt percent in non magnetic samples. Kleyenstüber (1985) reported Fe_2O_3 values for hausmannite from 0,56 wt percent for hausmannite replacing oolites in Mamatwan-type ore, in transition zones with Wessels-type ore, to values up to 10,06 wt percent in hausmannite present in braunite-rich matrix outside of oolites. Gutzmer (1993) reported Fe_2O_3 values for hausmannite ranging from 0,36 wt percent to as much as 8,25 wt percent from N'Chwaning Mine. High iron-contents for hausmannite have also been reported from Otjosundu, Namibia (Fe_2O_3 23.59 wt percent) from Mason County, USA (Fe_2O_3 15,39 wt percent), and from Darmstadt, Germany (Fe_2O_3 15,6 wt percent) (Roy, 1981).

6.3 BRAUNITE-GROUP

A close relationship exists between the crystal chemistry and the mechanics of silica substitution amongst bixbyite, braunite and braunite II. These minerals can be described with the general formula M_8O_{12} (M = Mn, Fe, Ca) and may be considered end members of a polysomatic series, together with neltnerite, the Ca-analogue of braunite as defined by Thompson (1978). There is a considerable range of composition among these minerals and their structural relations are complex. Braunite (new) (Kleyenstüber, 1985), a silica poor member, occurs within the braunite II-bixbyite transition. Braunite (new) can also be regarded as a silica poor braunite II. The different braunites of this study

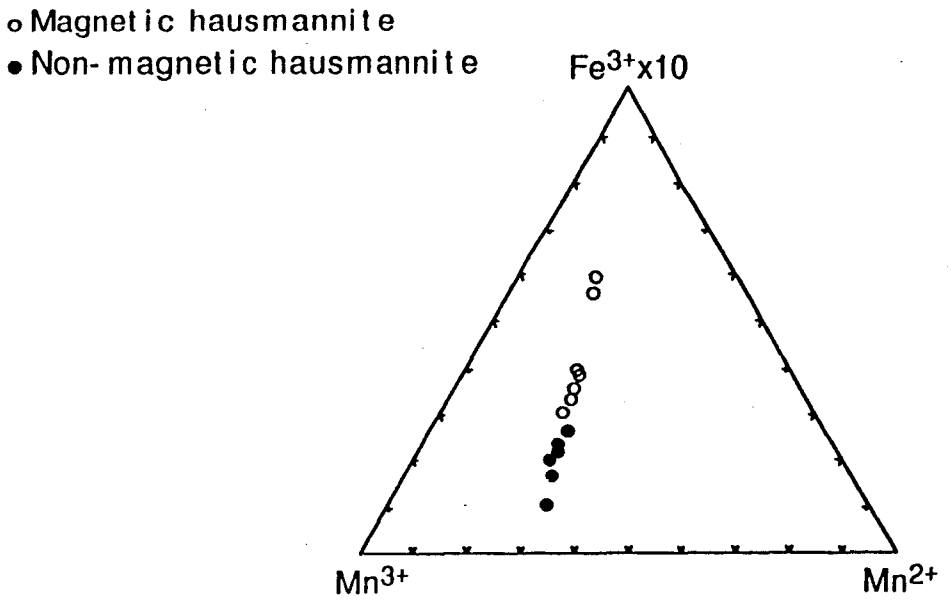

Figure 6.1 EDS analyses of magnetic and less-magnetic hausmannites of section N200, plotted on a ternary diagram to display the difference in Fe-content in the different hausmannites. Note that Fe^{3+} is multiplied by 10.

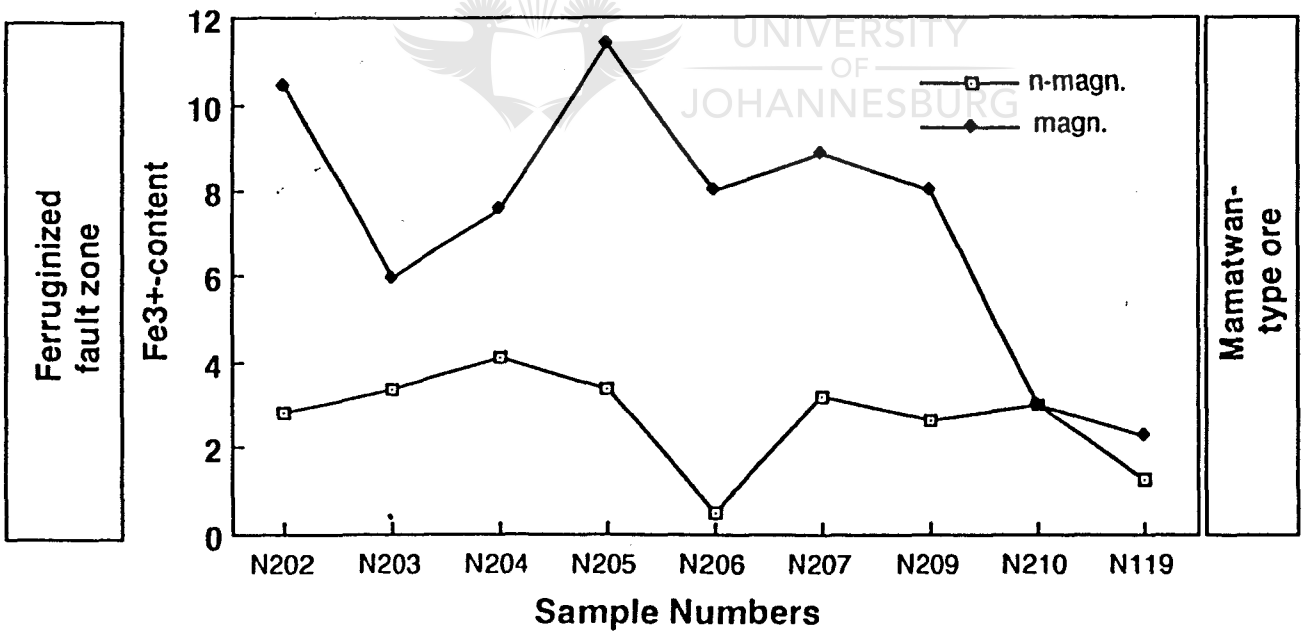

Figure 6.2 Fe^{3+}-content in wt percent of hausmannites from section N200 and a few samples from section N100, plotted against sample numbers, with N202 closest to the ferruginized fault zone and N119 bordering Mamatwan-type ore.

are plotted in figure 6.3 on a ternary diagram with SiO_2, $Mn_2O_3.Fe_2O_3$ and CaO at the apices.

6.3.1 BRAUNITE

Mn^{3+}-values were obtained during microprobe analyses and Mn^{2+}-values were calculated stoichiometrically after Kleyenstüber (1985). Braunites were analyzed in samples along section N200 from Mamatwan-type ore, through Wessels-type ore into the zone of ferruginization. The values given in table 6.2 are the averages of several analyses, of which the statistical data is given in Appendix I. Sample N201M consists of braunite separated from the rest of the sample by hand magnet, thus probably representing a magnetic braunite phase. The braunites contain on average 9 - 11 wt percent SiO_2 and 0,6 - 3,7 wt percent CaO.

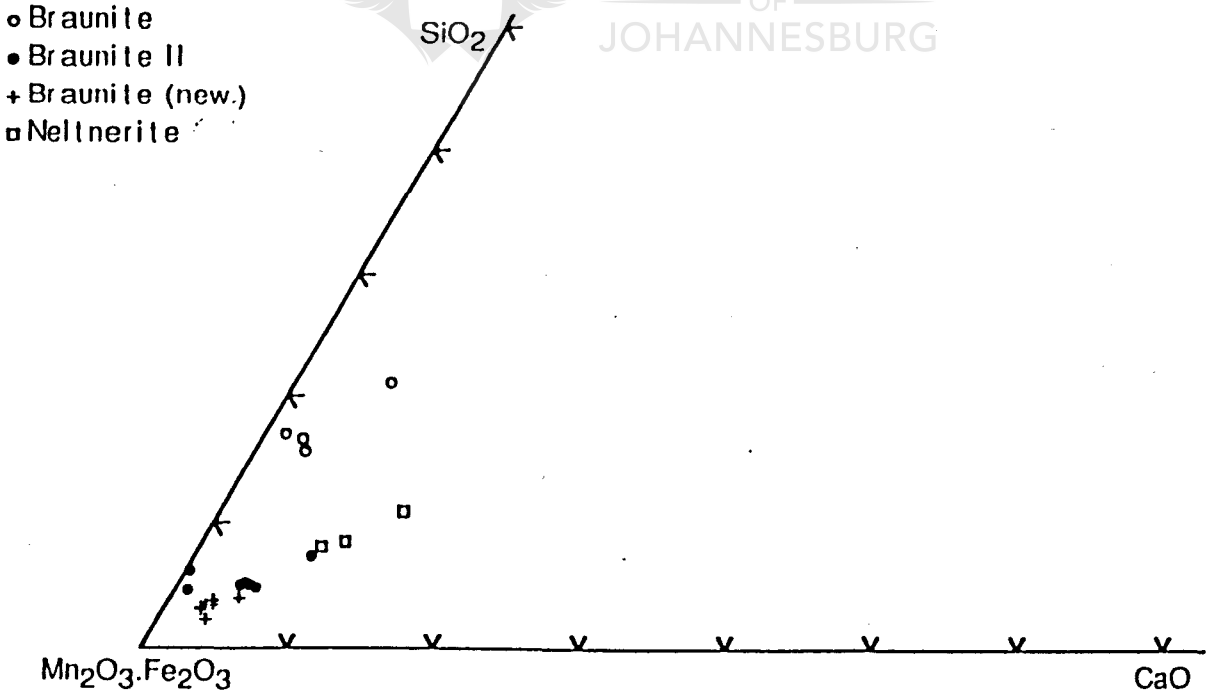

Figure 6.3. Different braunite end members of the braunite-group plotted on a ternary diagram to display the differences in the SiO_2- and CaO-contents.

Table 6.2. Mean values of several EDS analyses of braunite of section N200 and some of N100, with magnetic samples indicated with an M at the end.

	N101	N201M	N201	N202	N206	N210	N119
SiO_2	9.03	8.21	9.41	9.29	11.73	10.69	10.69
Al_2O_3	*	*	*	*	*	*	*
MnO	43.78	36.97	45.02	43.95	43.56	31.70	44.80
Fe_2O_3	10.84**	17.10**	8.89	2.73	5.89	4.54	3.23
Mn_2O_3	35.08	37.48	36.21	42.62	34.64	50.95	39.29
MgO	0.24	*	*	*	0.60	*	0.46
CaO	1.15	0.57	0.76	1.57	3.73	2.31	1.78
BaO	*	*	*	*	*	*	*
Na_2O	*	*	*	*	*	*	*
Total	100.15	100.61	100.39	100.24	100.44	100.43	100.44

* values < 0,20 wt%

** high Fe maybe due to fine intergrowths of hematite, not discernable under the microprobe

The iron-contents of the braunites display a definite increase from that in low-grade Mamatwan-type ore (sample N119) to that in samples bordering the ferruginized zone (sample N201M) (Fig. 6.4). Samples N201M to N202 consist of secondary braunite (replacing hausmannite), while the braunite of samples N206 to N119 consist of primary braunite (being replaced by hausmannite). The Fe:Mn ratios in the primary braunites are rather constant, compared to those in the secondary braunites associated with the ferruginized fault zone. The Fe_2O_3 contents varies between 2,73 and 17,10 wt percent in all the braunites analyzed along the section.

Kleyenstüber (1985) reported Fe_2O_3 values of 5-10 wt percent with 10,84 wt percent reported in high-grade Hotazel-type ore. Gutzmer (1993) also reported Fe_2O_3 values for braunite in the range of 4-8 wt percent. Sample N201M displays an extraordinary high Fe_2O_3 contents of 17,1 wt percent, which may be the reason why it is magnetic. The SiO_2 content of this sample (N201M) is low (8,21 wt percent) compared to that of other braunites, suggesting an intermediatery braunite phase, bordering on the composition of braunite II.

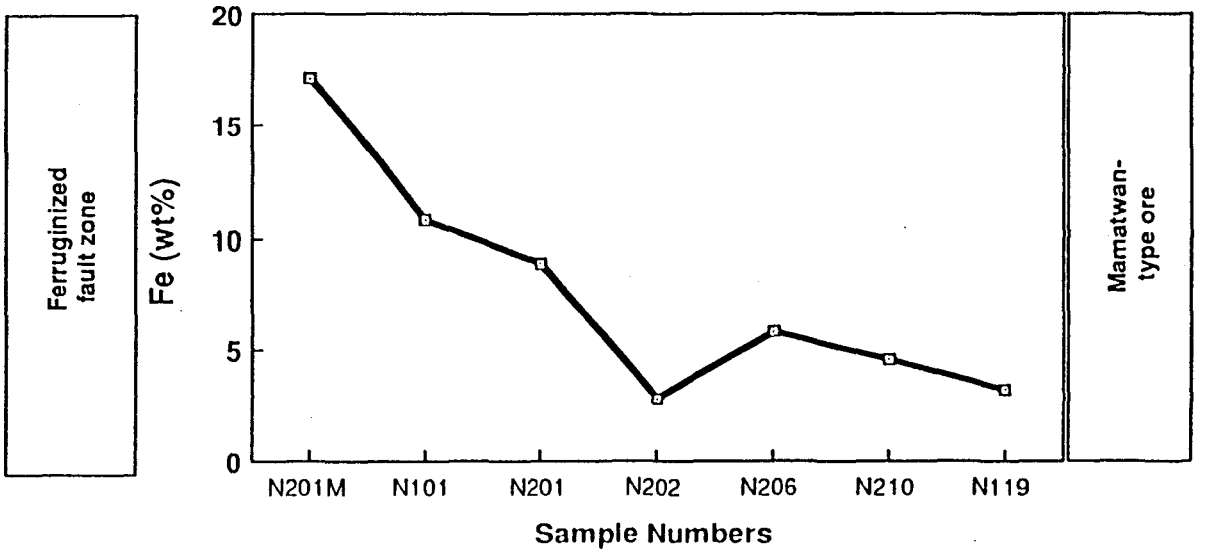

Figure 6.4 Fe^{3+}-content in wt percent of braunite from section N200, plotted against sample numbers, with N201M closest to the ferruginized fault zone and N119 bordering Mamatwan-type ore.

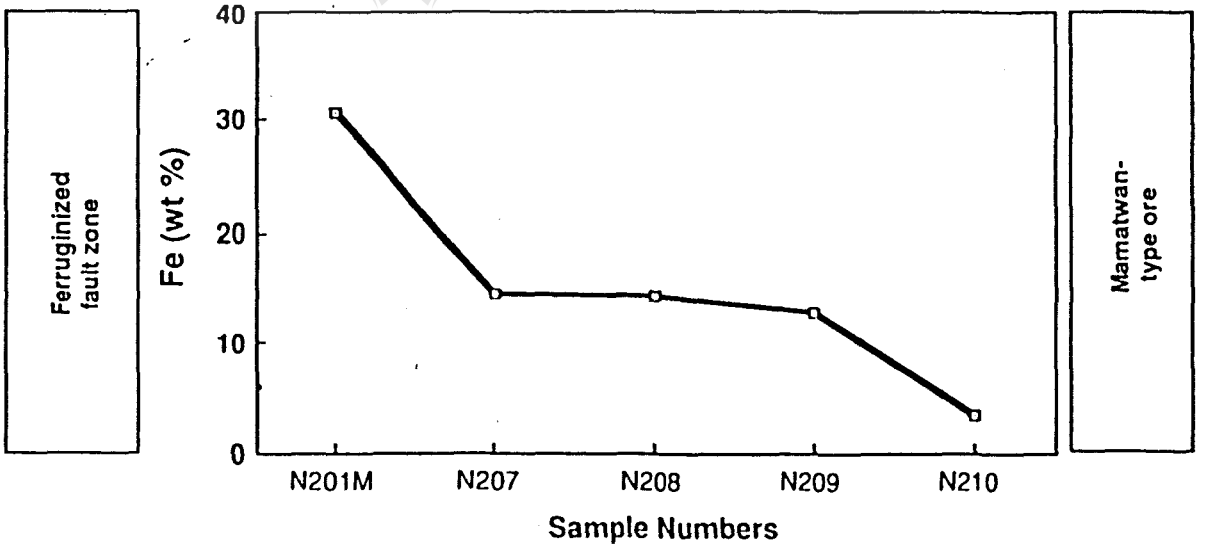

Figure 6.5 Fe^{3+}-content in wt percent of braunite II from section N200, plotted against sample numbers, with N201M closest to the ferruginized fault zone and N210 bordering Mamatwan-type ore.

6.3.2 BRAUNITE II

Braunite II analyses are given from samples near the ferruginized zone, through the high-grade Wessels-type ore into the low-grade Mamatwan-type ore. The values given in table 6.3 are averages of several analyses, of which the statistical data are given in Appendix I.

Table 6.3. Mean values of EDS analyses of several braunite II samples, with the magnetic sample indicated with an M at the end.

	N201M	N106	N207	N208	N209	N210
SiO_2	4.88	4.88	5.39	5.15	4.95	4.87
Al_2O_3	*	*	*	*	*	*
Fe_2O_3	30.62	12.95	14.33	14.63	12.73	3.39
Mn_2O_3	68.34	76.80	76.36	75.06	78.40	93.99
MgO	0.51	*	*	0.79	*	0.31
CaO	0.26	4.89	4.63	4.59	4.76	0.91
Na_2O	0.21	*	*	*	*	*
Total	104.69	99.76	100.90	100.33	101.35	103.83

* Values < 0,20 wt%

Comparison of braunite II from low-grade Mamatwan-type ore (sample N210) to that of secondary braunite II bordering the ferruginized zone (sample N201M), indicates an increase in the iron contents of the braunite II towards the ferruginized zone (Fig. 6.5). Samples N201M and N106 contain secondary braunite II replacing hausmannite, whereas samples N207 - N210 contain earlier formed braunite II which is replaced by hausmannite. The iron content increases in the direction of the ferruginized zone, especially in sample N201M which contains braunite II with 30,6 wt percent Fe_2O_3 (Table 6.3). Sample N201M was also separated by hand magnet and may contain magnetic braunite II. The total of this analysis is very high, again possibly due to small hematite inclusions not detectable under the microprobe. The silica contents are slightly lower in the second generation of braunite II (samples N201M, N106), relative to earlier braunite II in ore in the transition zone to Mamatwan-type ore. The Ca-content of the high-grade ore areas, samples N106, N207, N208, N209, is slightly higher when compared to the Ca-content of braunite II from Mamatwan-type ore in Wessels Mine, and also to that in secondary braunite II immediately adjacent to the ferruginized zone (Table 6.3).

Kleyenstüber (1985) reported Fe_2O_3 values in braunite II of between 13 wt percent and 16 wt percent and Gutzmer (1993) Fe_2O_3 values of between 8 and 15 wt percent in Wessels-type ore. The Fe_2O_3 values obtained during this study fall in the same range as those obtained by Kleyenstüber (1985) and Gutzmer (1993). However, sample N201M, which is magnetic, contains an exceptionally high iron content.

6.3.3 BRAUNITE (NEW)

Braunite (new), as defined by Kleyenstüber (1985), was found only in very finely skeletal crystals, in close association with skeletal low Si braunite crystals. The values given in table 6.4 are the averages of several analyses, of which the statistical data are given in Appendix I.

Table 6.4. Mean values of EDS analyses for braunite (new) from the different samples.

	N512.1.13	N106.2.6	N107 (avg)
SiO_2	3.18	3.89	3.01
Al_2O_3	*	*	0.35
Fe_2O_3	15.87	13.48	13.40
Mn_2O_3	79.86	77.46	80.86
MgO	*	*	*
CaO	2.74	4.87	3.01
Na_2O	*	*	*
Total	102.04	100.19	100.83

* Values < 0,20 wt%

In figure 6.3 the different braunite phases are plotted on a ternary diagram with SiO_2, $Mn_2O_3.Fe_2O_3$ and CaO on apices, to show the difference in CaO and SiO_2 in the different phases. The SiO_2 contents of 3,18 to 3,89 wt percent are slightly higher than the values reported by Kleyenstüber (1985) (2,85 - 3,66 wt percent) and Gutzmer (1993) (1,72 - 2,5 wt percent), but fall well below that of braunite II. Too few analyses were obtained to be able to distinguish a lateral trend in any chemical components of braunite (new). The braunite (new) contain abundant Fe_2O_3 (13,4 - 15,9 wt percent). This may be related to the fact that hematite was apparently replaced during formation of braunite (new) by the reaction:

$6Mn^{2+}Mn^{3+}_6SiO_{12} + 3Fe_2O_3 + 2CaCO_3 + {}^3/_2O_{2(aq)}$ ---->

$6Ca_{0,34}(Mn,Fe)^{3+}_6Si_{0,34}O_{10} + 3Mn^{3+}_2O_3 + 4SiO_{2(aq)} + 2CO_{2(aq)}$

(Gutzmer, 1993).

6.3.4 BIXBYITE

Bixbyites, developed after braunite II in hausmannite-rich ore, contain 20,7 - 25,2 wt percent Fe_2O_3 (Table 6.5). No hematite inclusions were found in the bixbyite grains, but abundant hematite inclusions are present in the surrounding ore. This means that the high Fe_2O_3-contents may have been derived from replacement of hematite during formation of the bixbyite. The composition of the bixbyites are near that of the ideal bixbyite composition (Table 6.5). The values given in table 6.5 are the averages of several analyses, of which the statistical data are given in Appendix I. Too few analyses were obtained to distinguish a lateral trend in any chemical components of bixbyite.

Table 6.5. Mean values of EDS analyses of bixbyite from two different samples.

	N512	N202M	ideal
SiO_2	0.87	1.00	*
Al_2O_3	*	*	*
Fe_2O_3	20.69	20.38	25.21
Mn_2O_3	78.93	83.87	74.78
MgO	*	0.47	*
CaO	0.67	*	*
Na_2O	*	*	*
Total	101.26	106.12	99.99

* Values < 0,20 wt%

6.3.5 NELTNERITE ($CaMn_6SiO_{12}$)

Neltnerite is a Ca-rich analogue of braunite (Bau-dracco-Gritti, 1982) and it is reported here for the first time from the Wessels-type ore. It occurs next to skeletal braunite II in association with gaudefroyite filling pores between skeletal crystals of braunite II. The neltnerite is present in sample N207 in braunite II-rich ore. It contains between 9,8 and 12,5 wt percent CaO and 16,5 - 17,25 wt

percent Fe_2O_3 (Table 6.6). Neltnerite has been reported in the Tachgagalt manganese deposit in Morocco, where it also occurs with braunite II and the minerals marokite, gaudefroyite and henritermierite (J.P.R. de Villiers et al., 1991). These analyses differ from that of the ideal composition, displaying lower SiO_2 and lower CaO. It is probably due to the high Fe_2O_3-content present in these samples.

Table 6.6. Mean values of EDS analyses of neltnerite from sample N207.

	N207.3.1	N207.3.5	N207.4.6	ideal
SiO_2	8.4	8.16	10.77	21.93
Al_2O_3	*	*	0.62	
Fe_2O_3	16.48	15.89	17.25	
Mn_2O_3	65.46	68.94	58.91	57.61
MgO	*	*	*	
CaO	9.78	8.33	12.49	20.46
Na_2O	*	*	*	
Total	100.23	101.12	100.32	100.00

* Values < 0,20 wt%

6.4 MAROKITE ($CaMn_2O_4$)

Marokite display very similar chemistry to that of hausmannite, it has however a different crystal structure and does not mix with hausmannite. The values given in table 6.7 are the averages of several analyses, of which the statistical data are given in Appendix I. Analyses of marokite indicated the composition to be very similar to that of the ideal composition, with a mean of about 72,1 wt percent Mn^{3+} and 24,5 wt percent CaO. The marokite differs from that of the ideal composition in that it contain about 3 wt percent Fe_2O_3 and 0,24 wt percent SiO_2 (Table 6.7).

Table 6.7. Mean values of EDS analyses of marokite from sample N510.

	ideal	N510
SiO_2	*	0.24
Al_2O_3	*	*
Fe_2O_3	*	3.52
Mn_2O_3	73.79	72.06
MgO	*	*
CaO	26.21	24.53
Na_2O	*	*
Total	100.00	100.41

* Values < 0,20 wt%

The analysis of bixbyite, neltnerite and marokite are plotted on a ternary diagram with Fe_2O_3, CaO and Mn_2O_3 at the apices in figure 6.6 to display its chemical contents. This plot clearly indicates that marokite contains high CaO and low Fe_2O_3 contents relative to bixbyite. Neltnerite is intermediate in composition between bixbyite and marokite (Fig. 6.6).

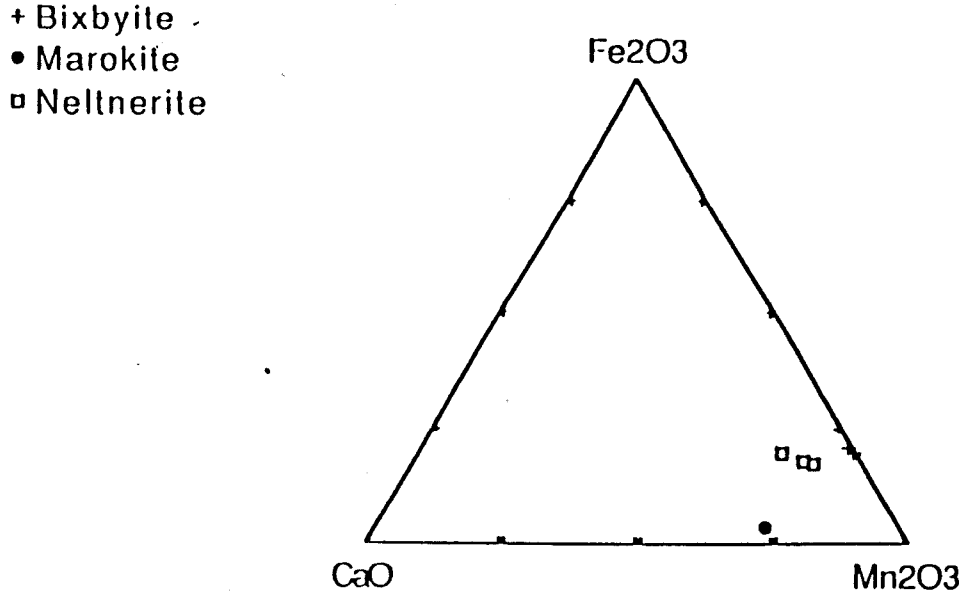

Figure 6.6. EDS analyses of marokite, neltnerite and bixbyite displaying the variations in chemical composition of the different phases.

6.5 ANDRADITE

Two types of andradite were analyzed namely,

(a) andradite replacing carbonate ovoids in braunite II-rich ore i.e. "mottled" andradite-rich ore as desrcibed in chapter 5 (Table 6.8a) and

(b) andradite occurring as gangue mineral associated with braunite II and hausmannite (Table 6.8b).

The andradite from ovoids apparently contain more CaO (34,7 wt percent) than that occurring as gangue mineral associated with hausmannite and braunite II (29 - 33,2 wt percent CaO). In comparison the andradites replacing ovoids apparently contain less iron (24 wt percent) than those associated with hausmannite and braunite II (22 - 31,4 wt percent) (Table 6.8a and 6.8b). The andradite plot in the field of MgO-poor andradite (Fig. 6.7) and Al_2O_3-poor andradite on the ternary plot for Fe-rich garnets (Fig. 6.8). Andradite occurring as gangue minerals in the Wessels-type ore, contain a high spessartine content, indicating that it formed from a Fe-rich source fluid, possibly at a later stage of hydrothermal activity than the main event responsible for the upgrading of the manganese ore.

Table 6.8.a. Mean values of EDS analysis of andradite filling earlier Mn-carbonate ovoids in braunite II-rich ore.

	N113
SiO_2	34.89
Al_2O_3	4.22
Fe_2O_3	24.17
Mn_2O_3	2.09
MgO	*
CaO	34.68
Total	100.02

* Values < 0,20 wt%

The values given in table 6.8a and 6.8b. are the averages of several analyses of which the statistical data are given in Appendix I.

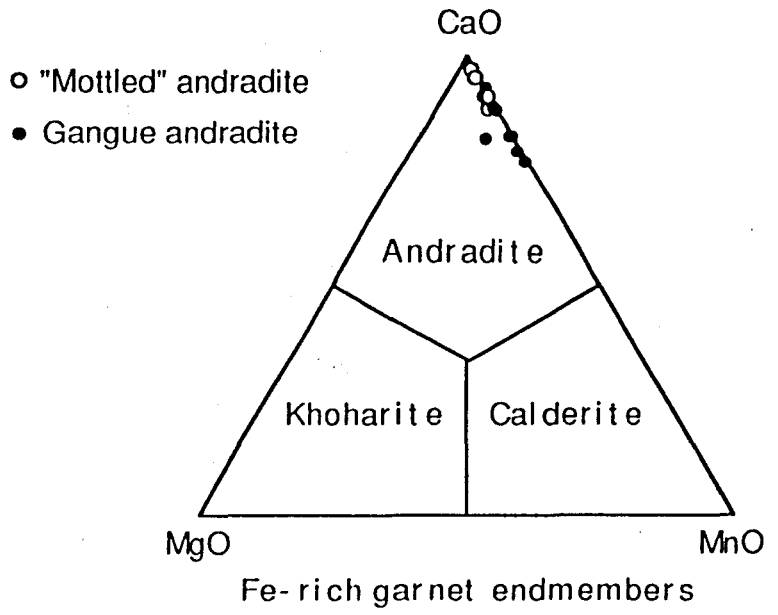

Figure 6.7 Fe-rich garnets plotted on a ternary diagram to determine if the garnets analysed, group under the andradite endmember.

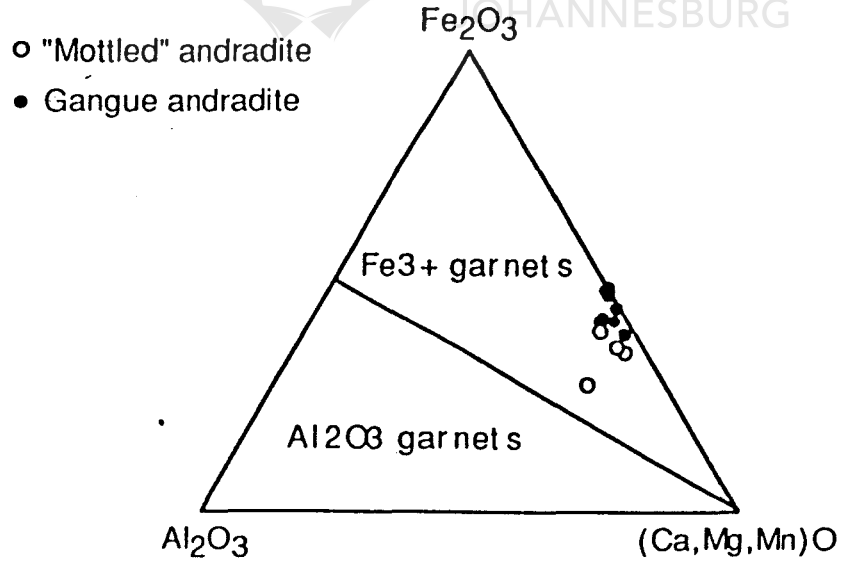

Figure 6.8 Ternary diagram with garnet analyses that show it to be Fe^{3+} garnet.

Table 6.8.b. Mean values of EDS analyses of andradite in Wessels-type ore.

	N203M	N210	theoretical
SiO_2	34.04	33.28	35.47
Al_2O_3	*	0.419	*
Fe_2O_3	31.39	22.03	31.42
Mn_2O_3	5.1	11.48	*
MgO	*	*	*
CaO	29.16	33.20	33.11
Total	100.12	100.58	100.00

* Values < 0,20 wt%

6.6 CALCITE

Analyses of calcite are given in table 6.9. The calcites contain less than 0,59 wt percent FeO and MgO values are most often below the level of 0,2 wt percent, with the exception of sample N205M, which contain up to 1,67 wt percent MgO. The calcites are manganese bearing containing 0,87 to 14,61 wt percent MnO. This may be as result of their replacing primary kutnahorite (Mn-carbonate), which occur as matrix mineral and filling ovoids in primary Mamatwan-type ore. In samples N202, N202M, N205M, N206 and N208, calcites occur as vugfilling, with sample N201M a small veinlet of calcite.

Table 6.9. Mean values of EDS analyses of calcite occurring in vugs and veinlets in the high-grade Wessels-type ore.

	N201M	N202	N202M	N205M	N206	N208
CaO	55.66**	59.99**	47.61	54.66**	51.29	58.94**
MgO	0.50	*	*	1.67	*	*
FeO	0.50	0.59	0.56	0.41	0.41	0.20
MnO	9.13	0.95	14.61	1.26	11.16	0.87
BaO	*	*	*	*	*	*
#CO_2	35.08	38.59	37.29	41.34	37.77	39.94
Total	100.00	100.00	100.00	100.00	100.00	100.00

* Values < 0,20 wt%

#CO_2 determined by difference

** High CaO-values due to evaporation of CO_2 during probe analyses

CHAPTER VII WHOLE ROCK CHEMICAL COMPOSITION

7.1 INTRODUCTION

Major element X-ray fluoresence (XRF) analyses of bulk powdered samples were done by the Analytical Chemistry Department of Samancor in Hotazel. They analyzed for Mn, Fe, Si, Ca and Mg. In addition some major and minor element analyses were done by the Analytical Chemistry Department of MINTEK. By means of emission spectroscopy, wet chemistry and atomic absorption methods fourteen representative samples were analyzed for Mn, Fe, SiO_2, CaO, Na, MgO, Al_2O_3, P_2O_5, K, TiO_2, CO_2, and H_2O.

7.2 RESULTS

7.2.1 SECTION N100

The Mn-contents of the ore along section N100 decrease to below 44 wt percent in the Mamatwan-type ore (sample N119) and in the ferruginized zone to 12,2 wt percent (sample N101). The secondary braunite ore (sample N102) bordering the ferruginized zone contains 48 wt percent Mn. Throughout the high-grade Wessels-type ore zone (samples N118-N103) the manganese-contents are between 49,9 and 63,6 wt percent with low iron contents of between 4,3 and 7,5 wt percent (Table 7.1 and Fig 7.1) The high-grade ores along section N100 represent some of the highest grade ore mined in the Wessels mine, designated as WH-type ore on the Mine. Sample N116 is the only exception with a Mn contents of 49.9 wt percent, i.e. WL-type ore.

On the border with the ferruginized zone (sample N102) a slight increase in iron-values to 9,5 wt percent and a decrease in manganese-values to 45,7 wt percent is visible (Fig. 7.1). The higher iron values may be due to the high iron-content in the manganese oxides (hausmannite, braunite II and braunite, refer to chapter 6). Wessels-type ore (sampled for this study) contain less iron i.e. 4,3 to 7,5 wt percent, compared to Mamatwan-type ore (Table 7.1), which contains about 5 wt percent Fe.

The SiO_2-contents of the manganese ores along section N100 (Fig. 7.2) are rather erratic with values ranging between 7 wt percent and 16 wt percent

(Table 7.1). There is a slight decrease in values from the low-grade braunite II-type ore (about 5 wt percent; Table 7.1) to the high grade ore (below 4 wt percent; Table 7.1). The almost pure hausmannite ore of samples N103 to N107, immediately adjacent to the ferruginized zone, display very low SiO_2-values (below 1 wt percent, except for sample N106 with 2,7 wt percent; (Fig. 7.2) Table 7.1). This is most probably due to the absence of silica bearing braunite-group minerals in this ore. The small amounts of SiO_2 present may be from gangue minerals such as clinochlore and andradite.

Table 7.1. Whole rock XRF analyses of samples from section N100 in wt% and ppm. Codes used for different ore types: M = Mamatwan-type ore; BII = braunite II-type ore; H = hausmannitic ore; B = secondary braunite ore and F = ferruginized ore. Codes for the different analyses are: SAM = Samancor; MIN = MINTEK.

Sample No.	Mn %	Fe %	Mn/Fe	SiO_2	CaO	CO_2	MgO	Al_2O_3	P_2O_5	K	Na	H_2O
N101(SAM) F	12.2	39.3	0.3	7.4	15.5		4.0					
N102(SAM) B	45.7	9.5	4.8	6.4	9.9		0.17					
N103(SAM)H	60.7	5.3	11.5	0.91	1.2		0.11					
N104(SAM)H	61.4	7.3	8.4	0.48	1.5		0.14					
N105(SAM)H	63.6	4.3	14.8	0.90	1.6		0.13					
N106(SAM)H	55.0	5.2	10.6	2.7	6.3		1.5					
N107(SAM)H	62.6	5.5	11.4	0.90	0.61		0.24					
N108(SAM)BII	54.0	7.5	7.2	5.4	9.5		0.15					
N109(SAM)H	60.2	5.5	10.9	3.0	4.3		0.13					
N110(SAM)BII	55.9	8.5	6.6	3.9	1.4		0.23					
N111(SAM)H	62.6	4.8	13.0	1.1	0.84		0.34					
N112(SAM)H	59.6	5.3	11.2	2.7	2.7		0.6					
N113(SAM)BII	52.9	4.9	10.8	7.2	5.5		2.2					
N114(SAM)H	60.8	6.2	9.8	1.8	0.31		0.19					
N115(SAM)BII	57.1	4.5	12.7	4.4	5.1		0.72					
N116(SAM)BII	49.9	6.5	7.7	16.2	5.3		10.9					
N117(SAM)BII	54.9	6.1	9.0	6.3	3.1		0.24					
N118(SAM)BII	52.7	5.3	9.9	9.6	2.4		0.03					
N119(SAM)M	44.2	5.3	8.3	5.8	9.4		1.4					
N119(MIN) M	44.0	5.1	8.6	7.3	8.8	7.5	1.5	*	485	17.3	100	0.1

*Values below 0,5 wt%
N.D = not determined

The SiO_2-contents increase towards the ferruginized zone, through samples N102 and N101 (up to 7,4 wt percent; Table 7.1), most probably because of the second generation of braunites present here. The erratic behavior of SiO_2 from

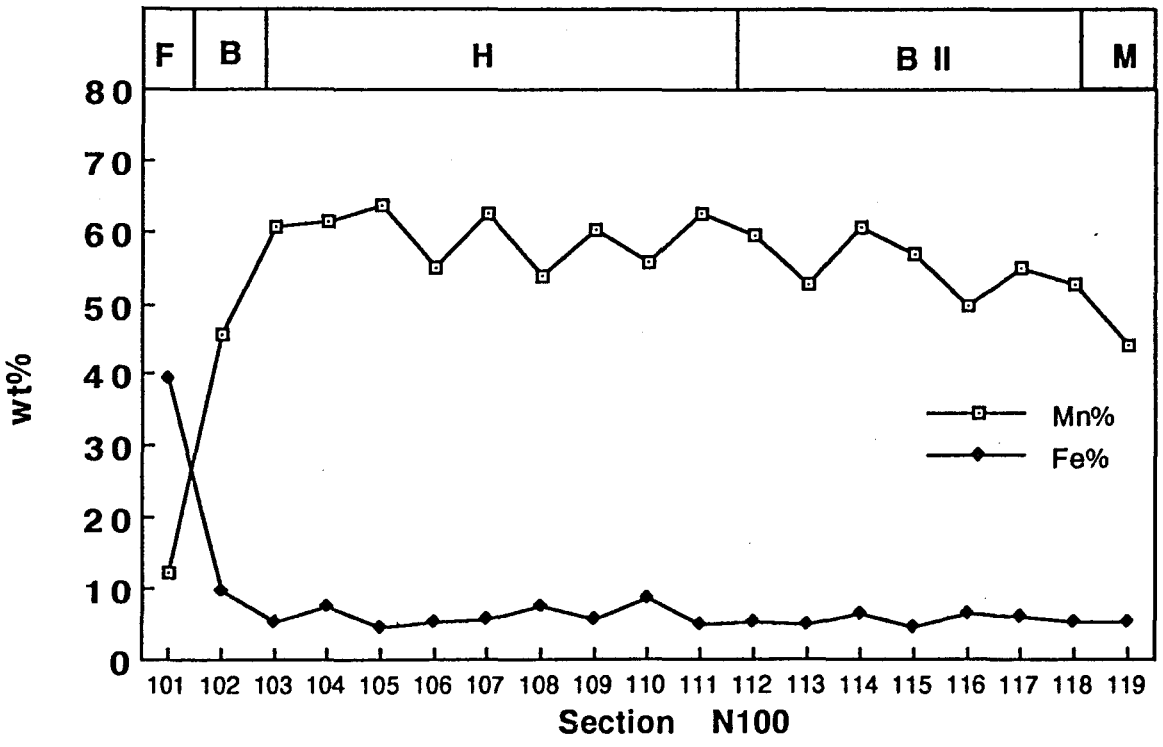

Figure 7.1 Mn and Fe contents of manganese ore along section N100.

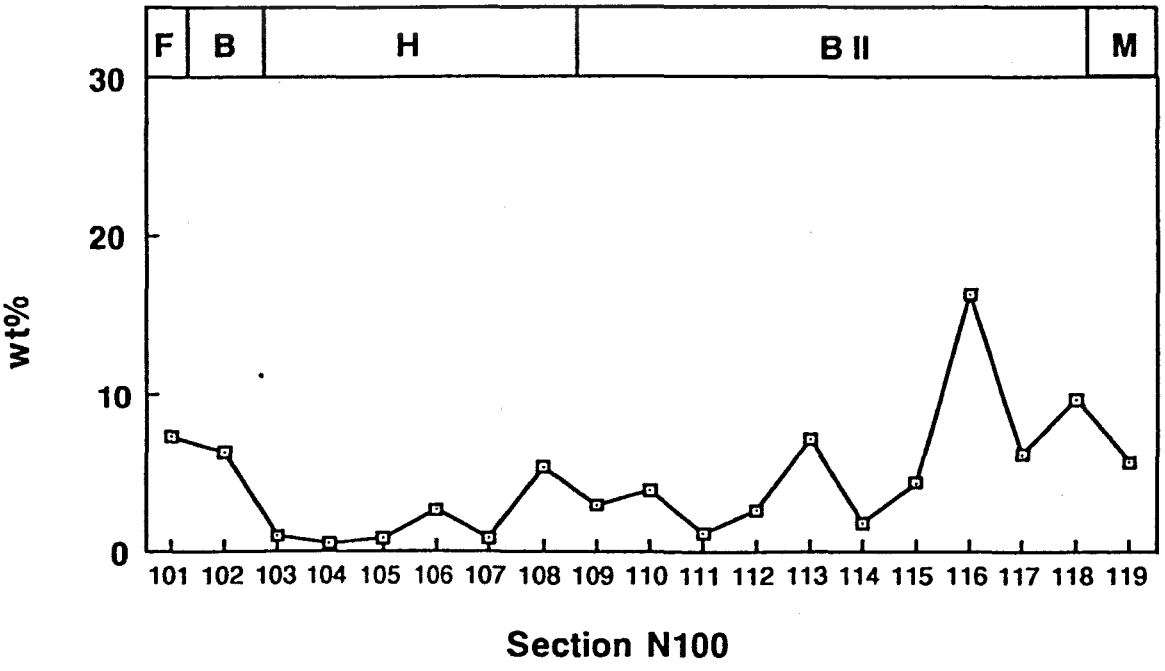

Figure 7.2 SiO_2-contents of manganese ore along section N100.

samples N108 - N118, in hausmannite rich and braunite II-type ore, is probably related to the braunite and andradite content of the ore. Low SiO_2 values can be ascribed to high-grade hausmannite-rich ore, with only gangue manganese silicates present. The higher peaks of SiO_2 indicate samples in which there are still braunite present, as is the case in samples N115 - N119, or because of andradite occurring as secondary gangue mineral in the ores. The high SiO_2 peak at sample N116 correlate with a high MgO peak (Fig. 7.4), this is probably due to the presence of clinochlore in the ore, also reported by XRD analyses.

The CaO content of the samples of Wessels-type ore range between 1,2 and 9,5 wt percent (samples N103 - N118) (the value of 9,5 wt percent CaO (sample N108) is very high for Wessels-type ore, the possibillity exists that a large calcite vug or joint was present in the sample submitted for chemical analyses). The CaO-content is up to 15, 5 wt percent in the ferruginized zone (sample N101) and 9,4 wt percent in Mamatwan-type ore (sample N119) (Fig. 7.3). In the hausmannite-rich, high-grade Wessels-type ore, the values are generally low (between 1,2 - 6 wt percent), with a few high peaks (6,3 - 9,5 wt percent; Table 7.1). The latter is ascribed, as previously mentioned, to the presence of calcite filled veinlets and vugs and to the gangue minerals gaudefroyite and andradite. Most of the high CaO peaks overlap with high peaks of SiO_2 (Fig. 7.3) which is an indication of the presence of andradite in the ore, for instance sample N113 which displays the "mottled" andradite ore texture (Pl. 5.4) and also high SiO_2 and CaO contents.

MgO-values in Wessels-type ore of section N100 (Fig. 7.4) are in general very low (< 0,2 wt percent; Table 7.1) with a few high peaks (1,5 - 10,9 wt percent; Table 7.1). The latter is due to the presence of clinochlore and especially brucite in the ore. The MgO-contents increase to 4 wt percent in the ferruginized zone and to 1,4 wt percent in the Mamatwan-type ore where kutnahorite occurs as matrix mineral.

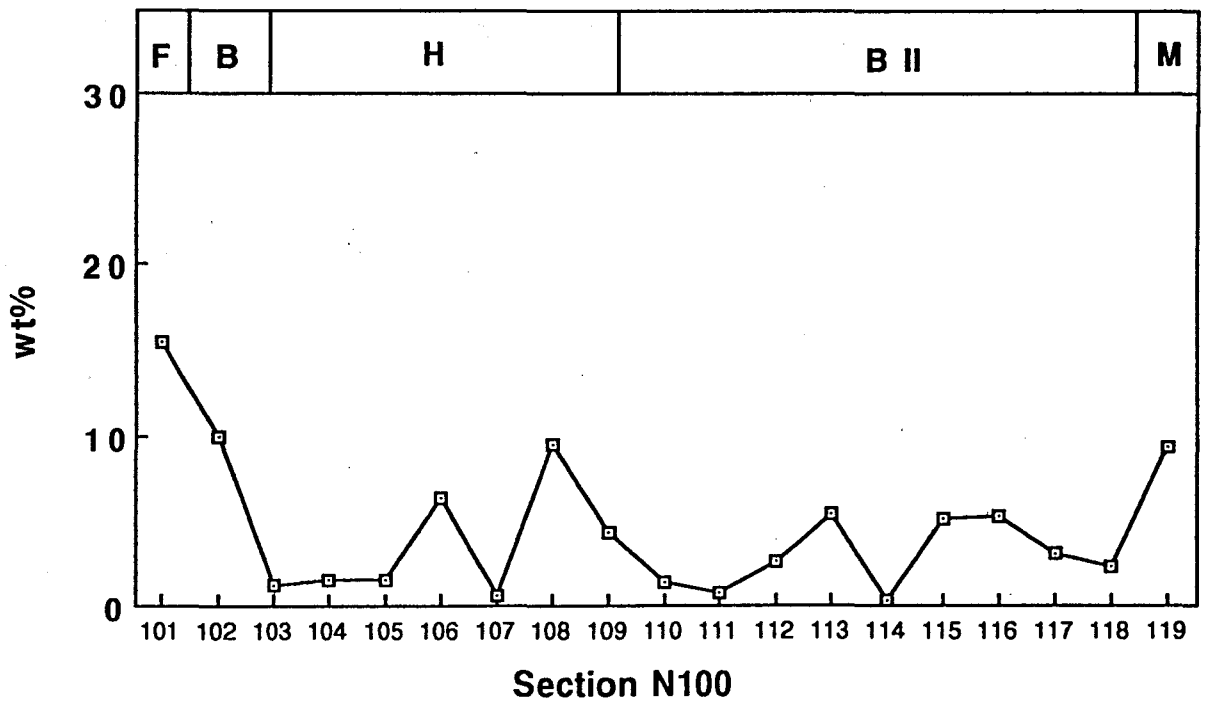

Figure 7.3 CaO-contents of manganese ore along section N100.

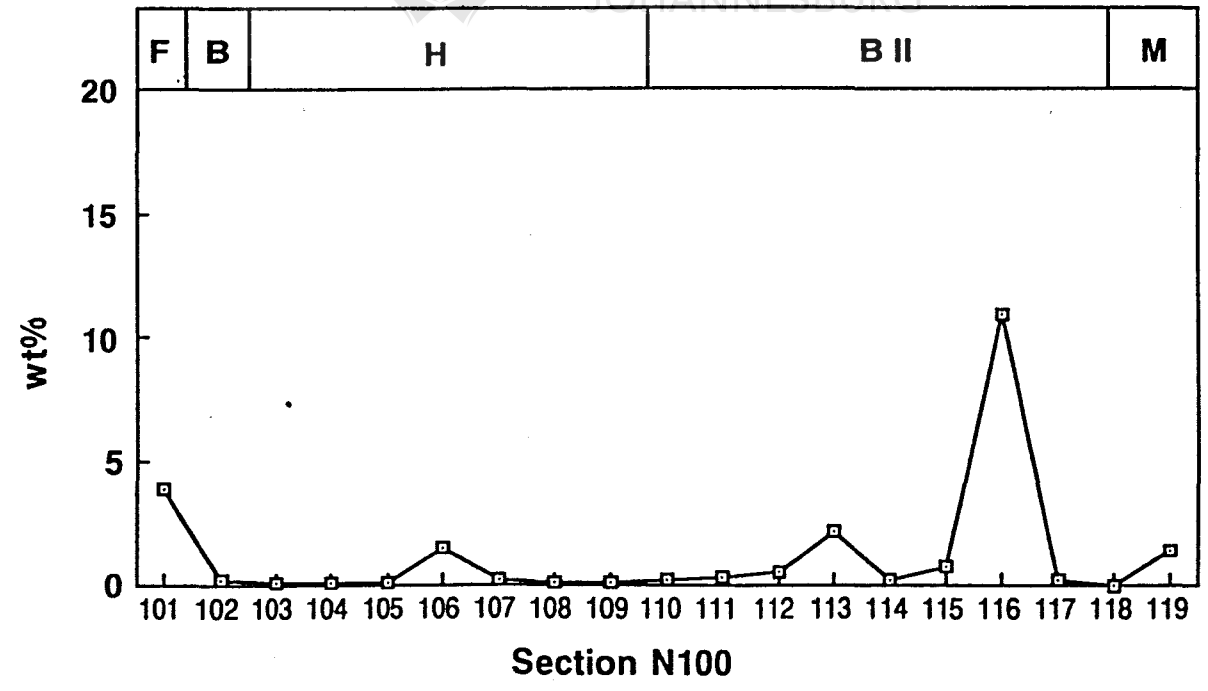

Figure 7.4 MgO-contents of manganese ore along section N100.

7.2.2 SECTION N200

Along section N200 the Mn-contents display high values of between 51 and 64 wt percent, i.e. high-grade WH-type ore (Table 7.2, Fig. 7.5). It should be noted that the low 47,6 wt percent Mn value of sample N207 as determined by Samancor, is determined by MINTEK analysis as 55,6 wt percent (Table 7.2), which is possibly the more accurate value. Highest Mn-contents (>60 wt% Mn) are present in the hausmannite-rich part of the Wessels-type ore, next to the ferruginized zone. It shows a slight decrease to values below 60 wt percent on the border with the ferruginized zone in the secondary braunite-rich ore (samples N202 and N201).

Table 7.2. Bulk rock XRF analyses of samples from section N200 in wt percent and ppm. Codes used for different ore types: M = Mamatwan-type ore; BII = braunite II-type ore; H = hausmannitic ore; B = secondary braunite ore and F = ferruginized ore. Codes for the different analyses are: SAM = Samancor; MIN = MINTEK.

Sample No.	Mn %	Fe %	Mn/Fe	SiO_2	CaO	CO_2	MgO	Al_2O_3	P_2O_5	K	Na	H_2O
N201(SAM) B	51.4	4.7	10.9	6.9	12.2		0.31					
N201(MIN) B	49.2	5.8	8.5	8.1	6.5	4.5	*	*	365	13	94	0.2
N202(SAM)B	58.8	6.3	6.2	5.7	22.9		1.9					
N202(MIN)B	62.3	7.6	8.2	4.4	14.6	10.1	1.2	*	616	38.6	302	*
N203(SAM)H	63.6	4.7	13.5	4.5	1.2		0.7					
N203(MIN)H	66.8	5.1	13.1	3.8	3.0	0.5	*	*	528	14.4	286	*
N204(SAM)H	62.5	5.2	12.0	1.3	1.7		0.08					
N204(MIN)H	60.2	3.5	17.2	0.7	2.2	1.5	*	*	519	15.1	170	0.1
N205(SAM)H	60.2	6.9	8.7	4.2	2.4		0.01					
N205(MIN)H	47.8	7.4	6.5	3.5	3.4	0.5	*	*	674	10	171	0.1
N206(SAM)BII	52.8	4.9	10.8	10.3	9.1		3.1					
N206(MIN)BII	49.1	3.8	12.9	10.0	7.5	3.3	2.6	0.9	397	13	120	*
N207(SAM)BII	47.6	7.1	6.7	3.8	3.1		14.5					
N207(MIN)BII	55.6	6.3	8.8	3.8	4.1	0.5	8.0	*	802	10	600	*
N208(SAM)BII	54.2	5.2	10.4	4.6	0.88		0.54					
N208(MIN)BII	55.7	4.8	11.6	4.7	6.9	1.6	*	*	312	3	60	0.1
N209(SAM)BII	52.7	6.3	8.4	3.3	7.6		2.3					
N209(MIN)BII	54.4	5.5	9.9	3.1	6.6	2.0	1.3	*	816	14.2	209	*
N210(SAM)BII	51.8	5.5	9.4	10.3	2.9		0.65					
N210(MIN)BII	53.9	4.8	11.2	11.7	5.0	0.5	*	*	490	9	199	*

*Values below 0,5 wt%
N.D. = not determined

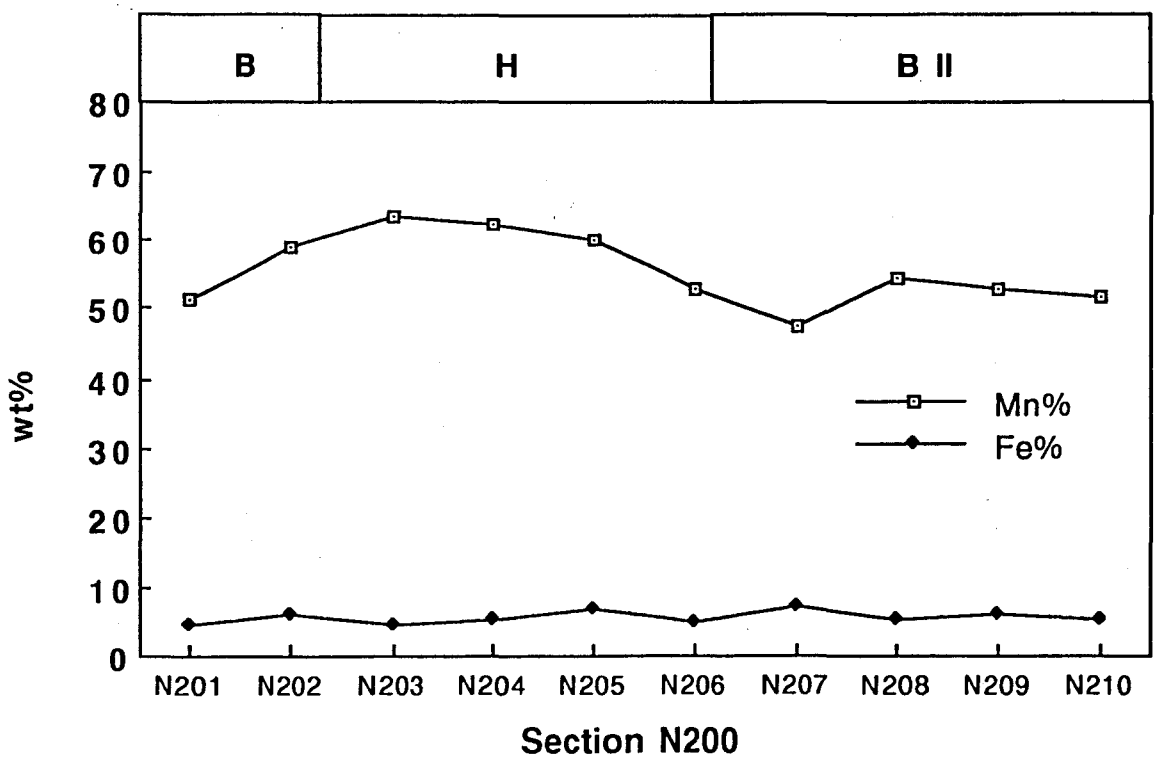

Figure 7.5 Mn and Fe contents of manganese ore along section N200.

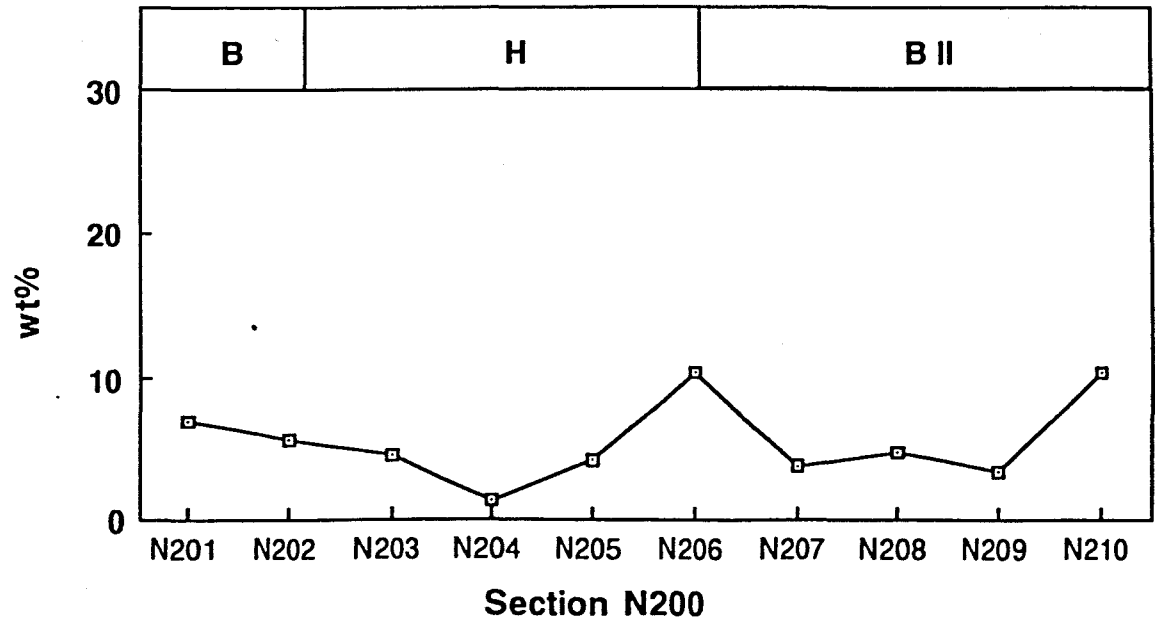

Figure 7.6 SiO_2-contents of manganese ore along section N200.

Hausmannite-rich high-grade ore (samples N203 to N205), displays a decrease in Mn-values into the lower grade, braunite II-rich ore more distal to the ferruginized zone, to values below 55 wt percent Mn (samples N206 - N210). The Fe-content shows no trend and stays rather constant throughout the section, ranging from 3,5 - 7,4 wt percent (Table 7.2 and Fig. 7.5).

The SiO_2-contents of samples from section N200 (Fig. 7.6) display low values of 0,7 - 4,5 wt percent in the high-grade hausmannite-rich ore (samples N203 - N209), except for sample N206 (10,8 wt percent; Table 7.2). Higher SiO_2 values of between 4,4 and 8,1 wt percent are present in the lower grade secondary braunite-rich ores bordering the ferruginized zone (samples N201-N202), and in braunite II-rich ores (sample N210) distal to the ferruginized zone. These higher SiO_2 values are associated with the braunite-group minerals present in the ores, as well as the presence of minerals such as clinochlore and andradite. Clinochlore is probably responsible for the high peak of 10,3 wt percent SiO_2 in sample N206, as it was indictaed to be present during XRD analyses (Fig. 4.2). The hausmannite-rich ores from sample N203 to N209 are depleted in SiO_2, because of the absence of the previously mentioned silicate phases, especially proximal to the ferruginized zone.

The CaO-contents of samples from section N200 (Fig. 7.7) display the same trend as the SiO_2-contents, where low values (0,88 - 4,1 wt percent; Table 7.2) occur in the hausmannite-rich ore and higher values (6,5 - 14,6 wt percent, Table 7.2) are associated with the secondary braunites bordering the ferruginized zone. The CaO content of sample N206 corresponds to a peak of CO_2 (3,3 percent), indicating the presence of calcite. The high CaO contents of samples N202 (14,6 wt percent according to MINTEK analysis) and N209 (7,6 wt percent) probably reflect the presence of calcite and gaudefroyite.

MgO-values from samples along section N200 (Fig. 7.8) are in general very low (<3,1 wt percent), except for in sample N207 (8 wt percent), which may be ascribed to the presence of brucite in the ore.

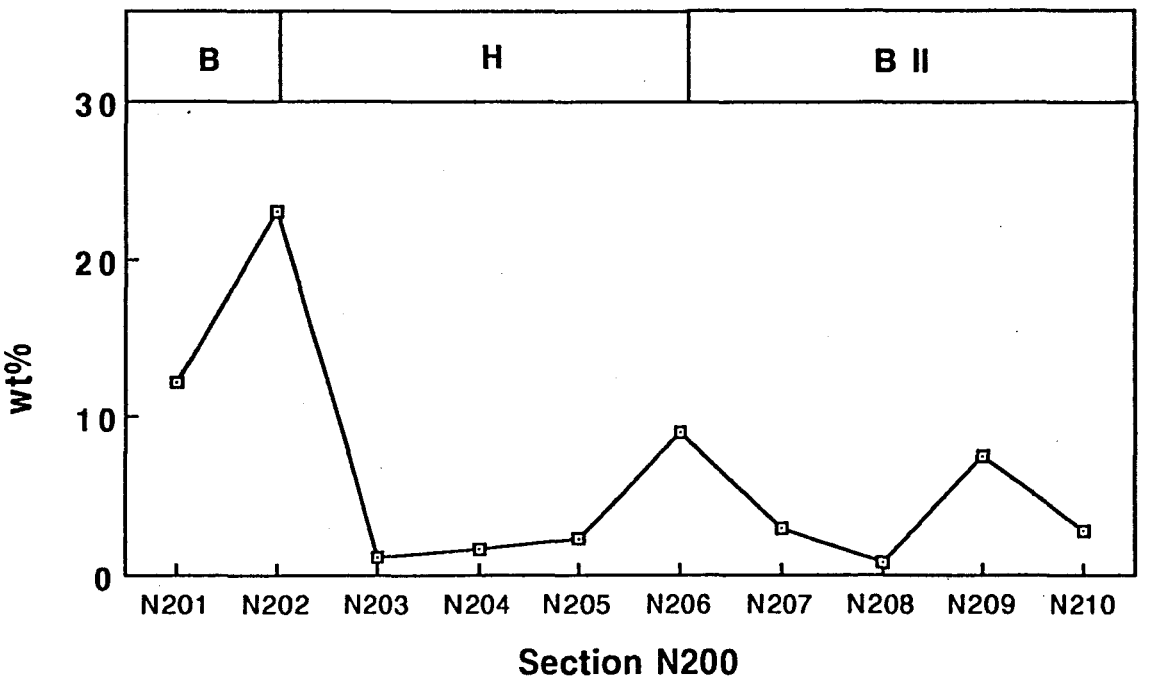

Figure 7.7 CaO-contents of manganese ore along section N200.

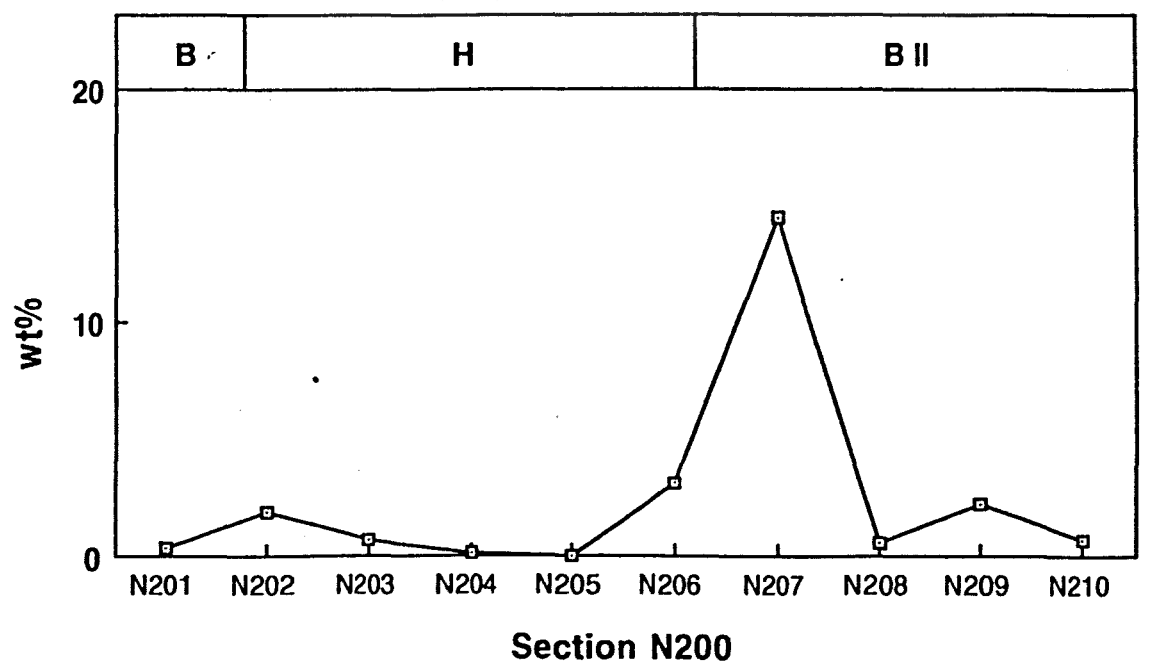

Figure 7.8 MgO-contents of manganese ore along section N200.

7.2.3 SECTION N300

Along section N300 high-grade hausmannite-rich ore (sample N220), with a Mn-content of 55,3 wt percent (Table 7.3), grades over into secondary braunite-rich ore (samples N230 - N222) more proximal to the ferruginized zone, with Mn-values ranging between 46,1 and 48,9 wt percent (Table 7.3 and Fig. 7.9). The ferruginized ore (samples N223 to N229) contains 0,1 - 0,7 wt percent Mn and 58,1 - 67,7 wt percent Fe (Table 7.3 and Fig. 7.9). Fe-values stay below 8 wt percent in the high-grade ore (samples N220 - N221; Table 7.3) and increase up to 10,3 wt percent on the border with the ferruginized zone (sample N222) (Table 7.3 and Fig. 7.5). Of interest is the fact that the Fe-content of sample N222, which represent mineable ore, is 10 wt percent. This may be due to the high Fe-content present in manganese oxides (hausmannite, braunite II and braunite) on the border with the ferruginized zone. It must again be noted that the ferruginized zone in this section may in actual fact represent the lower part of the manganese bed at Wessels. Reasons are that the ore marker could not be identified during sampling and samples may have been taken at a lower level in the ore bed.

Table 7.3. Whole rock XRF analyses (wt percent and ppm) of samples from section N300. Codes used for different ore types: H = hausmannitic ore; B = secondary braunite ore and F = ferruginized ore. Codes for the different analyses are: SAM = Samancor; MIN = MINTEK.

Sample No.	Mn %	Fe %	Mn/Fe	SiO_2	CaO	CO_2	MgO	Al_2O_3	P_2O_5	K	Na	H_2O
N220(SAM)H	55.3	6.9	8.01	0.97	4.8	1.1						
N230(SAM)B	46.1	7.5	6.15	0.86	6.4	0.29						
N221(SAM)B	48.9	2.8	17.46	8.2	11.2	0.82						
N221(SAM)B	48.5	2.6	18.7	7.8	11.4	3.1	0.8	0.6	462	2	52	*
N222(SAM)B	46.7	10.3	4.53	6.5	8.9	1.9						
N223(SAM)F	0.3	58.1	0.005	7.8	4.9	2.9						
N223(MIN)F	0.4	60.1	0.007	5.2	4.0	2.9	2.5	*	808	172	302	0.2
N224(SAM)F	0.7	66.6	0.011	0.87	0.19	0.05						
N224(MIN)F	0.4	70.1	0.006	0.5	1.24	1.2	*	*	606	11.7	91	0.1
N225(SAM)F	0.2	67.9	0.003	0.88	1.6	0.09						
N226(SAM)F	0.1	67.7	0.001	2.6	0.67	0.18						
N227(SAM)F	0.5	62.3	0.008	3.1	1.3	0.10						
N229(SAM)F	0.2	60.6	0.003	29.5	7.0	0.12						

*Values below 0,5 wt%
N.D. = not determined

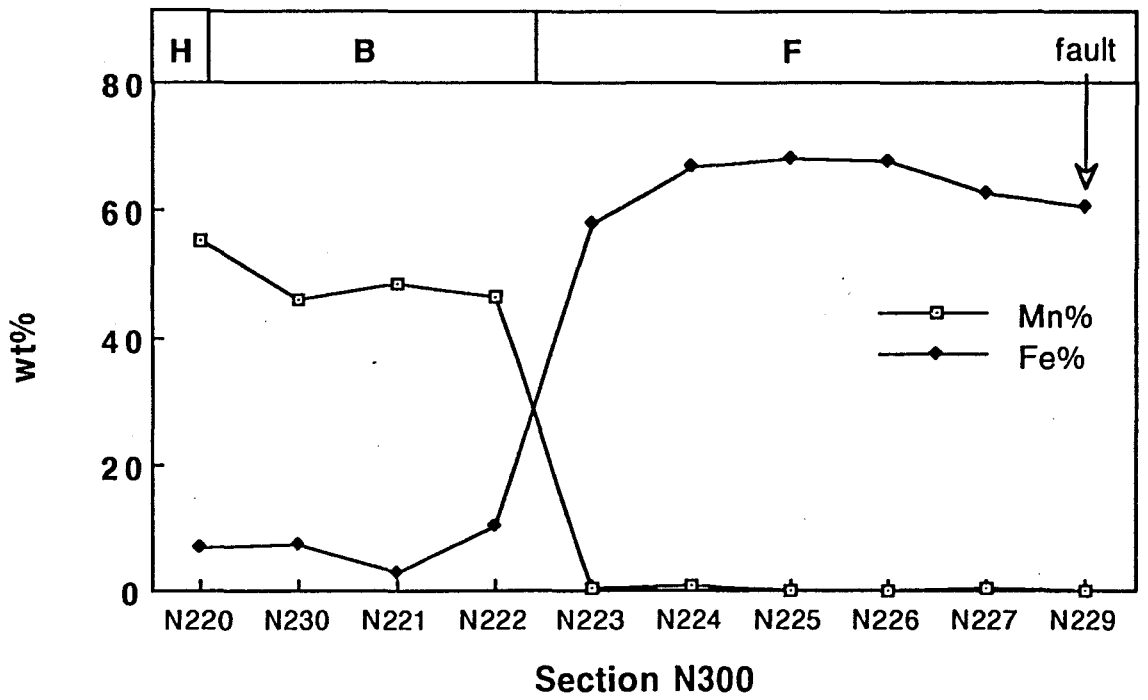

Figure 7.9 Mn and Fe contents of manganese ore along section N300.

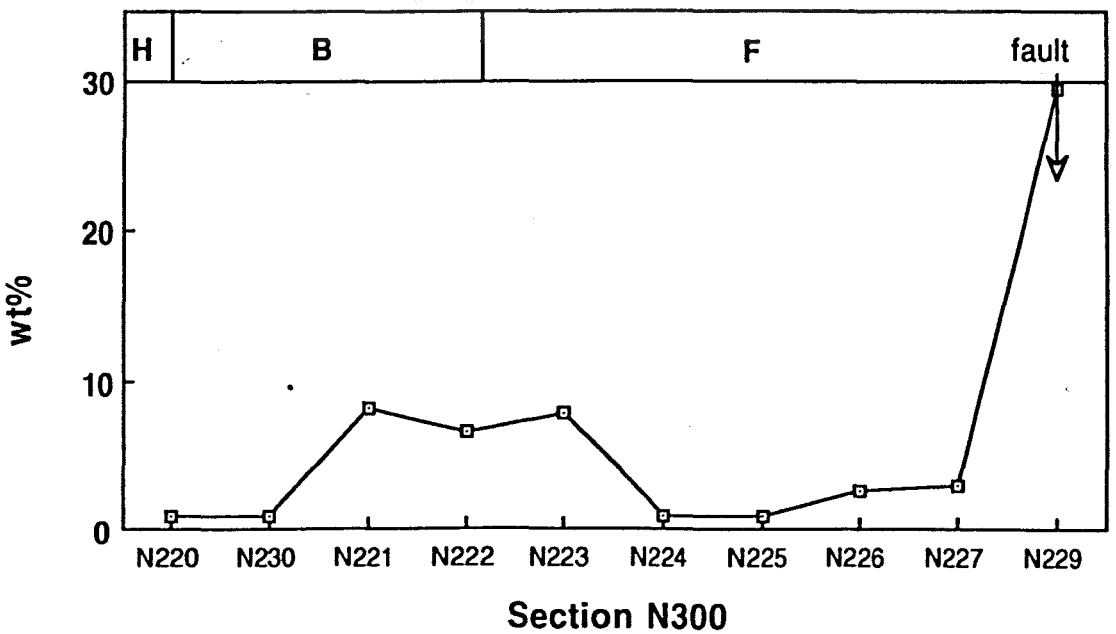

Figure 7.10 SiO_2-contents of manganese ore along section N300.

The SiO_2-contents of samples along section N300 (Fig. 7.10) in the higher grade ore (samples N220 and N230) display low values (<1 wt percent SiO_2), which increase to >6 wt percent in the secondary braunite-rich ore bordering the ferruginized zone (samples N221 - N223). The ferruginized zone (samples N224 - N227) displays very low SiO_2-contents (between 0,88 - 3,1 wt percent; Table 7.3), because the samples consist primarily of hematite and trace amounts of calcite. Sample N229 displays an anomalously high SiO_2-value (29,5 wt percent), this sample display botyroidal texture in hematite (Pl.3.8). No XRD analyses were done on this sample and therefore it is speculated that the anomaly may be caused by andradite, or even chert present in the sample.

The CaO-contents of samples along section N300 (Fig 7.11) display low values (between 4,8 and 6,4 to 11 wt percent CaO; Table 7.3) in the high-grade ore (samples N220 - N230). It increases in the secondary braunite-rich ore bordering the ferruginized zone (samples N221 and N222). This is the result of calcite veins and vugs present in the ore. Low values occur in the ferruginized zone where the ore consists mainly of hematite. Numerous calcite filled vugs occur in the fault plane (sample N229). The CO_2 value for this sample is low (0,12 wt %) and the high CaO contents of 7,0 wt percent in sample N229. is therefor speculated to be related to the presence of andradite.

The two MgO-values observed are relatively low (<3 wt percent) compared to sections N100 and N200, with one relatively high value (2,5 wt percent) observed in sample N223 in the ferruginized ore (Fig. 7.12). This is probably due to the presence of clinochlore in the ore, as analyses indicate the presence of Al_2O_3 (below 0,5 wt%). The ferruginized zone (samples N224 - N229) along the fault plane display MgO-values of below 0,2 wt percent (Fig. 7.12).

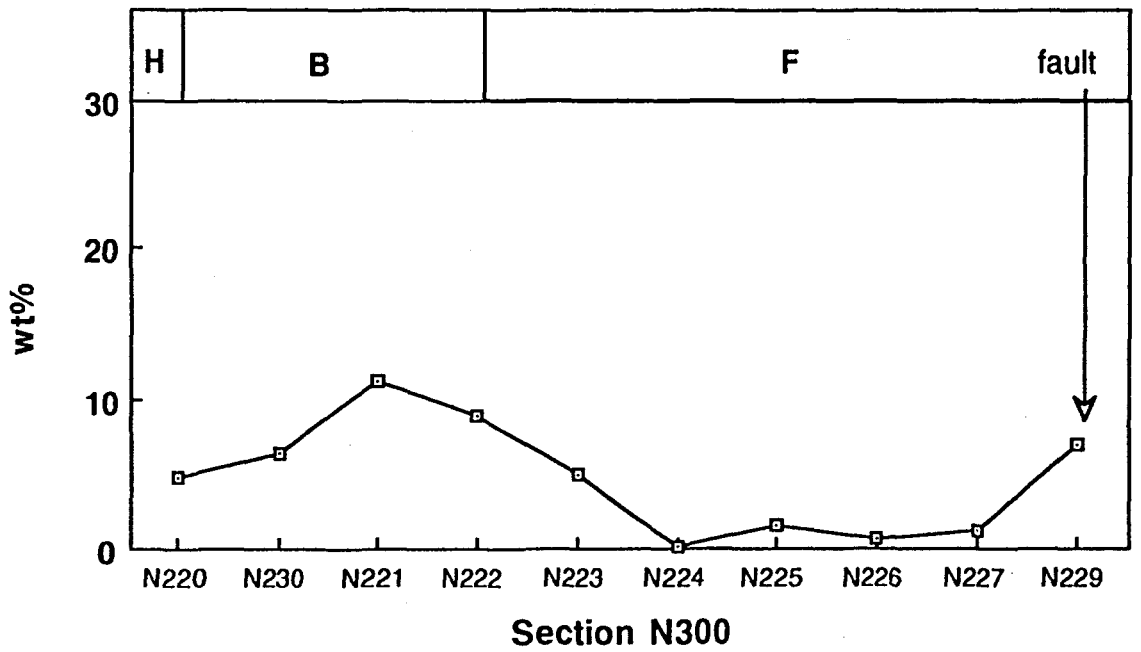

Figure 7.11 CaO-contents of manganese ore along section N300.

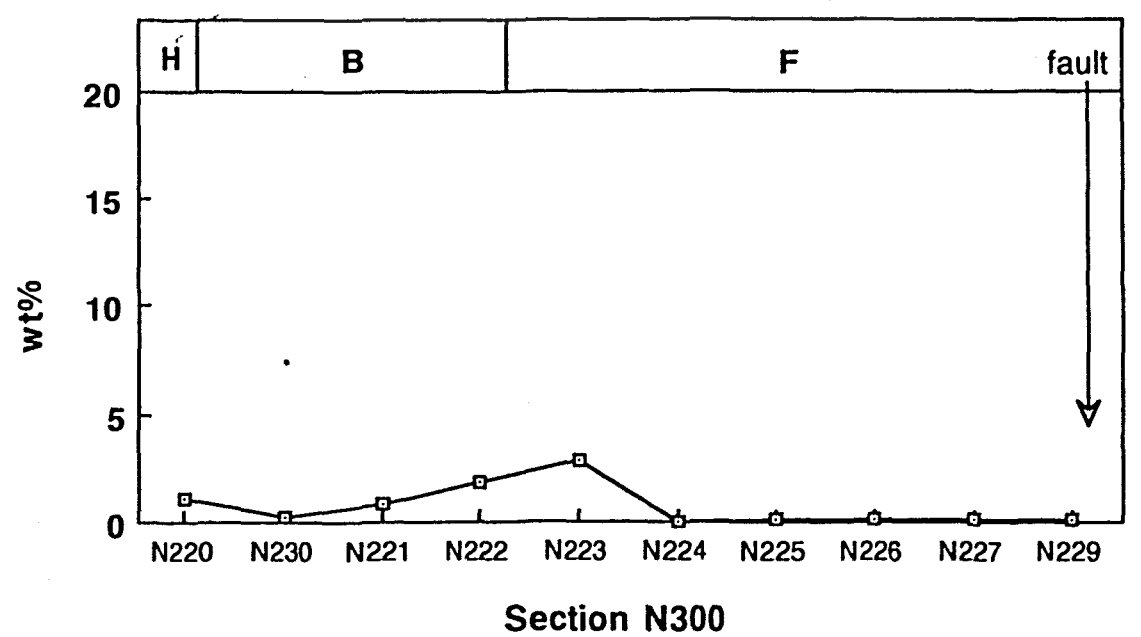

Figure 7.12 MgO-contents of manganese ore along section N300.

7.2.4 SECTION N500

High-grade hausmannite-manganite-rich ore occurs in the most southern (samples N501 to N502) and most northern parts (samples N511 to N512) of section N500, distal to the "fault zone". Mn-values range between 47,2 and 62,6 wt percent in the hausmannite- and manganite-rich ore (Table 7.4). Secondary braunite-rich ore, with Mn contents of between 41,8 and 48 wt percent, occurs adjacent to the fault zone (samples N503, N504, N509 and N510). The Fe-contents of the Mn ores adjacent to the fault zone, remain low between 5,7 and 10,3 wt percent and increase to 15,7 wt percent in the fault zone (samples N508 and N505). In the centre of the fault zone the iron content is very low at 0,7 wt percent Fe (sample N506; Fig. 7.13 and Table 7.4). The Mn/Fe ratio values of the ores in the fault zone (samples N505 to N508) are too low for mining (between 0,2 and 2,3; Table 7.4). Immediately adjacent to the fault zone (sample N509), the manganese ore contains a higher Fe content of 10,3 wt percent (Fig. 7.13). This may again be related to the relatively high Fe-contents present in the manganese oxides (hausmannite, braunite II and braunite) adjacent to the ferruginized zone (refer to chapter 6).

Table 7.4. Whole rock XRF analyses (wt percent) of samples from section N500. Codes used for different ore types:BII = braunite II-type ore; H = hausmannitic ore.

Sample No.	Mn %	Fe %	Mn/Fe	SiO_2	CaO	MgO
N501 BII	47.2	7.0	6.7	1.3	16.6	0.85
N502 BII	49.7	8.2	6.1	3.5	6.5	5.4
N503 BII	41.8	5.7	7.3	1.4	12.7	6.9
N504 BII	48.0	6.7	7.2	1.9	10.5	0.2
N505	3.7	15.7	0.2	47.2	1.6	0.3
N506	1.6	0.7	2.3	71.9	0.4	2.3
N507	3.6	1.7	2.1	68.4	1.2	0.2
N508	2.4	13.2	0.2	32.5	4.5	0.1
N509 BII	43.6	10.3	4.2	4.4	7.7	1.4
N510 BII	42.2	6.9	6.1	1.5	14.0	0.4
N511 H	61.6	3.9	15.8	2.4	1.4	1.4
N512 H	53.1	4.3	12.3	1.0	4.7	0.3

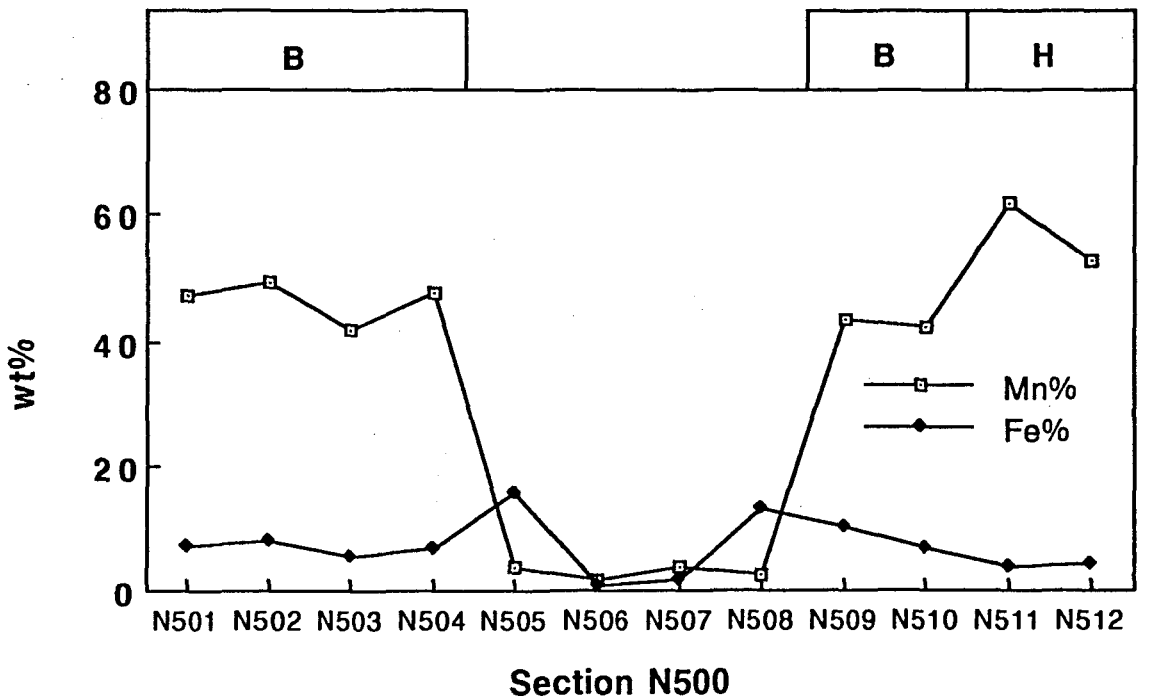

Figure 7.13 Mn and Fe contents of manganese ore along section N500.

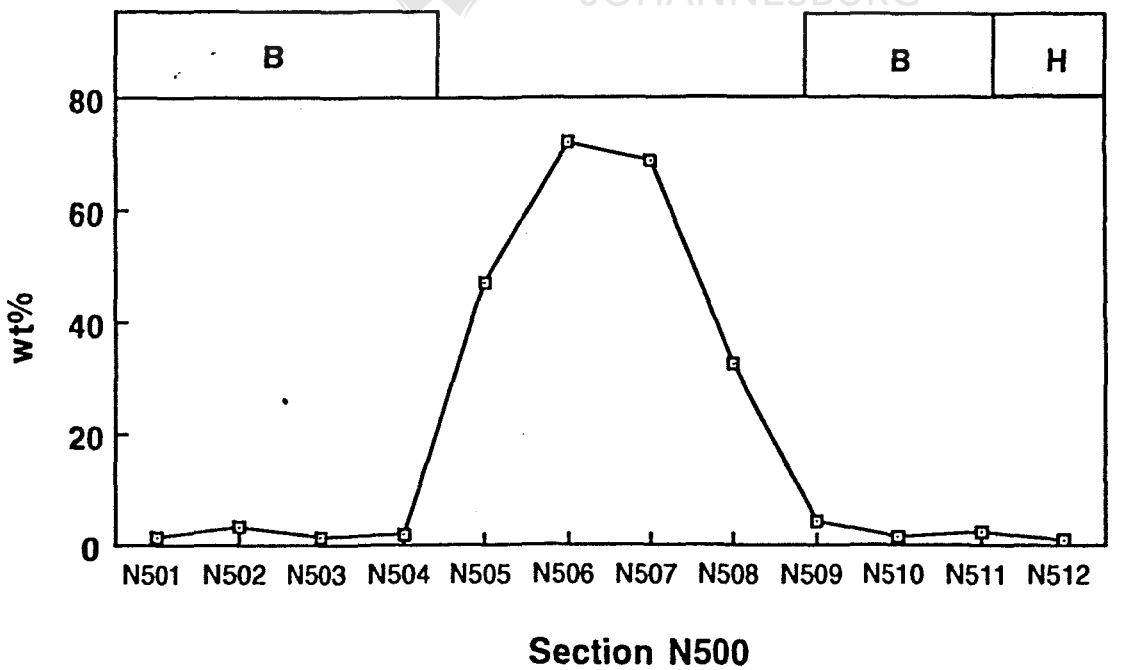

Figure 7.14 SiO_2-contents of manganese ore along section N500.

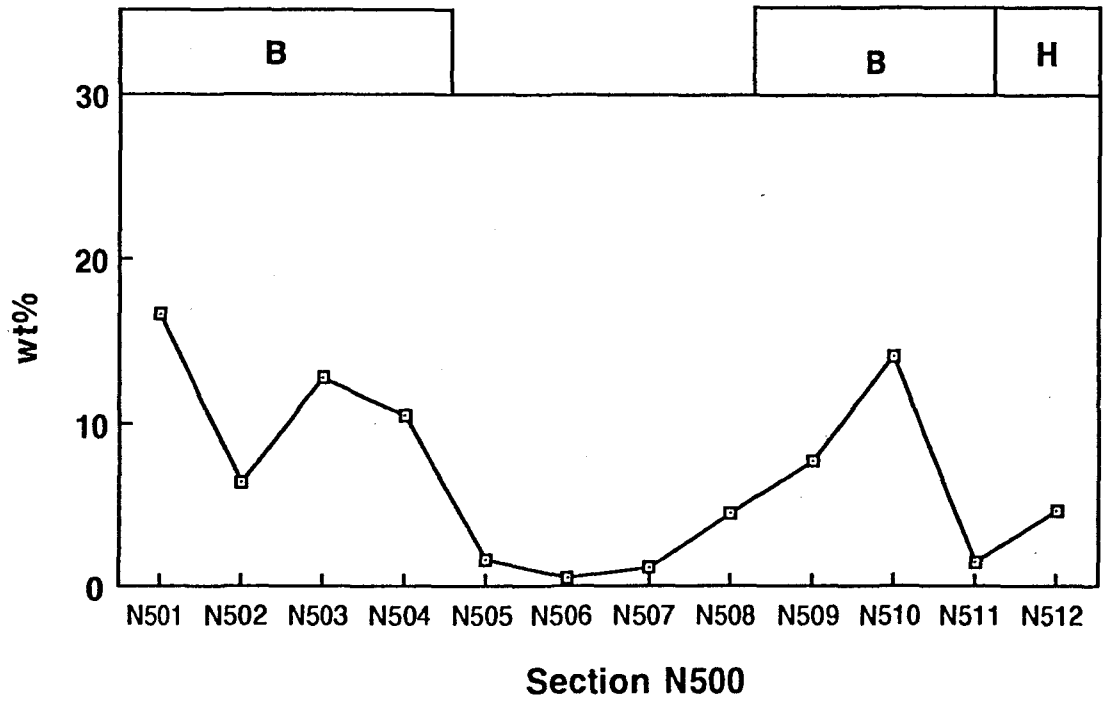

Figure 7.15 CaO-contents of manganese ore along section N500.

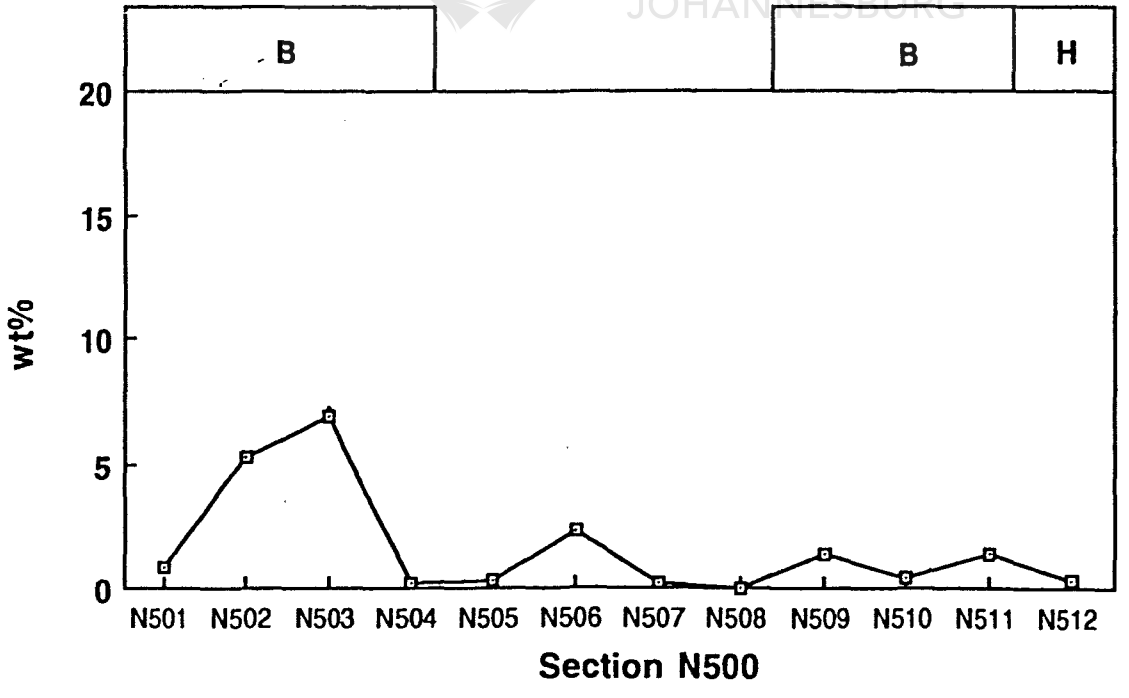

Figure 7.16 MgO-contents of manganese ore along section N500.

The SiO_2-contents of samples from section N500 (Fig. 7.14) display very high values of up to 70 wt percent inside the "fault zone" (samples N505 - N508). This is due to the presence of quartz and Mn-diopside in the fault zone. The SiO_2 contents in the high-grade secondary braunite-rich and hausmannite-rich ores adjacent to the fault zone are low (samples N501 - N504 and N509 - N512) i.e. between 1 and 4,4 wt percent.

The CaO-contents of samples from section N500 (Fig. 7.15) are low in the "fault zone" (0,4 - 4,5 wt percent in samples N505 - N508). These low values could be explained by the absence of calcite, andradite and gaudefroyite in the samples. In contrast the high values (14,0 and 16,6 wt percent) present in the surrounding high-grade ore (samples N501 and N510) are indicative of the presence of gaudefroyite and andradite in the ore as vein or vugfilling.

The MgO-contents for samples from section N500 are low (Fig. 7.16), compared to that in sections N100 and N200. Exceptions are samples N502 and N503 in the high-grade ore with MgO values of 5,4 and 6,9 wt percent (Fig. 7.16). These values reflect the presence of clinochlore and/or brucite in the samples.

7.3 MODEL OF LATERAL VARIATION IN CHEMICAL COMPOSITION

Fourteen samples, chosen to represent an idealized section from low-grade Mamatwan-type ore, through high-grade Wessels-type ore into the ferruginized ore associated with the north-south trending fault zone, are used to give a model of lateral variation in major element concentrations. The samples used for the model are: N119, N210, N209, N208, N207, N206, N205, N204, N203, N202, N221, N201, N223, N224 (Table 7.5). Sample positions relative to an idealized section are shown in figure 7.17.

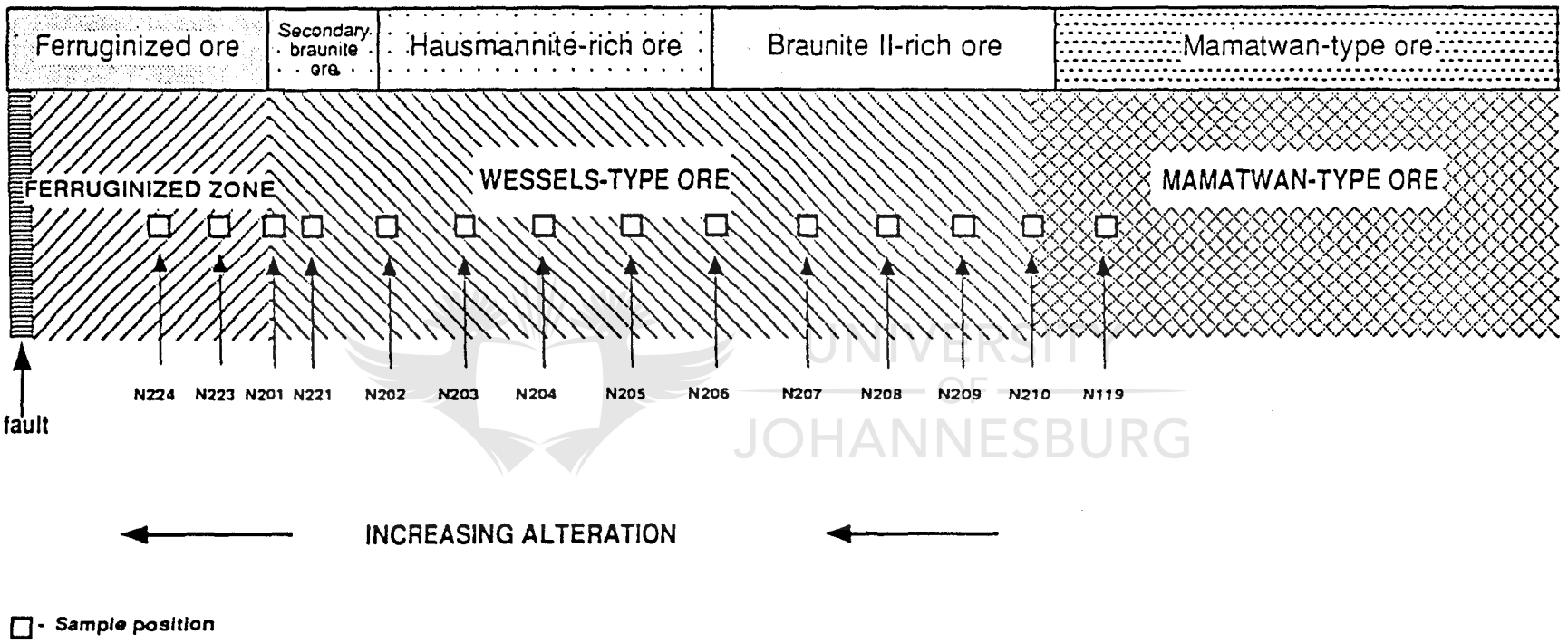

Figure 7.17. Sample positions of an idealized section, sampled from the ferruginized zone associated with a normal fault, through high-grade Wessels-type ore, into low-grade Mamatwan-type ore.

Table 7.5. Bulk rock chemical composition of samples (wt percent and ppm) used to construct an idealized section. Codes used for different ore types: M = Mamatwan-type ore; BII = braunite II-type ore; H = hausmannitic ore; B = secondary braunite ore and F = ferruginized ore. All analyses were done by MINTEK.

Sample No.	Mn %	Fe %	Mn/Fe	SiO_2	CaO	CO_2	MgO	Al_2O_3	P_2O_5	K	Na	H_2O
									ppm	ppm	ppm	
N119 M	44.1	5.1	8.6	7.31	8.83	7.5	1.45	*	485	17.3	100	0.1
N210 BII	53.90	4.80	11.2	11.7	4.95	0.5	*	*	490	9	199	*
N209 BII	54.40	5.50	9.9	3.1	6.62	2.0	1.34	*	816	14.2	209	*
N208 H	55.70	4.80	11.6	4.66	6.87	1.6	*	*	312	3	60	0.1
N207 H	55.60	6.30	8.8	3.78	4.10	0.5	8.01	*	802	10	600	*
N206 H	49.10	3.8	12.9	9.99	7.48	3.3	2.6	0.88	397	13	120	*
N205 H	47.8	7.4	6.46	3.46	3.41	0.5	*	*	674	10	171	0.1
N204 H	60.2	3.5	17.2	0.66	2.17	1.5	*	*	519	15.1	170	0.1
N203 H	66.8	5.1	13.1	3.76	3.01	0.5	*	*	528	14.4	286	*
N202 H	62.3	7.6	8.2	4.37	14.6	10.1	1.2	*	616	38.6	302	*
N221 B	48.9	3.75	13.04	7.79	11.4	3.1	0.79	0.64	462	2	52	*
N201 B	49.2	5.8	8.5	8.06	6.53	4.5	*	*	365	13	94	0.15
N223 F	0.49	58.35	0.008	5.23	4.03	2.9	2.48	*	808	172	302	0.15
N224 F	0.50	66.6	0.008	0.53	1.24	1.2	*	*	606	11.7	91	0.1

* Values below 0.5 wt%

For purpose of comparison chemical analyses of typical Mamatwan-type ore and Wessels-type ore are given in Tables 7.6 and 7.7 respectively. The comparison indicates that sample N119 represents rather typical Mamatwan-type ore bordering braunite II-rich ore (compare Table 7.5 with Table 7.6). In contrast eleven of the samples represent Wessels-type ore i.e. samples N210 to N201 (compare Table 7.5 with Table 7.7). Two samples come from the ferruginized ore zone along faults (samples N223 and N224).

Table 7.6. Chemical analysis of typical Mamatwan-type ore (wt percent) (After Kleyenstüber, 1993).

Mn_2O_3 *	54.97
Fe_2O_3 *	4.75
SiO_2	4.07
CaO	12.62
MgO	3.17
CO_2	15.02
Al_2O_3	0.19
Mn/Fe	11.52

* Total manganese expressed as Mn_2O_3 .
* Total iron expressed as Fe_2O_3 .

Table 7.7. Chemical analysis of typical Wessels-type ore (wt percent) (After Kleyenstüber, 1993).

Mn_2O_3 *	65.76
Fe_2O_3 *	18.00
SiO_2	4.66
CaO	7.12
MgO	1.14
CO_2	2.13
Al_2O_3	0.26
Mn/Fe	3.63

Mn- and Fe-values display the same opposite trend as is the case for all four sections sampled and described above (Fig 7.18). Low Fe-values coincide with high Mn-values. Mamatwan-type ores display low Mn-values (<45 wt percent Mn) with Fe-contents of <6 wt percent. The Fe-contents stay relatively constant in Wessels-type ore, between about 4 - 6 wt percent Fe, with values increasing in the ferruginized zone to >60 wt percent.

The braunite II-rich ores, in the zone between Mamatwan-type ore and very high-grade hausmannite-rich Wessels-type ore, display Mn-contents of about 50-55 wt percent Mn. In the hausmannite-rich Wessels-type ore, more proximal to the ferruginized zone, the Mn-content is very high, between 60-67 wt percent Mn. This reflects the almost pure hausmannite-rich composition of the ores, with only minor gangue minerals such as andradite and calcite present. The secondary braunite-rich ore zone, on the border with the ferruginized zone, displays lower Mn-values of 45 - 50 wt percent. In the ferruginized zone, the Mn-content is <1 wt percent.

The Mamatwan-type ores display a silica-content of about 7 wt percent (Fig. 7.19), which decreases in the Wessels-type ore to <5 wt percent. High peaks of silica of up to about 10 wt percent is encountered in the braunite II- and

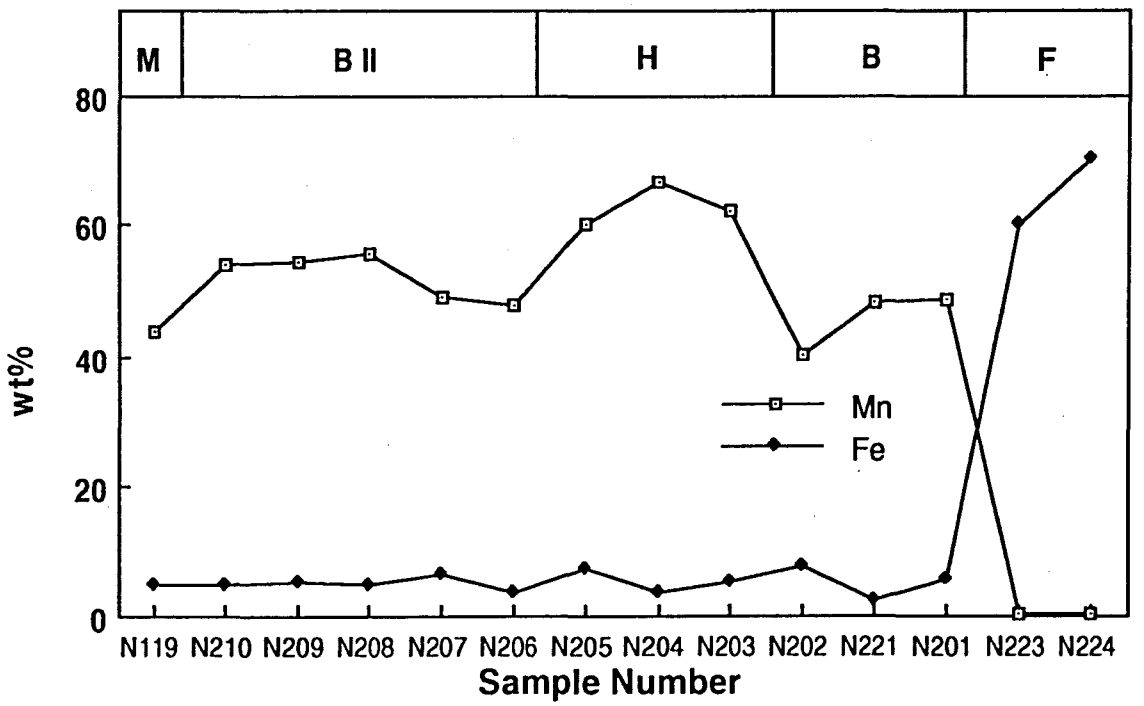

Figure 7.18 Mn and Fe contents of manganese ore along an idealized section.

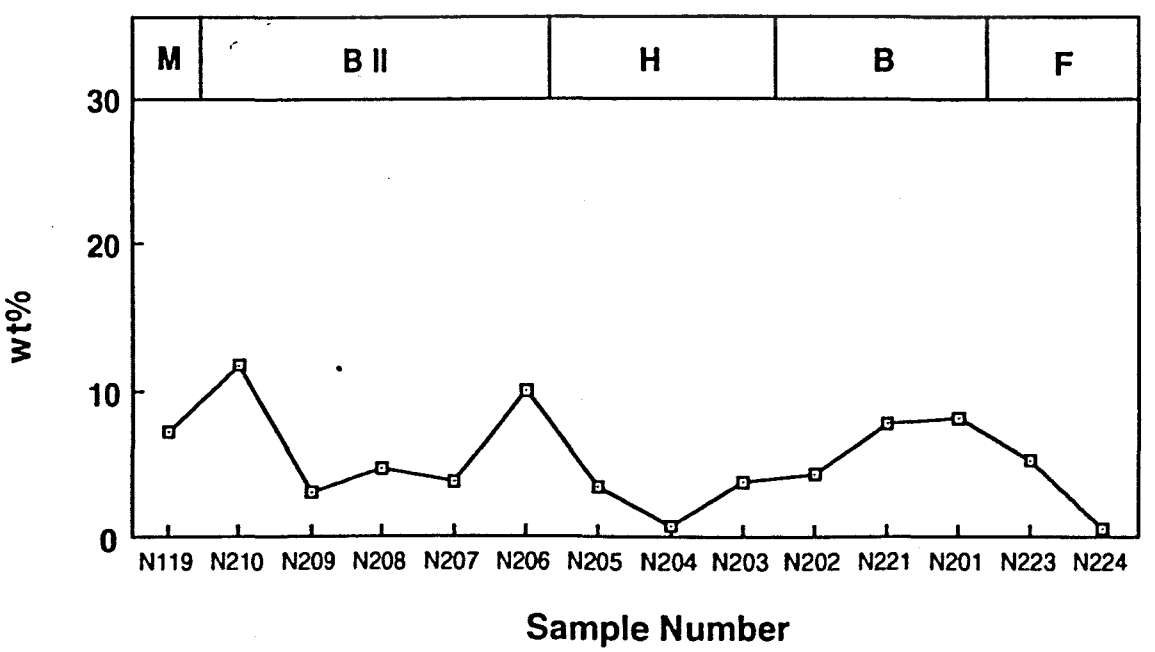

Figure 7.19 SiO_2-contents of manganese ore along an idealized section.

hausmannite-rich areas more distal to the ferruginized zone (Fig. 7.19), reflecting the presence of andradite and clinochlore as secondary minerals. Very low values of about 1 wt percent SiO_2 is encountered in the hausmannitic ore proximal to the ferruginized zone due to the pureness of the hausmannitic ore and the absence of braunites and gangue silicate minerals. An increase in the SiO_2-content of up to about 8 wt percent, is encountered in the zone of secondary braunite-rich ore on the border with the ferruginized zone. The silica-content of the ferruginized zone is mostly <1 wt percent, but higher values of up to 5 wt percent may occur. This is due to the presence of hydrothermal andradite and trace amounts of braunites.

The CaO and CO_2-values in the Mamatwan-type ore (Fig. 7.20) are in the order of 9 to 7 wt percent. In Wessels-type ore the CO_2-content decrease to less than 3 wt percent. The CaO-content decrease sympathetically, but to a lesser degree, because it is taken up in minerals such as braunite II and andradite. Slightly higher CaO and CO_2-values appear in the ferruginized zone (samples N202 and N221), where numerous calcite veins crosscut the ore.

MgO-values (Fig. 7.21) in all the different ore-types show very low values, with a few high peaks of up to about 8 wt percent MgO. These may be due to the presence of brucite and clinochlore. No definite trend was observed for MgO contents along sections sampled.

The contents of Al_2O_3, P_2O_5, K, Na (Fig. 7.22) and H_2O (Fig. 7.22C) display no definite trends, possibly due to the fact that they occur in very low concentrations. These elements are associated with gangue minerals, which are all irregularly distributed in the ores. Thus high values for these elements are possible indicators of the presence of hydrothermal minerals in the ore. It is perhaps worthwhile to note that P_2O_5, K and Na-values vary sympathetically (Fig. 7.22B).

The main geochemical trends observed is thus an inverse relationship between Fe and Mn, where in highest grade ore, with highest Mn-content, the SiO_2-content also decrease significantly, due to a possible leaching of silica during hydrothermal activity. The Mn-content is the best indicator of the different ore types, as it is relatively low in Mamatwan-type ore, increases gradually as Wessels-type ore is encountered, with maximum values present in the highest grade hausmannite-rich Wessels-type ore, from where it decrease sharply towards the ferruginized zone, where it is an insignificant low value. In the

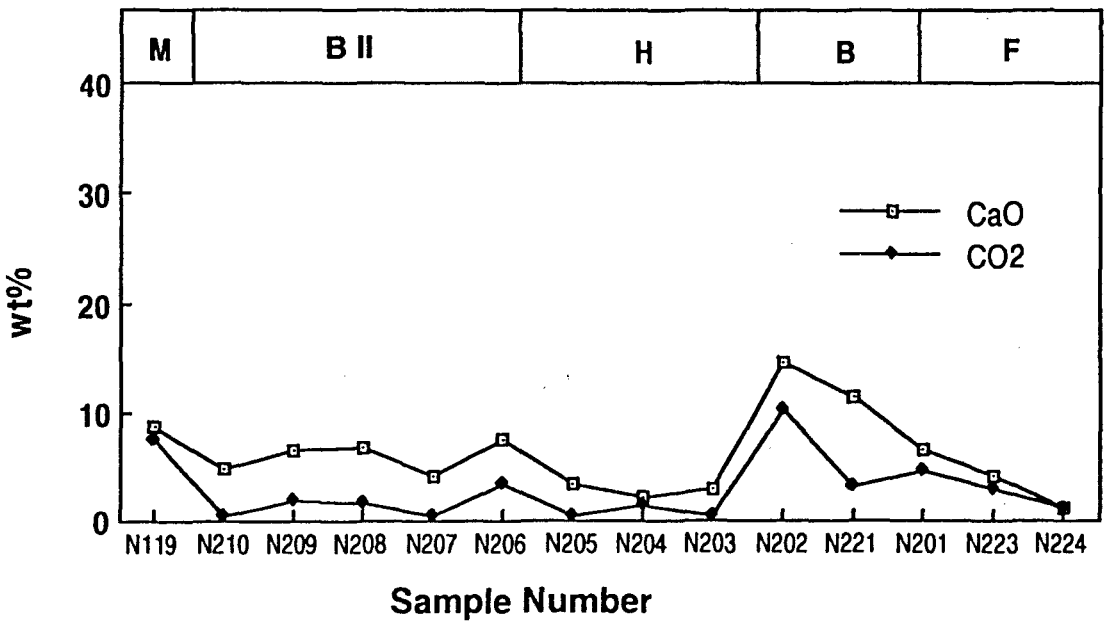

Figure 7.20 CaO- and CO_2-contents of manganese ore along an idealized section.

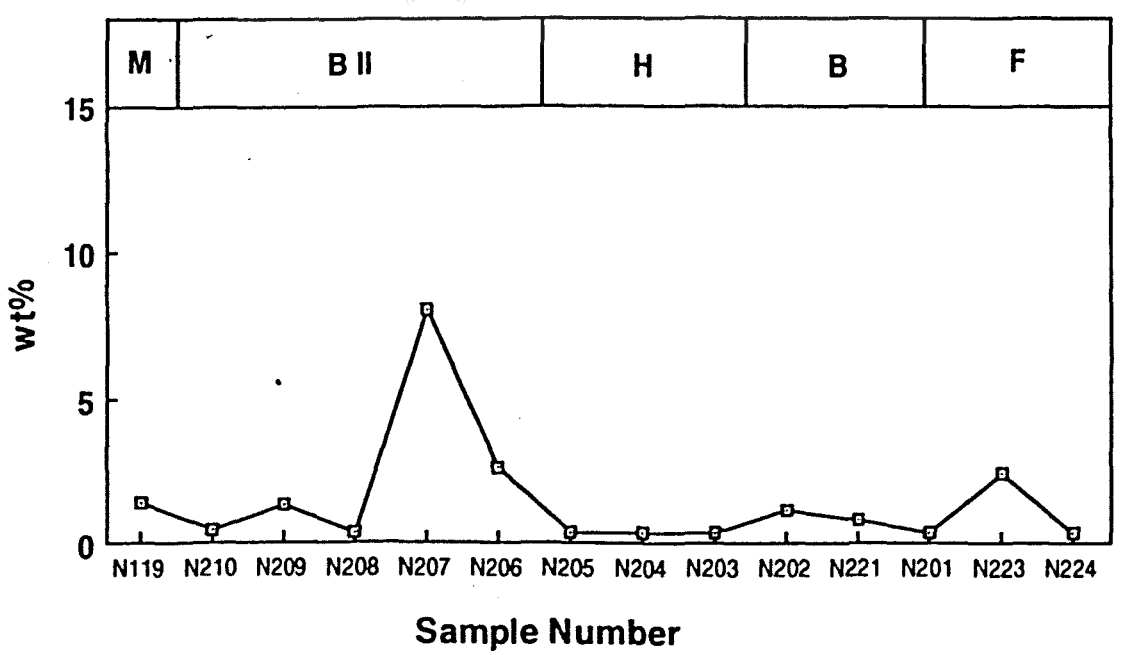

Figure 7.21 MgO-contents of manganese ore along an idealized section.

ferruginized zone the Fe-contents increase sharply to very high values, whereas the Fe-contents stays low and relatively constant throughout the other ore types.

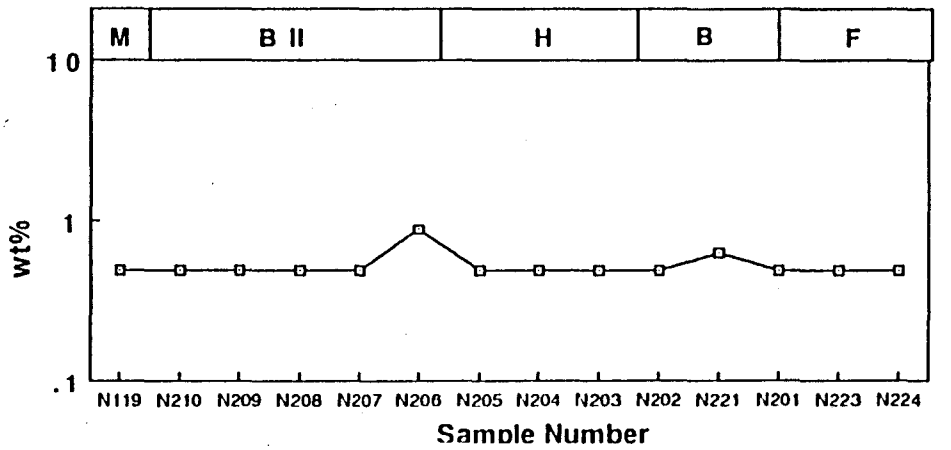

Figure 7 22A. Al_2O_3-values plotted in wt% against their relative sample numbers.

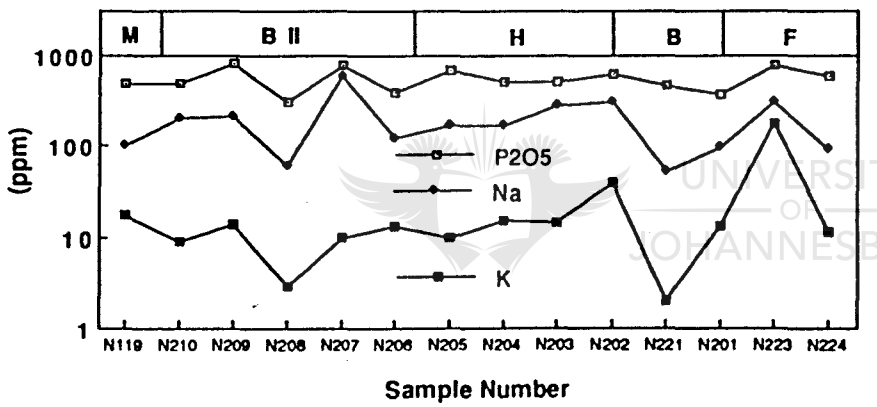

Figure 7.22B. P_2O_5, K and Na-values plotted in ppm against their relative sample numbers.

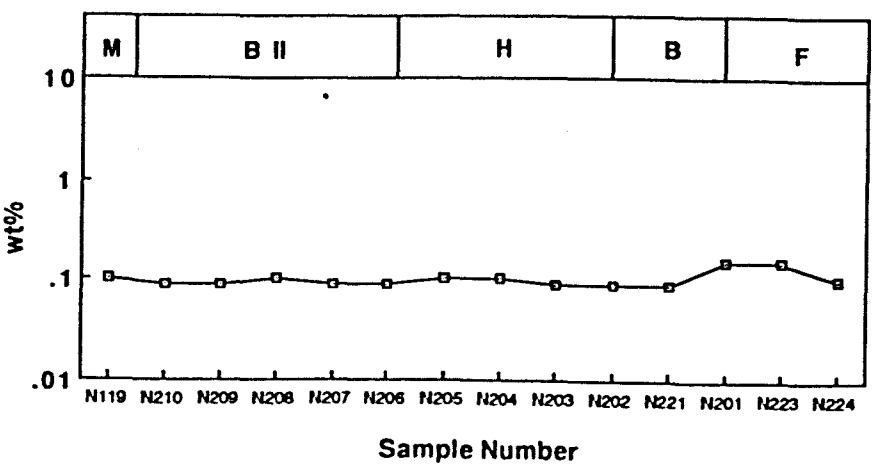

Figure 7.22C H_2O-values plotted in wt% against their relative sample numbers.

7.4 STABLE ISOTOPES

Stable isotope analyses of some carbonate samples were done by Dr. H. W. Yeh of the Hawaii Institute of Geophysics in Honolulu, USA. Carbon and oxygen isotopic ratios ($\delta^{13}C$ and $\delta^{18}O$) were measured, as well as sulfur ($\delta^{34}S$). These analyses were done to have a possible indication of the temperature at which the carbonates formed, and to maybe determine a source of carbon for the carbonates.

Nine samples were analyzed. Three samples (IMB 6, 7 and 8) came from Wessels-type ore along section N200. They represent calcite that was drilled out with a microdrill from vugs in the ore. Another sample (N228 = IMB9) came from a calcite filled vug in a ferruginized fault plane. The other five samples (IMB1- IMB5) came from a calcite-barite filled veinlet in secondary braunite type ore (sample N504 from section N500) and were drilled out vertically as well as horizontally along the veinlet (Fig 7.23 A). Results are given in Table 7.8.

A mean value for Mamatwan-type ore was obtained for $\delta^{13}C_{(PDB)}$, $\delta^{18}O_{(PDB)}$ and $\delta^{18}O_{(SMOW)}$ values of calcite- and kutnahorite samples (Gutzmer, personal communication).

Table 7.8. Carbon and oxygen isotopic composition of calcites from Mamatwan-type ore, Wessels-type ore, secondary braunite ore and a ferruginized fault zone.

Ore type	Sample No.	$\delta^{13}C_{(PDB)}$	$\delta^{18}O_{(PDB)}$	$\delta^{18}O_{(SMOW)}$	$\delta^{34}S_{(CDT)}$
Mamatwan-type ore	Mean	-12,0‰	-13.0‰	23,0‰	
Wessels-type ore	IMB6	-14,8‰	-13,9‰	16,5‰	
	IMB7	-11,5‰	-4,2 ‰	26,5‰	22,6‰
	IMB8·	-13,1‰	-1,5 ‰	29,3‰	
Secondary braunite ore	IMB1			13,3‰	21,6‰
	IMB2	-7,9‰	-8,5 ‰	22,1‰	
	IMB3	-22,3‰	-13,5‰	16,8‰	
	IMB4	-17,1‰	-12,0‰	18,5‰	
	IMB5	-11,1‰	-9,7 ‰	20,9‰	21,5‰
Fault plane	IMB9	-9,5‰	-11,6‰	18,9‰	

PDB = Peedee Belemnite; SMOW = standard mean ocean water; CDT = Canyon Diablo Troilite (internationally accepted reference standards)

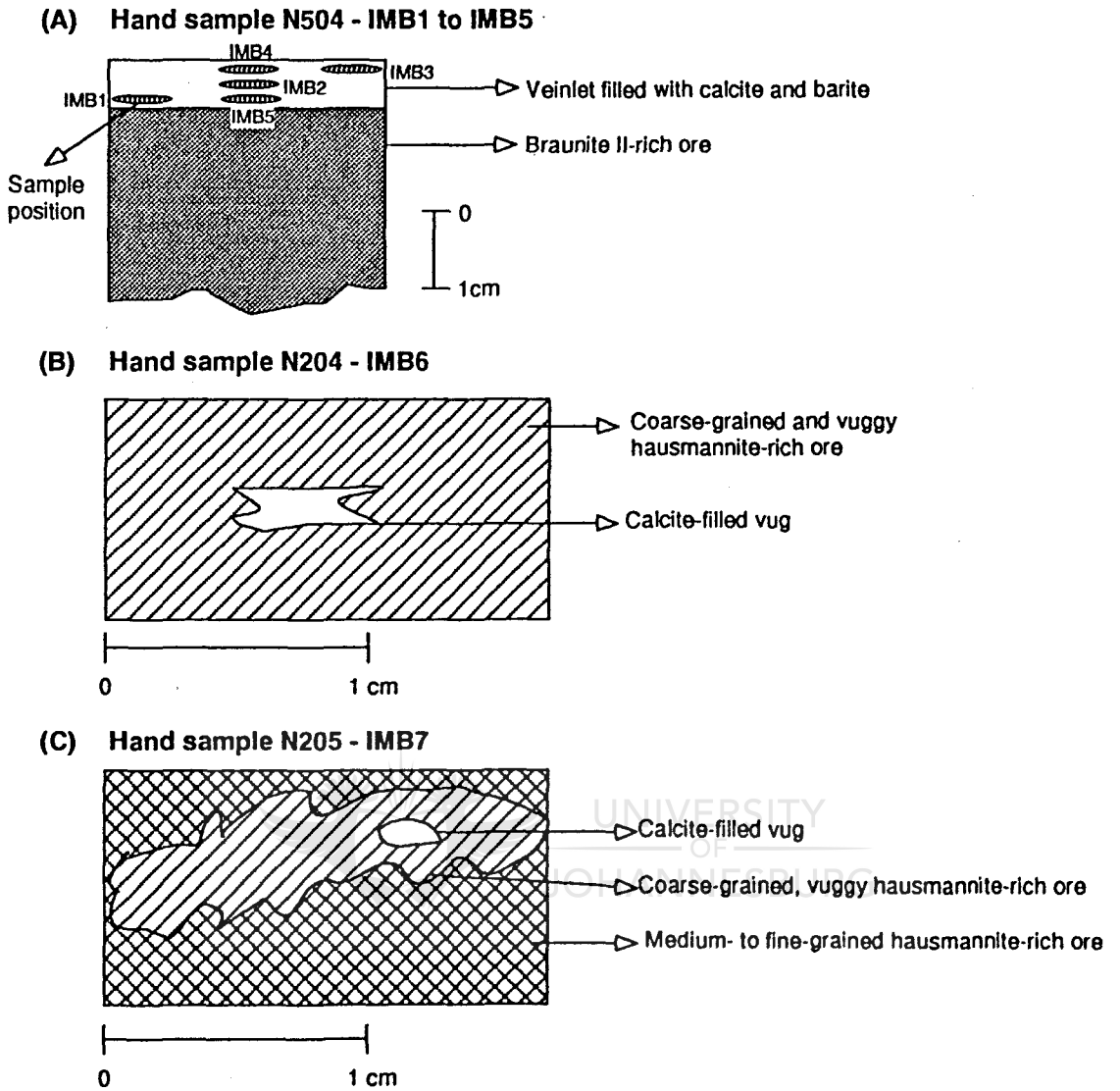

Figure 7.23. Diagrammatic description of the samples IMB1 - IMB5 from hand sample N504 (A), sample IMB6 from hand sample N204 (B), and sample IMB7 from hand sample N205 (C).

In figure 7.24 the data is presented relative to zones of ferruginization and Mamatwan-type ore along an idealized section. The mean value obtained for Mamatwan-type ore is used as a reference standard. In samples from the veinlet (samples IMB1 - IMB5), samples from near the walls display low $\delta^{18}O_{(PDB)}$-values of -13,6, -12,0 and -7,9 ‰, whereas the centre sample (IMB2) display a heavier ^{18}O-isotope value (-8,5 ‰). Thus higher temperature was present during the formation of the vein on the outside, and the fluids probably cooled, before the carbonates in the centre of the vein crystallized. The samples on the rims also display more depleted ^{13}C-values, -11,1 to -22,3 ‰ in

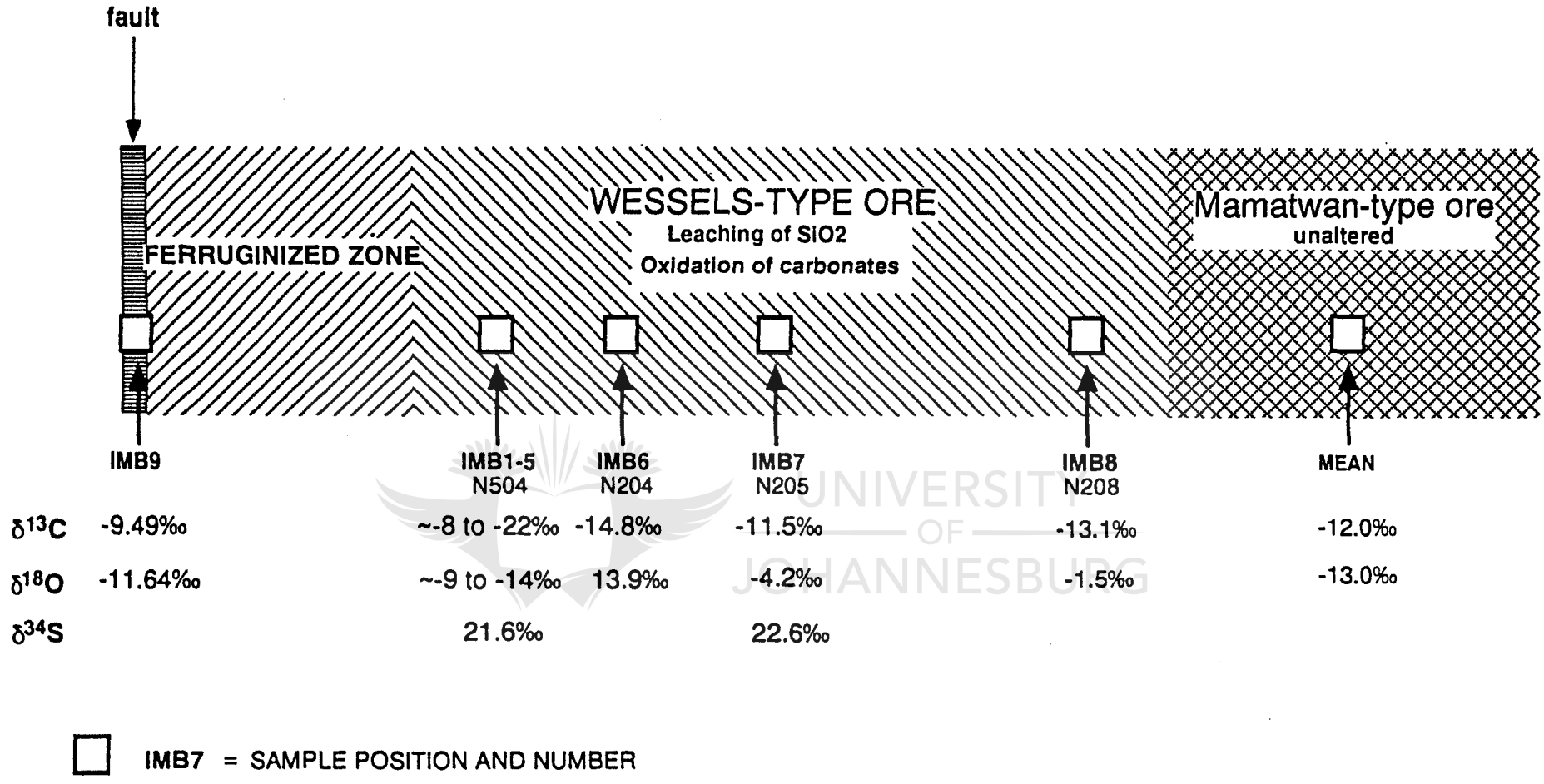

Figure 7.24. Sample positions and results of stable isotope analyses of nine carbonate samples, in an idealized section from ferruginized fault zone through Wessels-type ore into Mamatwan-type ore.

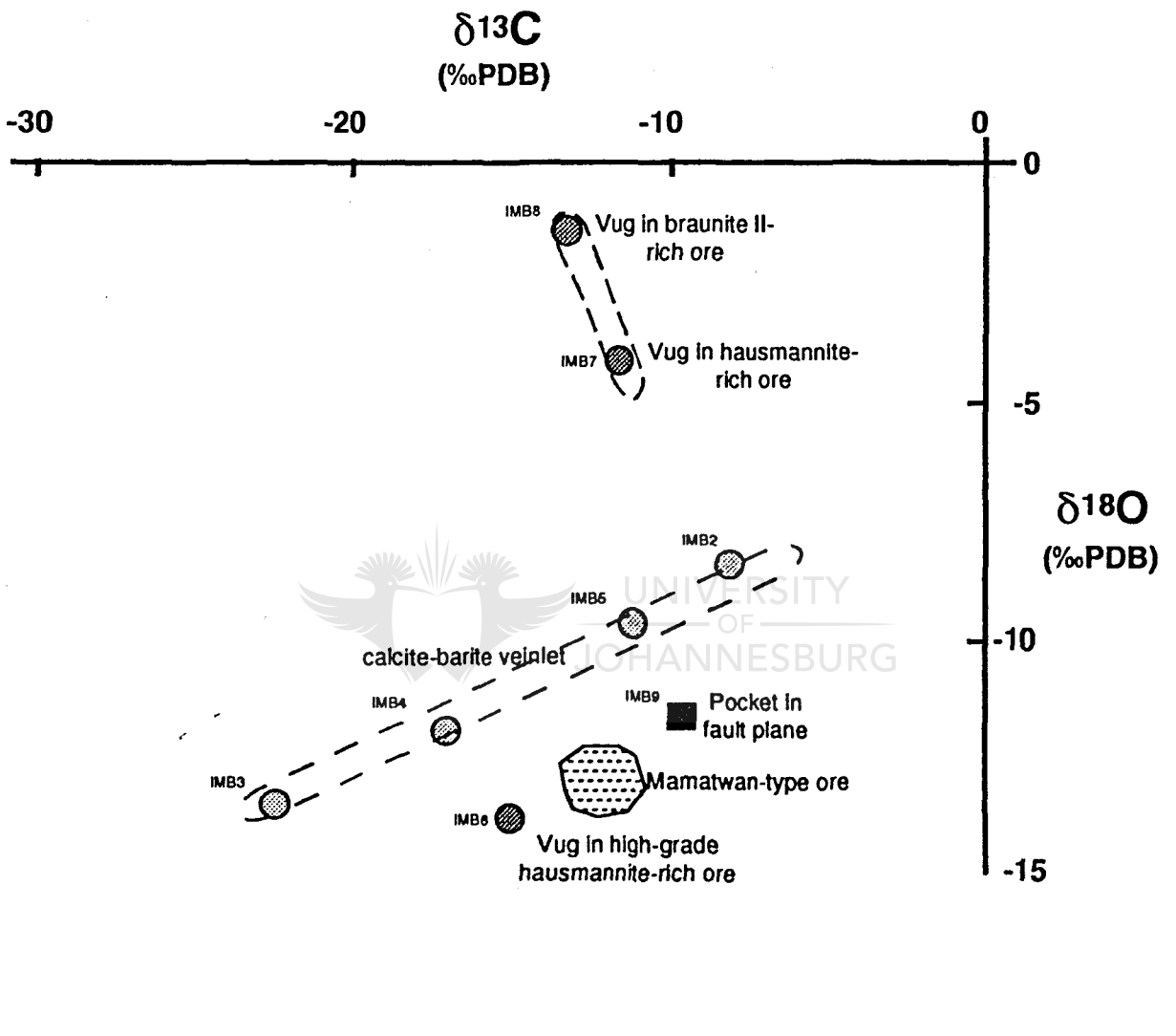

Figure 7.25 Carbon and oxygen isotopic composition of the carbonates present in the calcite vugs and calcite-barite veinlets in the different ore types.

comparison with the heavy centre value (-7,9 ‰), thus possibly indicating different sources of carbon.

In the other samples $^{18}O_{(PDB)}$-values range from -1,5 and -4,2 ‰ (IMB7, IMB8) further away from the ferruginized zones to -13,9 and -11,6 ‰ in samples IMB6 and IMB9 (Fig. 7.25) situated in the fault plane itself. This is a trend of lower temperatures of formation in calcite vugs, nearer to the ferruginized zone, with a different source of carbon present in the calcite of the vug in the fault plane, indicated by its heavy ^{13}C-value (-9,49‰). Carbon ^{13}C-Values in the Wessels-type ore are mostly heavier than that of the Mamatwan-type ore, indicative of a different source of carbon in the hydrothermal fluids.

CHAPTER VIII MAGNETIC PROPERTIES OF WESSELS-TYPE ORE

8.1 INTRODUCTION

Magnetic measurements were done on Wessels-type ore on a macro- as well as micro scale. The magnetic susceptibility of the samples were determined to investigate possible trends in magnetic properties along sampled sections. It was thought that such information may be of use in geophysical exploration for different manganese ore types. All samples in the different sections were measured for magnetic susceptibility. On a micro-scale, magnetic mineral phases were examined by various means.

8.2 MAGNETIC SUSCEPTIBILITY

Magnetic susceptibility is a measurement of the intensity of magnetization induced in a mineral or rock, by a magnetic field of given strength (Dunning, 1970). The susceptibility of rocks are almost entirely determined by their content of ferromagnetic minerals (Dunning, 1970). It is determined by a magnetometer or other magnetism measuring apparatus.

Measurements were done at MINTEK using a KLY-2, GEOFYZYKA BRNO kappabridge. Measurements entail taking the mass of the sample in grams, as well as that of the measuring cup that is being used in the instrument. The readings obtained are then substituted into the following equation:

$\chi = {}^{1}/_{0,4\pi}\,[({}^{\text{range x reading}}/_{\text{mass(g) (sample)}} - {}^{\text{(range x reading)}}/_{\text{mass(g) (cup)}})]\text{x}10^{-6}$

$= \text{x cm}^3/\text{g}$, where χ is the magnetic susceptibility of the sample (Svoboda, 1987).

Samples used were off-cut's of ore produced while making polished thin sections and had sizes of approximately 20x30x3 mm. Results are given in table 8.1.

8.2.1 SECTION N100

Along section N100 magnetic susceptibility displays a rather erratic pattern (Fig. 8.1). However, interesting enough peaks of high magnetic susceptibility correlate with relatively high Fe values in the ore (compare figure 7.1). The hausmannite-rich Wessels-type ores, close to the ferruginized zone, display

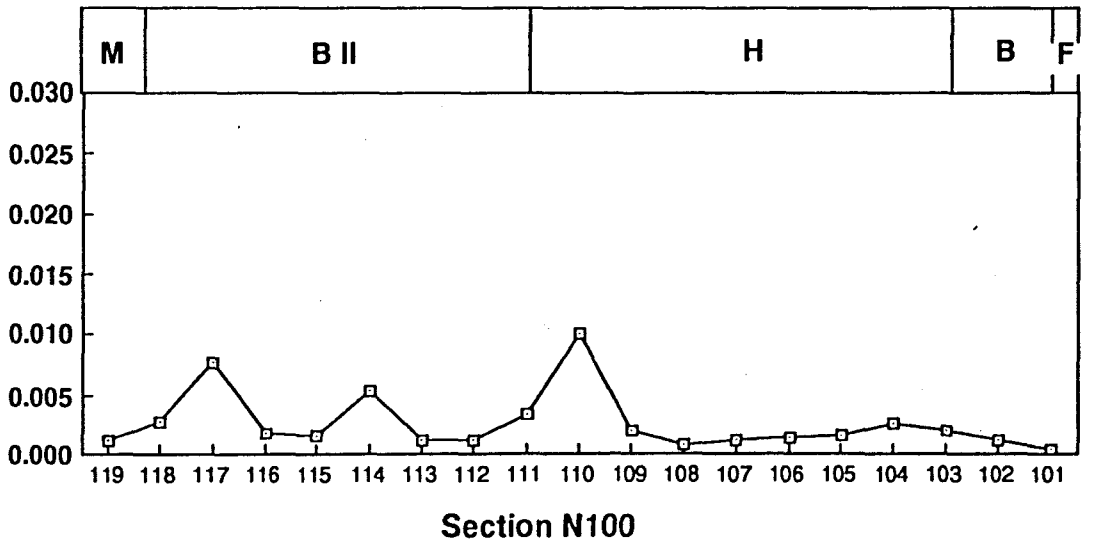

Figure 8.1 Magnetic susceptibility measurements of manganese ore along section N100.

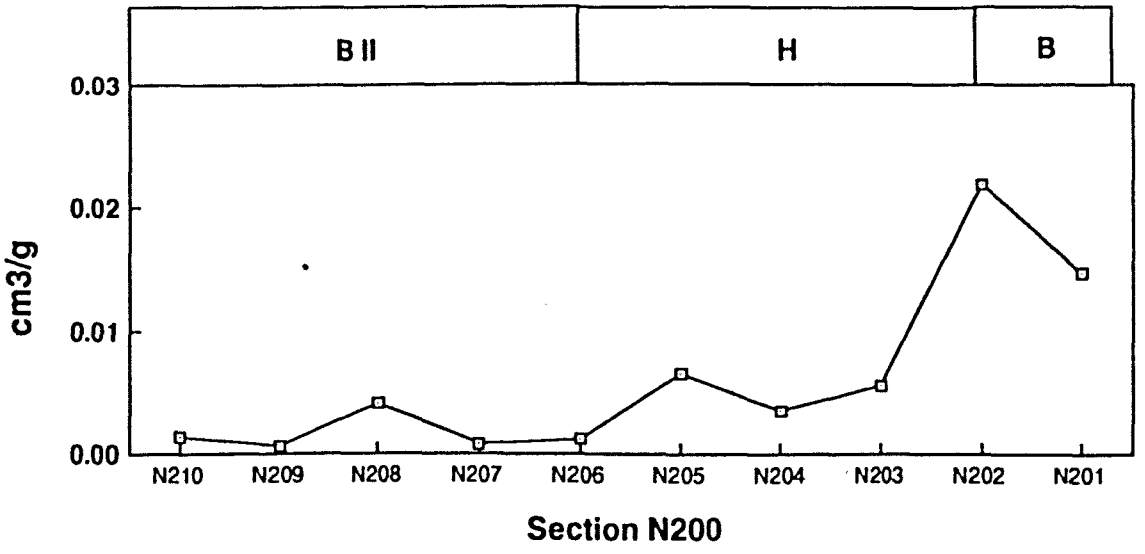

Figure 8.2 Magnetic susceptibility measurements of manganese ore along section N200.

overall low magnetic susceptibility. There is a slight increase in magnetic susceptibility in samples N105, N104 and N103 and then the susceptibility decreases (sample N102) to a very low value in the ferruginized zone (sample N101). Initially it was thought that the high readings were due to the presence of small amounts of jacobsite in the ore. However, no jacobsite could be traced and therefore it is concluded that it is related to the presence of Fe-rich magnetic hausmannite in the ore (see sections 6.2 and 8.4). The low readings in, and bordering the ferruginized zone (samples N101 - N102), are probably due to lower hausmannite contents and the presence of hematite. Hematite displays very low magnetic susceptibility (Smit et al., 1959).

Table 8.1. Magnetic susceptibility values of manganese ores along various sections, expressed as $1x10^{-3}$ cm^3/g.

N100	cm^3/g	N200	cm^3/g	N300	cm^3/g	N500	cm^3/g
N101	0.36	N201	14.75	N220	0.73	N501	0.05
N102	1.27	N202	21.91	N230	0.99	N502	0.074
N103	1.98	N203	5.66	N221	1.36	N503	0.067
N104	2.62	N204	3.57	N222	1.18	N504	0.068
N105	1.60	N205	6.58	N223	0.23	N505	0.053
N106	1.29	N206	1.16	N224	0.45	N506	0.002
N107	1.15	N207	0.68	N225	0.28	N507	0.020
N108	0.82	N208	2.23	N226	0.31	N508	0.049
N109	1.89	N209	0.64	N227	0.23	N509	0.077
N110	10.03	N210	1.28	N229	0.38	N510	0.044
N111	3.34					N511	0.036
N112	1.11					N512	0.061
N113	1.19						
N114	5.41						
N115	1.64						
N116	1.86						
N117	7.77						
N118	2.84						
N119	1.21						

8.2.2 SECTION N200

Along section N200 magnetic susceptibility of the ore is low in the transition zone between Mamatwan-type ore and Wessels-type ore. The susceptibility increases steadily towards the margin of the ferruginized zone (Fig. 8.2). In the

ferruginized zone it decreases to very low values (Fig. 8.2). Petrography and XRD analyses again indicate that only hausmannite is present in the samples with high magnetic susceptibility. In the sample with very high magnetic susceptibility (sample N202) trace amounts (<5 %) of jacobsite are present. In this specific section it was found that some of the hausmannite is so magnetic, that it could be separated with a hand magnet from a crushed sample. These magnetic hausmannites are Fe-rich, containing up to 10 weight percent Fe (Fig. 6.2). The hausmannite ore in the high-grade samples (N203 - N205) are also very pure, with very little other mineral phases present (Fig. 4.2 and table 6.1)

8.2.3 SECTION N300

In the high-grade ore bordering the ferruginized zone of section N300 (samples N220 - N222), the magnetic susceptibility values are relatively high (Fig. 8.3). Readings drop down to very low values in the ferruginized ore zone, where the main mineral phase is hematite with accessory calcite. The readings for section N300 are on average 10 times lower than those of sections N200 and N100. XRD and petrographic data (chapters IV and V) indicate that braunite and braunite II are the main phases present in the area with relatively high readings. The absence of hausmannite as main phase may be the reason for the relative low values, compared to sections N100 and N200. The samples with relatively high magnetic susceptibility in section N300 contain relatively high Fe-content (up to 10 wt percent in sample N222). The Fe is most probably present in the braunites that constitute the main phases.

8.2.4 SECTION N500

In section N500 relatively high magnetic susceptibility values are present in high-grade Mn-ore. In the quartz-rich zone, where Mn-diopside and quartz are the main mineral phases, the magnetic susceptibility is very low (Fig. 8.4). Again highest magnetic susceptibility readings are obtained immediately adjacent to the ferruginized zone. These values may again be due to the high Fe-content of the ore in this area as can be seen in its whole rock geochemistry (Fig. 7.13). Minerals present in this ore and having a high Fe-contents are braunite II, bixbyite and hausmannite. The readings are low relative to section N100 and N200, although the same trend is observed. These low magnetic susceptibility values may again be due to the absence of hausmannite as main phase, with braunite II and manganite occurring as main phases here.

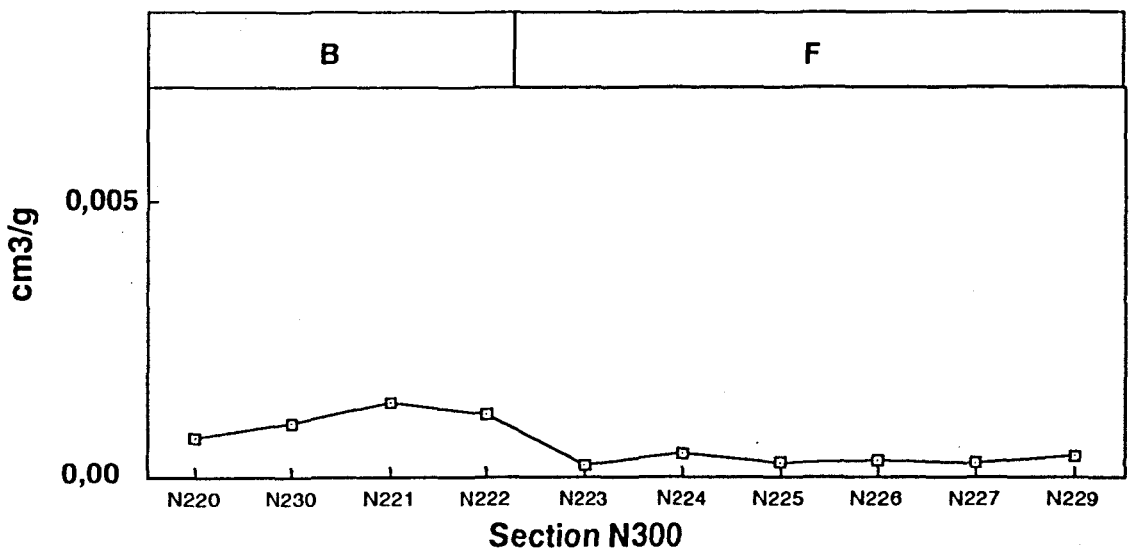

Figure 8.3 Magnetic susceptibility measurements of manganese ore along section N300. Sample N229 is situated in the fault plane.

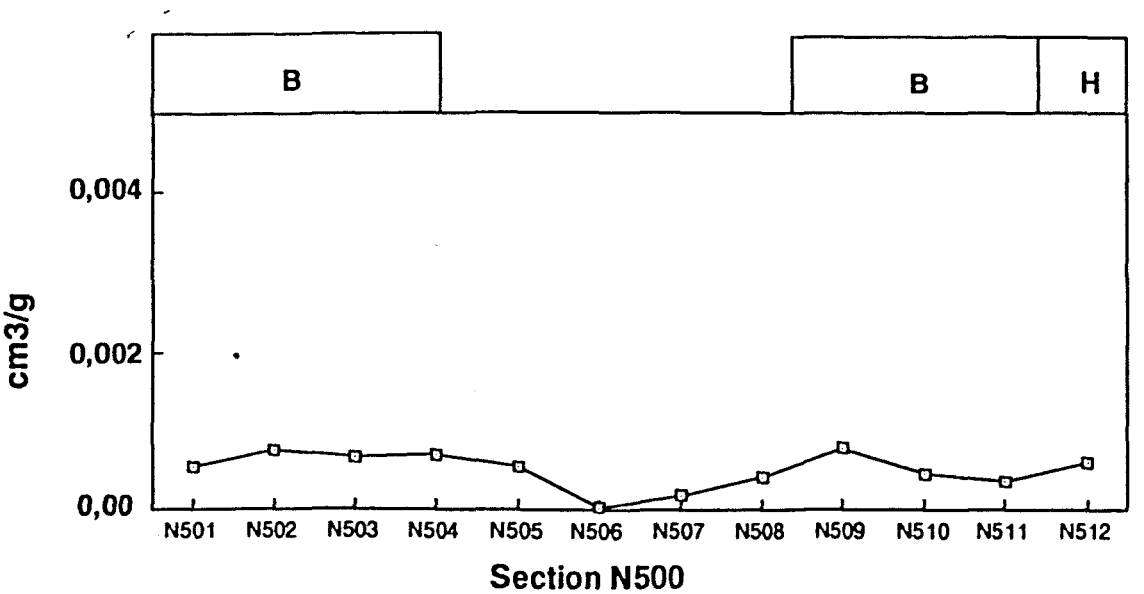

Figure 8.4 Magnetic susceptibility measurements of manganese ore along section N500. Samples N505 to N508 are situated in the "ferruginized" zone.

8.2.5 GENERAL MAGNETIC SUSCEPTIBILITY

Only sections N100 and N200 display any significant trend in its magnetic susceptibility patterns. Higher susceptibility occurs in high-grade hausmannite ore and are most likely linked to its hausmannite content, especially the magnetic hausmannite phases. In section N200 there also exist a posibillity that secondary braunite and braunite II also cause high magnetic susceptibility. In sections N300 and N500 it is seen that fault structures and its accompanying ferruginized and silicified zones, display significant absence of susceptibility due to the mineralogy present in these structures, which are mostly hematite-calcite and also quartz and diopside in section N500. The ores surrounding these structures also display very low susceptibility, probably due to the absence of magnetic phases such as hausmannite and jacobsite (present in the orebed near the hanging- and footwall) as main constituents of the ore. Minerals such as manganite dominate here and does definitely not display any magnetic properties. Due to the ease of measuring magnetic susceptibility in the orebeds it would be worthwhile to conduct a thorough study on a much larger scale in the Wessels Mine to determine more representative magnetic signatures.

8.3 MAGNETIC STUDIES ON INDIVIDUAL MINERAL PHASES

8.3.1 HAUSMANNITE

As already mentioned, some of the hausmannite in Wessels-type ore display unusual magnetic properties. Small pieces of hausmannite grains are strongly magnetic, so much so that it can be separated from the rest of a sample with a common hand magnet. This is very unusual for hausmannite as it is known that pure hausmannite with no Fe in its structure has a Curie temperature of 42 °K. Above that temperature hausmannite is known to be paramagnetic (Boucher et al., 1971). However, nothing is known about the influence of Fe^{3+} substitution for Mn in the structure of hausmannite. The magnetic character of the hausmannites were initially thought to be due to possible inclusions of jacobsite. However, microscopic studies, XRD, EDS and SEM analyses, failed to indicate the presence of any jacobsite. It is not even present as sub microscopic exolutions in the hausmannite, as shown by SEM images (Fig. 8.5). The images only indicated the presence of tiny, 3 microns in diameter, hematite inclusions in the hausmannite (Fig. 8.5).

Hausmannite, separated by hand magnet, has been analyzed by EDS and shows Fe_2O_3-content of up to 16 wt percent in some cases. The strongest magnetic hausmannite samples studied during this study (sample N205M) display a mean Fe_2O_3-content of 11,32 wt percent. Mössbauer spectroscopy was done on magnetic hausmannite at the University of Potchefstroom by Dr. F. Waanders. Results indicated that all iron present is in the form of Fe^{3+}.

Powdered and small block subsamples of magnetic hausmannite from samples N204 and N205 from section N200 were investigated for their magnetic properties by N.J. Beukes at the Paleomagnetic Laboratory of J. Kirschvink at the California Institute of Technology. Steplike thermal demagnetization experiments were conducted from room temperature (25 °C) to 700 °C. The powdered hausmannite samples were ordered by a very strong magnet and then demagnetized. They gave an initial high magnetism that demagnetized at ~280 °C and a second demagnetization temperature (blocking temperature) of ~475 °C (Fig. 8.6). Above 475 °C almost no magnetism is left. The small amount left, < 10%, is due to small amounts of hematite present in the hausmannite. It demagnetized at 700 °C which confirms that it is related to hematite; the Curie temperature of hematite is about 680 °C.

Blocks of hausmannite-rich ores were also thermally demagnetized. The initial demagnetization at ~275 °C observed in the powdered samples are much less pronounced (Fig. 8.7) and almost absent in some cases. Again a demagnetization temperature of ~475 °C is attained, with < 10% magnetism left at higher temperatures (Fig. 8.7).

The demagnetization, that took place at 280 °C, is close to the Curie temperature of jacobsite of 300 °C (Goodenough, 1966). Thus this initial demagnetization temperature was thought to be related to the possible presence of jacobsite in the samples. However, this was disproved as mentioned earlier, because no jacobsite could be traced in any of the samples. The demagnetization that took place at 470 °C is also much lower than that of the Curie temperature of magnetite, which is 580 °C (Goodenough, 1966). It is thus considered to represent the blocking temperature of the iron-bearing magnetic hausmannite from the Kalahari manganese field. Blocking temperatures approximate the Curie temperatures (Goodenough, 1966).

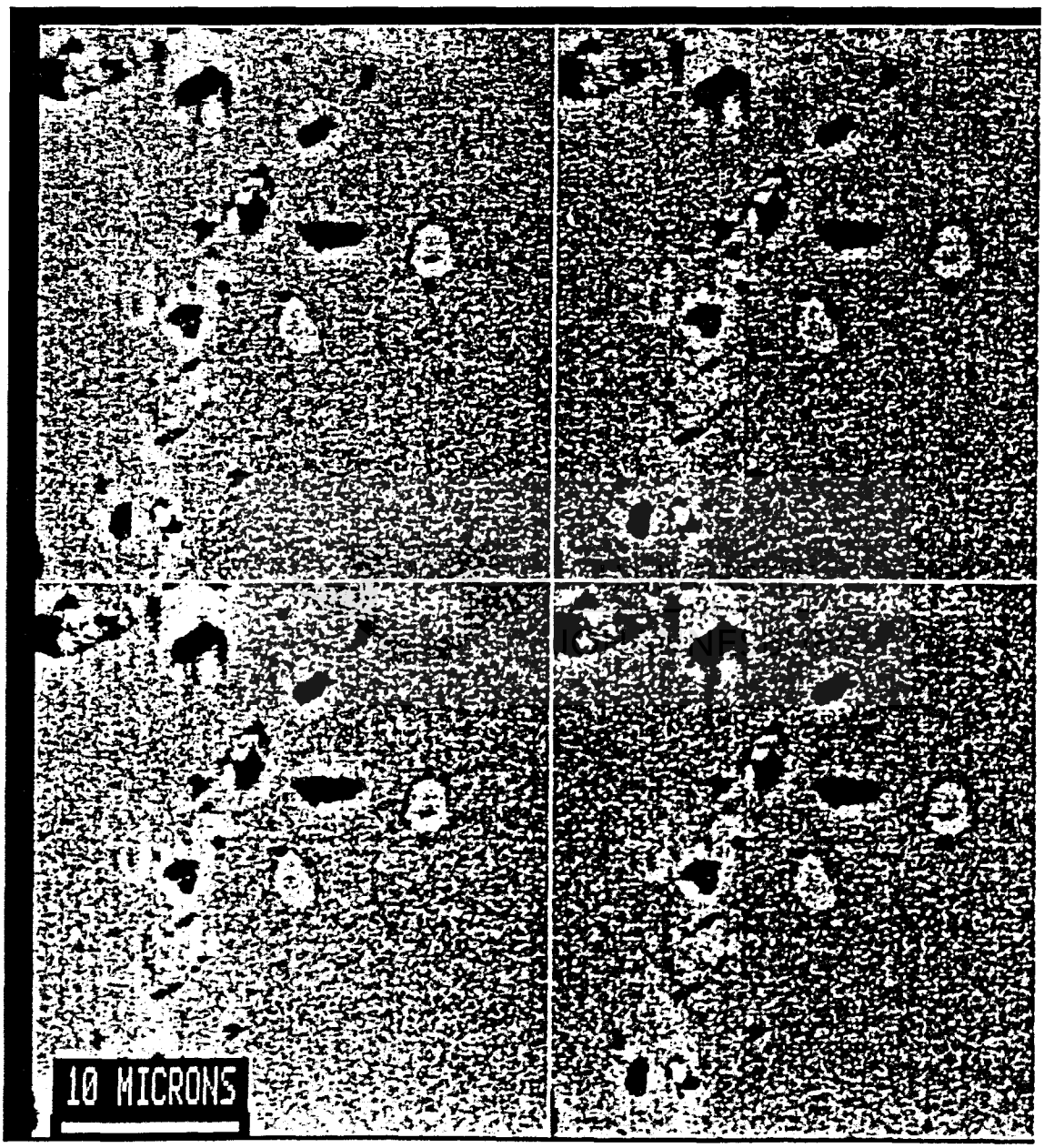

Figure 8.5. Photomicrograph of magnetic hausmannite displaying tiny inclusions of hematite (lighter grey colour).

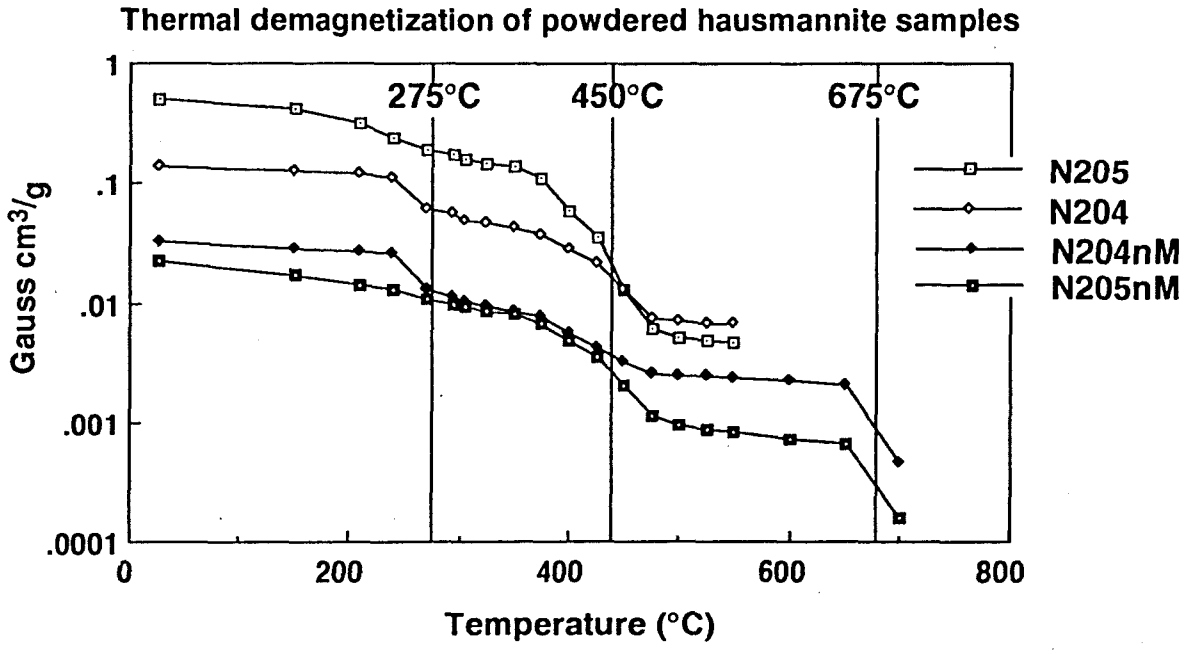

Figure 8.6 Demagnetization temperatures of powdered hausmannite samples.

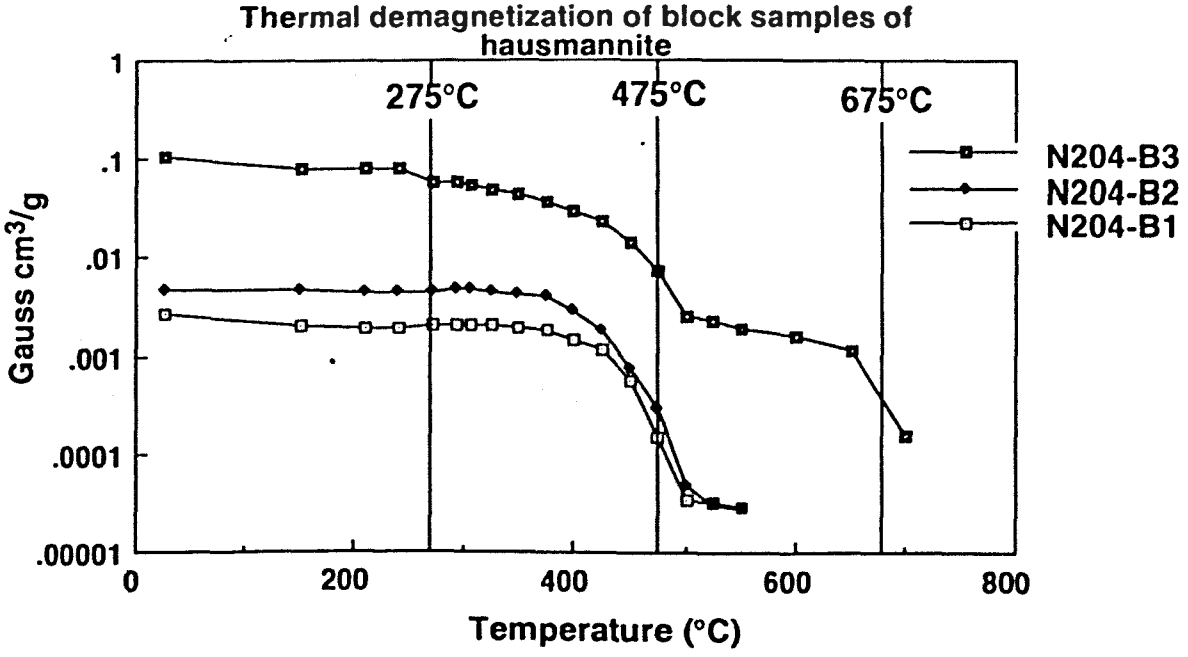

Figure 8.7 Demagnetization temperatures of blocks of hausmannite.

8.3.2 BRAUNITE-GROUP

During the process of trying to separate magnetic hausmannite, it was found that some braunite and braunite II also were attracted by hand magnet. These braunites consists of secondary braunite and braunite II, occurring in the secondary braunite-rich ore zone on the border between hausmannite-rich ore and ferruginized ore. Material came from sample N201. These samples were analyzed by EDS and found to have anomalous high Fe-content of up to a mean of 17,10 wt percent for braunite and 30,6 wt percent for braunite II (Figs. 6.4 and 6.5; sample N201M). No further work has been done on these magnetically seperated high Fe braunites, but it definitely deserves further attention. It may well be that tiny jacobsite grains are present, because it was found in trace amounts (<5 %) by XRD analyses in sample N202.

8.4 CAUSE OF MAGNETISM IN HAUSMANNITE

Fine grained hausmannite occurring in the high-grade hausmannite-rich ores proximal to the ferruginized zone, displays anomalous magnetic properties. It exhibits strong ferrimagnetism at room temperature. This hausmannite has been found to have a Curie temperature of approximately 475 °C (Beukes et al. (1994), which is high above the Curie temperature of 42,5 °K determined for pure hausmannite by Boucher et al. (1971). The Curie temperature (T_C) of a mineral is the critical temperature below which spontaneous electron spin ordering occurs (Goodenough, 1966).

Hausmannite has a tetragonally distorted spinel lattice. Work was done by Boucher et al. (1971) on the structure and magnetic properties of Mn_3O_4. He describes hausmannite to be ferrimagnetic at 4,2 °K, with a magnetic structure which may be derived from tetragonally coordinated cations and from 6 octahedrally coordinated cations, of distinct electron spin orientation (Fig. 8.8). Hausmannite displays a resultant magnetic moment of 1,85 bohr magnetons.molecule^{-1} and possesses a T_C of 42,5 °K according to Boucher et al. (1971). Thus pure Mn_3O_4 displays no magnetic properties at room temperature.

The replacement of Mn^{3+} by Fe^{3+} in hausmannite, confirmed through Mösbauer spectroscopy, may cause thermal stabilization of ordered spin configuration and therefore an increase in the Curie temperature observed, as seen during thermal demagnetization of magnetic hausmannite during this present study.

Further work is necessary to establish the magnetic structure of the magnetic hausmannite. This may be done by neutron diffractometry, which will determine the spin configuration of this magnetic hausmannite.

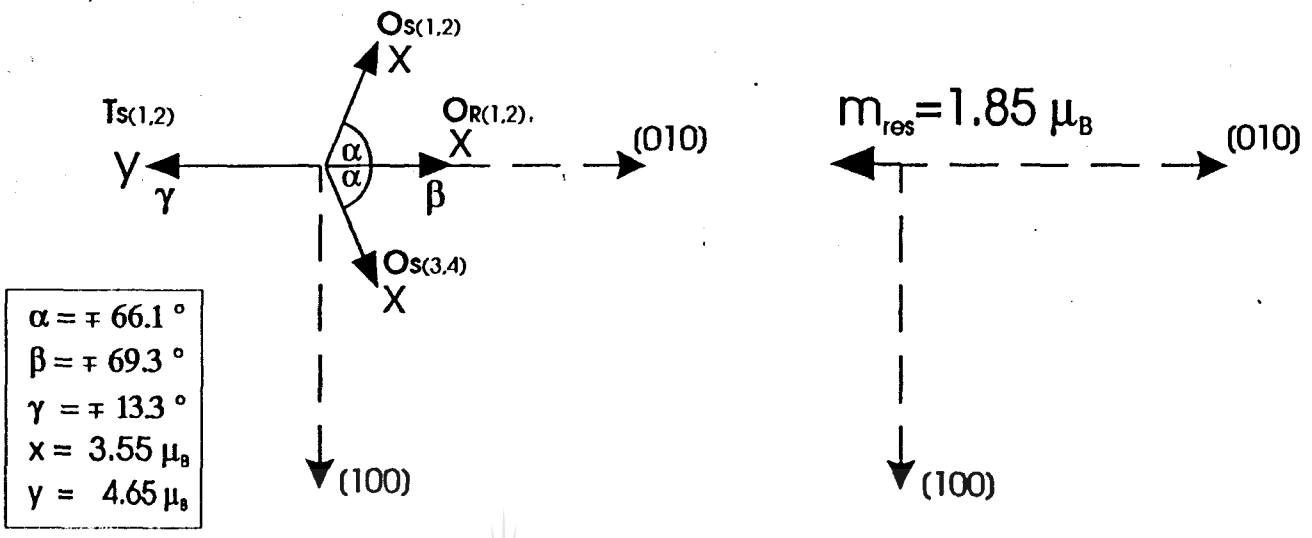

Figure 8.8 Spin configuration of ordinary hausmannite at 4,2 °K as given by Boucher et al. (1971).

CHAPTER IX DISCUSSION AND CONCLUSION

9.1 DISCUSSION

After the systematic mineralogical study of the alteration of low-grade Mamatwan-type ore to high-grade Wessels-type ore, a definite textural, as well as mineralogical pattern was found to exist when moving from low-grade ore, through high-grade ore into the ferruginized zones. This pattern is also supported by geochemical data obtained during the study.

One of the main observations of this study is that alteration of Mamatwan-type ore to Wessels-type ore is closely related to north-south trending normal faults. Highest grade Wessels-type ore occurs immediately adjacent to the ferruginized fault zones. The Wessels-type ore grades laterally into Mamatwan-type ore in central parts of fault blocks. Alteration of Mamatwan-type ore to Wessels-type ore is accompanied by an increase in the porosity of ores, recrystallization of the primary fine grained Mamatwan-type ore to a coarser grain size, and a dissolution of carbonates and leaching of silica from braunites. This type of alteration is best explained by hydrothermal action. The proposed model is that fluids moved from fault conduits into the adjacent ores and caused the alteration. Mineralogically it was observed that when moving from the kutnahoritic braunite-rich sedimentary Mamatwan-type ore, upgrading to braunite II occur, which grades into even higher-grade hausmannite in the central part of the Wessels-type ore. In a small zone between the high-grade Wessels-type ore and the hematite-rich ferruginized zone, a secondary braunite II-braunite assemblage was encountered, indicating a downgrading of the ore in this area.

The hydrothermal fluids must have been carrying ferrous iron in solution, which precipitated along fault conduits after oxidation to Fe^{3+} to form hematite. The fluids must also have become neutral to alkaline and relatively hot, to have been able to dissolve silica (Fig. 9.1). Indications are also that the fluids may have been slightly oxidizing for transformation of manganese carbonates to manganese oxides and calcite. They must also have contained certain amounts of Mg, Na and Al to form the hydrothermal minerals brucite, clinochlore and natrolite present in Wessels-type ore. In addition to these gangue minerals, Kleyenstüber (1985) and Gutzmer (1993) also described K-feldspar

(orthoclase), acmite, richterite, xonotlite and datolite in Wessels-type ore, indicating the presence of potassium in the hydrothermal fluids. (Fig. 9.2)

In the transition zone between primary Mamatwan-type ore and Wessels-type ore, the first alteration encountered is in the transformation of kutnahorite ovoids into calcite and hausmannite probably through a reaction such as:

$3CaMn(CO_3)_2 + {}^1/_2O_2 \text{ ----> } Mn_3O_4 + 3CaCO_3 + 3CO_2$

Moving laterally in zones of higher grades of alteration, a desilification of the ores took place in which braunite is being reconstituted to form braunite II by the removal of silica. A reaction such as the following may have been responsible:

braunite + hematite + calcite ----> braunite II + CO_2 + SiO_2

In this reaction Fe_2O_3 is taken up into the crystal structure of braunite II, explaining why it normally contains higher Fe contents than associated braunite. In turn the braunite II may be transformed into low Si braunite by a reaction:

braunite II + hematite + calcite ----> low Si braunite + CO_2 + SiO_2

Further liberation of silica and CO_2 could have led to the formation of bixbyite by a reaction such as:

low Si braunite + hematite + calcite ----> bixbyite + CO_2 + SiO_2

In most of these reactions CO_2 and SiO_2 are liberated. The braunite-bixbyite composition and the phases intermediate, is in actual fact reflecting the availability of SiO_2. Any composition (SiO_2-content) is thus possible between bixbyite and braunite (10-0% SiO_2).

The next step was the formation of hausmannite-rich ore. The hausmannite apparently formed due to reduction of some Mn^{3+} to Mn^{2+} and total desilification of the braunite II and braunite (new) by the reactions:

Braunite II ----> low Si braunite + SiO_2 ----> hausmannite + SiO_2

The very high-grade Wessels-type ore which consists mainly of hausmannite, found very close to the fault zone immediately adjacent to the ferruginized zone, might have formed from the mobilization of manganese from fault planes into adjacent Mn ore beds. Mobilization of manganese may have been made possible by reduction of Mn^{3+} to Mn^{2+} through the ferrous iron in solution in the hydrothermal fluids according to:

$$Fe^{2+}_{(aq)} + Mn^{3+}_{(s)} \text{ <----> } Mn^{2+}_{(aq)} + Fe^{3+}_{(s)}$$

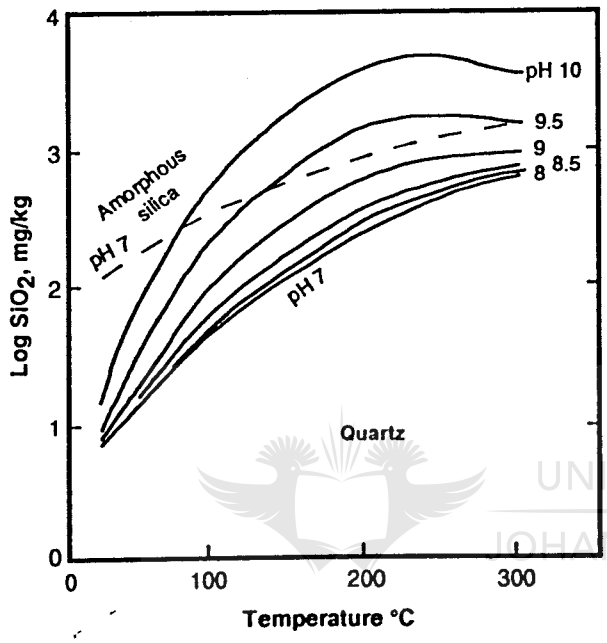

Figure 9.1. Solubility of quartz as a function of pH and temperature. It is seen that a neutral solution dissolve almost the same amount of silica at 300 °C, as a solution with a pH of 8 at the same temperature. After Fournier (1986).

The iron would have precipitated as hematite to form the ferruginized zone along faults, with manganese transported into the manganese beds to form very high-grade hausmannite-rich Wessels-type ore (Fig. 9.2). Recrystallization, or replacement of the finer grained hausmannite by the coarser grained, low Fe hausmannites possibly took place due to these Mn^{2+}-rich fluids.

The secondary braunite-rich ore zone, developed between the ferruginized zone and the very high-grade hausmannite-rich ore, may have formed from the reprecipitation of silica that was leached from braunites in the low-grade ores distal from the fluid conduits (Fig. 9.2). Oversaturation of silica and cooling of the fluids may have caused reprecipitation of the silica (Fournier, 1986). This would also explain the presence of quartz in some of the fault planes, such as

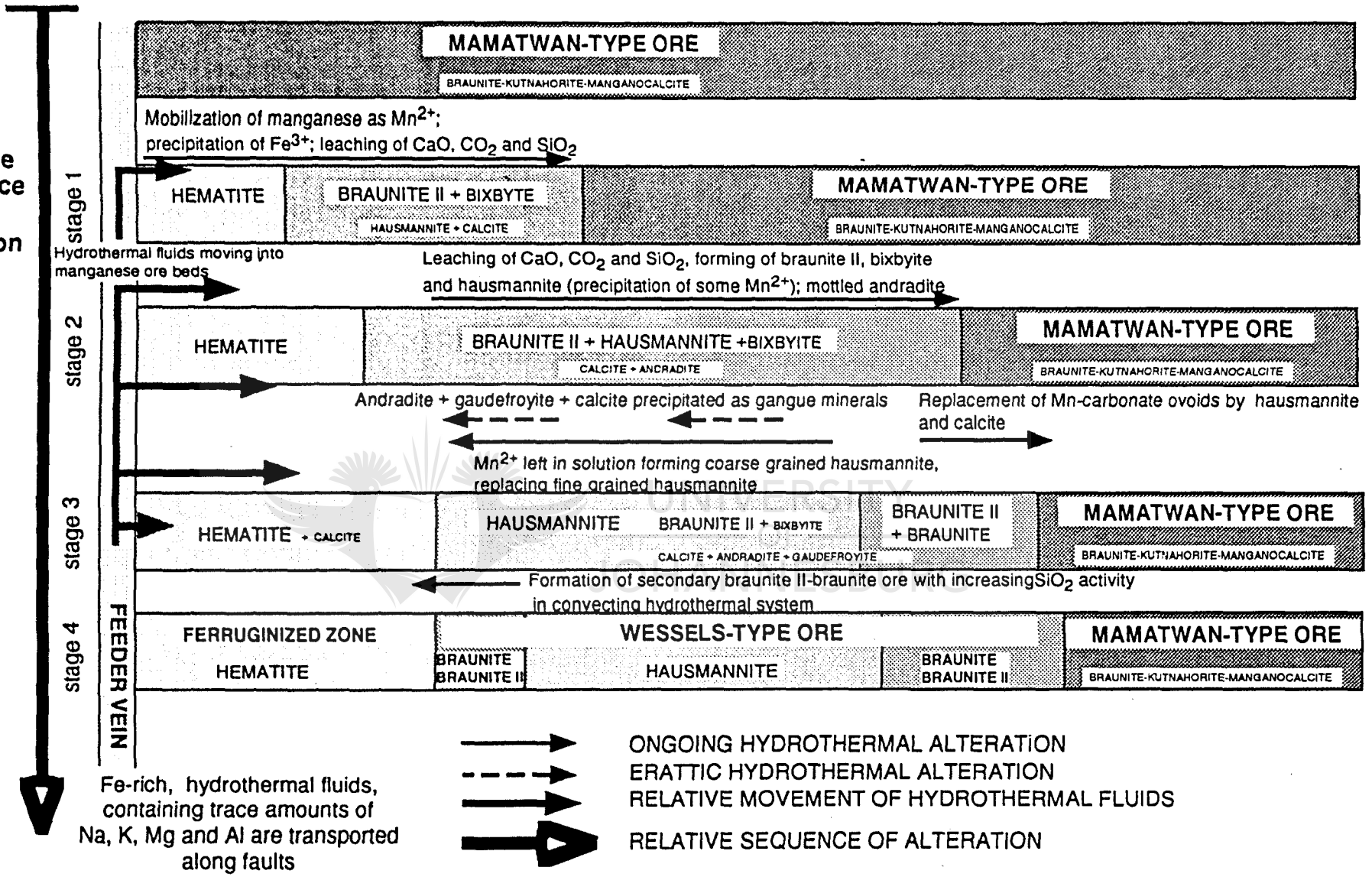

Figure 9.2. Conseptual model of the hydrothermal convection system that was responsible for the alteration and ferruginization of primary sedimentary Mamatwan-type manganese ores in the Kalahari manganese field. Only main mineral phases and a few of the gangue hydrothermal minerals are shown.

along section N500 where metasomatized quartz cement quartzcitic clasts. The silica was also precipitated as gangue andradite or as euhedral andradite, replacing primary carbonate ovoids and forming a "mottled" textured ore. According to Kleyenstüber (1985) andradite may have precipitated from the following reaction:

$3CaCO_3 + Fe_2O_3 + 3SiO_2 \text{ ----> } Ca_3Fe_2Si_3O_{12} + 3CO_2$

Manganite also formed due to oxidation of the parent rock, where manganese ore was in contact with possibly oxidising surface waters that apparently moved through the fault structure in section N500. However it is later replaced by hausmannite through transformation of some Mn^{3+} to Mn^{2+}. Ca liberated from the carbonates resulted in the formation of marokite which replaced manganite and braunite II. Such CaO may also have led to the formation of gaudefroyite and andradite (as mentioned above) in the form of gangue minerals associated with mainly hausmannite and braunite II. CO_2 liberated during the hydrothermal process may have reacted with Ca to form calcite that filled vugs and veinlets (Fig. 9.2). Calcite is especially abundant in the ferruginized zones where conditions for reprecipitation of Ca and CO_2 in the form of $CaCO_2$, were apparently most suited. Isotopic ^{18}O-values for calcites also indicate lower temperature of precipitation (-1,5 to -4,2 ‰) more distal to the primary ores (-13 ‰), proximal to the ferruginized zone. Thus indicating precipitation during the waning stages of alteration, from remnant hydrothermal liquid. Some calcite present as vugfilling also suggests a possible source of carbon originating from Mamatwan-type ore, seen in their more depleted values of ^{13}C (<-12 ‰). Most calcite occurring as vugfilling, however indicated different sources of carbon (>-12 ‰) than the primary ore.

The pattern of zonation found in the manganese ore beds relative to ferruginized fault zones is rather similar to that described by Gutzmer (1993) and Gutzmer and Beukes (in press) in the N'Chwaning Mine. They postulated two possible hydrothermal models that may have been responsible for the formation of Wessels-type ore and ore zonation. In the first model hydrothermal action leached silica from the original braunite-kutnahorite-manganocalcite ore and upgraded the ore to Wessels-type ore. A secondary influx of silica into the ore caused the formation of secondary, hydrothermal braunites next to ferruginized fault zones.

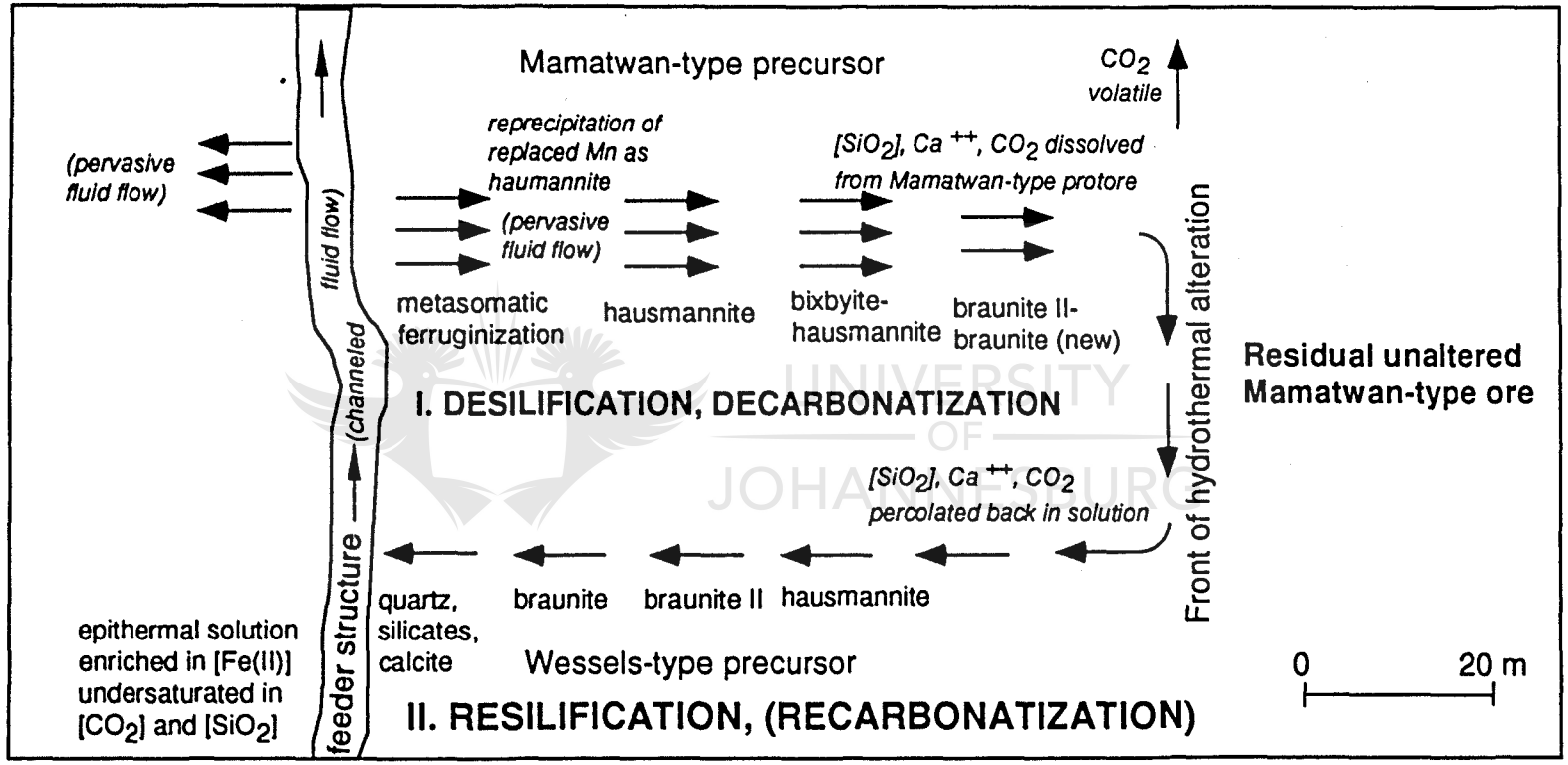

Figure 9.3. Conceptual model of the hydrothermal convecting system that was responsible for the hydrothermal alteration and ferruginization of ores in the Kalahari manganese field. Modified after Gutzmer (1993) and Gutzmer and Beukes (In press).

The second model is a convection model (Fig. 9.3) where faults or fractures acted as feeder veins from which fluids migrated through the wallrock. Here the fluids started to dissolve Mn^{3+} minerals, through reduction of Mn^{3+} to Mn^{2+} by Fe^{2+} and precipitation of Fe^{3+} as hematite. More distal to the feeder channels, the hot fluids caused leaching and recrystallization of original braunite-kutnahorite-manganocalcite bearing Mamatwan-type ore to high-grade hausmannite-rich Wessels-type ore and liberation of CaO, CO_2 and SiO_2. These components were transported to the feeder channel to be partly reprecipitated as calcite, quartz and other silicate minerals. Immediately adjacent to the ferruginized zone some of the silica reprecipitated in the form of secondary braunite. This secondary braunite-rich ore replaces some earlier formed high-grade hausmannite-rich ore (Fig. 9.3).

According to all available data the convection model seems to be the more plausible one. The system was temperature dependent. Fluids lost heat on the way through the wall rocks and fluids that penetrated far into the manganese beds away from the feeder channels (faults), had the least influence on the primary ore. Distal from feeder channels, replacement of ovoids by calcite and hausmannite is found in Mamatwan-type ore bordering Wessels-type ore (Fig. 9.2). As the system heated up this front moved deeper into the wall rocks, with already altered ore being overprinted by mineral assemblages like braunite II and hausmannite, representing a higher degree of alteration at higher temperatures. Closer to the fault zone, where the solutions caused the leaching of some of the silica to form braunite II from braunite and the liberation of CaO from the primary carbonate, possible oversaturation of CaO and CO_2 in parts of the fluids caused the precipitation of calcite-filled veins and vugs (Fig. 9.2).

The very high-grade hausmannite-rich ore immediately adjacent to ferruginized fault zones probably formed from leaching of all SiO_2 and introduction of Mn^{2+} from the zone of ferruginization where manganese was replaced by hematite (Fig. 9.2). In proximity to the ferruginized fault zone, secondary braunite formed through oversaturation of SiO_2 leached from Mamatwan-type ore. The secondary braunite also contains a high Fe-content, compared to the primary braunite.

9.2 CONCLUSION

In the northwestern part of the Kalahari manganese deposit, at Wessels Mine, north-south trending normal faults, with subordinate east-west trending normal faults, acted as feeder channels for hydrothermal fluids which reconstituted and thereby upgraded low-grade, primary sedimentary Mamatwan-type ore to high-grade Wessels-type ore. The Mn-ores in immediate vicinity of the faults are hematitized with no original sedimentary structures and textures preserved. On a macroscopic scale it is possible to observe areas of ferruginized ore, porous coarse-grained high-grade hausmannite-rich ore mixed with fine- and coarse-grained slightly porous braunite II-rich ore and microcrystalline dense laminated primary sedimentary Mamatwan-type ore, containing abundant ovoids of kutnahorite.

A systematic lateral mineralogical variation is encountered in the ores when sections are measured from ferruginized fault zones, through the high-grade Wessels-type ore, into the unaltered Mamatwan-type ore. This is found to be consistent for all sections sampled and possibly will apply for the whole mine. The generalized lateral variation in mineralogy of the ore is as follows: hematite-calcite ore -> secondary braunite-braunite II ore -> hausmannite ore -> hausmannite-braunite II ore -> braunite II-braunite ore -> braunite-kutnahorite Mamatwan-type ore. The hausmannite ores immediately adjacent to zones of ferruginization is of very high grade (up to 60 weight percent Mn) containing little SiO_2 (< 4 weight percent). In proximity to ferruginized zones the Fe contents of minerals, such as braunite, braunite II and hausmannite increases. Fe-rich hausmannites in this area are highly magnetic. The magnetism is probably related to high iron contents in the hausmannite.

Hydrothermal alteration must have been caused by an alkaline hydrothermal fluid with ferrous iron.in solution, as well as small amounts of K, Na, Mg and Al. These fluids mobilized SiO_2, CO_2 and CaO as it migrated through the wallrock. Mn^{2+} liberated by reduction of Mn^{3+} by Fe^{2+} and precipitation of Fe^{3+} (hematite) in the fault zones, reprecipitated adjacent to fault zones to form very high-grade hausmannite-rich Wessels-type ore. In the transition zone to primary Mamatwan-type ore kutnahorite was altered to hausmannite and calcite and silica leached from braunite to form braunite II, braunite (new) and/or bixbyite. Secondary minerals which precipitated from the hydrothermal fluids include gaudefroyite, clinochlore, barite and andradite.

Carbon isotopic ($\delta^{13}C$) values indicate different sources of carbon for calcite vugfilling occurring in the Wessels-type ore and ferruginized zone, than that of the carbonates present in the primary Mamatwan-type ore, supporting the theory of hydrothermal fluids entering Mn-ore beds from fault planes, which acted as fluid conduits.

Oxygen isotopic ($\delta^{18}O$) values indicate a decrease in temperature of formation of calcites, precipitated in vugs in the ore during the waning stages of hydrothermal alteration, when hydrothermal fluids regressed back towards the direction of the ferruginized fault zones, thus supporting the convection model of formation (Fig. 9.2).

The presence of magnetic hausmannite in the high-grade Wessels-type ore may possibly in future be used as a geophysical exploration tool for high-grade Mn-ores in the Kalahari manganese field, as high magnetic susceptibility is only present in Wessels-type ore consisting mainly of hausmannite and secondary braunite phases as ore minerals. However, sections containing ore minerals such as manganite, as main phase, display weak magnetic susceptibility. This observation should be further investigated. It would also, theoretically, be possible to upgrade Wessels-type ore by means of magnetic separation, thereby seperating very high-grade hausmannite ore from the bulk ore. It might even be possible to seperate ore with a Mn-content of more than 70 wt%. The mineralogical zonations defined, could in future lead to mapping out of different high-grade types of ore which may in turn promote selective mining of ores for more effective utilization of different ore grades.

REFERENCES

Armstrong, R.A., (1987). Geochronological studies on Archean and Proterozoic formations of the foreland of the Namaqualand front and possible correlates on the Kaapvaal craton. *Ph. D. thesis (unpubl.), Univ. of the Witwatersrand, Johannesburg,* 274 p.

Associated Manganese Mines of South Africa Ltd., (1992). Manganese operations. *Technical report*, 36 pp.

Baudracco-Gritti, C., Caye, R., Permingeat, F. and Protas, J., (1982). La neltnerite $CaMn_6SiO_{12}$, une nouvelle espece minerale du groupe de la braunite. *Bull. Mineral.*,**105**, 161 - 165.

Beukes, N.J., (1980). Stratigrafie en litofasies van die Cambellrand-Subgroep van die Proterofitiese GhaapGroep, Noord-Kaapland. *Trans. geol. Soc. S. Afr.*, **83**, 141 - 170.

------, (1984). Iron-formations and the evolution of iron and manganese deposits, Transvaal Supergroup, South Africa. *Abstr., 27th Int. Geol. Congr. Moscow,* **2**, p. 20.

------, (1984). Sedimentology of the Proterophytic Kalahari Manganese Deposit, Transvaal Supergroup, South Africa. *Abstr., 27th Int. Geol. Congr. Moscow.* **6**, 32 - 33.

------, (1985). W.N.N.R., K.W.P., N.G.P. - Transvaal en Griekwaland-Wes: Kalaharimangaan- en Sishenystererts afsettings. *Unpl. CSIR open file report, Pretoria,* 50 pp.

------, (1986). Environment of deposition and diagenesis of the Kalahari Manganese Deposits. *Abstr., 12th Int. Sed. Congr. Austr.*, p. 30.

------, (1988). Depositional setting of early Proterozoic manganese deposits of the Transvaal Supergroup, Griqualand West, South Africa. *Abstr., Int. Symp. on Sediments related to Mineral deposits, Beijing, China*, p.6.

------, (1989). Precamrian iron-formation and manganese deposits: Some paleo-environmental implications. *Abstracts: IGCP, Project 226, Hungary*, p1-2.

------, (1989). Sedimentological and geochemical relationships between carbonates, iron-formation and manganese deposits in the early Proterozoic Transvaal Supergroup, Griqualand West, South Africa. *Abstr., 28th Int. Geol. Congr. USA.*, 1, p. 143.

------, (1992). Some comments on the view by J.E. de Villiers that the Griqualand West manganese and iron ore deposits are of hydrothermal origin. *S. Afr. Journ. of Sci.*, **88**, 15-17.

------, (1993). A review of manganese deposits associated with the early Proterozoic Transvaal Supergroup in Northern Cape Province, South Africa. *Abstr., 16th Colloquium of African Geol. Swaziland.*, 1, 37-38.

------, (1994). Giant Early Proterozoic manganese and iron ore deposits of the Transvaal Supergroup, Northern Cape Province, South Africa. *Abstr. Vol., DMG-Tagung Freiberg, in: Eur. Journ. Min., Vol.6, No.4*, 3-4.

------, Burger, A.M., Gutzmer, J. & Kleyenstüber, A.S.E. (1994). Magnetic hausmannite from hydrothermally altered manganese ore in the Proterozoic Kalahari manganese deposit, Transvaal Supergroup, South Africa. *Abstr., Fermor Lecture Meeting, Geol. Soc. London, London*, p. 6.

------ & Gutzmer, J. (1994). Petrography and geochemistry of carbonates associated with early Proterozoic sedimentary manganese ore, Kalahari manganese field, Transvaal Supergroup, South Africa. *Abstr.,Fermor Lecture Meeting, Geol. Soc. London, London*, p. 5.

------, Kleyenstüber, A.S.E. & Nel, C.J., (1982). Volcanogenic-sedimentary cycles in the Kalahari Manganese Field. *Extended abstract for Sedimentology '82, Third Symposium of the sedimentology Division of the Geol. Soc. of S. Afr.*, 93-97.

------ & Kleyenstüber, A.S.E., (1986). Sedimentology, diagenesis and hydrothermal alteration of the Kalahari Manganese Deposit, Transvaal, Sequence, Griqualand West. *Abstr., Geocongress '86, RSA.*, 497-500.

------ & Smit, C.A., (1987). New evidence for thrust faulting in Griqualand West, South Africa: implications for stratigraphy and the age of the red beds. *S. Afr. J. of Geol.*, **90**, 378-394.

Boardman, L.G., (1941). The Black Rock manganese deposit in the south-eastern Kalahari. *Trans. Geol. Soc. S. Afr.*, **44**, 51-60.

------, (1961). Manganese in the Union of South Africa. *7th Commonwealth Mineralogical and Metallurgical Congress*, **1**, 201-215.

Boucher, B., Buhl, R. & Perrin, M., (1971). Properties et structure magnetique de Mn_3O_4. *J. Phys. Chem. Solids*, **32**, 2429-2437.

Burger, A.M., Beukes, N.J. & Gutzmer, J. (1994). Compositional variation in Mn-oxides associated with hydrothermal alteration in the early Proterozoic Kalahari Manganese Field, South Africa. *Abstr. Vol., DMG-Tagung Freiberg, in: Eur. Journ. Min., Annexture I, Vol.6, No.4*, 6-7.

De Villiers, J. (1956). Manganese, Union of South Africa. *Papers, 20th Int. Geol. Congr. Mexico. Symposium on manganese. Vol. II, Africa*, 34-72.

De Villiers, J., (1960). *The manganese deposits of the Union of South Africa.* Handbook **2**, The Government Printer, Pretoria, p280.

De Villiers, J.E., (1983). The manganese deposits of Griqualand West, South Africa: Some mineralogical aspects. *Econ. Geol.*, **78**, 1108-1118.

------, (1992). On the origin of the Griqualand West manganese and iron deposits. *S. Afr. journ. Sc.*, **88**, 12 - 15.

De Villiers, J.P.R. (1975). The crystal structure of braunite with reference to its solid-solution behavior. *Am. Miner.*, **60**, 1098-1104.

------ & Buseck, P.R. (1989). Stacking variations and nonstoichiometry in the bixbyite-braunite polysomatic mineral group. *Am. Miner.*, **74**, 1336-1989.

------, (1980). The crystal structure of braunite II and its relation to bixbyite and braunite. *Am. Miner.*, **65**, 756-765.

------, Dobson, S.M. and Buseck, P.R., (1991). Refinement of the crystal structure of neltnerite, a member of the bixbyite-braunite group of minerals. *Eur. journ. Miner.*, **3**, 567-573.

De Villiers, P.R., (1970). The geology and mineralogy of the Kalahari Manganese Field north of Sishen, Cape province. *Mem.,59, Geol. Surv. S. Afr.*, p.84.

------ & Herbstein, F.H., (1967). Distinction between two members of the braunite group. *Amer. Min.*, **52**, 20-30.

Dixon, R., (1988). Sugillite and associated metamorphic silicate minerals from Wessels mine, Kalahari Manganese Field. *M Sc. thesis, Univ. of Cape Town,* p. 150.

Dunning, F.W., (1970). *Geophysical exploration.* Her Majesty's Stationery Office, London, p.69.

Fournier, R. O., (1986). The behaviour of silica in hydrothermal solutions. *Rev. Econ. Geol.*, **2**, 45-59.

Goodenough, J.B., (1966). *Magnetism and the chemical bond.* J. Wiley and sons, New York, p.393.

Grobbelaar, W.S., (1988). The N'chwaning manganese mine of the Kalahari manganese field. *Geobulletin; Geol. Soc. S. Afr., Vol 31, No. 2*, 34-35.

Gutzmer, J. (1993). Hydrothermale alteration von Manganerzen der N'Chwaning-Mine, Kalahari-manganerzfeld, Südafrika., *M. Sc. thesis (unpubl.), T.U. Clausthal, Clausthal-Zellerfeld,* 161 pp.

------ & Beukes N.J., (1993). Fault zone controlled hematitization and upgrading of manganese ores in the Kalahari Manganese Field, South Africa. *Abstr., 16th Colloquium of African Geol., Swaziland.*, 1, 139-140.

------ & Beukes, N.J. (1993). Hydrothermal alteration and ferruginization of sedimentary manganese ore at the N'Chwaning mine, Kalahari manganese field, Early proterozoic Transvaal Supergroup, South Africa. *Unpbl. Report.* 152 pp.

------ & Beukes, N.J. (in press). Fault controlled metasomatic alteration of Early Proterozoic sedimentary manganese ores in the Kalahari manganese field, South Africa. *Accepted for publication Econ. Geol.*

------ & Cairncross, B. (1993). Recent discoveries from the Wessels Mine, South Africa. *Min. Rec.*, **24**, 365-368.

Hocking, A., (1983). *Kaias and cocopans*. Hollards, Johannesburg, 185 pp.

Jennings, M., (1986). The Middelplaats manganese ore deposit, Griqualand West. . In: Anhaeusser, C.R. and Maske S. (Eds), *Mineral deposits of southern Africa*., The Natal Witness, Pietermaritzburg, 979-983.

Kleyenstüber, A.S.E., (1979).'n Mineralogiese ondersoek van hoë-temperatuur-reduksie-produkte van mangaanerts vanuit die Mamatwanmyn, Kalaharimangaanveld. *M Sc. thesis (unpubl.), Rand Afrikaans Univ, Johannesburg,* 125 pp.

------ (1984). The mineralogy of the manganese-bearing Hotazel Formation, of the Proterozoic Transvaal Sequence in Griqualand West, South Africa. *Trans. Geol. Soc. S. Afr.*, **87**, 257-272.

------ (1985). A regional mineralogical study of the manganese-bearing Voëlwater Subgroup in the northern Cape province. *Ph.D. thesis (unpubl.), Rand Afrikaans Univ, Johannesburg,* 328 pp.

------ (1986). The mineralogy of the manganese-bearing Hotazel Formation of the Proterozoic Transvaal Sequence in Griqualand West, South Africa. *Trans. Geol. Soc. S. Afr.*, **89**, 421-425.

------ (1988). The correlation of the mineralogy with sedimentary cycles of the Proterozoic manganese-bearing Hotazel Formation in South Africa. *Abstr. Int. Symp.Sed. related to Min Dep., Beijing, China,* 107-108.

------ (1993). Significant characteristics of the manganese ores and some of the minerals occurring in the Proterozoic Kalahari Manganese Field, South Africa. *Resource Geol. Spec. Issue*, **17**, 2-11.

Kupferburger, W., Boardman, L.G., & Bosch, P.R. (1956). New considerations concerning the manganese ore deposits in the Postmasburg and Kuruman areas, northern Cape Province, Union of South Africa. *Papers, 20th Int. Geol. Congr. Mexico, Symposium on manganese. vol. II, Africa,* 73-87.

Lotgering, F. K. & Van Diepen, A. M., (1973). Valencies of manganese and iron ions in cubic ferrites as observed in paramagnetic Mössbauer spectra. *J. Phys. Chem. Solids*, **34**, 1369-1377.

Miyano, T. & Beukes, N.J., (1987). Physiochemical environments for the formation of quartz-free manganese oxide ores from the early Proterozoic Hotazel Formation, South Africa. *Econ. Geol.*, **82**, 706-718.

------ & Beukes, N.J., (1988). Estimation of carbon dioxide fugacity and braunite II stability in quartz-free manganese oxide ores from the Kalahari Manganese Field, South Africa. *S. Afr. J. Sci*, **84**, 244-246.

Moen, H.F.G., (1977). Postmasburg: Map and explanatory notes. *Geol. Surv. S. Afr., Pretoria,* Map 2822.

------ (1979). Kuruman: Map and explanatory notes. *Geol. Surv. S. Afr., Pretoria,* Map 2722.

Murray, J.W., Dillard, J.G., Giovanoli, R., Moers, H and Strumm, W., (1985). Oxidation of Mn(II): Initial mineralogy, oxidation state and ageing. *Geochim. et Cosm.*, **49**, 463-470.

Nel, C.J., (1984). Die mineralogie en geochemie van die Mamatwanertsliggaam, Kalaharimangaanveld, Transvaal-Supergroep. *M Sc. thesis (unpubl.), Rand Afrikaans Univ, Johannesburg.*, 119 pp.

------, Beukes, N.J. & De Villiers, J.P.R., (1986). The Mamatwan Mine of the Kalahari Manganese Field. In: Anhaeusser, C.R. and Maske S. (Eds), *Mineral deposits of southern Africa.* The Natal Witness, Pietermaritzburg, 963-978.

Ramdohr, P. (1969). *The ore minerals and their intergrowths.* 3rd Ed. Pergamon Press, Branschweig, 1174 pp.

Rogers, A.W., (1908). Geological survey of parts of Vryburg, Kuruman, Hay and Gordonia. *Cape Town, Annual Report, geol. Comm., C.G.H. for 1907*, 11-122.

Roy, S., (1981). *Manganese deposits.* Academic Press, London, 458 pp.

Smit, J. & Wijn, H.P.J., (1959). *Ferrites.* Wiley, New York, 136 pp.

Söhnge, P.G., (1977). Timing aspects of the manganese deposits of the northern Cape province (South Africa). In: Klemm, D.D. and Schneider, H.J. (Eds.), *Time- and stratabound ore deposits.* Springer-Verlag, Heidelberg, 115-122.

Stowe, C.W., (1986). Synthesis and interpretation of structures along the north-eastern boundary of the Namaqua tectonic province, South Africa. *Unpbl. Report., Samancor, Johannesburg.*, p. 7.

Svoboda, J., (1987). *Magnetic methods for the treatment of minerals*. Elsevier Science publishers, New York, USA, 113 pp.

Taljaardt, J.J., (1982). Major manganese ore fields, Republic of South Africa. *Unpubl. Report., Samancor, Johannesburg.*, 7 pp.

Thompson, J.B., (1978). Biopyriboles and polysomatic series. *Amer. Miner.*, **63**, 239 - 249.

Tsikos, H. (1994). The mineralogy and geochemistry of the Voëlwater banded iron-formation, Nothern Cape Province. *M.Sc. Thesis (unpubl.), Univ. Grahamstown, Grahamstown*, 152 pp.

Von Bezing, K.L., Dixon, R.D., Pohl, D. & Cavallo, G., (1991). The Kalahari Manganese Field: An update. *Min. Rec.*, **22**, 279-297.

Wilson, W.E. & Dunn, P.J. (1987). Famous mineral localities: The Kalahari Manganese Field. *Min. Rec.*, **9**, 137-153.

Appendix I

STATISTICS OF PROBE ANALYSES

1 HAUSMANNITE

N202M (7 analyses)

Element	Std. dev.	Max.	Min.	Mean
SiO_2	0.23	0.73	*	0.23
Al_2O_3	0.08	*	*	*
MnO	0.75	33.67	31.23	32.45
Fe_2O_3	2.55	10.45	2.82	5.27
Mn_2O_3	3.15	64.94	55.20	61.71
MgO	0.14	0.74	.036	0.54
CaO	0.07	*	*	*
Total	0.16	100.67	100.22	100.35

N203 (9 analyses)

Element	Std. dev.	Max.	Min.	Mean
SiO_2	0.04	0.22	*	*
Al_2O_3	0.23	0.78	*	*
MnO	0.92	33.84	30.80	32.57
Fe_2O_3	0.91	3.36	0.48	1.95
Mn_2O_3	1.13	66.76	30.80	64.98
MgO	0.07	0.21	*	*
CaO	0.06	*	*	*
Total	0.04	100.20	100.06	100.14

* Values < 0.2 wt%

N203M (5 analyses)

Element	Std. dev.	Max.	Min.	Mean
SiO_2	0.06	*	*	*
Al_2O_3	0.11	0.33	*	*
MnO	0.20	33.42	32.80	33.09
Fe_2O_3	1.50	5.96	1.79	3.77
Mn_2O_3	1.47	64.81	60.67	62.93
MgO	0.06	*	*	*
CaO	0.06	*	*	*
Total	0.10	100.40	100.13	100.23

N204 (9 analyses)

Element	Std. dev.	Max.	Min.	Mean
SiO_2	0.05	0.23	*	*
Al_2O_3	0.12	0.34	*	*
MnO	0.64	33.45	31.21	32.47
Fe_2O_3	1.89	5.11	0.13	2.76
Mn_2O_3	1.90	67.49	61.44	64.38
MgO	0.05	0.32	*	*
CaO	0.04	*	*	*
Total	0.10	100.30	100.03	100.19

* Values < 0.2 wt%

N204M (15 analyses)

Element	Std. dev.	Max.	Min.	Mean
SiO_2	0.04	*	*	*
Al_2O_3	0.05	0.11	*	*
MnO	0.61	33.30	31.31	32.45
Fe_2O_3	1.23	7.46	2.50	4.81
Mn_2O_3	1.33	65.01	59.29	62.64
MgO	0.10	0.47	*	*
CaO	0.05	*	*	*
Total	0.08	100.50	100.18	100.24

N205 (4 analyses)

Element	Std. dev.	Max.	Min.	Mean
SiO_2	0.05	*	*	*
Al_2O_3	0.07	*	*	*
MnO	0.46	32.98	31.97	32.62
Fe_2O_3	1.58	3.35	*	1.12
Mn_2O_3	1.05	66.64	64.31	65.78
MgO	0.02	*	*	*
CaO	0.02	*	*	*
Total	0.08	100.18	100.02	100.08

* Values < 0.2 wt%

N205M (5 analyses)

Element	Std. dev.	Max.	Min.	Mean
SiO_2	0.04	0.26	*	*
Al_2O_3	0.09	*	*	*
MnO	0.39	33.34	32.19	31.79
Fe_2O_3	4.55	11.08	0.47	11.32
Mn_2O_3	4.56	66.97	55.89	57.14
MgO	0.10	0.26	*	*
CaO	0.08	0.22	*	*
Total	0.29	100.76	100.05	100.73

N205ML (3 analyses)

Element	Std. dev.	Max.	Min.	Mean
SiO_2	0.01	*	*	0.20
Al_2O_3	0.00	*	*	*
MnO	0.54	32.34	31.25	32.87
Fe_2O_3	0.05	11.36	11.27	5.93
Mn_2O_3	0.38	57.52	56.76	61.14
MgO	0.06	*	*	*
CaO	0.17	0.37	*	*
Total	0.05	100.77	100.67	100.39

* Values < 0.2 wt%

N207 (3 analyses)

Element	Std. dev.	Max.	Min.	Mean
SiO_2	20.67	0.21	*	*
Al_2O_3	20.73	*	*	*
MnO	6.25	31.75	30.35	31.09
Fe_2O_3	20.55	6.61	0.29	2.47
Mn_2O_3	11.32	68.16	61.35	65.79
MgO	20.68	0.41	*	0.23
CaO	20.63	0.29	*	*
Total	26.43	100.34	100.03	100.16

N207M (4 analyses)

Element	Std. dev.	Max.	Min.	Mean
SiO_2	0.15	0.46	*	0.21
Al_2O_3	0.06	*	*	*
MnO	0.82	32.89	30.90	32.30
Fe_2O_3	3.38	8.90	0.47	6.24
Mn_2O_3	3.31	66.61	57.94	61.20
MgO	0.20	0.55	*	0.29
CaO	0.09	*	*	*
Total	0.20	100.51	100.02	100.36

* Values < 0.2 wt%

N209 (12 analyses)

Element	Std. dev.	Max.	Min.	Mean
SiO_2	0.06	*	*	*
Al_2O_3	0.04	*	*	*
MnO	0.94	32.69	29.86	31.11
Fe_2O_3	1.62	7.97	2.63	4.93
Mn_2O_3	1.76	65.98	60.22	63.06
MgO	0.52	1.73	*	0.92
CaO	0.11	0.37	*	*
Total	0.07	100.42	100.20	100.29

N210 (2 analyses)

Element	Std. dev.	Max.	Min.	Mean
SiO_2	0.09	0.26	*	*
Al_2O_3	0.04	*	*	*
MnO	0.07	32.19	32.06	32.13
Fe_2O_3	0.24	3.21	2.73	2.97
Mn_2O_3	0.23	64.91	64.45	64.68
MgO	0.06	*	*	*
CaO	0.01	*	*	*
Total	0.04	100.21	100.13	100.17

* Values < 0.2 wt%

N119 (14 analyses)

Element	Std. dev.	Max.	Min.	Mean
SiO_2	0.39	0.98	*	0.67
Al_2O_3	0.01	*	*	*
MnO	0.59	32.31	30.89	31.68
Fe_2O_3	0.42	2.22	1.24	1.82
Mn_2O_3	0.97	65.03	62.69	63.98
MgO	0.25	0.67	*	0.43
CaO	0.06	0.48	0.36	0.40
Total	0.02	100.22	100.17	100.20

* Values < 0.2 wt%

2 BRAUNITE

N101 (5 analyses)

Element	Std. dev.	Max.	Min.	Mean
SiO_2	1.01	10.27	7.76	9.03
Al_2O_3	0.06	*	*	*
MnO	2.04	46.27	41.22	43.78
Fe_2O_3	7.38	18.97	3.46	10.84
Mn_2O_3	4.98	40.38	28.93	35.08
MgO	0.15	0.48	*	0.24
CaO	0.31	1.56	0.68	1.15
Total	0.13	100.32	99.96	100.15

N201M (10 analyses)

Element	Std. dev.	Max.	Min.	Mean
SiO_2	0.84	10.40	7.79	8.21
Al_2O_3	0.07	*	*	*
MnO	1.53	47.58	42.64	36.97
Fe_2O_3	5.62	20.25	4.56	17.10
Mn_2O_3	3.59	39.82	29.06	37.48
MgO	0.06	*	*	*
CaO	0.39	1.32	0.20	0.57
Total	0.20	100.92	100.20	100.61

* Values < 0.2 wt%

N201

Element	Std. dev.	Max.	Min.	Mean
SiO_2				9.41
Al_2O_3				*
MnO				45.02
Fe_2O_3				8.89
Mn_2O_3				36.21
MgO				*
CaO				0.76
Total				100.39

N202

Element	Std. dev.	Max.	Min.	Mean
SiO_2	0.94	10.12	7.70	9.29
Al_2O_3	0.17	0.26	*	*
MnO	1.73	45.89	41.26	43.95
Fe_2O_3	1.10	3.74	1.05	2.73
Mn_2O_3	2.31	46.09	40.01	42.62
MgO	0.03	*	*	*
CaO	0.85	2.41	0.56	1.57
Total	0.17	100.45	100.06	100.24

* Values < 0.2 wt%

N206 (6 analyses)

Element	Std. dev.	Max.	Min.	Mean
SiO_2	1.37	14.25	10.23	11.73
Al_2O_3	0.30	0.76	*	*
MnO	0.78	44.95	42.76	43.56
Fe_2O_3	1.31	8.30	4.64	5.89
Mn_2O_3	3.90	39.00	27.36	34.64
MgO	0.66	2.02	0.14	0.60
CaO	1.35	6.19	1.72	3.73
Total	0.19	100.71	100.16	100.44

N210 (11 analyses)

Element	Std. dev.	Max.	Min.	Mean
SiO_2	0.42	11.54	10.15	10.69
Al_2O_3	0.08	*	*	*
MnO	8.93	41.29	9.66	31.70
Fe_2O_3	0.83	6.65	3.44	4.54
Mn_2O_3	7.62	69.38	41.69	50.95
MgO	0.11	0.43	0.04	*
CaO	1.39	5.79	1.0	2.31
Total		100.89	100.03	100.43

* Values < 0.2 wt%

N119 (14 analyses)

Element	Std. dev.	Max.	Min.	Mean
SiO_2	0.88	13.16	9.76	10.69
Al_2O_3	0.14	0.51	*	*
MnO	1.86	48.31	40.50	44.80
Fe_2O_3	2.54	8.41	*	3.23
Mn_2O_3	3.52	44.10	34.24	39.29
MgO	0.99	3.75	*	0.46
CaO	1.20	4.88	0.88	1.78
Total	0.32	101.03	99.75	100.44

* Values < 0.2 wt%

3 BRAUNITE II

N201M (2 analyses)

Element	Std. dev.	Max.	Min.	Mean
SiO_2	1.46	7.79	4.88	4.88
Al_2O_3	0.04	*	*	*
Fe_2O_3	5.19	30.62	20.25	30.62
Mn_2O_3	2.02	72.39	68.34	68.34
MgO	0.24	0.51	*	0.51
CaO	0.00	0.26	0.25	0.26
Total	1.87	104.69	100.96	100.69

N106 (5 analyses)

Element	Std. dev.	Max.	Min.	Mean
SiO_2	0.21	5.09	4.54	4.88
Al_2O_3	0.09	0.24	*	*
Fe_2O_3	0.77	13.90	11.64	12.95
Mn_2O_3	0.67	77.80	75.77	76.80
MgO	0.08	*	*	*
CaO	0.28	5.40	4.59	4.89
Total	0.47	100.63	99.29	99.76

* Values < 0.2 wt%

N207 (7 analyses)

Element	Std. dev.	Max.	Min.	Mean
SiO_2	0.11	5.57	5.29	5.39
Al_2O_3	0.08	*	*	*
Fe_2O_3	0.76	15.06	13.19	14.33
Mn_2O_3	0.54	77.04	75.50	76.36
MgO	0.06	*	*	
CaO	0.15	4.92	4.53	4.63
Total	0.39	101.61	100.49	100.90

N208 (19analyses)

Element	Std. dev.	Max.	Min.	Mean
SiO_2	0.21	5.57	4.84	5.15
Al_2O_3	0.07	*		*
Fe_2O_3	0.88	16.08	13.13	14.63
Mn_2O_3	1.13	76.83	72.60	75.06
MgO	1.06	2.97	0.01	0.79
CaO	0.27	5.42	4.37	4.59
Total	0.73	101.80	98.57	100.33

* Values < 0.2 wt%

N209 (5 analyses)

Element	Std. dev.	Max.	Min.	Mean
SiO_2	0.26	5.27	4.63	4.95
Al_2O_3	0.08	*	*	*
Fe_2O_3	2.19	16.07	10.30	12.73
Mn_2O_3	2.42	81.40	74.61	78.40
MgO	0.04	*	*	*
CaO	0.21	5.07	4.46	4.76
Total	0.14	101.47	101.08	101.35

N210 (2 analyses)

Element	Std. dev.	Max.	Min.	Mean
SiO_2	0.58	5.46	4.29	4.87
Al_2O_3	0.03	*	*	*
Fe_2O_3	0.25	4.13	3.64	3.39
Mn_2O_3	0.31	94.30	93.78	93.99
MgO	0.01	0.31	0.30	0.31
CaO	0.32	1.23	0.59	0.91
Total	0.21	104.04	103.62	103.83

* Values < 0.2 wt%

4 BRAUNITE (NEW)

N107 (7 analyses)

Element	Std. dev.	Max.	Min.	Mean
SiO_2	0.47	3.62	2.11	3.01
Al_2O_3	0.18	0.75	*	0.35
Fe_2O_3	1.66	14.9	10.00	13.40
Mn_2O_3	2.02	84.79	78.31	80.86
MgO	0.04	*	*	*
CaO	0.27	3.37	2.68	3.01
Total	0.65	101.29	99.46	100.83

* Values < 0.2 wt%

5 BIXBYITE

N512 (4 analyses)

Element	Std. dev.	Max.	Min.	Mean
SiO_2	0.34	1.33	0.38	0.87
Al_2O_3	0.06	*	*	*
Fe_2O_3	0.63	21.46	19.72	20.69
Mn_2O_3	1.25	81.00	77.71	78.93
MgO	0.03	*	*	*
CaO	0.18	0.83	0.38	0.67
Total	0.33	101.64	100.73	101.26

N202M (3 analyses)

Element	Std. dev.	Max.	Min.	Mean
SiO_2	0.26	1.36	0.73	1.00
Al_2O_3	0.06	*	*	*
Fe_2O_3	8.90	32.05	10.45	20.38
Mn_2O_3	9.08	94.25	72.13	83.87
MgO	0.14	0.67	0.36	0.47
CaO	0.04	0.22	*	*
Total	0.40	106.64	105.67	106.12

* Values < 0.2 wt%

6 MAROKITE

N510 (10 analyses)

Element	Std. dev.	Max.	Min.	Mean
SiO_2	0.30	1.02	*	0.24
Al_2O_3	0.07	0.04	*	*
Fe_2O_3	3.93	11.87	0.36	3.52
Mn_2O_3	3.11	74.49	64.40	72.06
MgO	0.07	*	*	*
CaO	2.50	26.27	18.47	24.53
Total	0.66	101.20	99.27	100.41

* Values < 0.2 wt%

7 ANDRADITE

N203M (3 analyses)

Element	Std. dev.	Max.	Min.	Mean
SiO_2	1.73	36.79	32.64	34.04
Al_2O_3	0.07	*	*	*
Fe_2O_3	1.12	32.63	30.15	31.39
Mn_2O_3	2.27	7.73	2.48	5.1
MgO	0.05	0.24	*	*
CaO	1.98	31.53	27.15	29.16
Total	2.13	104.53	99.86	100.12

N210 (4 analyses)

Element	Std. dev.	Max.	Min.	Mean
SiO_2	5.11	36.61	24.46	33.28
Al_2O_3	0.58	1.27	*	0.42
Fe_2O_3	11.95	31.71	1.68	22.03
Mn_2O_3	13.04	33.64	0.80	11.48
MgO	0.05	0.24	*	*
CaO	0.85	34.37	31.97	33.20
Total	3.58	103.39	94.37	100.58

* Values < 0.2 wt%

N113 (5 analyses)

Element	Std. dev.	Max.	Min.	Mean
SiO_2	0.51	35.49	34.14	34.89
Al_2O_3	0.19	4.41	3.86	4.22
Fe_2O_3	0.13	24.31	23.97	24.17
Mn_2O_3	0.43	2.90	1.62	2.09
MgO	0.04	*	*	*
CaO	0.55	35.51	33.88	34.68
Total	0.57	100.7	99.01	100.02

* Values < 0.2 wt%